

# ALTERNATE VERTICAL SHEAR REINFORCEMENT IN PRESTRESSED CONCRETE BEAMS: FINAL REPORT

William R. Burkett, W. Pennington Vann,  
Rafael Cedeno-Rosete, and Selim Turkyilmaz

Department of Civil Engineering  
Texas Tech University

Center for Multidisciplinary Research in Transportation  
Texas Tech University ♦ Lubbock, TX 79409

Submitted to:

Texas Department of Transportation

## NOTICE

The United States Government and the State of Texas do not endorse products or manufacturers. Trade or manufacturers' names appear herein solely because they are considered essential to the object of this report.

**TECHNICAL REPORT DOCUMENTATION PAGE**

1. Report No. TX 00/0-1853-2	2. Government Accession No.	3. Recipient's Catalog No.	
4. Title and Subtitle Alternate Vertical Shear Reinforcement in Prestressed Concrete Beams: Final Report		5. Report Date November, 2002	
		6. Performing Organization Code TechMRT	
7. Author(s) William R. Burkett, W. Pennington Vann, Rafael Cedeno-Rosete, Selim Turkyilmaz		8. Performing Organization Report No. 0-1853-2	
9. Performing Organization Name and Address Texas Tech University Center for Multidisciplinary Research in Transportation Box 41023 Lubbock, Texas 79409-1023		10. Work Unit No. (TRAIS)	
		11. Contract or Grant No. Project 0-1853	
12. Sponsoring Agency Name and Address Texas Department of Transportation Research and Technology P. O. Box 5080 Austin, TX 78763-5080		13. Type of Report and Period Cover Final Report – Draft 1	
		14. Sponsoring Agency Code	
15. Supplementary Notes: Study conducted in cooperation with the Texas Department of Transportation. Research Project Title: "Alternate Vertical Shear Reinforcement in Prestressed Concrete Beams"			
16. Abstract: The Texas Department of Transportation (TxDOT) commonly uses prestressed I-beams to construct bridges. Currently, TxDOT permits the substitution of welded wire fabric (WWF) for the traditional, 60-ksi, steel shear reinforcement, but load tests were needed to verify the behavior. WWF stirrups consist of deformed, vertical, cold-drawn wires anchored by a pair of smooth horizontal wires that are attached to the stirrups by electrical resistance welds. Forty-three load tests were conducted on the 18 specimens using four different load/support configurations. Load comparisons were made against AASHTO limits, and beam response comparisons were made against the standard TxDOT design. All of the beams had adequate shear and flexural strengths when compared to AASHTO limits and similar responses in terms of load/deflection curves, ductilities, failure modes, and crack sizes and distributions. A digital image analysis technique was developed and used to evaluate beam cracking.			
17. Key Words: Prestressed Concrete I-beams, Welded Wire Fabric, Shear Reinforcement Details, Normal Strength Concrete, High Strength Concrete, Full-scale Load Test, 60-ksi Steel Design Strength, 80-ksi Steel Design Strength, Digital Image Crack Analysis Technique		18. Distribution Statement:  No restrictions. This document is available to the public through the National Technical Information Service, Springfield, Virginia 22161	
19. Security Classif. (of this report) Unclassified	20. Security Classif. (of this page) Unclassified	21. No. of Pages 201	22. Price



ALTERNATE VERTICAL SHEAR REINFORCEMENT IN  
PRESTRESSED CONCRETE BEAMS: FINAL REPORT

by

William R. Burkett, Ph.D., P.E.  
W. Pennington Vann, Ph.D., P.E.  
Rafael Cedenro-Rosette, Ph.D.  
Selim Turkyilmaz, MSCE  
Texas Tech University  
Lubbock, Texas

Research Report Number 0-1853

conducted for

Texas Department of Transportation

by the

CENTER FOR MULTIDISCIPLINARY RESEARCH IN TRANSPORTATION  
TEXAS TECH UNIVERSITY

November 2002

Draft 1



## IMPLEMENTATION STATEMENT

The potential for positive, usable results from this project is high. The results of this study should provide recommended modifications to TxDOT's Prestressed Concrete I-beam Details IBA (M) standard. Recommendations could include changes to the WWF substitution note, standardization of WWF details (wire area, spacing, and anchorage), and an improved or alternate R Bar detail. Improved WWF details could lead to lower WWF fabrication costs resulting in construction cost savings to TxDOT.

Research could provide test data to allow modification of current AASHTO design codes. Test data could support increasing the design yield strength of deformed WWF used as shear reinforcement from the current limit of 420 MPa (60 ksi) to 550 MPa (80 ksi).

Prepared in cooperation with the Texas Department of Transportation and the U.S. Department of Transportation, Federal Highway Administration.



## **AUTHOR'S DISCLAIMER**

The contents of this report reflect the views of the authors who are responsible for the facts and the accuracy of the data presented herein. The contents do not necessarily reflect the official view of policies of the Department of Transportation or the Federal Highway Administration. This report does not constitute a standard, specification, or regulation.

## **PATENT DISCLAIMER**

There was no invention or discovery conceived or first actually reduced to practice in the course of or under this contract, including any art, method, process, machine, manufacture, design or composition of matter, or any new useful improvement thereof, or any variety of plant which is or may be patentable under the patent laws of the United States of America or any foreign country.

## **ENGINEERING DISCLAIMER**

Not intended for construction, bidding, or permit purposes.

## **TRADE NAMES AND MANUFACTURERS' NAMES**

The United States Government and the State of Texas do not endorse products or manufacturers. Trade or manufacturers' names appear herein solely because they are considered essential to the object of this report.

# SI\* (MODERN METRIC) CONVERSION FACTORS

## APPROXIMATE CONVERSIONS TO SI UNITS

Symbol	When You Know	Multiply By	To Find	Symbol	When You Know	Multiply By	To Find	Symbol
<b>LENGTH</b>								
in	inches	25.4	millimeters	mm	millimeters	0.039	inches	in
ft	feet	0.305	meters	m	meters	3.28	feet	ft
yd	yards	0.914	meters	m	meters	1.09	yards	yd
mi	miles	1.61	kilometers	km	kilometers	0.621	miles	mi
<b>AREA</b>								
in <sup>2</sup>	square inches	645.2	square millimeters	mm <sup>2</sup>	square millimeters	0.0016	square inches	in <sup>2</sup>
ft <sup>2</sup>	square feet	0.093	square meters	m <sup>2</sup>	square meters	10.764	square feet	ft <sup>2</sup>
yd <sup>2</sup>	square yards	0.836	square meters	m <sup>2</sup>	square meters	1.195	square yards	yd <sup>2</sup>
ac	acres	0.405	hectares	ha	hectares	2.47	acres	ac
mi <sup>2</sup>	square miles	2.59	square kilometers	km <sup>2</sup>	square kilometers	0.386	square miles	mi <sup>2</sup>
<b>VOLUME</b>								
fl oz	fluid ounces	29.57	milliliters	mL	milliliters	0.034	fluid ounces	fl oz
gal	gallons	3.785	liters	L	liters	0.264	gallons	gal
ft <sup>3</sup>	cubic feet	0.028	cubic meters	m <sup>3</sup>	cubic meters	35.71	cubic feet	ft <sup>3</sup>
yd <sup>3</sup>	cubic yards	0.765	cubic meters	m <sup>3</sup>	cubic meters	1.307	cubic yards	yd <sup>3</sup>
NOTE: Volumes greater than 1000 l shall be shown in m <sup>3</sup> .								
<b>MASS</b>								
oz	ounces	28.35	grams	g	grams	0.035	ounces	oz
lb	pounds	0.454	kilograms	kg	kilograms	2.202	pounds	lb
T	short tons (2000 lb)	0.907	megagrams (or "metric ton")	Mg (or "t")	megagrams (or "metric ton")	1.103	short tons (2000 lb)	T
<b>TEMPERATURE (exact)</b>								
°F	Fahrenheit temperature	5(F-32)/9 or (F-32)/1.8	Celsius temperature	°C	Celsius temperature	1.8C + 32	Fahrenheit temperature	°F
<b>ILLUMINATION</b>								
fc	foot-candles	10.76	lux	lx	lux	0.0929	foot-candles	fc
fl	foot-Lamberts	3.426	candela/m <sup>2</sup>	cd/m <sup>2</sup>	candela/m <sup>2</sup>	0.2919	foot-Lamberts	fl
<b>FORCE and PRESSURE or STRESS</b>								
lbf	poundforce	4.45	newtons	N	newtons	0.225	poundforce	lbf
lbf/in <sup>2</sup>	poundforce per square inch	6.89	kilopascals	kPa	kilopascals	0.145	poundforce per square inch	lbf/in <sup>2</sup>

\* SI is the symbol for the International System of Units. Appropriate

(Revised September 1993)

## TABLE OF CONTENTS

<b>CHAPTER I - INTRODUCTION</b> .....	1
1.1 Background.....	1
1.2 Scope.....	2
1.3 Objective.....	3
<b>CHAPTER II – TEST PLAN</b> .....	4
2.1 General Approach.....	4
2.2 Test Matrix.....	4
2.3 Beam Details.....	12
2.4 Cast-in-Place Concrete Deck Slab.....	15
2.5 Test Arrangements.....	15
2.5.1 Flexural Tests.....	16
2.5.2 First End Region Shear Tests.....	17
2.5.3 Second End Region Shear Tests.....	19
2.5.4 Intermediate End Region Shear Tests.....	21
2.6 Calculations for Load and Support Placement.....	22
2.6.1 Capacities of Specimens in Middle Region Tests.....	22
2.6.2 Capacities of Specimens in the First End Region Shear Tests.....	26
2.6.3 Capacities of Specimens in the Second End Region Shear Tests...	29
2.6.4 Shear Capacity of Specimens in the Intermediate End Region Tests	32
2.7 Test Specimen Identification.....	35
2.8 Fatigue Considerations.....	36
<b>CHAPTER III – TEST SETUP AND PROCEDURES</b> .....	37
3.1 Introduction.....	37
3.2 Specimen Fabrication.....	37
3.3 Test Sequence.....	39
3.4 Load Equipment and Load Sequence.....	41
<b>CHAPTER IV – INSTRUMENTATION AND DATA ACQUISITION</b> .....	44
4.1 Introduction.....	44
4.2 Electronic Instrumentation.....	44
4.2.1 Embedded Strain Gages.....	44
4.2.2 Concrete Strain Gages.....	45
4.2.3 Linear Variable Differential Transducers.....	45
4.2.4 Load Cell and Pressure Transducers.....	47
4.2.5 Data Acquisition.....	47
4.3 Mechanical Instrumentation.....	48
4.3.1 Dial Gages.....	48
4.3.2 Wire Gage.....	48
4.3.3 Strand End-slip Measurements.....	50

<b>CHAPTER V – DIGITAL IMAGING FOR CRACK QUANTIFICATION.....</b>	<b>52</b>
5.1 Objective and Scope .....	52
5.2 Introduction to Digital Imaging .....	52
5.3 Algorithms for Crack Determination.....	53
5.3.1 RGB to Grayscale Image Conversion.....	53
5.3.2 Edge Detection.....	55
5.3.3 Binarization.....	58
5.3.4 Spot Removal.....	61
5.3.5 Hole Filling .....	66
5.3.6 Crack Thinning .....	66
5.4 Algorithms for Crack Quantification .....	68
5.4.1 Crack Labeling.....	69
5.4.2 Crack Area .....	72
5.4.3 Crack Length.....	72
5.4.4 Crack Width.....	73
5.5 Accuracy of the Technique .....	73
5.6 Calculations for the Example Beam Image .....	77
5.7 Taking of Digital Images .....	77
<b>CHAPTER VI – MIDDLE REGION FLEXURAL TESTS .....</b>	<b>79</b>
6.1 Objective and Scope .....	80
6.2 Normal Strength Concrete .....	80
6.2.1 Load –Deflection Behavior.....	80
6.2.2 Cracking Behavior .....	86
6.3 High Strength Concrete.....	88
6.3.2 Cracking Behavior .....	91
6.4 Summary .....	94
<b>CHAPTER VII – FIRST END REGION SHEAR TESTS .....</b>	<b>95</b>
7.1 Objective and Scope .....	95
7.2 Normal Strength Concrete .....	97
7.2.1 Load-Deflection Behavior .....	97
7.2.2 Cracking Behavior .....	107
7.3 High Strength Concrete.....	110
7.3.1 Load-Deflection Behavior .....	111
7.3.2 Cracking Behavior .....	111
7.4 Summary .....	118
<b>CHAPTER VIII – SECOND END REGION SHEAR TESTS.....</b>	<b>119</b>
8.1 Objective and Scope .....	119
8.2 Normal Strength Concrete .....	120
8.2.1 Load-Deflection Behavior of Flexural Beams.....	120
8.2.2 Load-Deflection Behavior of Pristine Beams.....	126
8.2.3 Cracking Behavior .....	129

8.3	High Strength Concrete.....	132
8.3.1	Load Deflection Behavior of Flexural Beams.....	132
8.3.2	Load-Deflection Behavior of Pristine Beams.....	137
8.3.3	Cracking Behavior.....	137
8.4	Summary.....	139
<b>CHAPTER IX – INTERMEDIATE END REGION SHEAR TESTS.....</b>		<b>140</b>
9.1	Objective and Scope.....	140
9.2	Load-Deflection Behavior.....	141
9.3	Cracking Behavior.....	145
9.4	Summary.....	148
<b>CHAPTER X – POTENTIAL FATIGUE PROBLEMS.....</b>		<b>149</b>
10.1	Background.....	149
10.2	Literature Review.....	150
10.3	I-Beam Related Concerns and Resolutions.....	150
10.4	Summary.....	153
<b>CHAPTER XI – SUMMARY, CONCLUSIONS, AND RECOMMENDATIONS.....</b>		<b>154</b>
11.1	Summary.....	154
11.1.1	Test Program.....	155
11.1.2	Test Results.....	155
11.2	Conclusions.....	155
11.3	Recommendations.....	156
11.3.1	TxDOT Policies and Standards.....	156
11.3.2	Future Research.....	157
<b>REFERENCES.....</b>		<b>158</b>

## LIST OF FIGURES

Figure 2.1	Traditional Reinforcing Steel R-bar and S-bar in a TxDOT Type A I-beam .....	6
Figure 2.2	Side View Detail of TxDOT Type A I-beam.....	6
Figure 2.3	Matching WWF Detail.....	8
Figure 2.4	Side View of Matching WWF Detail.....	8
Figure 2.5	Simplified WWF Detail .....	9
Figure 2.6	Side View of Simplified WWF Detail .....	9
Figure 2.7	Equivalent Strength WWF Detail .....	10
Figure 2.8	Side View of Equivalent Strength WWF Detail. ....	11
Figure 2.9	Alternate R-bar Detail.....	12
Figure 2.10	Type A I-beam Cross-section and Dimensions .....	13
Figure 2.11	Strand Pattern for Normal Strength Concrete Beams .....	14
Figure 2.12	Strand Pattern for High Strength Concrete Beams .....	14
Figure 2.13	Cast-in-Place Concrete Deck Slab Geometry and Reinforcement .....	15
Figure 2.14	Configuration for the Middle Region Flexural Test .....	16
Figure 2.15	Assumed Reaction Stress Distribution.....	17
Figure 2.16	Configuration for the First End Region Shear Test .....	18
Figure 2.17	Expected Cracking Behavior in the First End Region Shear Test .....	19
Figure 2.18	Configuration for the Second End Region Shear Test.....	20
Figure 2.19	Expected Cracking Behavior for the Second End Region Shear Test..	20
Figure 2.20	Configuration for the Intermediate End Region Shear Test .....	21
Figure 2.21	Expected Cracking Behavior for the Intermediate End Region Shear Test.....	22
Figure 2.22	Applied and Resisting Shears and Moments: Flexural Test .....	25
Figure 2.23	Applied and Resisting Shears and Moments: First End Region Shear Test.....	28
Figure 2.24	Applied and Resisting Shears and Moments: Second End Region Shear Test.....	31
Figure 2.25	Applied and Resisting Shears and Moments: Intermediate End Region Test.....	34
Figure 3.1	General Test Setup.....	41
Figure 4.1	Locations of Vertical Displacement Measurements .....	46
Figure 4.2	Wire Gage Deflection Device.....	49
Figure 4.3	End-Slip Measurement Brackets.....	50
Figure 5.1	Sample RGB Crack Image and its Grayscale Conversion.....	54
Figure 5.2	Eight-Pixel Neighborhood of a Grayscale Image .....	55
Figure 5.3	Edge Enhanced Images of Fig. 5.2 by First Method (Eqs. 5.2 & 5.3)..	57
Figure 5.4	Edge Enhanced Images of Fig. 5.2 by Second Methods (Eqs. 5.2 and 5.4) .....	60
Figure 5.5	Edge Enhanced Images of Fig. 5.2 by Third Method (Eqs. 5.3 & 5.5)	61
Figure 5.6	Edge Enhanced Images of Fig. 5.3 After Binarization .....	63
Figure 5.6	Edge Enhanced Images of Fig. 5.4 After Binarization .....	64

Figure 5.8	Edge Enhanced Images of Fig. 5.5 After Binarization .....	65
Figure 5.9	Spot Removing Process .....	66
Figure 5.10	Spot Removed Images of Figure 5.8.....	67
Figure 5.11	Images of Figure 5.8 after the Hole Filling Process .....	68
Figure 5.12	Crack Images after the First Thinning Process .....	70
Figure 5.13	Final Crack Images after the Second Thinning Process .....	71
Figure 5.14	Crack Length Calculation Process .....	72
Figure 5.15	Crack Quantification Control Image.....	74
Figure 5.16	Crack Determined Image of Figure 5.15 .....	75
Figure 5.17	Digital Image Representation of a 15° Straight Line.....	76
Figure 5.18	Digital Image Regions Associated with the Load Conditions .....	78
Figure 6.1	Configuration for the Middle Region Flexural Test .....	79
Figure 6.2	Load-Deflection Curves for NSC Flexural Beam Middle Region Tests	81
Figure 6.3	Final Deflected Shape of the Specimen TNRFm.....	84
Figure 6.4	Retrofitted Bottom Flange Reinforcement for Specimen WNRfM .....	85
Figure 6.5	Flexural Cracking in the TNRFm and WNRfM Specimens at 128 & 123 Kips.....	88
Figure 6.6	Load-Deflection Curves for HSC NSC Flexural Beam Middle Region Tests.....	89
Figure 6.7	Crack Images for Middle Region Flexural Tests on HSC Specimens..	93
Figure 7.1	Configuration for the First End Region Shear Test .....	96
Figure 7.2	Load-Deflection Curves for the NSC Flexural Beam First End Region Tests.....	98
Figure 7.3	Load-Deflection Curves for the NSC Pristine Beam First End Region Tests.....	99
Figure 7.4	Punching and Shear Failure of the Slab of the TNRFf Specimen .....	102
Figure 7.5	Compression Strut Failure of the TNRFf Specimen.....	103
Figure 7.6	Load vs. Strand Slip for the TRNFf Specimen .....	104
Figure 7.7	Strand-Slip Numbering Identification.....	104
Figure 7.8	Load-Deflection Curve for the TNRFf Beam.....	105
Figure 7.9	Typical Strand Slip Crack Pattern.....	106
Figure 7.10	Crack Images for First End Region Tests on NSC Flexural Beams .....	108
Figure 7.11	Crack Images for First End Region Tests on NSC Pristine Beams .....	110
Figure 7.12	Load-Deflection Curves for the HSC Flexural Beam First End Region Tests .....	112
Figure 7.13	Load-Deflection Curves for the HSC Pristine Beam First End Region Tests .....	113
Figure 7.14	Crack Images for First End Region Tests on HSC Flexural Beams .....	116
Figure 7.15	Crack Images for First End Region Tests on HSC Pristine Beams .....	117
Figure 8.1	Configuration for the Second End Region Shear Tests .....	119
Figure 8.2	Load-Deflection Curves for Second End Region Tests on NSC Flexural Specimens .....	122
Figure 8.3	Load-Deflection Curves for Second End Region Tests on NSC Pristine Specimens .....	127

Figure 8.4	Second End Region Shear Failure of the Specimen WNEP .....	128
Figure 8.5	Detail of Second End Region Stirrup Failure in the WNEP Beam.....	128
Figure 8.6	Crack Images for Pristine Beams in NSC Second End Regions Tests.	131
Figure 8.7	Load-Deflection Curves for Second End Region Shear Tests on HSC Flexural Specimens .....	134
Figure 8.8	Shear Failure of the Second End Region Test on Specimen WHEFs...	136
Figure 8.9	Load-Deflection Curves for Second End Shear Region Tests on HSC Pristine Specimens .....	138
Figure 9.1	Configuration for the Intermediate End Region Shear Test .....	141
Figure 9.2	Load-Deflection Curves for Intermediate End Region Shear Tests .....	142
Figure 9.3	Shear Failure of the Specimen WNSPi.....	144
Figure 9.4	Shear Failure of the Specimen TNRPi2.....	144
Figure 9.5	Final Crack Image of TNRPi1 at 319 kips (S3 & S2) .....	145
Figure 9.6	Final Crack Image of TNRPi2 at 318 kips (N2 & N3).....	145
Figure 9.7	Final Crack Image of WNSPi at 317 kips (S3 & S2) .....	146
Figure 9.8	Final Crack Image of WNEPi at 318 kips (N2 & N3).....	146
Figure 9.9	Final Crack Image of TNAPi1 at 319 kips (S3 & S2).....	146
Figure 9.10	Final Crack Image of TNAPi2 at 319 kips (N2 & N3).....	147
Figure 10.1	Fatigue Related Strain Gage Installations.....	153



## LIST OF TABLES

Table 2.1	Test Parameters .....	5
Table 2.2	Beam Capacity, Middle Region Flexural Test with P = 124 kips .....	23
Table 2.3	Beam Capacity, First End Region Shear Test with P = 248 kips .....	27
Table 2.4	Beam Capacity, Second End Region Shear Test with P = 195 kips .....	30
Table 2.5	Beam Capacity, Intermediate End Region Shear Test with P = 86 kip .....	33
Table 3.1	Normal Strength Concrete Specimen Material Properties .....	38
Table 3.2	High Strength Concrete Specimen Material Properties .....	39
Table 4.1	Sample Load and LVDT Displacement Output Data .....	51
Table 5.1	Crack Widths and Lengths for the Control Image of Figure 5.15 .....	76
Table 5.2	Properties of the Cracks of Figure 5.13 .....	77
Table 6.1	Middle Region Flexural Test Load-Deflection Data for Normal Strength Concrete .....	82
Table 6.2	Middle Region Flexural Test Terminal Loads for Normal Strength Concrete .....	83
Table 6.3	Crack Results for Normal Strength Concrete Flexural Tests .....	87
Table 6.4	Load-Deflection Data for the HSC Middle Region Flexural Tests .....	90
Table 6.5	Terminal Loads and Failure Modes for the HSC Middle Region Flexural Tests .....	90
Table 6.6	Crack Results for High Strength Concrete Flexural Tests .....	92
Table 7.1	Load-Deflection Parameters for the NSC First End Region Tests .....	100
Table 7.2	Terminal Loads and Failure Modes for the NSC First End Region Tests .....	101
Table 7.3	Calculated Crack Results for the NSC First End Region Tests .....	109
Table 7.4	Load-Deflection Parameters for the HSC First End Region Tests .....	114
Table 7.5	Terminal Loads and Failure Modes for the HSC First End Region Tests .....	115
Table 7.6	Calculated Crack Results for the HSC First End Region Tests .....	118
Table 8.1	Load-Deflection Data for Second End Region Shear Tests on NSC Specimens .....	123
Table 8.2	Terminal Loads for Second End Region Shear Tests on NSC Specimens .....	124
Table 8.3	Crack Results in the NSC Second End Region Tests of Pristine Specimens .....	132
Table 8.4	Load-Deflection Data for Second End Region Shear Tests on HSC Specimens .....	135
Table 8.5	Terminal Loads for Second End Region Shear Tests on HSC Specimens .....	135
Table 8.6	Crack Results in the High-Strength Concrete Second End Region Shear Tests .....	139
Table 9.1	Load-Deflection Parameters for Intermediate End Region Shear Tests .....	143
Table 9.2	Terminal Loads and Failure Modes for Intermediate End	

	Region Shear Tests .....	143
Table 9.3	Crack Results in NSC Intermediate End Region Shear Tests.....	147
Table 10.1	PSTRS-14 Analyses Parameters .....	151

**APPENDICES**

APPENDIX A – Beam Reinforcement Details ..... A-1

APPENDIX B – Alternate R-Bar Surveys..... B-1

# CHAPTER I

## INTRODUCTION

### 1.1 Background

The use of precast, prestressed concrete I-beams with cast-in-place concrete deck slabs in highway bridge construction in the United States is a common practice. Efficient material utilization and cost effectiveness have led to the popularity of this construction technique and its widespread use. Through the years, its popularity has led to many innovations and improvements in the fabrication and construction process as well as the materials used. One such improvement and innovation is the use of Welded Wire Fabric (WWF) in lieu of traditional reinforcing bars to control tensile and shear stresses in the concrete; therefore, control cracking of the concrete. A large number of traditional reinforcing bars, of various configurations and sizes, must be individually placed and tied throughout the I-beam in addition to the prestressing steel. A large number of these bars are located in each end region of the beam where high tensile and shear stresses are caused by the transfer of forces from the prestressing strands to the concrete and by the applied transverse service loads. Using WWF allows a large number of these bars to be prefabricated into a single unit and set into place at one time, saving time and labor, during the fabrication of the prestressed I-beam, which is a time critical process.

Current Texas Department of Transportation (TxDOT) policy, per the standard Prestressed Concrete I-beam Details (IBA), permits the substitution of, “An equal area of welded wire fabric for Bars R, V, S, or X if approved by the engineer.” The R-bars are bent bars that are placed vertically in the beam at various spacings along the entire length of the beam. These bars are stirrups and are used to help carry the shear forces in the beam. The V-bars are bent bars that are placed in the lower flanges of the I-beam in each end region. They are used to provide confinement to the concrete and to control radial tensile stresses and concrete cracking in the prestress transfer region of the lower flange of the beam. The S-bars are straight vertical bars that are placed in pairs between the R-bars only in each end region of the I-beam. They are used to control tensile stresses and horizontal cracks in the thin web of the I-beam caused by the large prestress force that is being applied primarily to the lower flange of the beam. The X-bars are bent bars that are placed in the upper flange of the I-beam at varying spacings along the entire length of the beam. They are used to provide confinement of the concrete in the upper flange of the beam. The exact locations, sizes, and details of these bars are provided in Chapter 2 and Appendix A of this report.

The R-bar, which provides shear reinforcement, is of primary interest in this research project due to the change in the anchorage mechanism used on the lower end of the R-bar when WWF is used in lieu of the traditional deformed bar. For the R-bar to function properly, its ends must remain fully anchored in the concrete, allowing it to carry an axial load equal to  $A_v$  times  $F_y$ , where  $A_v$  is the area of the bar and  $F_y$  is the tensile yield stress of the material. R-bars made, using the traditional deformed bar and WWF, are both hairpin shaped bent bars with the U-portion of the hairpin extending beyond the top of the precast I-beam. This is done so that the upper portion of the bar can be encased in the cast-in-place deck concrete to

provide adequate horizontal shear capacity at the beam/deck interface so that composite action will occur. Because the upper anchorage detail is identical for both types of R-bars (traditional and WWF), and because the embedded hairpin configuration of the upper detail provides more than adequate anchorage, only the lower anchorage detail of the WWF is of concern.

The standard TxDOT R-bar detail for the traditional deformed bar uses 4-inch long, 90-degree hooks on the lower ends of the R-bar to provide adequate anchorage. The typical anchorage detail used with WWF to date uses a pair of smooth cross-wires, two inches apart, welded to the straight ends of each primary reinforcing wire. The primary wire is typically a deformed wire. The smooth cross-wires are oriented perpendicular to the primary reinforcing wire and are attached to the primary wire using an electrical resistance welding process. The materials and fabrication processes used with WWF, for smooth and deformed wires, are covered by ASTM specifications A82, A185, A496, and A497. To meet the requirements of A497 or A185, the areas of the cross-wires must be at least 40% of the primary wire area. This anchorage detail is specified by the American Concrete Institute (ACI 318, 1999), American Association of State Highway and Transportation Officials (AASHTO, 1996), Prestressed Concrete Institute (PCI, 1985), and Wire Reinforcement Institute (WRI, 1993). Research has shown that the WWF anchorage detail performs satisfactorily as shear reinforcement in T-beams under static, cyclic, and ultimate load conditions (Robertson, 1987; Xuan, 1988; Pincheira, 1989). In addition, the described WWF anchorage detail has been successfully used in other structural applications (Ayyub, 1994; Griezic, 1994; Lin, 1998; Mansur 1986). However, there were some distinctive differences between these applications and the Texas prestressed I-beam details. Therefore, a detailed investigation was conducted using the specific details of the Texas prestressed concrete I-beam along with several modifications under consideration by the research team. The specific details of these modifications and the parameters of this research are provided in Chapter 2. In general, they include various combinations of reinforcing steel configurations, concrete strengths, and steel strengths.

## **1.2 Scope**

This research project consisted of a series of 43 full-scale load tests conducted on 18 test specimens with multiple load tests conducted on each specimen at different locations along its length. The basis of each specimen was a 36-foot long, TxDOT Type “A” prestressed concrete I-beam that was prefabricated by Southwest Prestressed Concrete Company in Amarillo, Texas. Each beam was transported to the Civil Engineering Structural Testing Laboratory at Texas Tech University in Lubbock, Texas, where a 6-foot wide, 8-inch thick, reinforced concrete deck slab was cast-in-place on top of each beam. Once the cast-in-place concrete deck slab reached adequate strength, each composite specimen was placed in the proper position and loaded by means of a one million pound hydraulic ram placed between the test specimen and a reaction load frame that was bolted down to the structural test deck in the laboratory. Both flexural tests and shear tests were conducted on the specimens. During the flexural tests, the specimens were subjected to loads that caused internal moments that exceeded the theoretical ultimate moment capacity of the specimens. The loading was stopped prior to complete flexural failure. This was done to preserve the specimens and allow additional shear tests to be completed on the basically unaffected end regions of the

specimens. During the shear tests, the specimens were loaded to complete failure. Specific details of the load and support configurations for the flexural and shear tests are provided in Chapter 2 of this report.

### **1.3 Objective**

The primary objective of this research project was to determine whether or not the typical WWF anchorage detail could be used successfully in other structural applications performed adequately as shear reinforcement in TxDOT prestressed concrete I-beams. One secondary objective of the project was to study the effects of modifying various geometric details of the reinforcing steel as well as the effect of using higher strength materials, both concrete and steel. This was accomplished by completing a series of full-scale load tests, in both flexure and shear, on specimens fabricated using various combinations of the parameters of interest. For each parameter of interest, a companion test was done on a specimen fabricated using standard TxDOT materials and details so that comparisons could be made. Points of comparison include; load-deflection curves, beam stiffnesses, crack patterns and sizes, and failure modes. Another secondary objective of this research project was to develop and evaluate a Digital Imaging Analysis Technique (DIAT) to quantify and compare crack patterns and sizes between test specimens with comparable parameters. A third secondary objective arose during the execution of this research project. It was to determine whether or not an observed brittle failure mode in several WWF wires near the electrical resistance welds would be a cause for concern about premature fatigue failures in prestressed concrete I-beams. Details about this observed phenomenon are provided in Chapter 10.

## CHAPTER II

### TEST PLAN

#### 2.1 General Approach

The general approach used during this research project was to conduct a parametric study on several variables of interest by conducting 43 full-scale load tests on 18 test specimens. Multiple load tests, in flexure and/or shear, were conducted on each specimen by moving the load and support points along the length of the specimen, thus allowing a more efficient utilization of the project's resources. The variables of interest included five shear reinforcement details, two beam concrete strengths, and two shear reinforcing steel strengths. Specific details about each of the variables used in this research project are provided and discussed in the following sections of this chapter. As a point of comparison for each load test conducted on the various parameters of interest in the project, a series of companion tests were completed on specimens using standard TxDOT materials and details. All of the test specimens were 36-feet long, TxDOT Type A, prestressed concrete I-beams, each with a 6-foot wide, 8-inch thick reinforced concrete cast-in-place deck slab.

#### 2.2 Test Matrix

Table 2.1 contains a summary of the test parameters of interest in this project. All of the beams were cast in pairs with identical parameters in each pair except Beam Pair No. 8. Pair No. 8 had a mix of parameters that were repeated from earlier beam pairs to allow additional tests to be conducted on some of the same parameters but with a modified load / support configuration. Details of the load and support configurations are provided later in this chapter.

**Table 2.1** Test Parameters

<b>Beam Pairs</b>	<b>Shear Steel Detail</b>	<b>Steel Yield * (ksi)</b>	<b>Concrete Strength (ksi)</b>
<b>1</b>	Standard Bar (#4 / #5)** (#4)***	60	5 – 7
<b>2</b>	Matching WWF (D20 / D31)** (D20)***	60	5 – 7
<b>3</b>	Simplified WWF (D26)** (D20)***	60	5 – 7
<b>4</b>	Equal Strength WWF (D20)** (D15)***	80	5 – 7
<b>5</b>	Standard Bar (#4 / #5)** (#4)***	60	10 – 12
<b>6</b>	Simplified WWF (D26)** (D20)***	60	10 – 12
<b>7</b>	Equal Strength WWF (D20)** (D15)***	80	10 – 12
<b>8</b>	Standard Bar (#4 / #5)** (#4)*** (both ends, 1 <sup>st</sup> beam)	60	5 – 7
	Simplified WWF (D26)** (D20)*** (1 <sup>st</sup> end, 2 <sup>nd</sup> beam)	60	
	Equal Strength WWF (D20)** (D15)*** (2 <sup>nd</sup> end, 2 <sup>nd</sup> beam)	80	
<b>9</b>	Alternate R-Bar (#4 / #5)** (#4)***	60	5 – 7

\* Design Values

\*\* R-bar / S-bar sizes in first end region of beam

\*\*\* R-bar size in second end region of beam

The main variable of interest in this research project was the shear reinforcing steel detail. For the traditional design, the R-bar shear steel is shown in Figure 2.1 on the left. In a standard TxDOT beam detail, shown in Figure 2.2, the R-bars are placed at a 4-inch center-to-center (c/c) spacing in the first 38 inches of beam length at each end of the beam. This first 38 inches is referred to as the “first end region” in this report. Also, in a standard TxDOT beam detail, the R-bars are placed at an 8-inch c/c spacing in the next 112 inches along the length of the beam. Any region where the R-bars are at an 8-inch c/c spacing is referred to as the “second end region” in this report. In addition, in a standard TxDOT beam, the R-bars are placed at an 18-inch c/c spacing along the remaining mid-region length of the beam. To help control shear forces in the test specimens and to control the failure location along the length of the specimens, the standard TxDOT 18-inch c/c spacing was not used in the middle region of the specimens tested in this project. A 4-inch c/c R-bar spacing was used in all of the first end regions of the specimens and an 8-inch c/c R-bar spacing was used along the remainder of each specimen’s length.



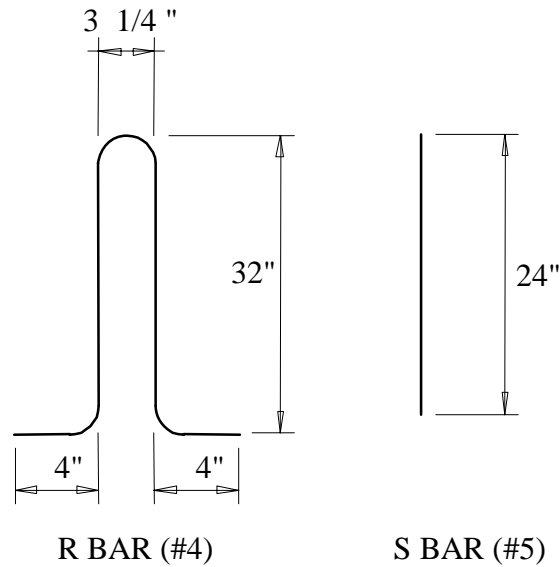


**Figure 2.1** Traditional Reinforcing Steel R-bar and S-bar in a TxDOT Type A I-beam

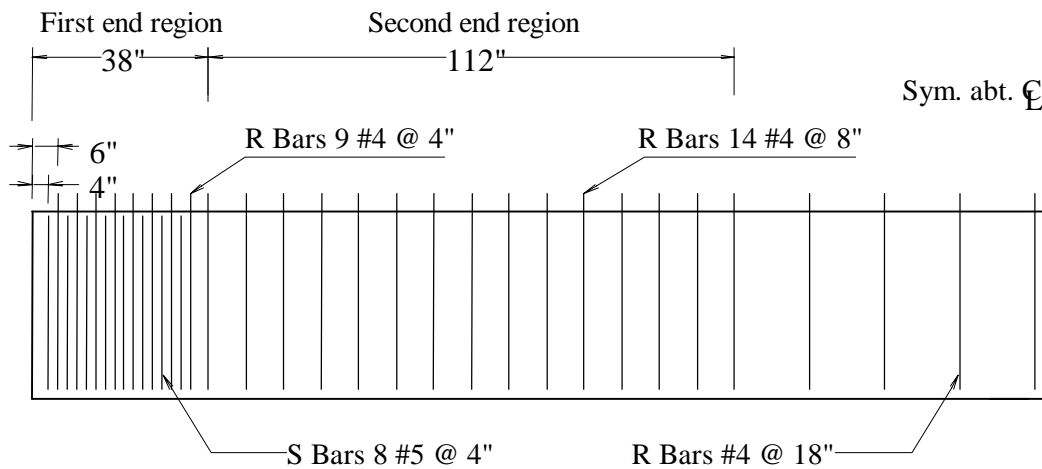


**Figure 2.2** Side View Detail of TxDOT Type A I-beam

The straight S-bars are also placed at a 4-inch *c/c* spacing in the first end region of the beam, as shown in Figure 2.2, and they are longitudinally centered between the 4-inch *c/c* spaced R-bars, providing alternating R-bars and S-bars at 2-inch *c/c* spacings in the first end regions. This combination of R-bars and S-bars in the first end region significantly impacted

the WWF detail used in the first end region of this research project. Even though the S-bars and the purpose that they serve in the beam were not of primary interest in this project, they were a part of the WWF cage in the first end region which caused them to become important in this project as several WWF shear reinforcement details located in the first end region were investigated.

The parameters used in Beam Pairs No. 1 and No. 5 are shown in Table 2.1. They were fabricated using Grade 60 standard deformed reinforcing steel bars and had concrete strengths in the 5,000 to 7,000 psi and 10,000 to 12,000 psi ranges, respectively. Concrete in the 5,000 to 7,000 psi range is referred to as “normal strength concrete” (NSC) while concrete in the 10,000 to 12,000 psi range is referred to as “high strength concrete” (HSC). The R-bars in the first and second end regions were all made from #4 bars while the S-bars, which were only located in the first end region, were made from #5 bars. The parameters used to fabricate the first beam of Beam Pair No. 8 matched exactly those used in Beam Pair No. 1. The decision to deviate from using matched pairs of beams was made during the project after reviewing some of the earlier test data. The need to re-test previously tested parameters using a modified load configuration brought about the decision to deviate from the matching beam pair scenario. The test data from the test specimens fabricated using TxDOT’s standard reinforcing details and standard deformed reinforcing bars were the control data and were used as the standard by which to compare the results from the other test specimens with the various parameters of interest.

The parameters used in Beam Pair No. 2 matched the parameters used in Beam Pair No. 1 except that WWF was substituted for standard deformed bars. This reinforcing detail is referred to as “Matching WWF” and is shown in Figures 2.3 and 2.4. Common terminology to call out the sizes of the reinforcing steel elements was used. For the standard bar, a #4 bar has a diameter of 4/8 of an inch and a cross-sectional area of 0.20 square inches. The equivalent size of WWF is called out as a D20, which indicates that the wire contains a deformed surface pattern and has a cross-sectional area of 0.20 square inches. Similarly, the #5 bar has a diameter of 5/8 of an inch and a cross-sectional area of 0.31 square inches and thus, an equivalent size of WWF is D31. A smooth wire with a cross-sectional area of 0.31 square inches is called out as W31. Test specimens using the Matching WWF reinforcing detail were only fabricated using NSC.

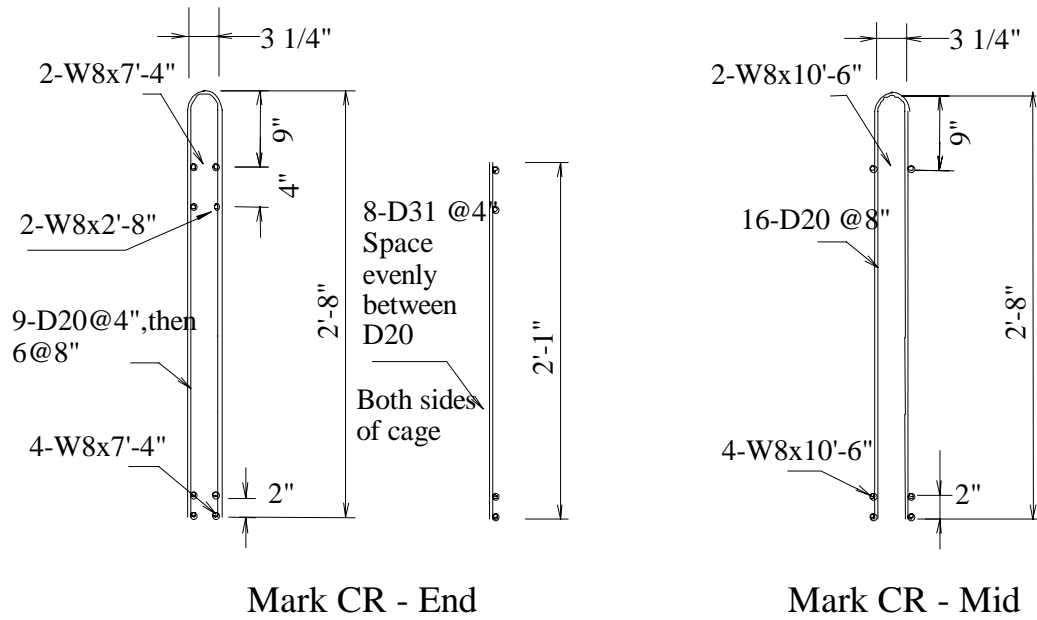


**Figure 2.3** Matching WWF Detail

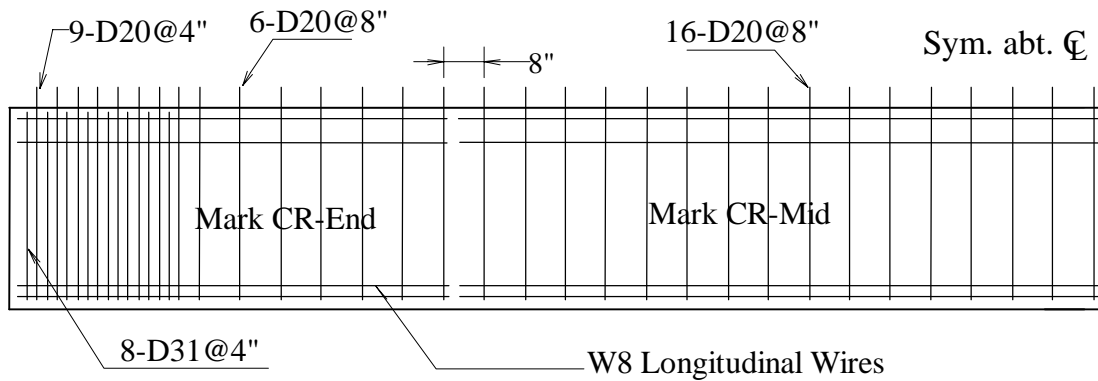


**Figure 2.4** Side View of Matching WWF Detail

A “Simplified WWF” reinforcing detail was used to fabricate all of the beams in Beam Pair No. 3 and Beam Pair No. 6 as well as one end of the second beam of Beam Pair No. 8. The Simplified WWF detail is shown in Figures 2.5 and 2.6. The Simplified WWF detail impacts only the reinforcing detail in the first end region. In an effort to economize the fabrication of the WWF cage, it was determined to combine the R-bars and S-bars in the first

end region into a single size wire with an equal area of steel. Thus D26 wires were placed at 2-inch c/c spacings in lieu of alternating D20 and D31 wires every 2 inches. The Simplified WWF reinforcing detail steel used a 60 Grade design wire value. However, it should be noted that the wire actually comes as a 70 Grade wire even if 60 Grade is specified. The basic wire material starts as a 60 Grade but when the first cold drawing occurs to make the wire the proper size, the wire material properties increase to a 70 Grade. Test specimens fabricated using the Simplified WWF detail were made using NSC and HSC as shown in Table 2.1.

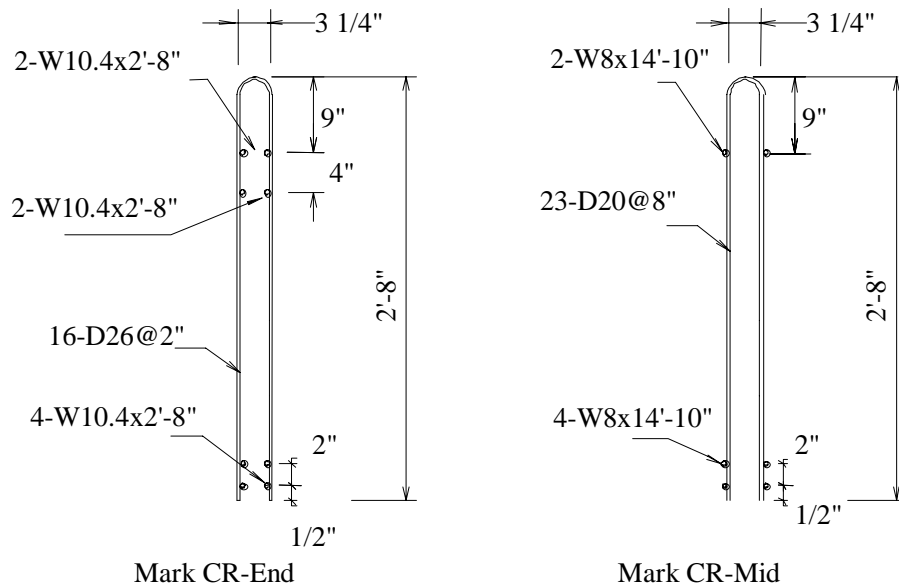


**Figure 2.5** Simplified WWF Detail

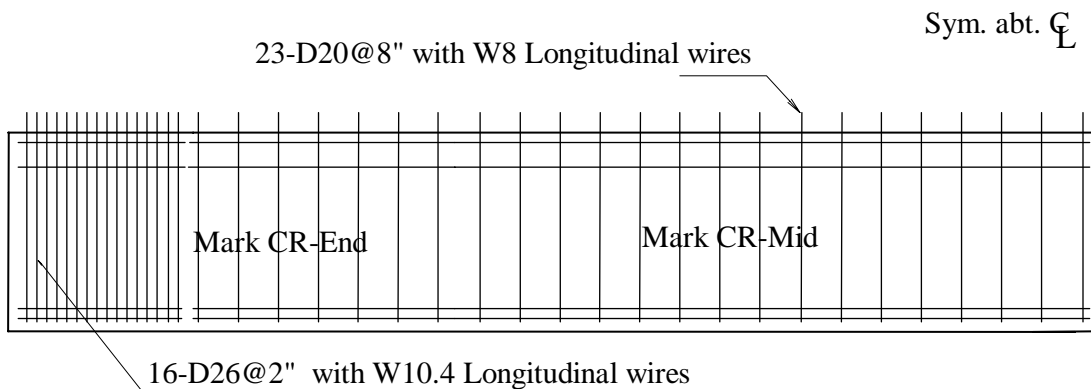


**Figure 2.6** Side View of Simplified WWF Detail

An “Equivalent Strength WWF” reinforcing detail was used to fabricate Beam Pair No. 4 and Beam Pair No. 7 as well as one end of the second beam of Beam Pair No. 8. This detail is shown in Figures 2.7 and 2.8. The Equivalent Strength WWF detail was developed to utilize the more common higher yield strength of the wire. Even though the wire begins as a Grade 60 wire, it is commonly cold drawn twice during sizing operations, which increases it to a Grade 80 wire. However, the current AASHTO codes, Standard and LRFD, restrict shear reinforcement design to a maximum material value of 60 ksi. By utilizing the wire’s common higher grade of 80 ksi, less material would have to be used to develop the same ultimate force in each wire. The simplified WWF detail concept (using only one size of wire in the first end region) described above was used in the Equivalent Strength WWF detail along with the higher Grade 80 wire. In the first end region, a D20 wire was used in lieu of a D26 wire, and in the second end region, a D15 wire was used in lieu of a D20 wire. Equivalent Strength WWF specimens were fabricated using both NSC and HSC as shown in Table 2.1. Caution must be used when substituting the higher strength wire due to increased crack sizes. Since less area of wire is used to develop the same force, higher levels of ultimate stress will occur in the smaller diameter wire and thus larger strains and larger cracks will occur in the concrete. However, since prestressed concrete beams remain uncracked at service loads, this is not anticipated to be an issue.

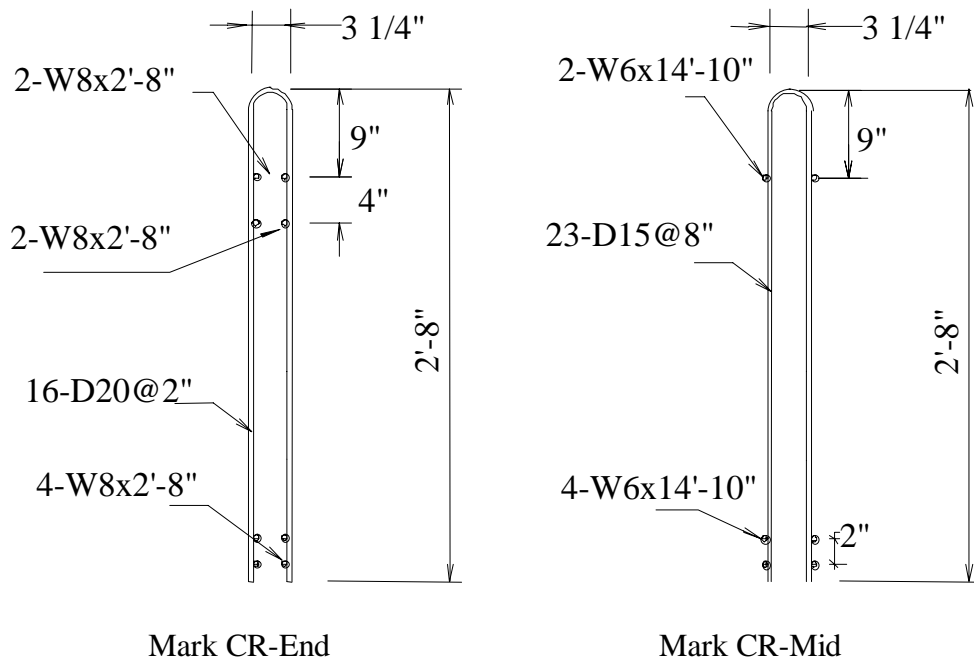


**Figure 2.7** Equivalent Strength WWF Detail

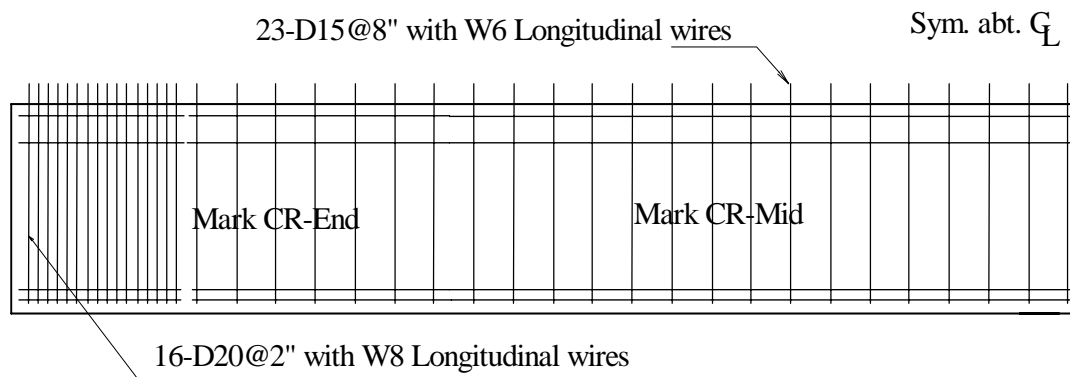


**Figure 2.8** Side View of Equivalent Strength WWF Detail

An “Alternate R-bar” reinforcing detail, shown in Figure 2.9, was used to fabricate Beam Pair No. 9. This detail used standard 60 Grade deformed reinforcing steel bars of the same size and distribution as used in the standard TxDOT detail. The standard TxDOT R-bar is a 2-dimensional bent hairpin bar with a 4-inch long, 90-degree hook on the lower end of each vertical leg. These hooks are perpendicular to the axis of the beam and are placed directly below the bottom row of prestressing strands. If the standard R-bar is not fabricated properly, the two 90-degree hooks are not in the same horizontal plane and concrete cover problems occur on the bottom of the beam. The 90-degree hook on the shorter vertical leg is placed against the bottom row of prestressing strands and forces the 90-degree hook on the longer leg to be nearer the bottom surface of the beam, typically violating concrete cover requirements. To resolve this problem, an Alternate R-bar detail was developed and tested. Many possible variations were considered and input was solicited from 5 Texas prestressed beam fabricators, 7 key TxDOT personnel, and 19 other state DOT personnel via 2 similar but slightly different surveys. Out of the surveys sent out, the number of responses received back were 4 from Texas fabricators, 4 from TxDOT personnel, and 12 from other state DOTs. Copies of these surveys and a summary of their results are provided in Appendix B. The Alternate R-bar detail that was selected for use in this project was a 3-dimensional bent hairpin bar with a 3.5-inch long, 90-degree hook on the lower end of each vertical leg. These 90-degree hooks were rotated 90-degrees about the axes of the vertical legs so that they were parallel to the axis of the beam in lieu of perpendicular to the beam. Since the R-bars are spaced at 4-inch c/c in the first end region, the length of the hooks were shortened to 3.5 inches to alleviate interference with the next R-bar located 4 inches away. Beams notated as Beam Pair No. 9 were fabricated with NSC.

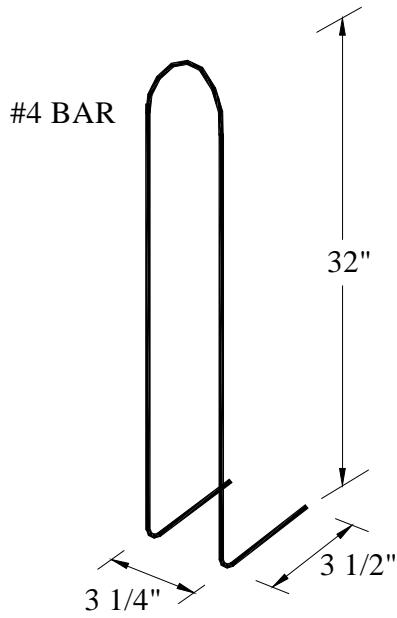


**Figure 2.9** Alternate R-bar Detail

### 2.3 Beam Details

TxDOT uses 6 standard sizes of I-beams that vary dimensionally and range in height from 28 inches to 72 inches. These 6 standard sizes carry the indicators of Type A, Type B, Type C, Type IV, Type 54, and Type 72. The smallest of these I-beams, Type A, was selected for use in this project. All of the beams used in this project were 36-feet long. The cross-sectional shape and dimensions for the Type A I-beam are shown in Figure 2.10.

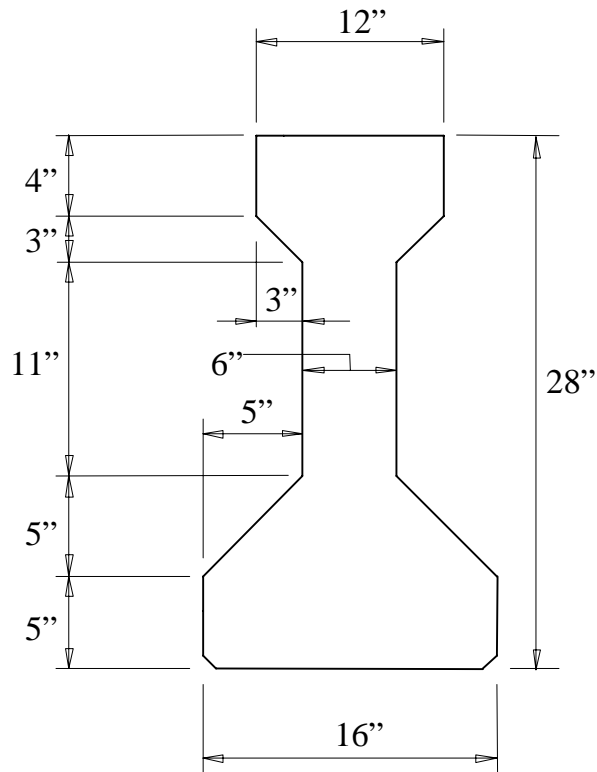


**Figure 2.10** Type A I-beam Cross-section and Dimensions

Two prestressing strand patterns were selected for use in this project, one for the NSC beams and another for the HSC beams. A 2-inch grid spacing was used throughout this project. A 10-strand pattern, shown in Figure 2.11, was selected for the NSC beams. Six of the strands were held straight along the entire length of the beam while 4 of the strands were harped with the hold-down points being located two feet from the beams' mid-length point. A 14-strand pattern, shown in Figure 2.12, was selected for the HSC beams. Eight of these strands were held straight along the entire length of the beam while 6 of the strands were harped, again with the hold-down points located 2-feet from the beams' mid-length point. All of the strands used in this project was 0.5-inch diameter, 270-ksi, low relaxation strand that was pretensioned to 75% of its guaranteed ultimate tensile strength or 31 kips per strand. Complete beam details that include all the reinforcing details are provided in Appendix A. All of the beams used in this research project were fabricate by Southwest Prestressed Concrete Company in Amarillo, Texas.



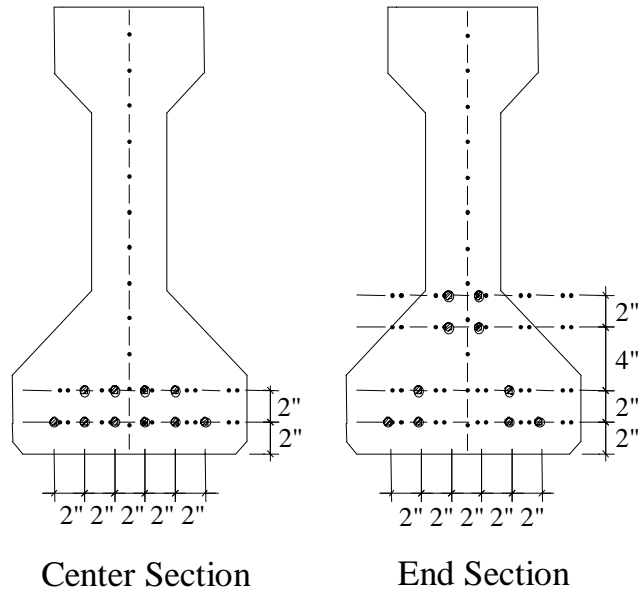


**Figure 2.11** Strand Pattern for Normal Strength Concrete Beams

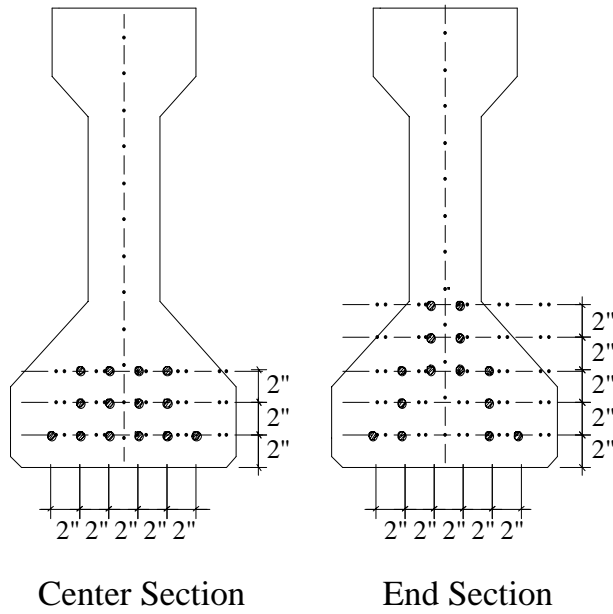


**Figure 2.12** Strand Pattern for High Strength Concrete Beams

## 2.4 Cast-in-Place Concrete Deck Slab

Once the beams reached sufficient strength, they were shipped in pairs to the Civil Engineering Structural Test Laboratory at Texas Tech University in Lubbock, Texas. When they reached the laboratory, they were set in position on the structural test deck and a cast-in-place concrete deck slab was cast on top of each beam to complete the test specimen. The purpose of the deck slab was to simulate, as well as possible, the in-situ response of a composite bridge beam and deck slab. A 6-foot wide, 8-inch thick, concrete slab was used and reinforced with standard TxDOT details as shown in Figure 2.13. The slab concrete strength was specified as 5,000 psi, and the reinforcing steel was specified as Grade 60 deformed bar.

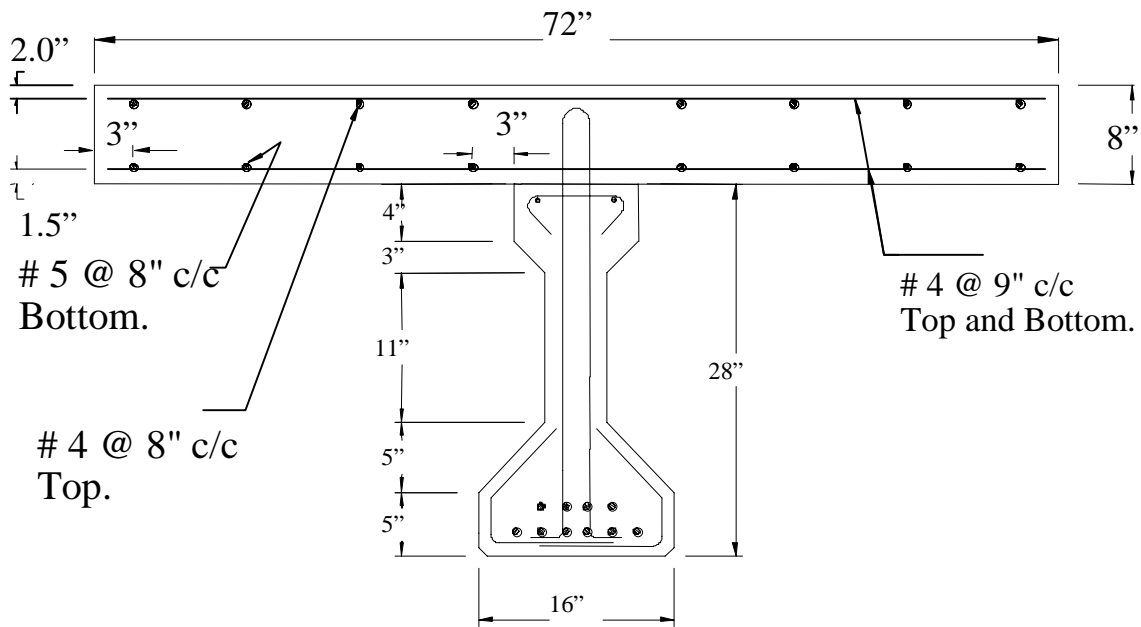


**Figure 2.13** Cast-in-Place Concrete Deck Slab Geometry and Reinforcement

## 2.5 Test Arrangements

In order to devise tests in which particular types of failure could be evaluated, extensive calculations were carried out on the specimen configuration of Figure 2.13. Specimens with traditional shear reinforcement and with welded wire fabric shear reinforcement were first tested to verify and compare their flexural behavior. For every pair of beams listed in Table 2.1, except Beam Pairs No. 8 and No. 9, one specimen was first tested in flexure and loaded slightly beyond its theoretical moment capacity but to less than its failure moment. These tests are referred to as flexural tests, and they occurred with loads symmetrically applied at midspan. Of the two beams in each pair, this beam is identified as the “Flexural Specimen.” In addition, the flexural specimen always had two shear tests conducted at its ends, one on each end. This resulted in 3 load tests per flexural specimen.

The second beam in each pair was tested twice and only in shear with one shear test on each end of the specimen. This specimen is referenced to as the “Pristine Specimen” due to the fact that it did not have the effects of previous flexural cracks as did the corresponding flexural specimen. Thus, a total of five tests were performed on every pair of beams except for Beam Pairs No. 8 and No. 9. The repetition of the shear tests at the two ends of each pair of beams gave a degree of repeatability. Although the stiffness was expected to be lower in each shear test on a flexural specimen due to its prior cracking, the failure loads and failure modes in shear were expected to be consistent for the two specimens of each pair.

One key point in designing the tests was to choose loading locations that would provide accurate measures of the shear strengths in the first end regions and in the second end regions of the beams. Another challenge in the design of the test program involved keeping as many parameters as possible constant while one parameter was varied. Thus, for instance, if the same load locations could produce a shear failure in a normal-strength beam and in a beam with 10,000-psi concrete, then the differences in behavior could be attributed exclusively to the concrete strength.

### 2.5.1 Flexural Tests

One specimen of every pair, except pairs No. 8 and No. 9, was tested for flexural behavior by supporting it at its ends and applying two symmetrically centered loads as shown in Figure 2.14. This test was conducted to demonstrate the type of structural performance for which such a prestressed bridge girder is primarily designed; that is, sized and reinforced to prevent flexural failure. It may be noted that the assumed locations of the end supports were 9.5 inches from the ends of the girder. This assumption was based on the use of an 11-inch wide elastomeric bearing pad and the assumption of a triangular reaction stress pattern on the inside 6 inches of the support pad, as shown in Figure 2.15. The two equal loads were three feet apart symmetrically placed about the midpoint of the specimen. The two applied loads were only allowed to cause an internal moment that slightly exceeded the theoretical ultimate moment capacity of the specimen but that was less than its actual failure moment. The specimen was not completely failed in flexure. This approach allowed later testing of each end of the flexural specimen in shear.

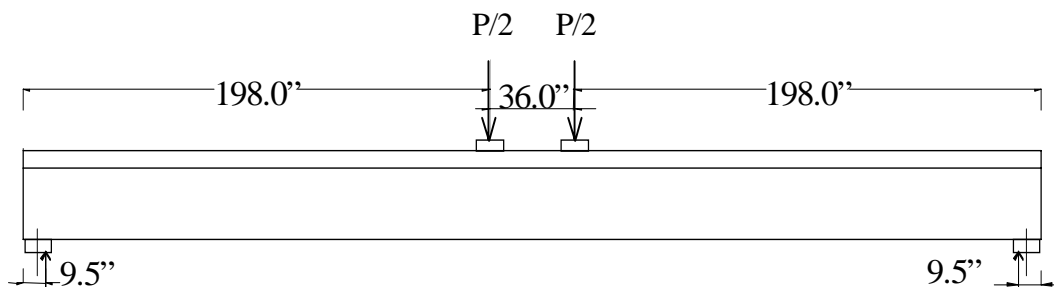


**Figure 2.14** Configuration for the Middle Region Flexural Test

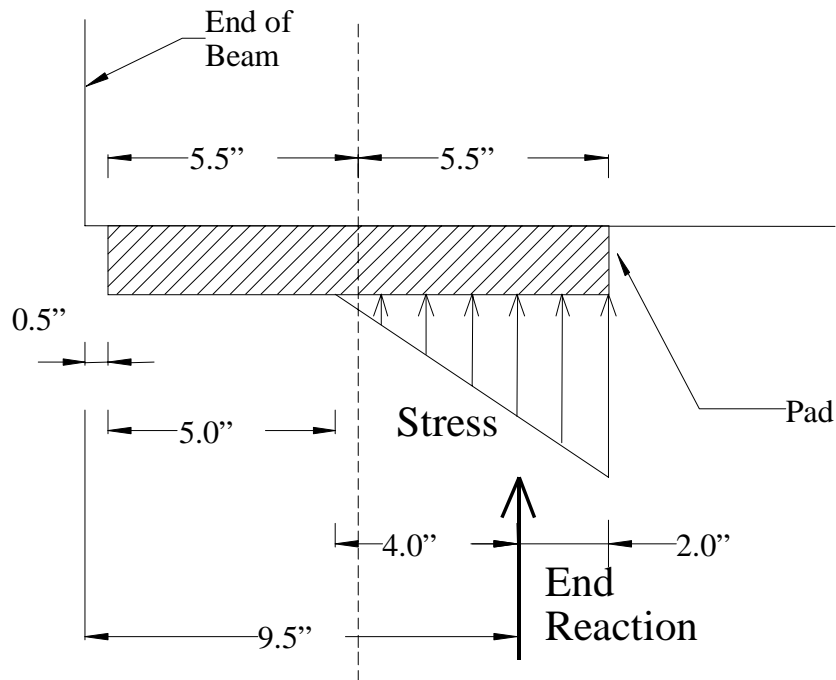


**Figure 2.15** Assumed Reaction Stress Distribution

### 2.5.2 First End Region Shear Tests

The first end region shear test was one of the three load conditions used to specifically study the shear behavior of the WWF reinforcement, and it is illustrated in Figure 2.16. It had two unequal loads that were three feet apart placed near the right end of the beam. Here the applied load nearest the end of the specimen was only 38 inches from the end, which was the location of the transition point between the first and second end regions. The three-fourths/one-fourth load ratio for “P” shown in Figure 2.16 was used to provide an approximately constant moment region between the load points during the second and intermediate end region shear tests. This ratio was maintained during the first end region shear tests for consistency. This choice was important in limiting the peak moment in the second and intermediate end region shear tests so that a premature flexural failure could be avoided if possible.

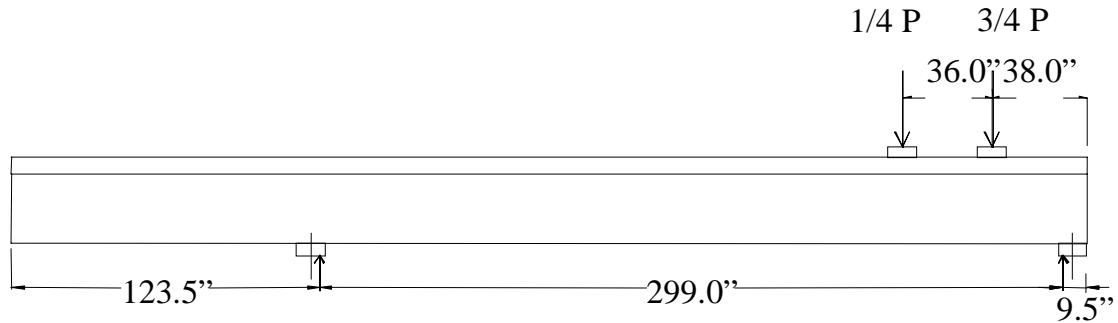


**Figure 2.16** Configuration for the First End Region Shear Test

A detailed view of the load positions and shear reinforcement for the first end region test is shown in Figure 2.17. This load arrangement should have caused a shear failure in the first end region if the added S-bars did not contribute to the shear strength, as assumed in the calculations. A diagonal compression strut effect could also develop between the pad support and the first applied load. It should be noted that the placement of the left support ten feet from the left end in Figure 2.16 had essentially no effect on the right end shear test behavior. At the shear failure load, the maximum moment was the same no matter where the left-hand support was placed if the load positions were the same and the dead weight of the beam was neglected. The chosen location of the left-hand support assured that a pristine segment of the left end of the beam was not affected by the loading of the right end except for dead weight effects. The 10-foot long segment cantilevered over the left-hand support was the longest possible segment without causing negative moment problems in the left end of the specimen.

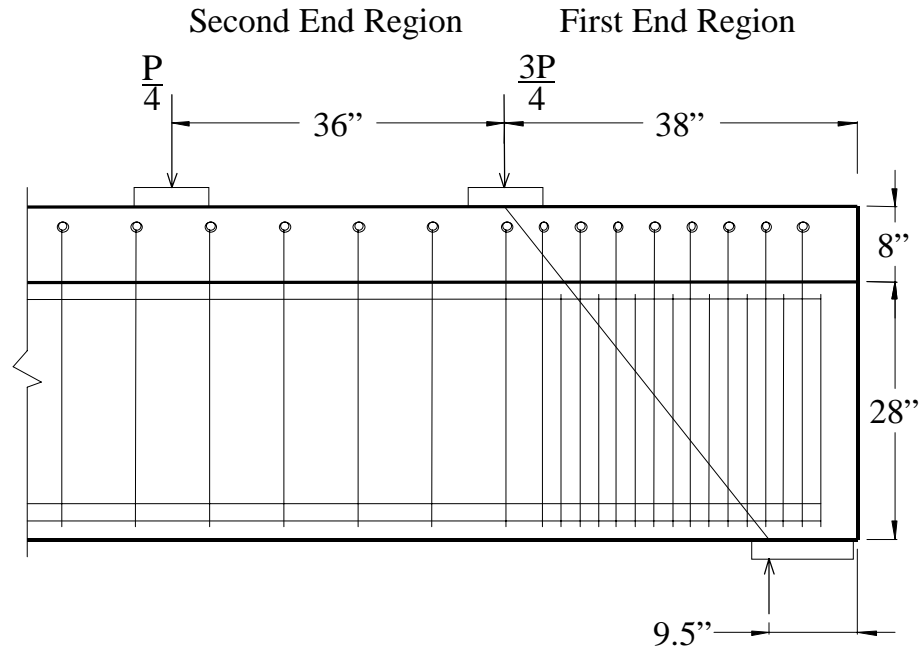


**Figure 2.17** Expected Cracking Behavior in the First End Region Shear Test

### 2.5.3 Second End Region Shear Tests

The second end region shear test was another of the three load conditions used to specifically study the shear behavior of the WWF reinforcement, and it is illustrated in Figure 2.18. It had two unequal loads three feet apart placed near the left end of the specimen. Also, the support for the right end of the beam was not at the very end of the specimen but about ten feet from its right end. This was done to remove the right end of the beam from the load path since the right end of the beam was previously tested to failure during the first end region shear test, which was always conducted prior to the second end region shear test.

The purpose of this set-up was to test the shear cracking and shear strength of the “second end region” on the left end of the specimen. The placement of the loads was carefully selected to develop a shear failure in the second end region without too much risk of a flexural (rather than shear) failure and without having any diagonal shear cracks that would develop in the second end region end up at their lower left extremity in the first end region.

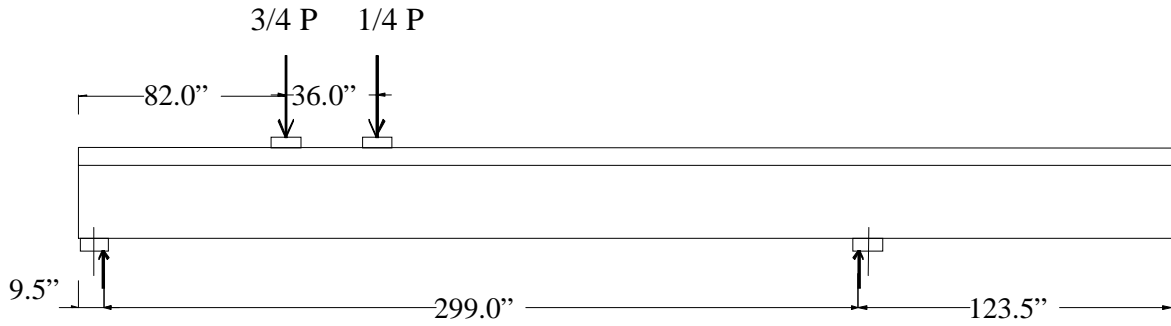


**Figure 2.18** Configuration for the Second End Region Shear Test

The dashed inclined line in Figure 2.19 illustrates how the cracking was expected to appear in relation to the end support, the two applied loads, and the shear reinforcement in the second end region test. The load nearest the end was again made to carry three-quarters of the total applied load  $P$ , so as to produce an approximately constant moment region between the loads. With this configuration, the theoretical moment capacity was at least 19 percent larger than the applied moment throughout the length of the beam. This 19 percent margin of safety against a moment failure instead of a shear failure could not have been maintained if the loads had been moved farther to the right. On the other hand, it was desirable to place the loads farther to the right to make the expected 45-degree shear cracks in the second end region reach the bottom of the beam before intersecting any of the vertical bars in the first end region. As shown in Figure 2.19, with the larger applied load 82 inches from the end of the beam, a 45-degree crack starting at that load would reach the bottom of the beam before reaching the second R-bar of the second end region. Thus, the effect of such a crack on the anchorage of that bar, as might occur in a real beam in service, would be fully tested.

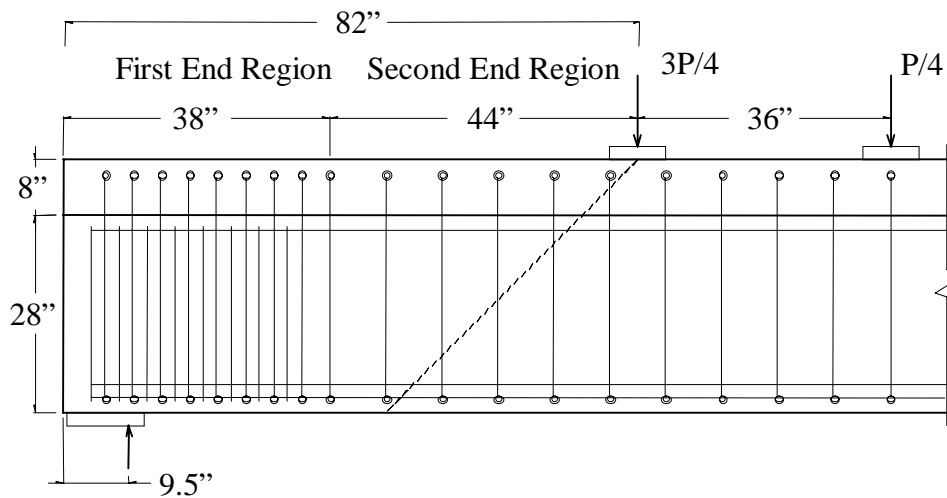


**Figure 2.19** Expected Cracking Behavior for the Second End Region Shear Test

The configuration of Figure 2.19 made the failure truly representative of the shear strength of the second end region, including the anchorage of the R-bars in that region. However, the second end region shear test configuration shown in Figure 2.18 and Figure 2.19 was not maintained for all of the second end region tests. The first test with this configuration conducted on the flexural specimen of Beam Pair No.1 failed in flexure rather than shear in spite of the 19 percent margin of safety predicted by the AASHTO equations. Accordingly, the loads were moved so that the closest one was only 74 inches from end of the specimen in the next second end region shear test, which was conducted on the flexural specimen of Beam Pair No. 2. When it again failed in flexure, despite a 26 percent margin of safety against premature flexure failure, the loads were again moved so that the closest one was only 66 inches from the end of the specimen for all the remaining second end region shear tests. This position was the closest that could be used without having a 45-degree shear crack, coming down from the 3/4 P load point, intersect more than two R-bars in the first end region. This final position gave a margin of safety against premature flexural failure of 40 percent.

#### 2.5.4 Intermediate End Region Shear Tests

The intermediate end region shear test was the last of the three load conditions used to specifically study the shear behavior of the WWF reinforcement, and it is illustrated in Figure 2.20. Three of the last four beams of this study were tested using this modified second end region test. It involved shifting the position of the left support as well as the load points. It provided an alternative to the second end region type of test by moving the left support to the inner edge of the first end region in order to reduce the bending moment in the second end region. Reducing the applied bending moment in this way greatly increased the probability of getting a shear failure instead of a flexural failure where there were only R-bars at an 8-inch spacing. The purpose of this set-up was to fail the specimen in shear in the second end region and observe the relative behavior of the WWF and the traditional shear reinforcement. Figure 2.21 shows a detail of the left support and how the expected 45-degree shear cracking would appear in relation to the end support, the two applied loads, and the shear reinforcement in the first and second end regions.

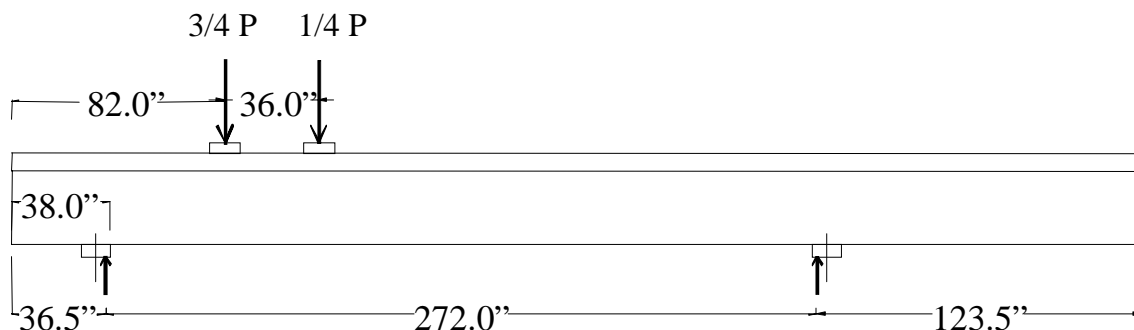


**Figure 2.20** Configuration for the Intermediate End Region Shear Test



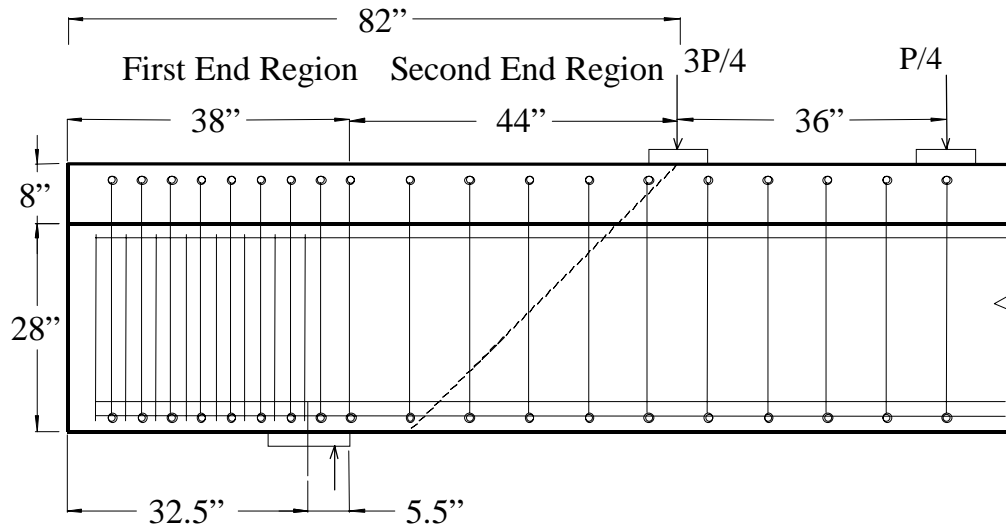


**Figure 2.21** Expected Cracking Behavior for the Intermediate End Region Shear Test

## 2.6 Calculations for Load and Support Placement

Detailed calculations were completed for each of the specified load tests in an effort to insure that the desired failure mode would control and to determine the total applied load that would cause internal forces to reach the member's theoretical ultimate values. To do this, the total applied load required to cause theoretical failure for a specific region was calculated. Then, this total applied load was used to plot the corresponding shear and moment diagrams for the given load and support geometry so that factors of safety against unwanted failure modes could be determined along the entire length of the beam. Specific details and calculations are provided in the following sections for each load test described in the previous section. The theoretical capacities of the specimens were obtained using AASHTO Standard Specifications for Highway Bridges, (AASHTO, 1996).

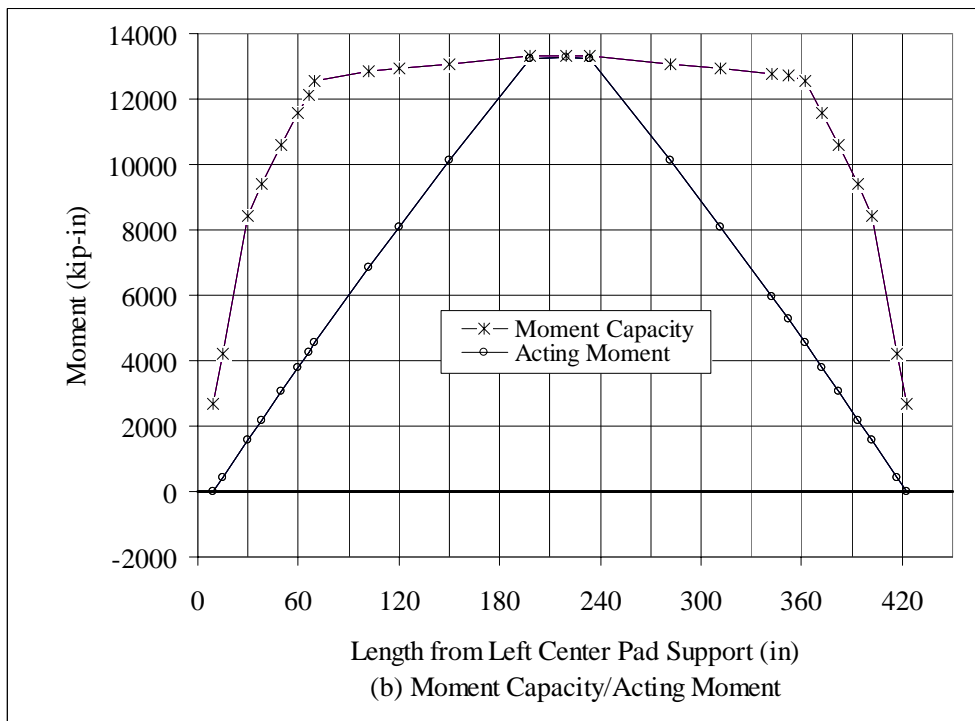
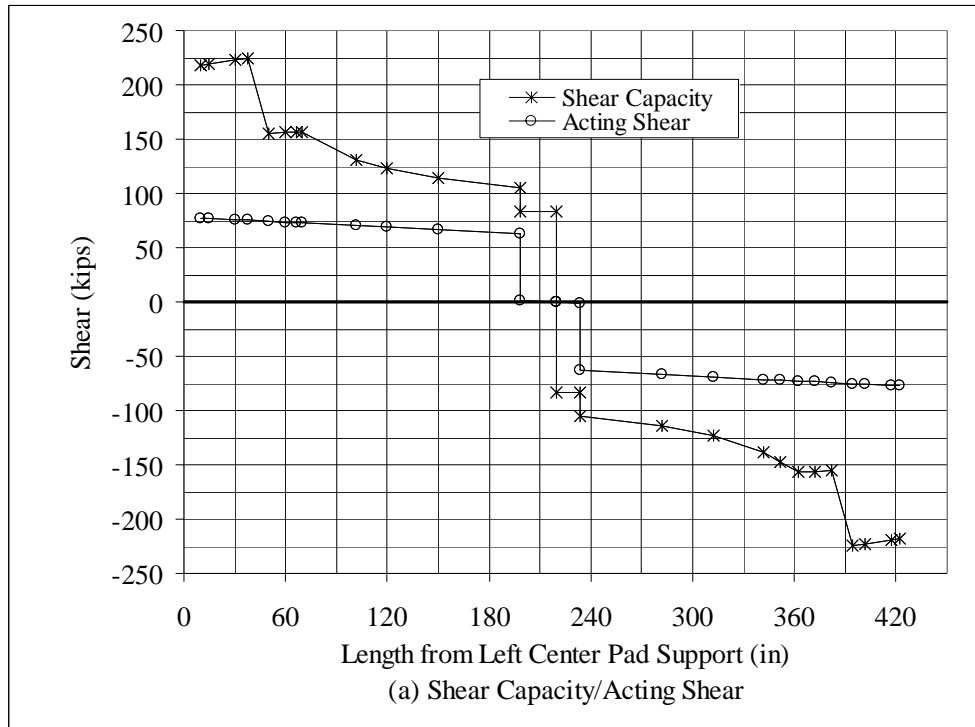
### 2.6.1 Capacities of Specimens in Middle Region Tests

Table 2.2 summarizes the results obtained considering the setup of supports and loads depicted in Figure 2.14 for the middle region flexural tests. Calculations were made at several sections along the length of each beam, as represented by the distance "x" from the left end. Special section positions were considered such as the transition between the first and second end regions as well as at the applied loads. The material properties were for traditional rebar with a normal concrete strength in the beam of 6,000 psi. The slab concrete strength for this table was 5,000 psi. The total applied load, which should have theoretically produced flexural failure, was  $P = 124$  kips. This total load was imposed on the middle region flexural test geometry, and the resulting internal shear and moment values were determined along with the specimen's shear and moment capacities at common points. Only one-half of the flexural beam was considered due to symmetry. The last two columns in Table 2.2 show the ratios between the resisting and applied shear forces and bending moments for a flexural test. These values are plotted in Figure 2.22.

**Table 2.2** Beam Capacity, Middle Region Flexural Test with P = 124 kips

<b>x</b> <b>inches</b>	<b>V<sub>t</sub></b> <b>kips</b>	<b>M<sub>t</sub></b> <b>kip-in</b>	<b>V<sub>ci</sub></b> <b>kips</b>	<b>V<sub>cw</sub></b> <b>kips</b>	<b>V<sub>c</sub></b> <b>kips</b>	<b>V<sub>s</sub></b> <b>kips</b>	<b>V<sub>n</sub></b> <b>kips</b>	<b>M<sub>n</sub></b> <b>kip-in</b>	<b>V<sub>n</sub>/V<sub>t</sub></b>	<b>M<sub>n</sub>/M<sub>t</sub></b>
9.5	77	0	511	81	81	138	218	2,676	2.82	---
15	77	424	511	82	82	138	220	4,224	2.86	9.97
30	76	1,569	238	84	84	139	223	8,442	2.94	5.38
38	75	2,172	178	84	84	140	224	9,404	2.98	4.33
50	74	3,069	128	85	85	70	155	10,575	2.09	3.45
60	74	3,808	104	85	85	71	156	11,557	2.12	3.04
66	73	4,248	93	86	86	71	157	12,149	2.14	2.86
70	73	4,540	88	86	86	71	157	12,544	2.15	2.76
102	70	6,831	59	87	59	72	131	12,835	1.86	1.878
120	69	8,087	50	88	50	73	123	12,928	1.78	1.60
150	67	10,126	40	89	40	74	114	13,083	1.70	1.29
198	63	13,251	29	88	29	76	105	13,300	1.65	1.00
220	0	13,262	7	88	7	76	83	13,300	---	1.00

$x$	Distance from the left end of the beam to the section.
$V_t$	Total shear force due to the self weight and applied loads.
$M_t$	Total bending moment due to the self weight and applied loads.
$V_{ci}$	Shear strength provided by concrete when diagonal cracking results from combined shear and moment.
$V_{cw}$	Shear strength provided by concrete when diagonal cracking results from excessive principal tensile stress in the web.
$V_c$	Nominal shear strength provided by the concrete.
$V_s$	Nominal shear strength provided by the shear reinforcement.
$V_n$	Total nominal shear strength of the section.
$M_n$	Total nominal moment strength of the section.



**Figure 2.22** Applied and Resisting Shears and Moments: Flexural Test

Part (b) of Figure 2.22 shows that the moment capacity is less near each end due to the reduced strand effectiveness in the transfer and flexural bond regions of the development length. Still, there is a sizable factor of safety against moment failure everywhere except

near the center. Similarly, Part (a) of Figure 2.22 shows that there is a sizable factor of safety against shear failure everywhere in the beam, even though the shear capacity varies quite a bit throughout the length.

### 2.6.2 Capacities of Specimens in the First End Region Shear Tests

In the same way, Table 2.3 presents the shear and flexural capacities of the first end region shear test depicted in Figure 2.16. The total load,  $P$ , which would develop the theoretical shear failure in the first end region, was 248 kips. This resisting shear was calculated using AASHTO formulas and assuming the S-bars not to be effective. The resisting shear varied with a number of parameters, including the shear reinforcement, the applied shear, and the applied moment. Thus, the shear resistances in the left- and right-end regions were not the same even though they had the same vertical reinforcement since the applied shears were not the same. Still, there were instantaneous changes in the shear resistance where the vertical reinforcement changed from a 4-inch spacing in the first end region to an 8-inch spacing in the second end region. Table 2.3 shows only values to a point a little beyond the critical region of the beam and does not show all of the values necessary to plot Figure 2.23.

Figure 2.23 shows the plots of the applied shears and moments in relation to the corresponding capacities for the first end region shear test. The moment diagram in Part (b) of Figure 2.23 shows that the peak applied moment in this test was less than 8,000 kip-inches with the nominal theoretical moment capacity at that same point more than 12,000 kip-inches. As can be seen in Table 2.3 and Figure 2.23, there was a large margin of safety against moment failure prior to shear failure throughout the length of the specimen. Also, Part (a) of Figure 2.23 and Table 2.3 show that the internal shear forces and the theoretical shear capacities in the first end region of the beam (the first 38 inches) were nearly equal to each other where the shear failure was anticipated. In addition, they show large factors of safety against shear failure in the remaining portions of the beam. While the capability to fail the first end region appears to be feasible if the shear contribution of the S-bars is neglected, it is not clear if the full shear capacity can be attained by testing if the S-bars are effective, as is expected in the WWF designs. The difference between the standard rebar case and the WWF case is due to the fact that in the WWF design the S-bars are welded to both top and bottom longitudinal wires, along with the R-bars, thus giving them sufficient anchorage to be effective in shear. Since the No. 5 S bars have approximately 50 percent more area than the R-bars, including them significantly increases the shear capacity of the first end region. Therefore, it was expected that for the WWF specimens, the test of the first end region in shear would indicate a greater shear capacity than for the standard design. This was assuming that bond slip between the strands and the concrete beam would not occur, which was very possible since the first load fell well within the development length of the strands.

**Table 2.3** Beam Capacity, First End Region Shear Test with P = 248 kips

<b>x</b> <b>inches</b>	<b>V<sub>t</sub></b> <b>kips</b>	<b>M<sub>t</sub></b> <b>kip-in</b>	<b>V<sub>ci</sub></b> <b>kips</b>	<b>V<sub>ew</sub></b> <b>kips</b>	<b>V<sub>c</sub></b> <b>kips</b>	<b>V<sub>s</sub></b> <b>kips</b>	<b>V<sub>n</sub></b> <b>kips</b>	<b>M<sub>n</sub></b> <b>kip-in</b>	<b>V<sub>n</sub>/V<sub>t</sub></b>	<b>M<sub>n</sub>/M<sub>t</sub></b>
9.5	226	0	511	81	81	138	218	2,676	0.97	
15	226	1,242	511	82	82	138	220	4,224	0.97	3.40
30	225	4,619	238	84	84	139	223	8,442	0.99	1.83
38	224	6,413	178	84	84	140	224	9,404	1.00	1.47
50	37	6,863	35	85	35	70	105	10,575	2.83	1.54
60	36	7,230	33	85	33	71	104	11,557	2.85	1.60
74	35	7,732	31	86	31	71	102	12,691	2.88	1.64
120	-30	6,425	32	88	32	73	-105	12,691	3.50	1.64
150	-32	5,489	38	89	38	74	-112	12,928	3.47	2.01
172	-34	4,760	46	90	46	75	-120	13,083	3.55	2.38
194	-36	3,995	56	88	56	76	-131	13,197	3.68	2.77
216	-37	3,194	69	88	69	76	-144	13,300	3.88	3.33

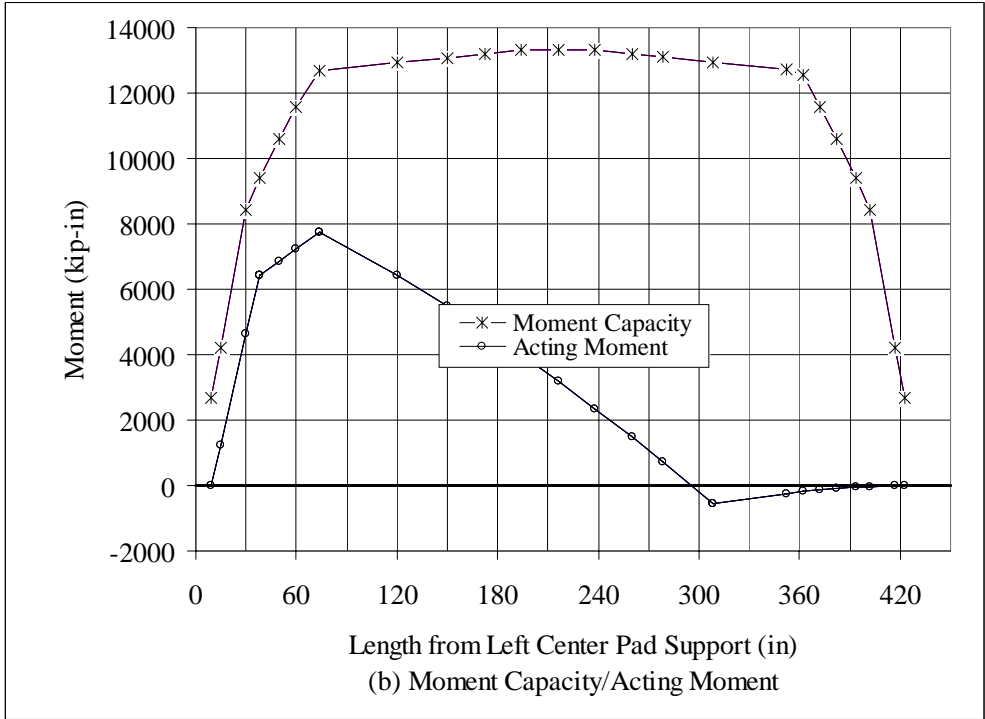
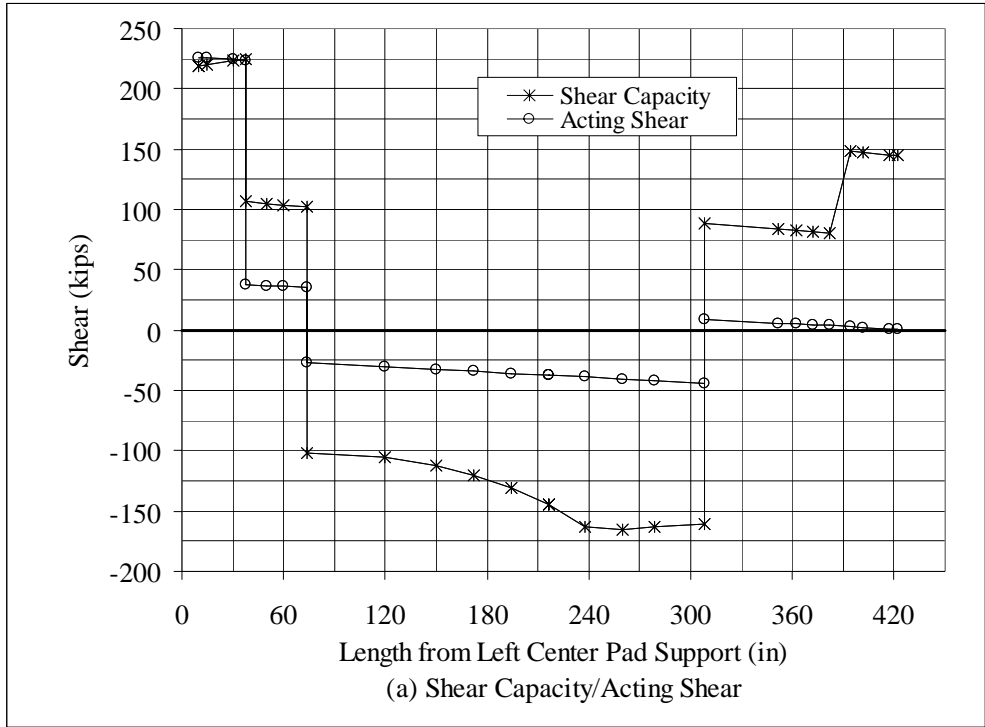


**Figure 2.23** Applied and Resisting Shears and Moments:  
First End Region Shear Test

### 2.6.3 Capacities of Specimens in the Second End Region Shear Tests

In the same way, Table 2.4 presents the shear and flexural capacities of the second end region shear test depicted in Figure 2.18. The total applied theoretical failure load in the shear was 195 kips. Part (a) of Figure 2.24 shows a detailed plot of the relationship between the applied shear and the resisting shear of the beam in the second end region test. It may be seen in Part (a) that the shear resistance in the first end region on the left end of the beam was about 46 percent larger than the applied shear without accounting for the S-bars, so that shear failure should not have occurred in the first end region. Again, Table 2.4 shows only values to a point a little beyond the critical region of the beam and does not show all of the values necessary to plot Figure 2.24.

Furthermore, everywhere to the right of the right-hand applied load, the resisting shear was at least twice the applied shear. Part (b) of Figure 2.24 shows that in spite of the rapid increase in the applied moment near the left end of the beam in the second end region shear test, the resisting moment remained larger than the applied moment. The moment margin was about 18 percent in the constant moment region and was greater elsewhere, despite the drop-off in capacity in the transfer length and flexural bond zones. It should be noted that the data in Table 2.4 and Figure 2.24 are for the first placement of the loads in a second end region test, where the first load was placed 82 inches from the end of the beam. Similar calculations for the final placement, with the first load only 66 inches from the end of the beam rather than 82 inches, showed a moment margin of safety of 40 percent against premature moment failure in the constant moment region.



**Table 2.4** Beam Capacity, Second End Region Shear Test with P = 195 kips

x inches	V <sub>t</sub> kips	M <sub>t</sub> kip-in	V <sub>ci</sub> kips	V <sub>cw</sub> kips	V <sub>c</sub> kips	V <sub>s</sub> kips	V <sub>n</sub> kips	M <sub>n</sub> kip-in	V <sub>n</sub> /V <sub>t</sub>	M <sub>n</sub> /M <sub>t</sub>
9.5	151	0	511	81	81	138	218	2,676	1.45	---
15	151	830	511	82	82	138	220	4,224	1.46	5.09
30	150	3,080	238	84	84	139	223	8,442	1.49	2.74
38	149	4,274	178	84	84	140	224	9,404	1.50	2.20
82	146	10,755	74	86	74	71	146	12,732	1.00	1.18
120	-52	10,581	32	88	32	73	-105	12,928	2.02	1.22
150	-54	8,983	38	89	38	74	-112	13,083	2.06	1.46
172	-56	7,769	46	90	46	75	-120	13,197	2.15	1.70
194	-58	6,519	56	88	56	76	-131	13,300	2.28	2.04
216	-59	5,234	69	88	69	76	-144	13,300	2.44	2.54

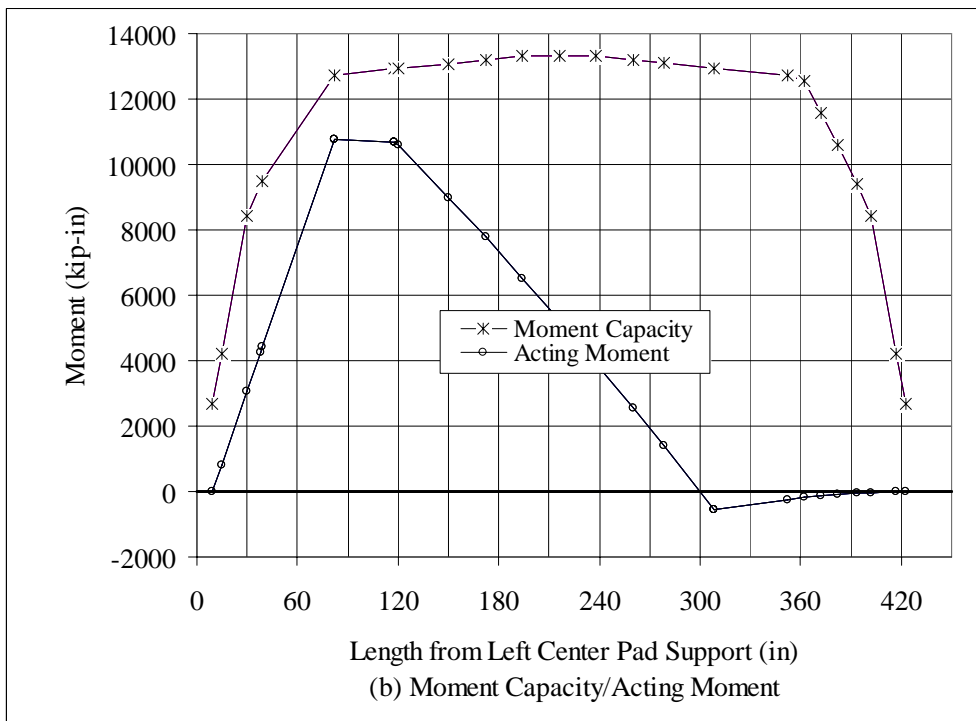
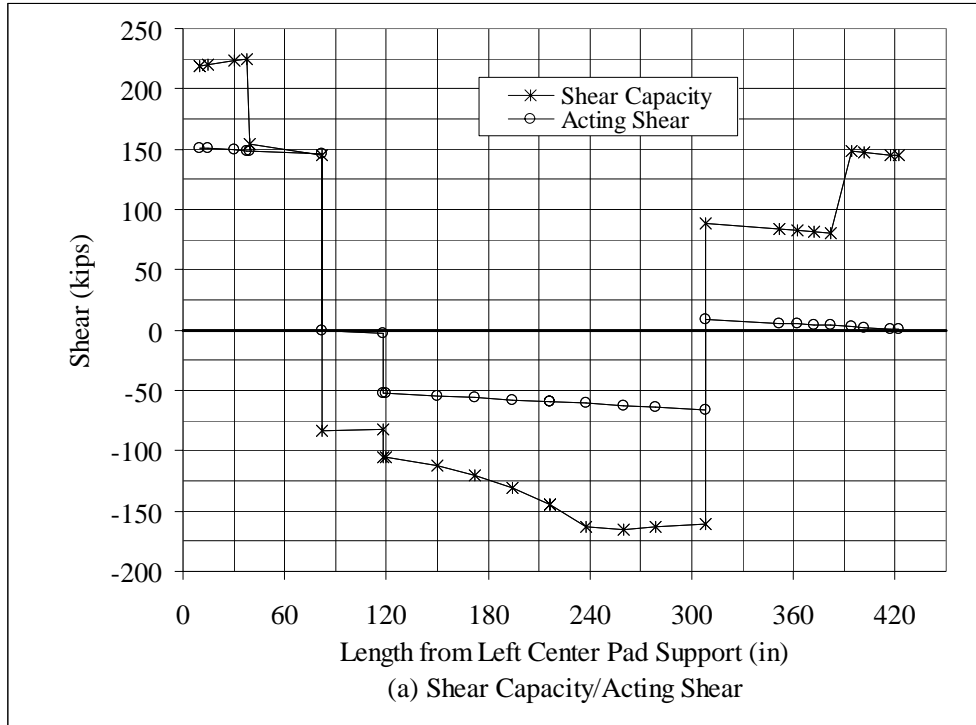


**Figure 2.24** Applied and Resisting Shears and Moments:  
Second End Region Shear Test

#### 2.6.4 Shear Capacity of Specimens in the Intermediate End Region Tests

In the same way, Table 2.5 presents the shear and flexural capacities of the intermediate end region shear test depicted in the Figure 2.21. The total applied load, which should have theoretically produced shear failure, was  $P = 186$  kips. In this case, the distance “x” in the first column of Table 2.5 is measured from the left pad edge of the left support instead of the left end of the beam. Figure 2.25 shows a detailed plot of the relationship between the applied shear and the resisting shear, as well as the applied moment and resisting moment of the beam in the intermediate end region shear test. The margin of safety against a flexural failure was about 55 percent in the constant moment region and was greater elsewhere. Also, the margin of safety against a shear failure was approximately zero in the region of interest, where a shear failure was desired, and significantly higher in the remaining regions of the specimen. Again, Table 2.5 shows only values to point a little beyond the critical region of the beam and does not show all of the values necessary to plot Figure 2.25.

**Table 2.5** Beam Capacity, Intermediate End Region Shear Test with P = 86 kips

<b>x</b> inches	<b>V<sub>t</sub></b> kips	<b>M<sub>t</sub></b> kip-in	<b>V<sub>ci</sub></b> kips	<b>V<sub>cw</sub></b> kips	<b>V<sub>c</sub></b> kips	<b>V<sub>s</sub></b> kips	<b>V<sub>n</sub></b> kips	<b>M<sub>n</sub></b> kip-in	<b>V<sub>n</sub>/V<sub>t</sub></b>	<b>M<sub>n</sub>/M<sub>t</sub></b>
<b>9.5</b>	156	0	511	81	81	69	150	2,674	0.96	---
<b>15</b>	156	860	511	82	82	69	151	4,222	0.97	4.91
<b>36</b>	155	4,121	191	85	85	70	155	9,211	1.00	2.24
<b>40</b>	154	4,739	167	85	85	70	155	9,603	1.00	2.03
<b>50</b>	153	6,277	128	85	85	70	156	10,586	1.01	1.69
<b>56</b>	153	7,189	113	86	86	71	156	11,174	1.02	1.55
<b>60</b>	13	7,250	17	86	17	71	88	11,575	6.74	1.60
<b>65</b>	13	7,314	16	86	16	71	87	12,071	6.92	1.65
<b>75</b>	12	7,436	16	87	16	71	87	12,724	7.32	1.71
<b>85</b>	11	7,551	15	87	15	72	87	12,779	7.77	1.69
<b>92</b>	11	7,627	14	87	14	72	86	12,818	8.13	1.68
<b>100</b>	-37	7,338	34	88	34	72	-106	12,863	2.91	1.75
<b>120</b>	-38	6,592	37	89	37	73	-110	12,973	2.89	1.97

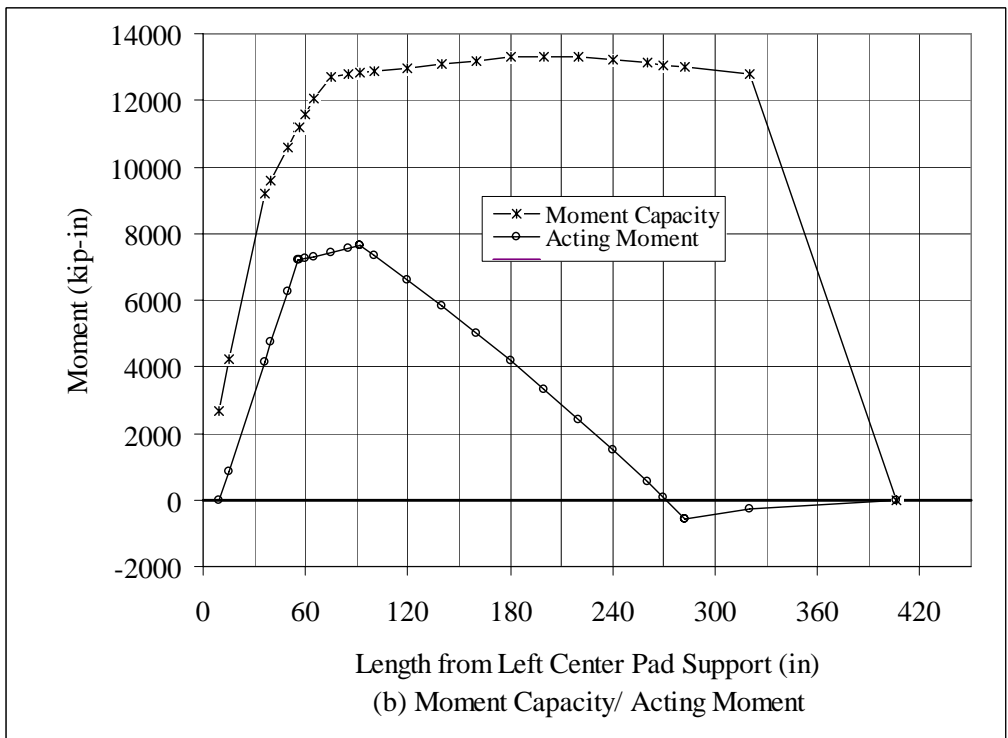
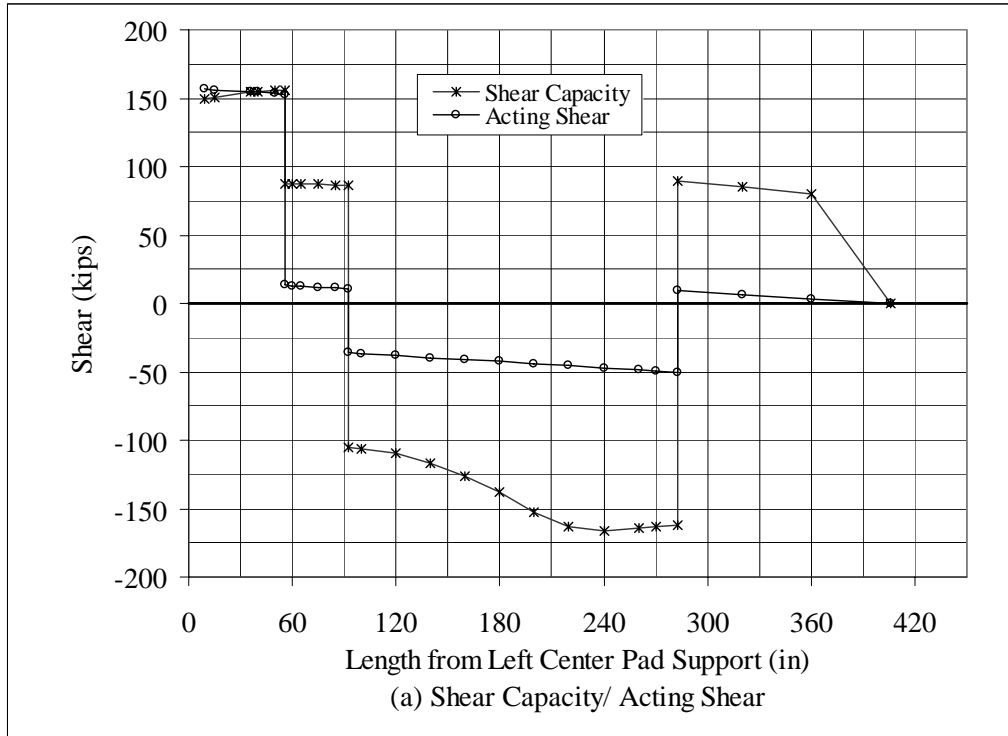


**Figure 2.25** Applied and Resisting Shears and Moments:  
Intermediate End Region Test

## 2.7 Test Specimen Identification

Initially, a 5-letter code was developed to identify and track each of the 43 load tests along with its associated material properties, shear reinforcement detail, and load geometry as well as to identify whether or not the specimen was in a pristine condition. This 5-letter code was used to identify 39 of the 43 load tests that were conducted during this project. Towards the end of the project, after reviewing some initial test data, modifications were made to the initial test plan that resulted in two sets of two beam tests that would have the exact same 5-letter code. For these 4 load tests, a sixth numeric digit was added to the 5-letter code to differentiate between the identical tests. The following describes the test identification code used during this project.

First letter: Shear reinforcement type

- T - Traditional Bar
- W - Welded Wire Fabric;

Second letter: Concrete strength

- N - Normal strength (5,000 to 7,000 psi)
- H - High strength (10,000 to 12,000 psi);

Third letter: Shear reinforcement detail

- R - Regular (TxDOT Standard, 60-ksi bar)
- S - Simplified (WWF, S- and R-bars of the same size, 60-ksi wire)
- E - Equal strength (WWF, S- and R-bars of same size, 80-ksi wire)
- A - Alternate (Alternate R bars, 90-degree hooks parallel to beam, 60-ksi bar);

Fourth letter: Beam type

- F - Flexural beam (with initial middle region test, significant prior cracking)
- P - Pristine beam (without initial middle region test, no significant prior cracking);

Fifth letter: Loaded region

- m - Middle region flexural test
- f - First end region shear test
- s - Second end region shear test
- i - Intermediate end region shear test;

Sixth digit: Numeric distinguisher (used only when necessary)

- 1 - First test with identical 5-letter code
- 2 - Second test with identical 5-letter code.

As an example, the specimen identified with the label WNSPf corresponds to the following test parameters:

- W - Welded Wire Fabric shear reinforcement
- N - Normal strength concrete (5,000 to 7,000 psi)
- S - Simplified shear reinforcement detail
- P - Test conducted on a pristine beam
- f - Shear test conducted on the first end region.

## **2.8 Fatigue Considerations**

Initially, only static load conditions were of interest in this research project. However, during full-scale testing, brittle tensile failures were observed in the lower longitudinal smooth wires near the electrical resistance welds in regions of high flexure-induced tension. Since brittle materials and joints subjected to cyclic tensile loads are susceptible to fatigue, two regions of concern, where fatigue failures in the WWF could adversely affect the shear capacity of the member, were given preliminary consideration against fatigue. In-depth background and details addressing potential fatigue issues are provided in Chapter 10 of this report.





## CHAPTER III

### TEST SETUP AND PROCEDURES

#### 3.1 Introduction

This chapter describes the overall process and procedures that were followed during the fabrication and testing of the specimens. The test specimens were fabricated using various combinations of test parameters identified in Table 2.1. Various test configurations (load and support geometries) were used, as described in Chapter 2.

#### 3.2 Specimen Fabrication

Each 36-foot long Type “A” prestressed concrete I-beam was prefabricated by Southwest Prestressed Concrete Company, in Amarillo, Texas, and shipped by truck to the Civil Engineering Structural Test Laboratory at Texas Tech University in Lubbock, Texas. The I-beams were unloaded and moved into the structural laboratory using a 10-ton overhead crane and a forklift, one on each end of the I-beam. In the structural laboratory, each beam was initially supported at its ends by 20-inch by 28-inch reinforced concrete pedestals 18-inches in height. Once the beam was in this initial position, the 8-inch thick, 72-inch wide reinforced concrete deck slab detailed in Figure 2.13 was cast in place. After several days, the deck slab formwork was stripped and the completed specimen was raised to its final test height and supported on 20-inch by 28-inch reinforced concrete pedestals that were 48-inch in height. The shorter pedestals were used to provide a safer working condition for laboratory personnel during the fabrication of the deck slab, and the taller pedestals were used for better access to the I-beam during testing. During fabrication of the test specimens, 6-inch by 12-inch standard concrete test cylinders were made for each beam and slab to experimentally determine the concrete’s strength and modulus of elasticity. The concrete material properties for the normal and high strength concrete test specimens are provided in Tables 3.1 and 3.2, respectively. It should be noted that these concrete strengths were determined during the week of specimen testing to identify the strengths on the concrete in each specimen at the time of testing. This caused the cylinders to be tested at various ages ranging from approximately 14 days to 3 months, depending on the specimen, rather than on the common typical age of 28 days.

**Table 3.1** Normal Strength Concrete Specimen Material Properties

Specimen	Beam	Concrete	Slab	Concrete
	$f_c'$ *	$E_c$ **	$f_c'$ *	$E_c$ **
	(ksi)	(ksi)	(ksi)	(ksi)
<b>TNRF</b>	7.25	4,750	5.57	4,290
<b>WNRF</b>	6.93	4,680	4.93	3,880
<b>WNSF</b>	5.97	4,400	5.05	4,620
<b>WNEF</b>	6.76	4,810	5.06	4,380
<b>TNRP</b>	8.37	4,830	5.80	4,330
<b>WNRP</b>	8.29	4,520	5.97	4,530
<b>WNSP</b>	6.05	4,340	5.08	4,540
<b>WNEP</b>	6.69	4,480	5.22	4,510
<b>TNAP</b>	9.00	5,030	5.80	5,200
<b>TNRPI</b>	7.42	4,900	5.04	4,180
<b>WNSPI/WNEPI</b>	7.52	4,970	5.14	4,520
<b>TNAPI</b>	8.70	4,980	5.54	4,040

\* Average of three compression tests.

\*\* Average of four modulus tests.

**Table 3.2** High Strength Concrete Specimen Material Properties

Specimen	Beam	Concrete	Slab	Concrete
	$f_c'$ *	$E_c$ **	$f_c'$ *	$E_c$ **
	(ksi)	(ksi)	(ksi)	(ksi)
<b>THRF</b>	10.78	5,750	5.31	5,200
<b>WHSF</b>	11.97	6,010	6.74	4,760
<b>WHEF</b>	10.31	5,950	4.19	3,630
<b>THRP</b>	10.80	5,800	5.17	4,280
<b>WHSP</b>	12.47	6,490	5.48	4,660
<b>WHEP</b>	10.98	5,790	4.53	4,060

\* Average of three compression tests.

\*\* Average of four modulus tests.

### 3.3 Test Sequence

A typical test sequence was used to conduct five separate load tests on each of the first seven beam pairs listed in Table 2.1. Between each load test, the load points and supports were adjusted to match the type of test and its associated geometry as defined in Chapter 2. The typical test sequence used for the first seven beam pairs listed in Table 2.1 was as follows.

Test 1: Perform a middle region flexural test of the first beam of each pair.

Test 2: Perform a first end region shear test on the first beam of each pair.

Test 3: Perform a second end region shear test on the first beam of each pair.

Test 4: Perform a first end region shear test on the second beam of each pair.

Test 5: Perform a second end region shear test on the second beam of each pair.

The test sequence used on the 8<sup>th</sup> and 9<sup>th</sup> pairs of beams listed in Table 2.1 was modified to account for adjustments made following the data review from earlier tests. An intermediate end region shear test was conducted on each end of each specimen fabricated from the 8<sup>th</sup> pair of beams. These 2 beams had a mix of previously tested parameters as shown in Table 2.1. The specimens fabricated from the 9<sup>th</sup> pair of beams listed in Table 2.1 had the same parameters but the typical test sequence was modified to provide the tests necessary for optimum comparisons to the other specimens. The test sequence used to test the two specimens fabricated from the 9<sup>th</sup> pair of beams listed in Table 2.1 is as follows.

Test 1: Perform a first end region shear test on the first beam.

Test 2: Perform a second end region shear test on the first beam.

Test 3: Perform an intermediate end region shear test on the second beam.

Test 4: Perform another intermediate end region shear test on the second beam.

During any one of the 4 basic types of load tests that were conducted during this project (middle region flexure test, first end region shear test, second end region shear test, or intermediate end region shear test), similar steps were followed. A view of the general test setup is shown in Figure 3.1. Each specimen and its support pedestals were properly located and aligned on the structural test deck in the horizontal, longitudinal, and vertical directions. Once proper alignment was achieved, 3-inch thick elastomeric bearing pads were placed between the specimen and the 48-inch tall support pedestals to allow longitudinal movement and rotation at the supports during loading. A 1/4-inch thick bearing pad was also placed on top of the concrete deck slab at each of the two load points to provide even bearing pressures between the top surface of the concrete deck slab and the bottom surface of the steel rocker bearing plates located at each end of the load spreader beam. Once the spreader beam was properly aligned, the load frame containing a hydraulic ram, described in Section 3.4, was located over the specimen and bolted down to the structural test deck. Once the instrumentation and the data acquisition system was in place, loading of the specimen was completed as described in Section 3.4. During middle region flexural tests, the specimens were loaded to magnitudes that caused internal moments greater than their theoretical ultimate moment capacities but not to failure to allow additional testing to be conducted on the flexural specimens. All first, second, and intermediate end region shear tests were loaded to failure. After a test was completed, the load frame and supports were moved to new locations along the length of the specimen, if additional tests were to be conducted on the specimen, and the overall setup and test procedure were repeated. If no additional test(s) was to be conducted on the specimen, all the instrumentation and load equipment were removed, and the specimen was lowered onto the test deck for demolition and disposal. Once the specimen was removed, another I-beam was set in place and the overall process was repeated until 43 load tests had been completed on 18 specimens.



**Figure 3.1** General Test Setup

### **3.4 Load Equipment and Load Sequence**

Load was applied to each specimen using a Power Team, Model RD50013, hydraulic ram having a 1,000-kip rated capacity at 10,000 psi, an effective cylinder area of 99.402 square inches, and a 13-inch stroke. As shown in Figure 3.1, the ram was attached to the reaction load frame that was bolted down to the structural test deck by 16, 2-inch diameter, high strength threaded steel rods. The structural test deck has a 30-foot by 60-foot floor area and a 2-foot center-to-center grid of tie-down points to provide adequate movement and alignment of the load frame. Hydraulic pressure was provided to the ram via a pneumatically actuated, manually controlled, Power Team, Model PA6D, hydraulic pump rated for 10,000 psi. The ram transmitted its load to the test specimen via a steel

spreader beam. This beam was supported on top of the specimen by two bearing plates that were 3 feet apart and centered over the longitudinal axis of the I-beam. The locations of these two bearing plates represent the two load points shown in the various test configurations in Chapter 2. The magnitude of the total load that went to each load point was controlled by the location of the ram with respect to the bearing plates at each end of the spreader beam. Final longitudinal alignment of the ram was accomplished after the load frame was bolted to the structural test deck. The final alignment of the ram was accomplished via a roller system between the ram and the overhead cross-beam seen in Figure 3.1. For all middle region flexural tests, the ram was centered between the bearing plates, resulting in two equal point loads and a constant internal moment region in the test specimens between the two load points. For all of the shear tests, the ram was positioned so that  $\frac{3}{4}$  of the ram load would be transmitted to the bearing plate closest to the end of the test specimen and  $\frac{1}{4}$  of the ram load would be transmitted to the other bearing plate. This load distribution was selected to provide an approximately constant internal moment region in the specimens for the second end region shear tests and was maintained for consistency in the first and intermediate end region shear tests.

Loads were applied incrementally to the specimens with short pauses between each load increment to allow time for data acquisition. Collected data included total applied load, vertical movements of the specimen at several points, strains in the witnesses bars embedded in the concrete, strains in the extreme fibers of the concrete deck slab, and end-slip measurements of the prestressing strands. Details about data collection methods and specific locations are discussed at length in Chapter 4. In addition, digital images were taken of specific regions and at specific load levels for use with a Digital Image Analysis Technique developed during the project to evaluate differences or similarities of the cracking of the specimens. Details of the digital images and the analysis technique are provided in Chapter 5.

Load increments were slightly modified depending on the general type of test that was being conducted: middle region flexure test or first, second, or intermediate end region shear test. An initial load increment of 15 kips was used for all of the tests while the specimens were in their linear elastic range prior to cracking. Once initial cracking occurred, smaller load increments were used to account for the reduced stiffness of the specimen. The second load increment that was used during the middle region flexure tests was 5 kips. This load increment was maintained until the test was stopped when the maximum strain in the top fiber of the concrete deck slab reached a value of 0.002, well below its assumed ultimate value of 0.003. The applied load causing the limiting strain of 0.002 also caused an internal moment in the specimen slightly above its theoretical ultimate moment. The middle region flexural tests were stopped at this point to prevent complete material failures since these test specimens were scheduled for subsequent shear tests. The second load increment that was used during the first end region shear tests was 10 kips. This load increment was maintained until failure of the specimen in the first end region. It did not have to be reduced due to the higher stiffness of these specimens. The second load increment that was used during the second and intermediate end region shear

tests was also 10 kips. However, during these two types of tests, larger deflections began to occur in the specimens when the longitudinal steel began to yield. Therefore, 10-kip load increments were used only until it produced a vertical deflection greater than  $1/10^{\text{th}}$  of an inch. Following this occurrence, only the amount of load necessary to cause an observed  $1/10^{\text{th}}$  of an inch deflection in the specimen was applied. This deflection controlled load increment was continued until failure of the second and intermediate end region shear test specimens.





## CHAPTER IV

### INSTRUMENTATION AND DATA ACQUISITION

#### 4.1 Introduction

This chapter describes the techniques and equipment used to instrument and collect data from the specimens tested during this project. Several physical measurements were monitored and recorded at each load increment. Test data was collected from both electronic and mechanical devices.

#### 4.2 Electronic Instrumentation

##### 4.2.1 Embedded Strain Gages

Strain gages were embedded in the concrete beams adjacent and parallel to several of the vertical shear reinforcing bars in the high shear regions of the test specimens in an attempt to measure the magnitudes of the tensile strains in the shear steel. These values could then be used to determine the magnitudes of the stresses in the shear steel at or near failure. These strain gages were embedded in the concrete via “witness” bars, which were fabricated using 100-ksi threaded rods approximately 9-inches long that were anchored at each end by a series of nuts and washers. A 1.5-inch long region of threads on each piece of threaded rod was ground smooth near its mid-length point to allow the installation of a 0.25-inch long, 350-ohm, encapsulated strain gage on the rod. These gages were general-purpose static gages manufactured by Measurements Group, Inc. After being mounted on the rod, each strain gage was wrapped with a sticky, elastomeric material and then with tape to protect the gage from moisture and mechanical damage during casting. These witness bars were then wired to the shear reinforcing steel during beam fabrication.

The first four beams, Beam Pairs No. 1 and 2 listed in Table 2.1, were each instrumented with approximately 28 witness bars, 16 in the first end region at one end of the beam and 12 in the second end region at the other end of the beam. Two results were observed during testing of these first four beams that prompted a revision to the initial witness bar embedment strategy in subsequent beams. First, the strain gages in the first end region shear tests showed mostly high compressive strains and a few very low tensile strains due to compression strut action that developed in the concrete between the near support and the near load point. These types and magnitudes of strain values were determined not to be of interest to the current project. Therefore, the installation of witness bars in the first end region shear tests was discontinued for subsequent test specimens. Second, the magnitudes of the tensile strains observed during the second end region shear tests were very low compared to the expected yield strain of the material. This was determined to be due to the fact that the shear cracks in the concrete were not crossing the witness bars at the locations of the strain gages, and anywhere away from the cracks, the steel and concrete were acting as an uncracked section where the steel only carries a small portion of the load due to the much larger volume of the concrete. Because of this and the lack of ability to predict exactly where the shear cracks would form, the number of witness bars installed in the second end region was reduced from 12 to 6 in the remainder of the

beams. These six witness bars were placed with their strain gages 7 inches above the bottom of the beam and were attached to the stirrups located 38, 46, and 54 inches from the end of the beam in the second end region of the reinforcing. Two witness bars were attached to each stirrup, one on the near side and one on the far side. These locations placed the strain gages on the three stirrups just above the bottom two longitudinal wires where a shear failure was most likely to occur. Review of the final test results showed that the magnitude of the measured strain, except in a couple of isolated cases, never approached the yield strain of the stirrups. This was simply due to the fact that the shear cracks did not intersect the gages.

The only other reason that witness bars were embedded in the beams was in an effort to resolve some potential fatigue issues that were raised during testing. A discussion of the fatigue issues and the locations of the associated witness bars are provided in Chapter 10.

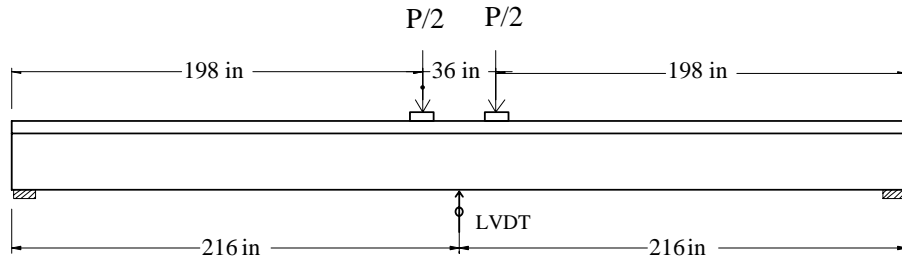
#### 4.2.2 Concrete Strain Gages

Two concrete strain gages were mounted to the top of the concrete deck slab in the test region during each test. These gages were located along the longitudinal centerline of the beam at the third points between the two applied load points that were 36-inches apart. During the flexural tests, these gages were used to monitor the maximum strain in the deck slab and to stop the test before complete flexural failure occurred. The flexural tests were stopped when the extreme concrete fiber compressive strain reached a value of 2,000 micro strains, well below the generally used compressive failure value of 3,000 micro strains. At a compressive strain value of 2,000 micro strains, the internal moment in each specimen was well above the theoretical moment capacity of the specimen. In all of the shear tests, the concrete strain gages were used to monitor the maximum compressive strain in the concrete deck slab in an effort to predict if a flexural failure was eminent. These gages were mounted directly on top of the slab after the concrete surface had been ground smooth and sealed with an epoxy. Each concrete strain gage was a 2.5-inch long, 120-ohm, uniaxial, narrow gage, encapsulated strain gage that was manufactured by Measurements Group, Inc.

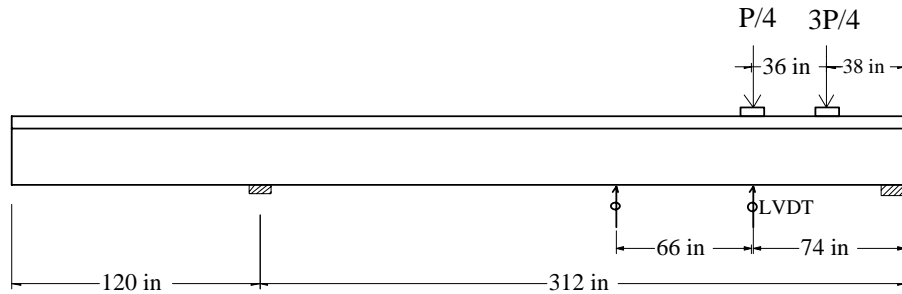
#### 4.2.3 Linear Variable Differential Transducers

Linear Variable Differential Transducers (LVDT's) were used to determine the vertical displacements of the beams at one or two locations as load was applied to each test specimen. Specific deflection locations for the four types of tests conducted during this project are shown in Figure 4.1. The LVDT closest to the near support, as shown in Parts (b), (c), and (d) of Figure 4.1, represented the estimated maximum plastic deflection, and this value was used to plot the load-deflection curves developed and discussed in this report. The LVDT farthest from the near support represented the estimated maximum elastic deflection and was used as backup data. Two lengths of Trans-Tec Series 240 LVDT's were used during this project. One length of LVDT that provided a total travel of 8 inches,  $\pm 4$  inches of active range, was used to measure the vertical movement of the beam relative to the floor as shown in Figure 4.1. The other length of LVDT provided a total travel of 1-inch,  $\pm 0.5$  inches of active range, was used to measure the vertical

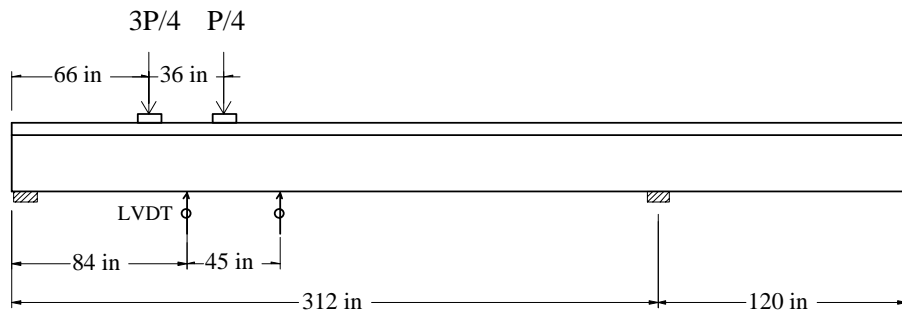
settlements of the elastomeric bearing pads at the beams' supports. These support settlement measurements were combined with the other relative deflection measurements to determine the absolute vertical deflections of the specimens at the given load increments.



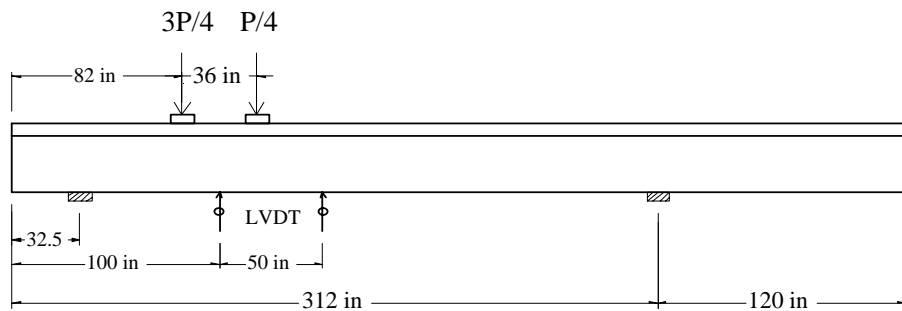
(a) Flexural Test



(b) First End Region Test



(c) Second End Region Test



(d) Intermediate End Region Test

**Figure 4.1** Locations of Vertical Displacement Measurements

#### 4.2.4 Load Cell and Pressure Transducers

The magnitude of the applied load was recorded at every load increment using three separate devices. The primary load-measuring device, whose data was used to plot the load-deflection curves associated with this project, was a 1,000-kip strain-gage load cell manufactured by Strainsense Enterprises, Inc., specifically for this project. The electronic output of the load cell was processed and recorded by the data acquisition system described in the following section. As backup, two Series P027 Pressure Transducers manufactured by Trans-metrics, both with 10,000-psi ratings, were also used to monitor the load. These hydraulic pressure transducers were connected directly into the hydraulic stream, near the ram, that was used to actuate the ram and load the specimens. The electronic output of each transducer was converted to pressure. Each pressure value was then multiplied by the ram piston area to yield the corresponding load. The electronic output from one pressure transducer was processed and recorded by the same data acquisition system used with the load cell. The electronic output from the other pressure transducer was fed into a P-3500 Digital Strain Indicator manufactured by Measurements Group, Inc. The readout from the Digital Strain Indicator was in psi and was recorded and processed by hand. The load cell output was used as the primary data, and the output from the two pressure transducers was used as backup and to verify the primary data during testing.

#### 4.2.5 Data Acquisition

The output from the electronic instrumentation devices (strain gages, LVDT's, load cell, and pressure transducers) was fed into, processed, and recorded via a National Instruments, Inc. (NI), PC-based signal conditioning and data acquisition system that utilized Signal Conditioning Extensions for Instrumentation (SCXI). The system used during this project was a NI SCXI-1000, 4-bay chassis that contained two NI SCXI-1121 modules and two NI SCXI-1122 modules. The SCXI-1121 is a 4-channel isolation amplifier module with transducer excitation. It includes an independent gain amplifier and low-pass noise filter on each channel with complete channel-to-channel electrical isolation. Each channel also includes a completely isolated excitation source and a half-bridge completion circuit. The SCXI-1122 is a 16-channel signal-conditioning module. It combines a 16-channel input multiplexer with a single programmable gain isolation amplifier for economical, isolated measurements. The SCXI-1122 also includes a half-bridge completion circuit and a single voltage excitation source. All output signals from the electronic instrumentation devices were fed through one of the four SCXI modules described above and multiplexed to a single DAQ board; in this case, a NI PCI 6024E card that was plugged into a Dell, Dimension XPS T500 personal computer. All of the witness bar strain gages were connected to one of the SCXI-1122 modules, while the concrete strain gages, the LVDTs, one pressure transducer, and the load cell were connected to one of the SCXI-1121 modules. The output signal from all of these devices was voltage.

As the electronic output data (changes in voltage) was collected from all of these devices and fed into the computer, a program was needed to organize, convert and store these voltage changes to the physical measurements they represented: strain, displacement, pressure, or load. LabVIEW, a computer software package from National Instruments,

Inc., was used to accomplish this process. LabVIEW is a graphical programming language that uses icons instead of lines of text to create applications. In contrast to text-based programming languages, where written text instructions determine program execution, LabVIEW uses dataflow programming, where data determines the execution. For a more in-depth discussion of LabVIEW and the program developed for use during this project see Cedeno (2001).

Several output data files were generated in every test as a result of collecting the electronic information corresponding to the different devices. Table 4.1 shows an example of the output data for the applied load and the four LVDT's used in a second end region test. In the first column, the load increment is recorded. The second and third columns correspond to the LVDT's used to monitor the settlements of the support pads. The ends of the beam are referred to as the South and North ends. The fourth and fifth columns correspond to the LVDT's used to track two vertical displacements along the beam. The plastic position refers to the LVDT located between the load points, see Figure 4.1(c), and the elastic position is where the maximum deflection should occur under purely elastic behavior. Similar files were generated for the pressure transducer, witness bar strain gages, and slab strain gages.

### **4.3 Mechanical Instrumentation**

In addition to the electronic instrumentation described in Section 4.2, several mechanical devices were also used to measure vertical deflections as a backup source of data, should problems occur with the electronic system during testing. A digital caliper was also used to take prestressing strand end-slip measurements during the first and second end region shear tests as an indicator of an impending bond slip failure mode. All mechanical devices were individually read and the data recorded by hand at each load increment.

#### 4.3.1 Dial Gages

A 10-inch range dial gage was located under the beam at the same location as the LVDT placed at the maximum plastic deflection position. This dial gage served two purposes. First, it provided backup vertical deflection data should the electronic system experience trouble during testing. Second, its large dial face was used to monitor loading during the final loading stages of the second and intermediate end region shear tests where 0.1-inch deflection increments controlled the load application. In addition, two 0.5-inch range dial gages were used. These two dial gages were located at the ends of the beams, opposite the shorter LVDT's at each support, to provide backup data for support settlement data at the elastomeric bearing pads.

#### 4.3.2 Wire Gage

A taut piano wire attached to the beam provided another source of information for the two vertical displacements of the specimens, maximum elastic and plastic. The piano wire was attached to a hilty bolt at the mid height of the web and centered over each support bearing pad. Thus, its end points moved as the supports settled. A straight chalk line previously drawn on the web of the beam behind the wire gave a visual reference line.

Scales with a precision of a hundredth of an inch and mirrors were attached to the beam at the elastic and plastic displacement points to furnish the numerical displacements values. By taking scale readings at every load increment, changes in vertical displacement could be determined. The mirrors were used to insure a horizontal line of sight between the wire and the scales. Vertical deflections determined from this method were deformations of the specimen itself since the ends of the wire moved as the elastomeric bearing pads settled at the supports. This arrangement also provided a visual sense of the deformed shape of the specimen throughout the load sequence. Figure 4.2 shows a view along a beam of this wire gage instrumentation.



**Figure 4.2** Wire Gage Deflection Device

### 4.3.3 Strand End-slip Measurements

Strand end-slip measurements were taken during first and second end region shear tests to monitor the potential for an impending bond-slip failure. End-slip measurements were only taken during first and second end region shear tests in which the maximum internal moments occurred within the theoretical development length of the strand. Strand end-slip measurements were initially taken at every other load increment until significant slippage began to occur, and then they were taken at every load increment. A small plastic plate glued to the concrete surface on the end of the beam provided a smooth reference surface. With a digital caliper, the length between the face of a bracket clamped to the strand and the plastic surface was read for each of the monitored strands. Initial readings at zero load were the references for future readings. Changes in readings represented strand end-slip. Figure 4.3 shows the setup of the metallic brackets attached to the strands. The small holes in the brackets provided consistent alignment of the digital caliper during measurements.

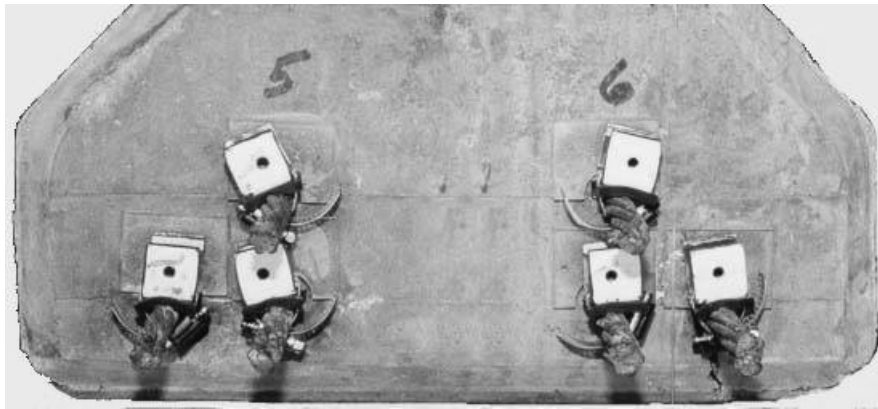


**Figure 4.3** End-Slip Measurement Brackets

**Table 4.1** Sample Load and LVDT Displacement Output Data

Welded Normal Simplified Pristine Second End Region Test				
Date	18-Jul-00	Time	9:58	
Load and LVDT Displacements				
Load	LVDT			
	South	North	Elastic	Plastic
kips	in	in	in	in
0.0	0.000	0.000	0.000	0.000
15.2	-0.003	-0.002	0.020	0.019
30.4	-0.005	-0.004	0.037	0.034
45.4	-0.005	-0.004	0.051	0.047
60.0	-0.005	-0.004	0.066	0.060
75.6	-0.005	-0.004	0.082	0.074
90.7	-0.005	-0.003	0.097	0.089
105.2	-0.005	-0.002	0.114	0.103
120.0	-0.005	-0.001	0.131	0.120
135.1	-0.005	0.001	0.154	0.141
150.2	-0.005	0.002	0.174	0.160
165.3	-0.002	0.004	0.198	0.182
179.3	-0.001	0.006	0.227	0.209
193.9	0.000	0.009	0.294	0.276
209.6	0.001	0.013	0.392	0.369
224.3	0.004	0.018	0.484	0.455
238.1	0.008	0.023	0.608	0.562
248.9	0.010	0.026	0.685	0.631
259.6	0.011	0.029	0.764	0.708
263.2	0.013	0.030	0.810	0.746
274.8	0.014	0.033	0.908	0.837
283.5	0.016	0.035	1.001	0.926
291.8	0.019	0.039	1.094	1.018
299.3	0.020	0.042	1.186	1.111
298.3	0.022	0.044	1.244	1.176
298.4	0.023	0.047	1.334	1.285
304.0	0.024	0.049	1.421	1.385
308.3	0.026	0.052	1.508	1.481
308.7	0.027	0.054	1.570	1.556
308.7	0.028	0.056	1.642	1.644
0.0	0.013	0.014	0.343	0.371



## CHAPTER V

### DIGITAL IMAGING FOR CRACK QUANTIFICATION

#### 5.1 Objective and Scope

In this project the ultimate shear capacities of the various welded wire fabric (WWF) designs were to be evaluated and compared to the shear capacities of traditionally reinforced beams of similar dimensions and longitudinal reinforcement; thus the research team considered a thorough analysis of the cracking of the different beams near failure to be of interest. While prestressed beams are designed not to crack under service loads, the shear reinforcement in the beams is what is counted on to guard against failure in shear. Furthermore, a shear failure can be quite sudden, and the cracking that develops prior to the failure is useful in understanding how the shear and moment effects combine in this failure mechanism. How two different shear reinforcement designs compare in control of cracking is a helpful supplement to the ultimate loads in evaluating the designs.

Cracks can be compared in different ways, but it is not easy by eye to establish a measure of the overall cracking in a beam. The cracks generally vary in spacing, length, maximum width, average width, and overall crack area, but only the first three of these are readily measured by eye. With the advent of digital imaging, however, it was expected that quantitative crack data could be extracted from digital pictures of the cracks in a way that would be more efficient and more reliable than measures obtained manually. Accordingly, extensive efforts were given to developing ways to quantify cracking in the specimens tested in this project.

The remainder of this chapter presents the methodology and the computer algorithms developed to quantify cracking in the beams tested in this project. The results obtained in various tests are presented in the chapters with the other test results. Further documentation of the methodology is given in Turkyilmaz (2001).

#### 5.2 Introduction to Digital Imaging

Digital imaging is the science of operating on digital pictures to obtain information. First, a digital picture is taken, which is a digitized form of a scene that can be stored, displayed, and processed by a computer. Digital images are stored as matrices with elements called “pixels,” a word derived from “picture element.” Each pixel has a value depending on the light intensities coming from the corresponding region in the picture. The more pixels in a given area or the greater “resolution” of the image, the better the representation is of the visual scene. The pictures taken in this project were in JPEG format, which is the most common type of color picture format in today’s cameras. JPEG stands for Joint Photographic Experts Group. This format involves compression of the original data and later decompression, and some information can be lost in this process.

In this research, the MATLAB Image Processing Toolbox (MATLAB, 2001) was used as the primary software. The JPEG images were stored as three-dimensional arrays, with the first plane for red intensities, the second plane for green intensities, and the third for blue intensities of the so-called RGB (red-green-blue) images. These images were then converted to “grayscale” images and later to binary (black and white) images, with the cracked areas represented by black pixels and the uncracked areas by white pixels. This process was called “crack determination.” Then counting the pixels in individual cracks and determining total cracked areas, individual crack areas and lengths, and average crack widths constituted “crack quantification.”

### 5.3 Algorithms for Crack Determination

Crack determination by digital imaging is the process by which the pixels in a digital image of a cracked surface are all set to be black and all the other pixels are set to be white. With the resulting binary image, the storage space required for the image is greatly reduced and the counting operations needed for crack quantification are greatly simplified.

A series of computer algorithms have been developed to carry out this process. After quite a bit of experimentation, it was found that the best sequence of steps were as follows: 1) conversion from RGB to grayscale; 2) edge detection to enhance the crack boundaries; 3) binarization with a threshold value of the illuminance; 4) “spot removal” to eliminate black pixels not on a crack; 5) “hole filling” to turn all white pixel within a crack black; and 6) thinning to reduce the crack widths closer to their original widths. Each of these steps is described and illustrated with an example in the subsections below. Computer codes for the algorithms themselves are given in the appendixes of Turkyilmaz (2001).

#### 5.3.1 RGB to Grayscale Image Conversion

The example RGB picture that will be used to illustrate crack determination is shown in part (a) of Figure 5.1. It is a picture of an 11 x 18-inch portion of the web of a beam in a second end region test. Conversion to a grayscale image, shown in part (b) of the figure, was performed with one of the built-in functions of the MATLAB Toolbox. The luminance of a pixel in a grayscale image is obtained by adding the intensities of the red, green, and blue components with certain proportions. These proportions are not all the same because of the human eye’s sensitivity to different colors:

$$L_m = 0.229R + 0.587G + 0.114B \quad (5.1)$$



(a) RGB Image of Shear Cracks



(b) Corresponding Grayscale Image of Shear Cracks

**Figure 5.1** Sample RGB Crack Image and its Grayscale Conversion

where  $L_m$  is the grayscale luminance and  $R$ ,  $G$ , and  $B$  represent the red, green, and blue intensities, respectively.

### 5.3.2 Edge Detection

An edge may be regarded as a boundary between two dissimilar regions of an image. In the present study, the regions of interest are a concrete background and the cracks within it. The logic of using an edge detection technique is that it evaluates the differences between the values of the background and crack pixels, rather than the absolute values of the pixels, so that cracks can be distinguished on images with different overall levels of lighting.

Several built-in edge detection methods are available in the MATLAB Toolbox, including the Sobel, Roberts, Rewitt, Canny, Zero-crossing, and Laplacian or Gaussian methods. However, these methods proved to be somewhat lacking for the present purpose because they were not detect thin cracks well. Accordingly, three original methods that account well for diagonal cracks as well as for vertical and horizontal cracks were developed. All three methods operate on the eight grayscale values around each pixel, as seen labeled  $a_1$  through  $a_8$  in Figure 5.2, to determine if the center pixel,  $a_0$ , is an edge.

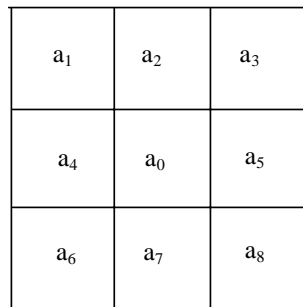


**Figure 5.2** Eight-Pixel Neighborhood of a Grayscale Image

The first of the original edge detection or “edge enhancing” methods initially takes differences in four directions among the pixels surrounding a given central pixel. In algebraic form these differences are, referring to Figure 5.2:

$$\text{The horizontal difference: } H = |a_1 - a_3| + |a_4 - a_5| + |a_6 - a_8| \quad (5.2a)$$

$$\text{The vertical difference: } V = |a_1 - a_6| + |a_2 - a_7| + |a_3 - a_8| \quad (5.2b)$$

$$\text{The first diagonal difference: } D1 = |a_1 - a_8| + |a_2 - a_5| + |a_4 - a_7| \quad (5.2c)$$

$$\text{The second diagonal difference: } D2 = |a_3 - a_6| + |a_5 - a_7| + |a_2 - a_4| \quad (5.2d)$$

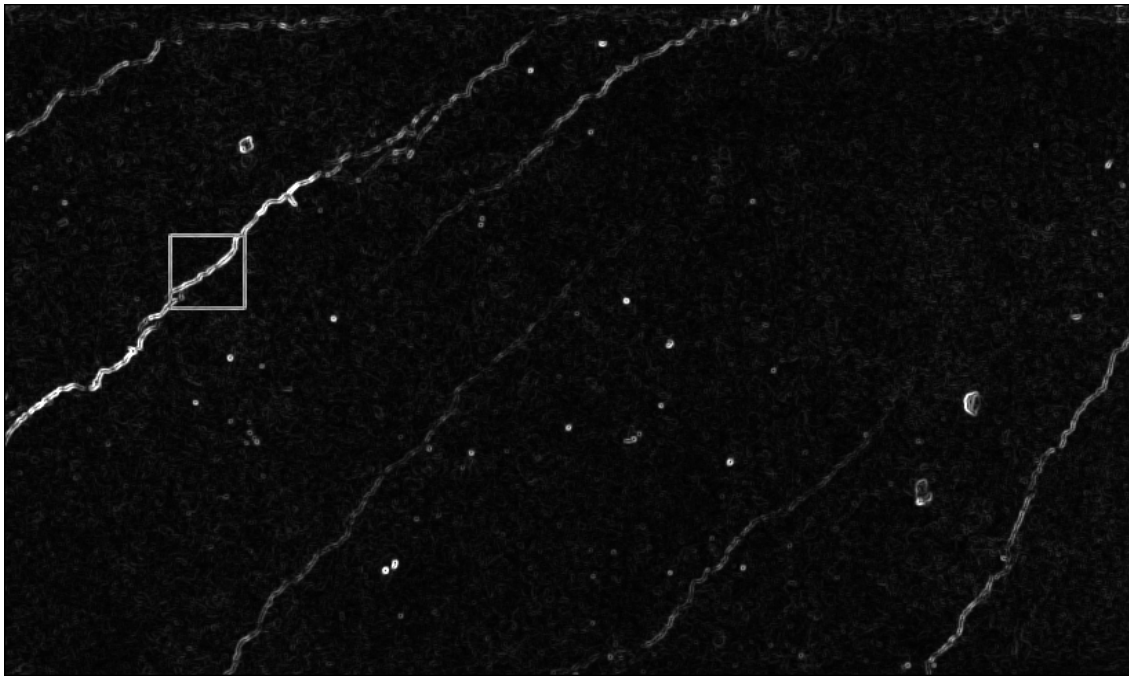
Then the value,  $E_0$ , assigned to the center pixel for the first edge-enhanced image is the largest of these four quantities:

$$E_0 = \max(H, V, D1, D2) \quad (5.3)$$

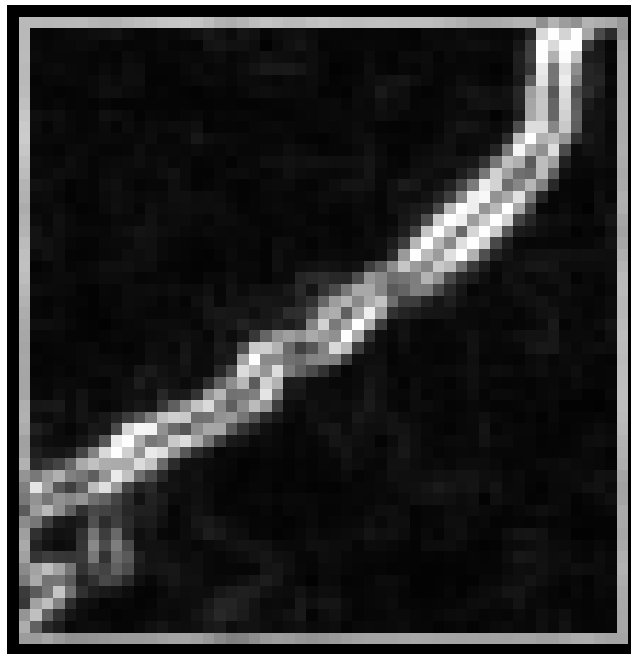
High values of  $E_0$  represent boundaries of cracks, holes, and other features of the grayscale image.

Part (a) of Figure 5.3 shows the edge-enhanced image of the grayscale image of Figure 5.1(b) as determined by the first original method. It is an intensity image, meaning that it is another grayscale image with the values determined by the preceding algorithm. Some of the values of  $E_0$  could have exceeded the maximum (pure white) intensity of 255 for a grayscale image; in which case, the value was set equal to 255. The values closest to or equal to 255 define the edges of the cracks and also show up as dots and splotches elsewhere in the figure. Part (b) of the figure shows an enlargement of the section outlined with a box in part (a), where the sizes of the pixels are evident.

In the second original edge detection method the same four differences as in Equation (5.2) are determined, but the value of the edge-enhanced image for the center pixel is determined by Equation (5.4) instead of Equation (5.3):



(a) Full Image



(b) Zoomed Section (Magnification of 7.85)

**Figure 5.3** Edge Enhanced Images of Fig. 5.2 by First Method (Eqs. 5.2 and 5.3)

$$E_0 = (H^2 + V^2 + D1^2 + D2^2)^{1/2} \quad (5.4)$$

The distinction of this method is that it considers the differences in all four directions, not just the maximum difference in one direction. Figure 5.4 shows the edge-enhanced image using this method. It may be seen that this image has somewhat brighter crack boundaries than in Figure 5.3, but otherwise the results are very similar.

In the third original edge detection method, the individual directional differences are magnified by taking the squares of the opposing intensities; as in the first method, only the largest of the four is used. Thus, in this method the quantities V, H, D1, and D2 are redefined as:

$$V = (a_1 - a_6)^2 + (a_2 - a_7)^2 + (a_3 - a_8)^2 \quad (5.5a)$$

$$H = (a_1 - a_3)^2 + (a_4 - a_5)^2 + (a_6 - a_8)^2 \quad (5.5b)$$

$$D1 = (a_1 - a_8)^2 + (a_2 - a_5)^2 + (a_4 - a_7)^2 \quad (5.5c)$$

$$D2 = (a_3 - a_6)^2 + (a_2 - a_4)^2 + (a_5 - a_7)^2. \quad (5.5d)$$

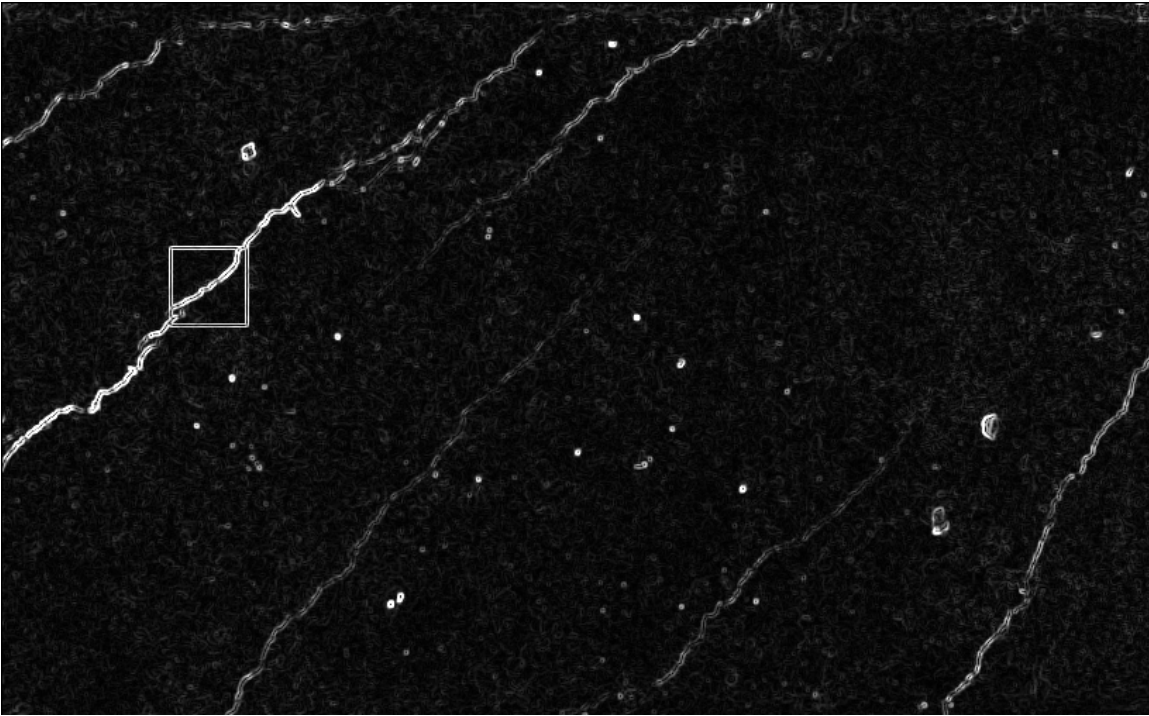
They are then used in Equation (5.3). Figure 5.5 (S 3.12) shows the edge-enhanced image using this method. In this image, the entire crack is essentially pure white as squaring the differences more easily increased the grayscale pixel values above 255. Also, the white portion representing the crack is wider than before and there are more white marks, considered to be “noise,” throughout the image.

### 5.3.3 Binarization

The grayscale edge-enhanced images of Figures 5.3, 5.4, and 5.5 can be converted to a binary image (each pixel either black or white) by means of a threshold binarization process. The MATLAB Toolbox has built-in routines for this operation. For the present application, a threshold value must be specified, which preserves the pixels on the cracks. In order to reverse the image as well, pixel values greater than the threshold value are assigned a value of zero (black) and pixel values less than the threshold are assigned a value of one (white). This operation may be expressed mathematically as:

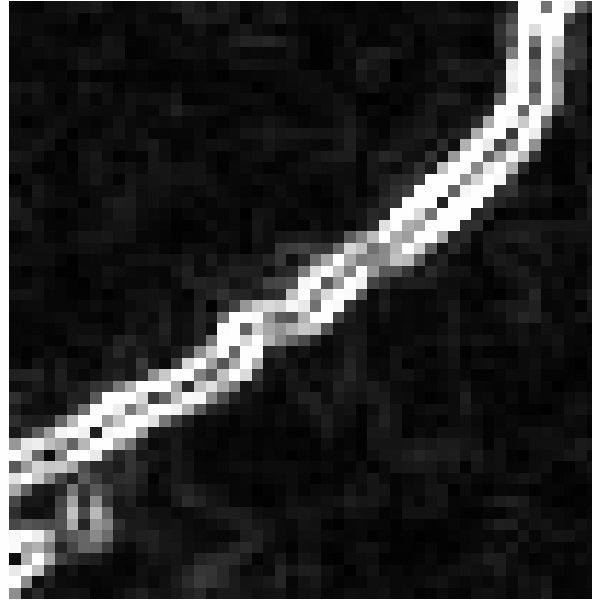
$$BW(x,y) = \begin{cases} 0 & \text{if } E(x,y) \geq k, \\ 1 & \text{otherwise.} \end{cases} \quad (5.6)$$

where  $BW(x,y)$  is the pixel value in the new binary image,  $E(x,y)$  is the pixel value in the edge-enhanced image, and  $k$  is the threshold value.



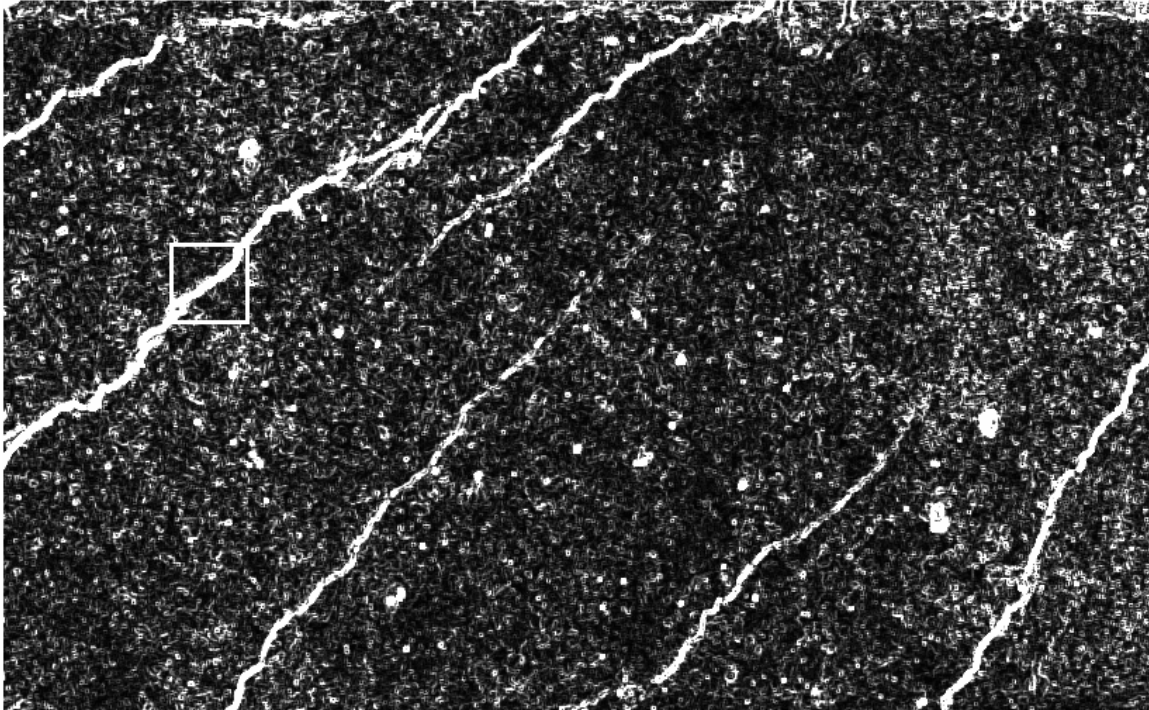
(a) Full Image



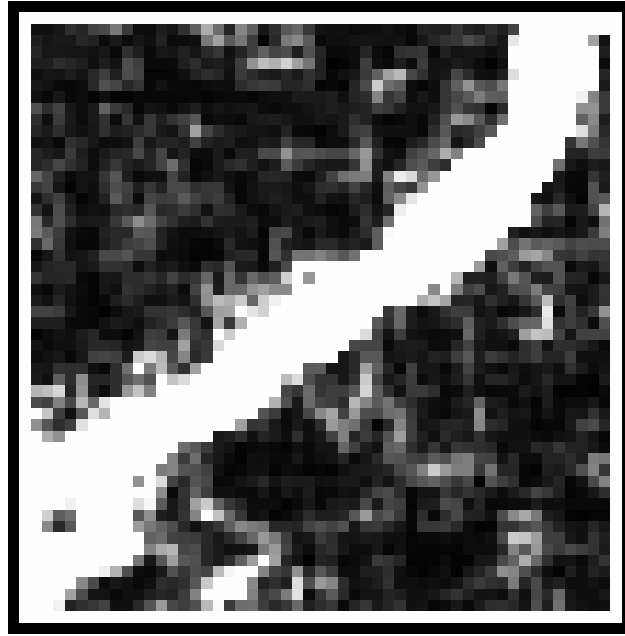


(b) Zoomed Section (Magnification of 7.85)

**Figure 5.4** Edge Enhanced Images of Fig. 5.2 by Second Method (Eqs. 5.2 and 5.4)



(a) Full Image



(b) Zoomed Section (Magnification of 7.85)

**Figure 5.5** Edge Enhanced Images of Fig. 5.2 by Third Method (Eqs. 5.3 and 5.5)

Figures 5.6, 5.7, and 5.8 show the binarized versions of Figures 5.3, 5.4, and 5.5, respectively. The threshold value,  $k$ , was set at 115 for the first two cases, with their similar amounts of background noise and crack widths, but for the third case  $k$  was set at 250 before the values were re-scaled to 255. The results in the third case have narrower cracks and less remaining noise than in the second method and are less dependent upon the choice of the threshold value than in the first method. The third method of edge enhancement and binarization was thus chosen for the remainder of the study.

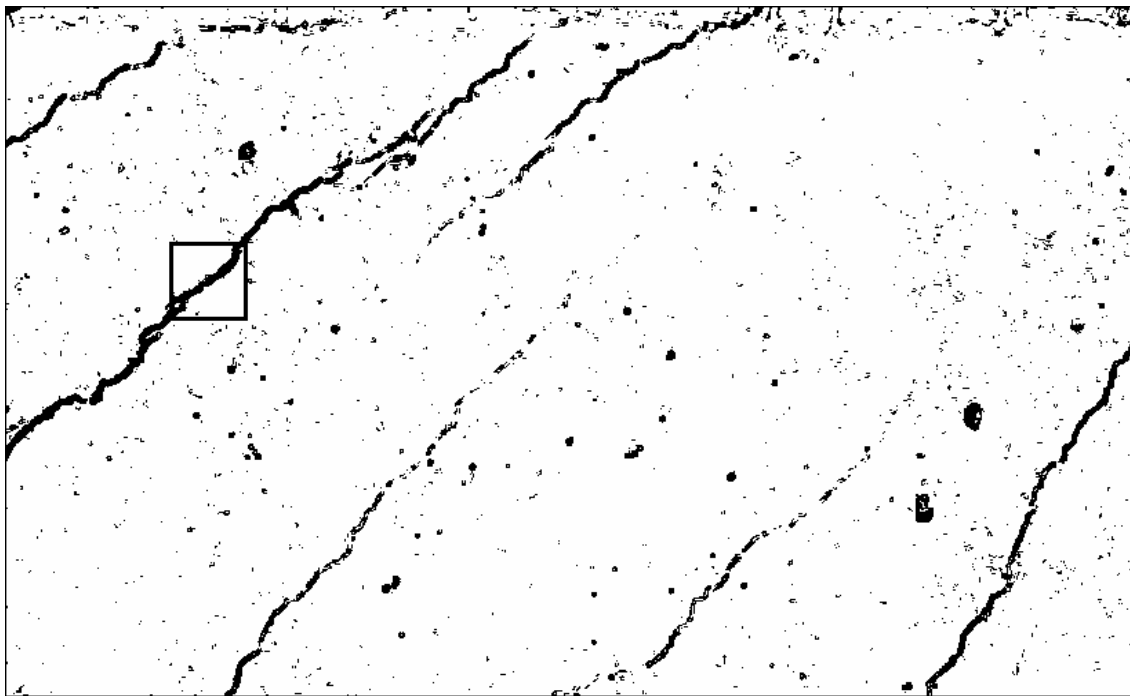
#### 5.3.4 Spot Removal

After being processed by the edge detection method and binarization, the resulting image has black spots off the cracks due to the impurity of the background and air voids in the concrete surface. Before crack quantification, it is necessary to remove this “noise.” Large spots can be removed manually with a cursor, but a “spot remover” algorithm was developed to eliminate the many small spots in a typical image.

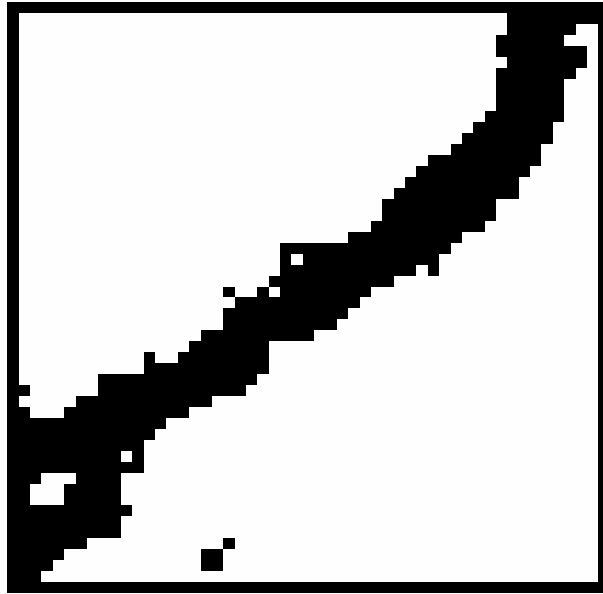
The spot remover moves through the image matrix, and when it comes to a black pixel, it checks the neighborhood of the pixel to determine whether or not the spot is continuous, that is, if it is part of a crack. Figure 5.9 shows the concept of the spot removing process. It starts with the first eight-pixel neighborhood around a black pixel that it comes to (labeled P in Figure 5.9) and checks if any of these surrounding pixels is also black. If not, then this central black pixel is assumed to be a spot and it is removed. Otherwise, the second-level surrounding neighborhood with sixteen pixels is checked in the same way. This process goes on for a predefined number of iterations or levels of surrounding pixel, depending on the user’s definition of the size of a spot.

For this research, this number was set at six iterations. In the example of Figure 5.9, three iterations are sufficient to show that the original pixel, P, is part of a spot, not a crack.

After applying the spot remover algorithm, in most cases there are still some spots on the output image because of thermal cracks, air holes on the concrete surface, and impurity of the surface. These spots remain if their sizes are bigger than the size of the last checked neighborhood. Another reason why some spots remain is that if two spots are too close, the neighborhood operation for one spot catches pixels from the other spot, and it may not sense the discontinuity. After use of the automated spot-removal algorithm, these remaining spots are removed manually. Figure 5.10 shows the final spot removed image of Figure 5.8.

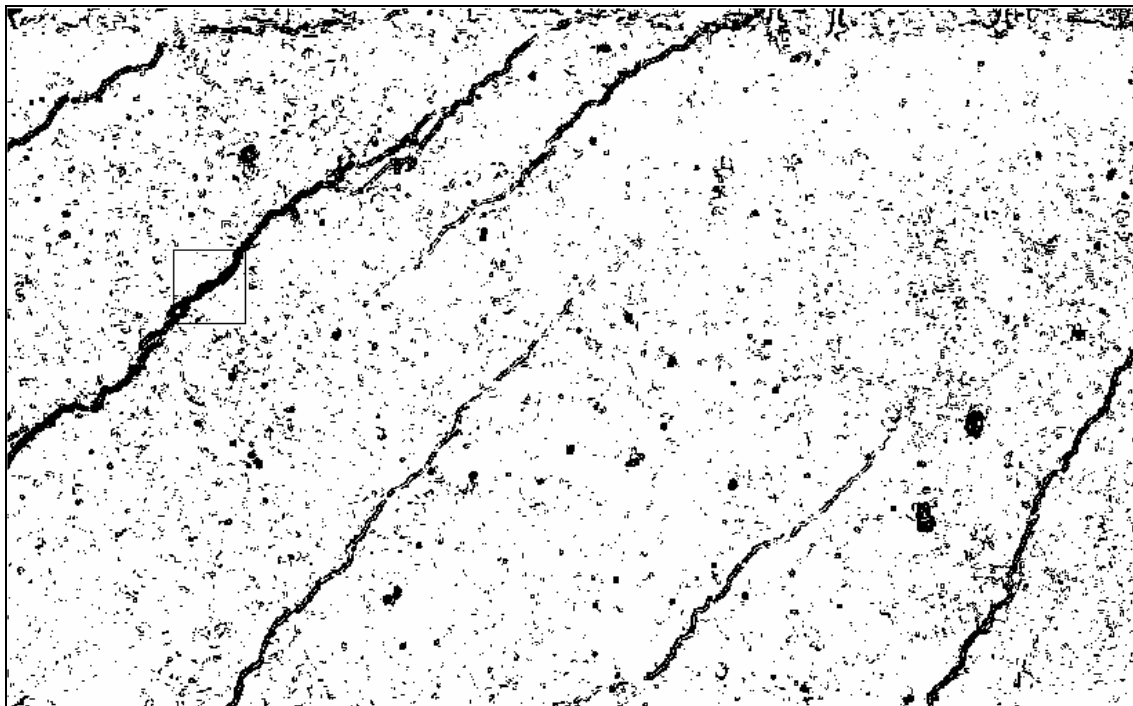


(a) Full Image



(b) Zoomed Section (Magnification of 7.85)

**Figure 5.6** Edge Enhanced Images of Fig. 5.3 After Binarization

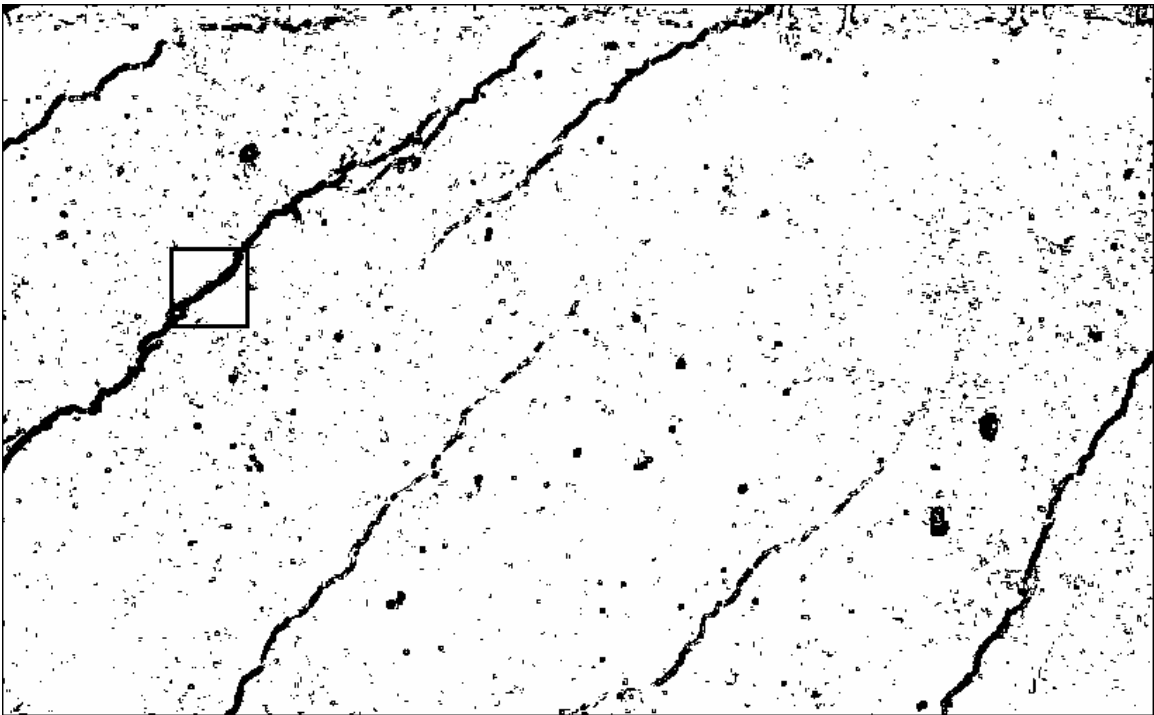


(a) Full Image

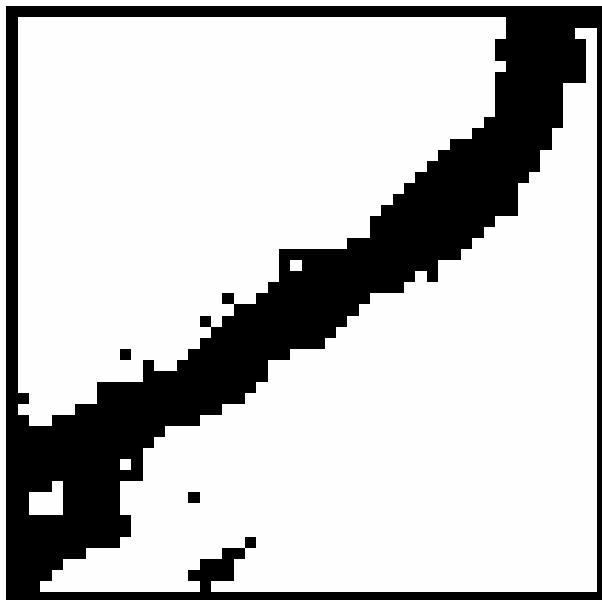


(b) Zoomed Section (Magnification of 7.85)

**Figure 5.7** Edge Enhanced Images of Fig. 5.4 After Binarization



(a) Full Image



(b) Zoomed Section (Magnification of 7.85)

**Figure 5.8** Edge Enhanced Images of Fig. 5.5 After Binarization

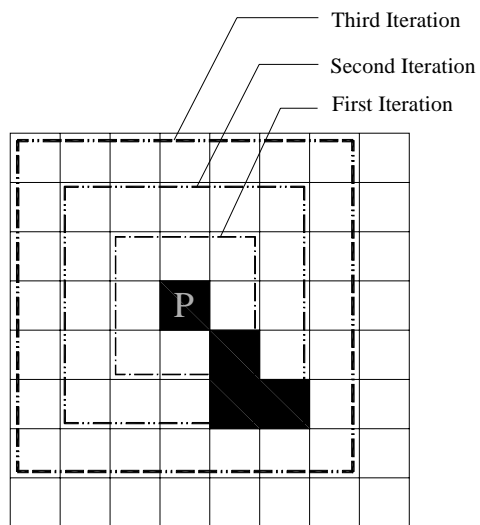


**Figure 5.9** Spot Removing Process

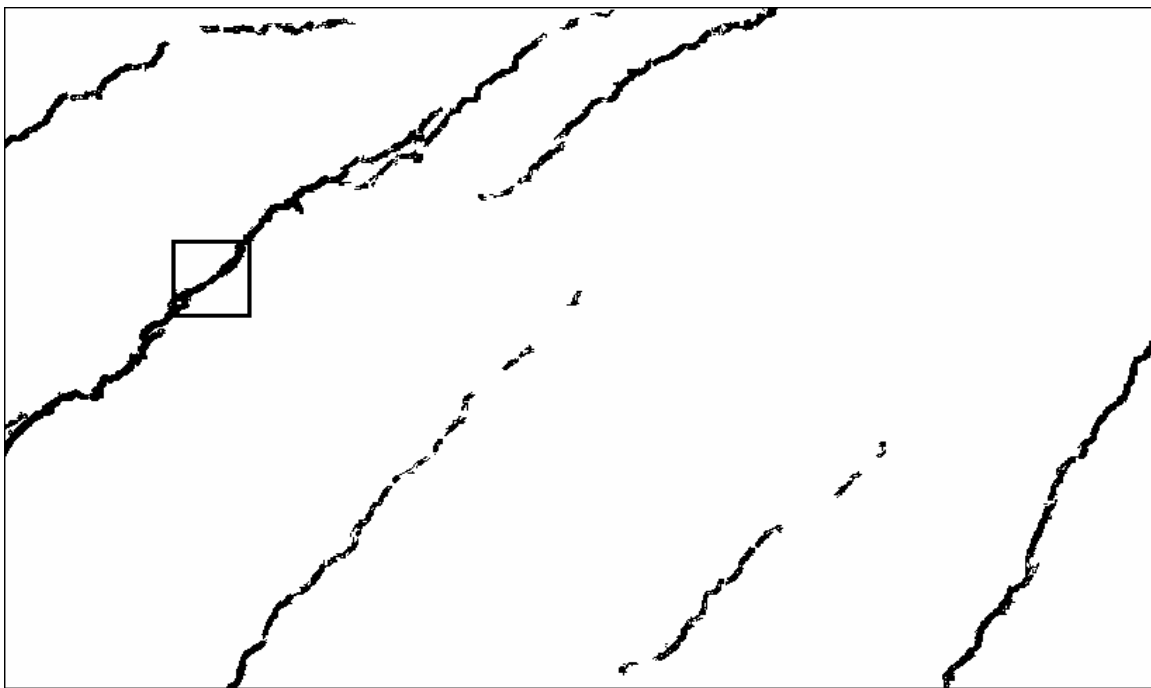
### 5.3.5 Hole Filling

An edge-enhanced image consists of depictions of the boundaries of the cracks, and they generally are not completely solid representations. The crack bodies usually have hollows and white spots after edge detection. These affect the quantitative analysis of the image. For this reason, these openings in the cracks are filled for more accurate analysis. Figure 5.11 shows the resulting image of Figure 5.8 after the hole-filling algorithm.

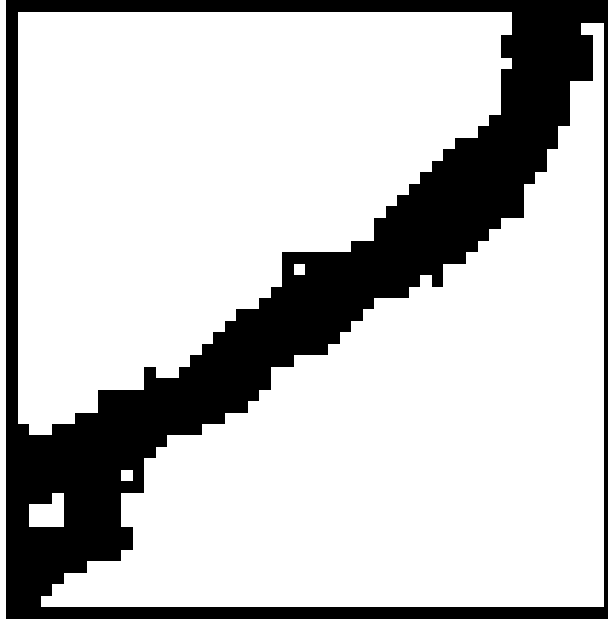
The hole-filling algorithm checks each white pixel's eight-pixel neighborhood. If the number of surrounding black pixels is four or more, then the central white pixel's value is set to zero (black). Since this algorithm adds black pixels to the crack boundaries, it generally results in wider cracks. It might also not work well for very thick cracks; since it only operates in an eight-pixel neighborhood of a pixel, large openings between the cracks edges might not be completely filled.

### 5.3.6 Crack Thinning

The foregoing edge detection algorithm results in representations of the cracks that are wider than the true widths. After the hole filling process, the crack images tend to be even wider. For this reason, MATLAB's thinning algorithm is used to strip off the extra black pixels from the crack images. For the images used in this research, the thinning algorithm was executed twice to get the best representation. A detailed verification with a test case was used to make this determination



(a) Full Image



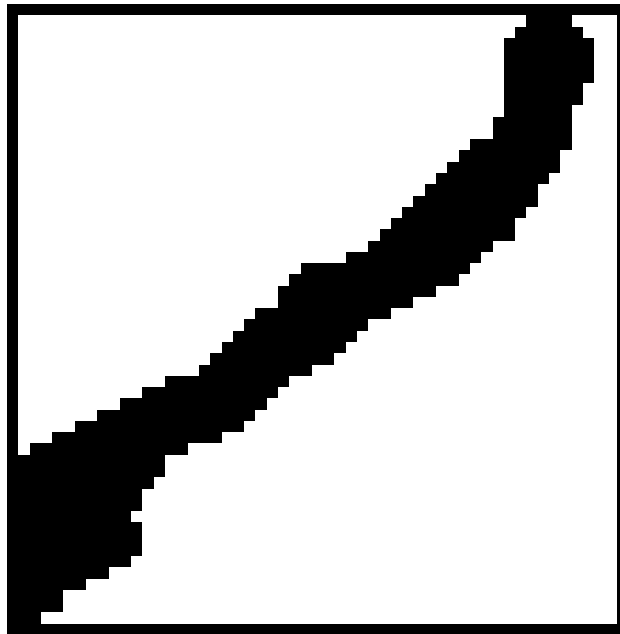
(b) Zoomed Section (Magnification of 7.85)

**Figure 5.10** Spot Removed Images of Figure 5.8



(a) Full Image





(b) Zoomed Section (Magnification of 7.85)

**Figure 5.11** Images of Figure 5.8 after the Hole Filling Process

After the thinning operation the images finally become ready for quantitative analysis. These final crack images are called “binary crack images.” Figure 5.12 shows the output of the first thinning process of Figure 5.11. Figure 5.13 shows the output of the second thinning process, which is considered to be the final crack determined image.

#### **5.4 Algorithms for Crack Quantification**

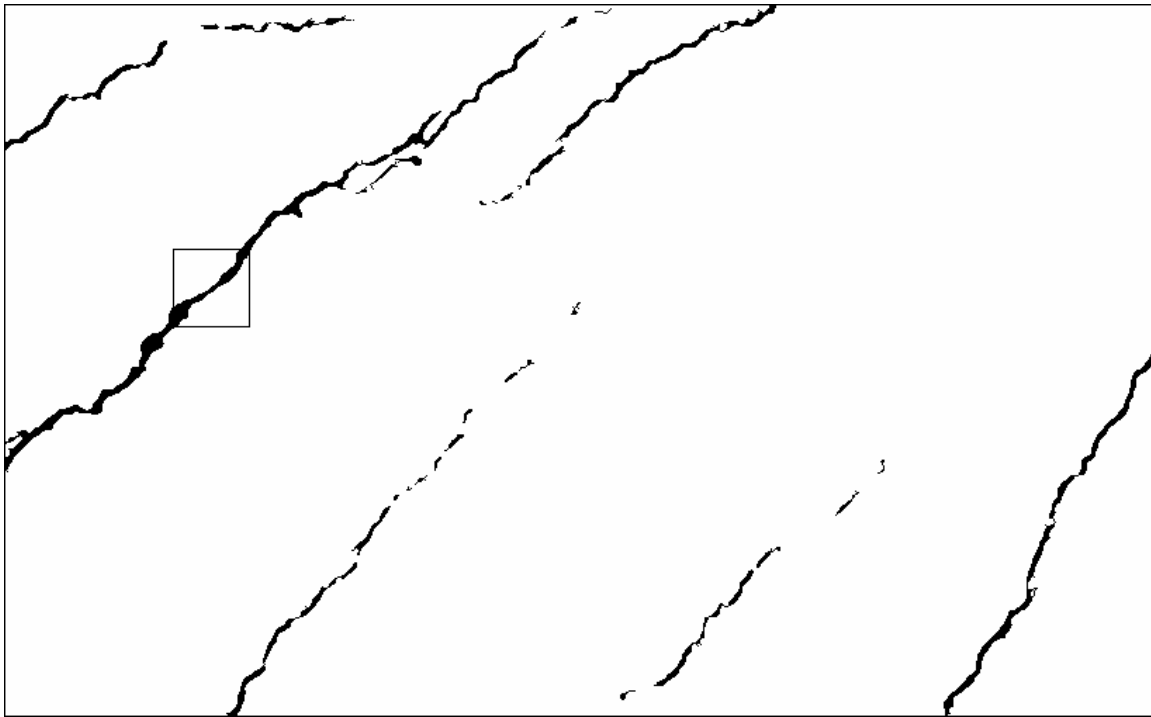
Once an original RGB crack image (JPEG photograph) has been reduced to a binary image with black pixels representing the cracks and white pixels everywhere else, it is fairly straightforward to have the computer count the black pixels for “quantification” of the cracks. When a crack has continuous black pixels along its length, it may be labeled as an “object” by MATLAB’s image processing toolbox and dealt with individually. In this process, the number of cracks in the image is determined automatically, although long cracks with a slight break or two are considered to be more than one crack. It is also of interest to evaluate the average and/or maximum width of a crack. A direct determination of the width, either at a given point along the length or at the point of maximum width, is quite problematic for cracks with any possible inclination. Even the crack length is not as easily determined as one might expect when the crack is inclined because the pixels are arranged as squares with vertical and horizontal sides.

In the following section, the quantities determined by computer algorithms are the number of cracks (carried out simply by labeling), the area of each crack, total crack area, the percentage of the image’s area that is cracked, the length of each crack, the average width of each crack, the overall average crack width, and the maximum among the average widths of the

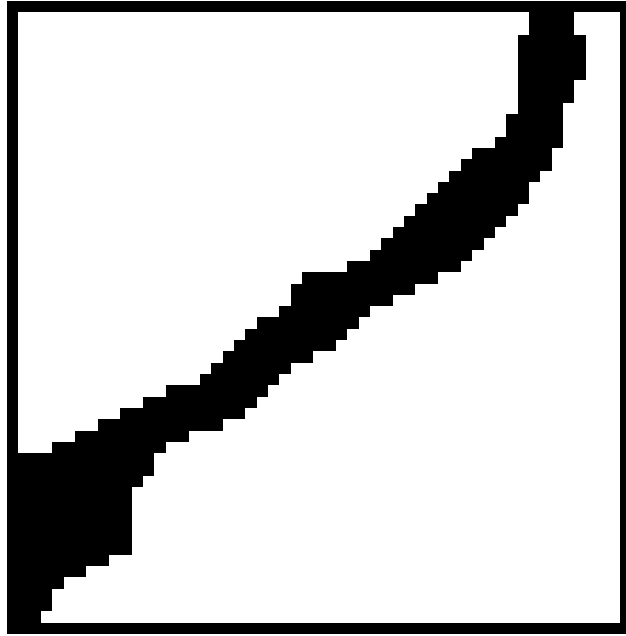
individual cracks. The accuracy of the calculations is evaluated by having the algorithms treat an image with known properties.

#### 5.4.1 Crack Labeling

As mentioned above, the cracks are first labeled with different numbers to investigate each one individually. With MATLAB's labeling function, each object in a binary image is identified. An object is defined as a set of connected black pixels for an image where the background is white and the cracks are black. MATLAB's labeling function returns a matrix of the same size as the input image in which each object is distinguished from the others by assigning all of them different integer numbers. For example, BW is a binary image with two objects as shown next:

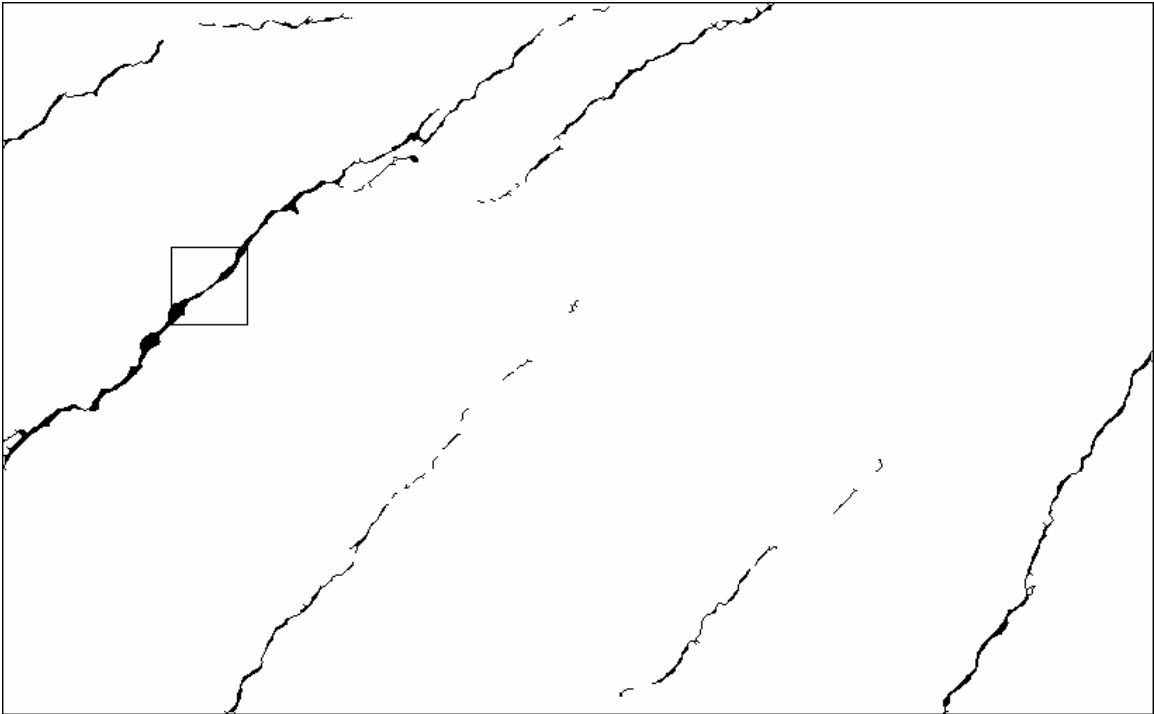


(a) Full Image

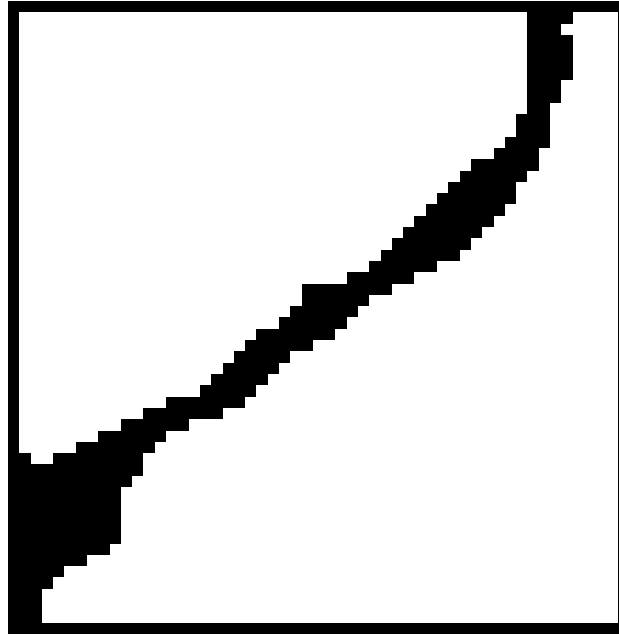


(b) Zoomed Section (Magnification of 7.85)

**Figure 5.12** Crack Images after the First Thinning Process



(a) Full Image



(b) Zoomed Section (Magnification of 7.85)

**Figure 5.13** Final Crack Images after the Second Thinning Process

$$\text{BW} = \begin{bmatrix} 0 & 0 & 1 & 1 & 0 & 0 & 1 & 1 & 1 & 1 & 0 \\ 0 & 1 & 1 & 1 & 0 & 0 & 0 & 1 & 1 & 0 & 0 \\ 0 & 1 & 1 & 1 & 0 & 0 & 0 & 1 & 1 & 0 & 0 \\ 0 & 0 & 1 & 1 & 1 & 0 & 0 & 1 & 1 & 1 & 0 \end{bmatrix}. \quad (5.7)$$

MATLAB's labeling function returns a labeled image BWL that is:

$$\text{BWL} = \begin{bmatrix} 0 & 0 & 1 & 1 & 0 & 0 & 2 & 2 & 2 & 2 & 0 \\ 0 & 1 & 1 & 1 & 0 & 0 & 0 & 2 & 2 & 0 & 0 \\ 0 & 1 & 1 & 1 & 0 & 0 & 0 & 2 & 2 & 0 & 0 \\ 0 & 0 & 1 & 1 & 1 & 0 & 0 & 2 & 2 & 2 & 0 \end{bmatrix}. \quad (5.8)$$

In the output image, BWL, the 1's represent the first object and the 2's represent the second object. By thresholding the output image through an object's index number, that object can be isolated from the image and investigated separately. This feature is used to automate the calculation process.

### 5.4.2 Crack Area

Crack areas are easily calculated by counting the number of black pixels in the crack image. This calculation can be processed for each individual crack from a labeled crack image. The sum of the black pixels in an object must be multiplied by a scale factor to get the actual area. In this research, the digital images were taken from 11" x 18" regions. For an image of 550x900 pixels, the pixel lengths must be scaled to the actual lengths in the image. If the total number of black pixels is 1700, the actual area  $A$  is:

$$A = 1700 \times \frac{11 \times 18}{550 \times 900} = 0.68 \text{ in}^2 \quad (5.9)$$

### 5.4.3 Crack Length

Before starting to calculate the lengths, the cracks are first skeletonized. The skeletonization is simply done by applying the MATLAB thinning algorithm repeatedly until the crack width is only one pixel. A portion of a skeletonized crack with a branch is shown in Figure 5.14. After a crack is skeletonized, the lengths of the connections between the pixels are checked. For two vertically or horizontally connected pixels, the distance between the centers of the pixels is one pixel length. For two diagonally connected pixels, on the other hand, the length between the centers is the length of a pixel diagonal. The algorithm detects how many pixels are connected to each individual pixel and the directions of these connections. In the example of Figure 5.14, for the pixel in row 4 and column 5 there are three connected pixels. Two of them are connected diagonally and one is connected horizontally. Thus, two diagonal and one perpendicular pixel length contribute to the total length from this pixel.

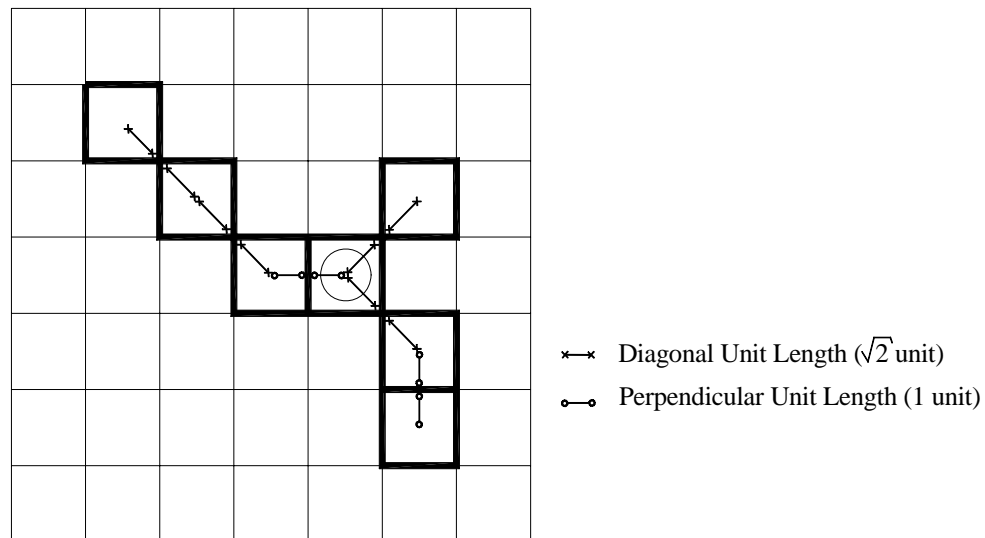


**Figure 5.14** Crack Length Calculation Process

Summing up the diagonal and perpendicular lengths gives the unit length of the crack. As in the determination of the crack areas, this length should be multiplied by a scale factor to get the actual length. For the present 11"x 18" images, if the sum of the pixel lengths of a crack is  $L_u$  for an m-by-n sized image, the actual length of the crack,  $L$ , is:

$$L = L_u \times \frac{11}{m} = L_u \times \frac{18}{n} \text{ (in).} \quad (5.10)$$

#### 5.4.4 Crack Width

Crack width is an important parameter for comparing the effectiveness of the various shear reinforcing details in prestressed concrete beams. Information about these widths can be helpful in understanding the crack controlling behaviors of different shear reinforcement details. In this project, the mean width of each crack is calculated by dividing the crack area by the crack length. Thus, for a crack with a length of  $L$  and an area of  $A$  the mean crack width,  $W$ , is simply:

$$W = \frac{A}{L} \text{ (in).} \quad (5.11)$$

### **5.5 Accuracy of the Technique**

A control image was processed to check the accuracy of the foregoing crack detection and quantification methods. The control image, as seen in Figure 5.15, consisted of a set of lines at different angles on a background similar to the beam web background. There were four groups of lines of equal length, with each group having a different width. These widths were: 0.1181 inches, 0.0591 inches, 0.0197 inches, and 0.0098 inches. Each group had lines with lengths of 3.54 inches at angles of  $0^\circ$ ,  $15^\circ$ ,  $30^\circ$ ,  $45^\circ$ ,  $60^\circ$ ,  $75^\circ$ , and  $90^\circ$ . The size of the image selected was the same as the standard image region of the beams, which was 11"x 18".

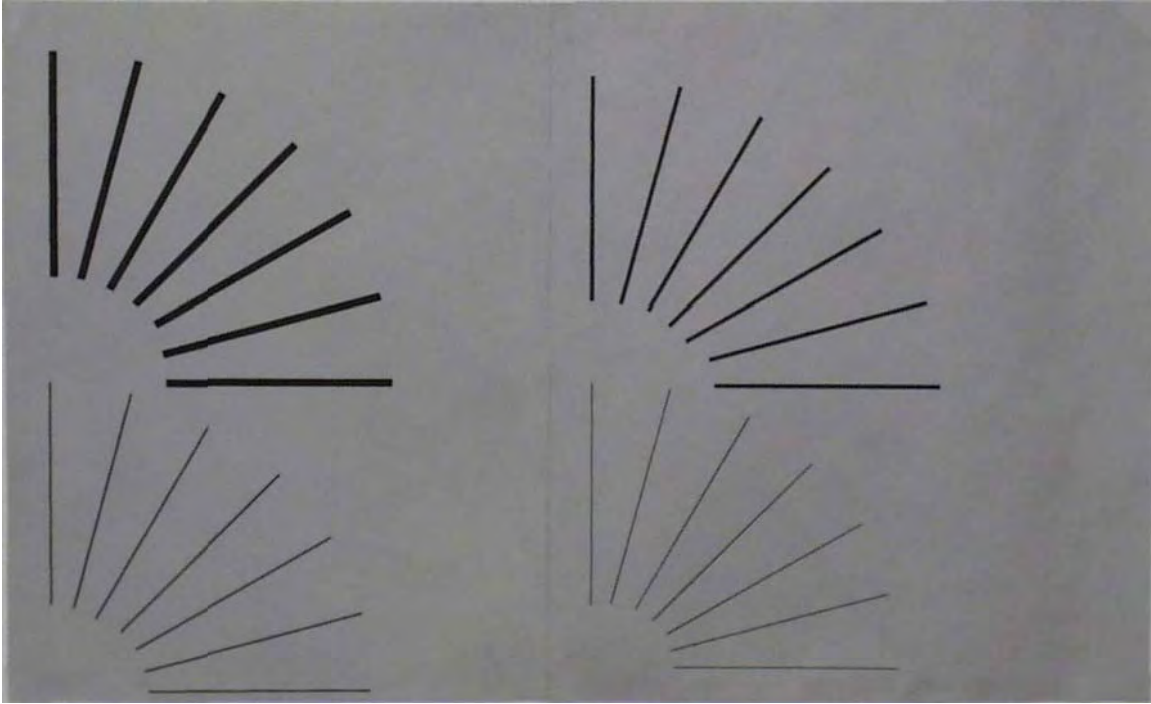


**Figure 5.15** Crack Quantification Control Image

The “crack determined” image of Figure 5.15 by the method of Section 5.2 is shown in Figure 5.16. Careful examination of this figure reveals there are some slight breaks and discontinuities in the borders of the lines. An example of this effect for an inclined line, where the image must represent the line with a horizontal layout of pixels, is shown enlarged in the inset. Irregularities are also seen, however, in the lines that are theoretically perfect vertically and horizontally. It should be remembered in this regard that in taking a picture of a sheet of paper with a camera, it is impossible to align the camera exactly. Nevertheless, the important concerns in this process are the total crack areas and the average crack widths. These line edge deviations did not affect the results very much.

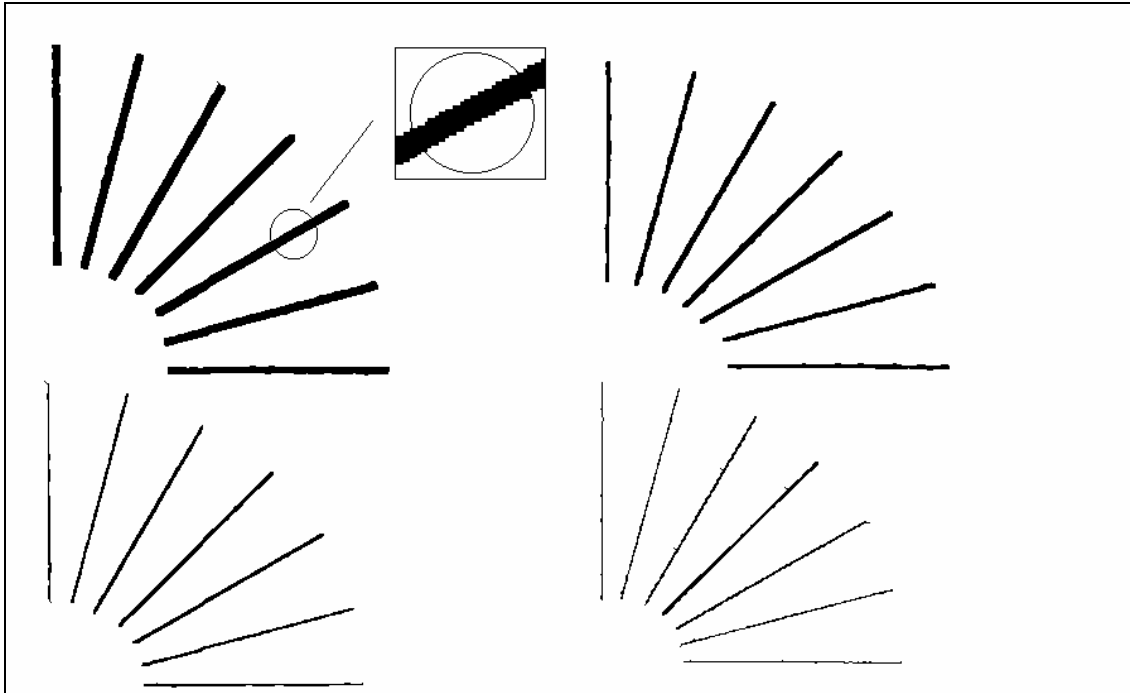


**Figure 5.16** Crack Determined Image of Figure 5.15

The most important problem in obtaining accurate results for the cracks was the resolution of the image. The crack images for this research generally had an approximate size of 550 x 900 pixels. Since the size of each image region on a beam web was 11"x 18", the width of a single pixel was about 0.02 inch. Therefore, the resolution used was insufficient for line widths less than 0.02 inches. For the test image of Figures 5.15 and 5.16, the lines with the smallest width of 0.0098 inches, or about half a pixel size, did not give the expected results. Using a higher resolution digital camera, choosing a smaller region, or taking a closer picture, could solve this problem.

Calculated results for the line for average line widths and the lengths of the lines in Figure 5.16 are given in Table 5.1. These results show that the method could not produce a width as small as 0.01 inches for the thinnest lines, but that it worked rather well for the other cases. There was a tendency for the calculated width to be low for the vertical and horizontal lines and high for the lines inclined at 45 degrees, and the accuracy was best for an actual line width of 0.02 inches, the width of one pixel. The maximum width errors were -30% for the thicker 0° and 90° lines and +15% for the thicker 45° lines. For the intermediate 30° and 60° lines, the width error ranged from -3% to -10%. For the 15° and 75° lines, the width errors ranged from -7% to -20%. Considering the fact that shear cracks are the primary concern of the present research, and that they tend to be inclined at about a 45° angle, it is expected that the errors in the average widths of the beam shear cracks will range from -10 to + 15 percent.



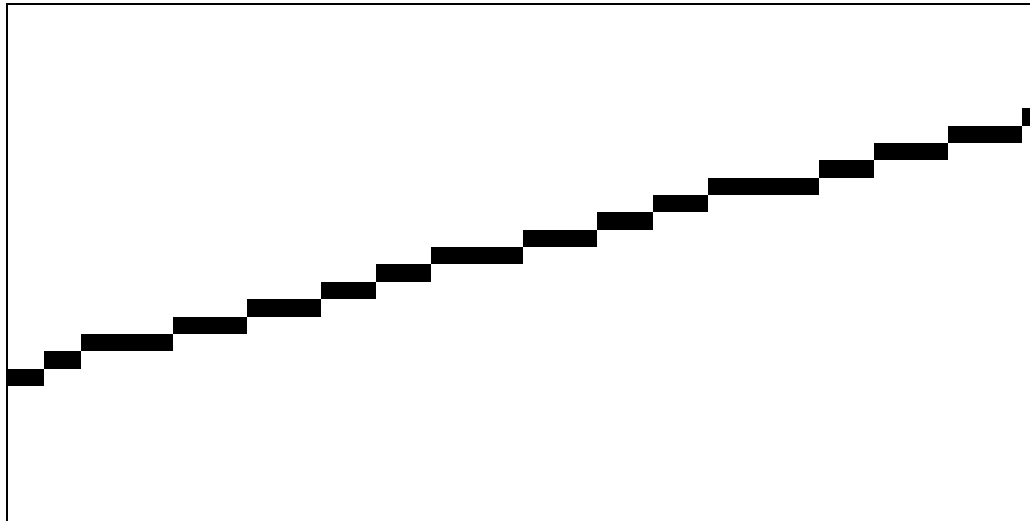
**Table 5.1** Crack Widths and Lengths for the Control Image of Figure 5.15

Actual Crack Width (in)	Calculated Crack Widths by Image Processing (in)						
	0°	15°	30°	45°	60°	75°	90°
0.118	0.096	0.101	0.112	0.134	0.113	0.101	0.098
0.059	0.042	0.053	0.055	0.068	0.056	0.052	0.044
0.020	0.019	0.019	0.020	0.022	0.020	0.020	0.018
0.010	0.018	0.020	0.019	0.020	0.020	0.020	0.018

Actual Crack Length (in)	Calculated Crack Lengths by Image Processing (in)						
	0°	15°	30°	45°	60°	75°	90°
3.543	3.515	3.750	3.635	3.567	3.637	3.731	3.498

The errors in the lengths of the lines in the control image were, as expected, smaller than those for the widths. The maximum length error was found to be 6% among all of the lines. This error depended on the irregular inclination of the pixels at certain angles. Figure 5.17 shows the digital image representation of a skeletonized line at a 15° angle, for which the maximum error occurred. The vertical and horizontal arrangement of the pixel did not accurately calculate the length in this case.



**Figure 5.17** Digital Image Representation of a 15° Straight Line

## 5.6 Calculations for the Example Beam Image

The main concerns of crack properties are the widths, lengths, and areas of individual cracks. The total area of all cracks, overall average crack width, total number of cracks, and maximum average crack width are also important for evaluation of each image. For the example beam image of Figure 5.1, with its crack determined image of Figure 5.13, Table 5.2 (S 4.2) shows the results for individual cracks and overall crack behavior.

**Table 5.2** Properties of the Cracks of Figure 5.13

Crack No	Crack Length (in)	Crack Area (in <sup>2</sup> )	Average Crack Width (in)
1	3.569	0.145	0.041
2	2.667	0.073	0.027
3	16.294	0.865	0.053
4	6.650	0.223	0.034
5	6.633	0.191	0.029
6	4.531	0.118	0.026
7	8.112	0.343	0.042

The other concerned crack properties:

Total Number of Cracks = 7

Total Crack Area = 1.958 in<sup>2</sup>

Overall Average Crack Width = 0.040 in

Maximum Average Crack Width = 0.053 in.

## 5.7 Taking of Digital Images

The west side of the web of each I-beam was marked off in 11" x 18" regions of interest as shown in Figure 5.18, defining the limits of each digital image to be used for crack analysis. Digital images of these regions were taken at various common load increments during testing of each specimen. Digital images of the cracks in these regions were taken at several common load increments as failure or test termination was approached in an effort to obtain images of cracks at common values as near as possible to the failure or termination load in an effort to get maximum crack sizes for evaluation. Even though the intermediate end region shear test configuration is

not shown in Figure 5.18, the region numbers with respect to the support was held similar to the second end region shear test. Regions of primary interest are regions F1 and F2 for the middle region flexural tests, regions S1 and S2 for the first end region shear tests, and regions N1, N2, N3, and N4 for the second and intermediate end region shear tests. Digital images at common load levels for common test parameters were processed and compared using the techniques described in this chapter.

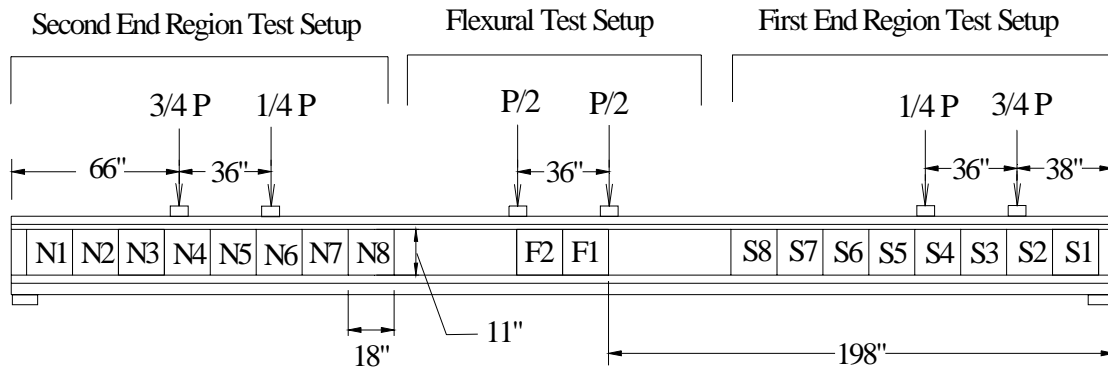


**Figure 5.18** Digital Image Regions Associated with the Load Conditions



## CHAPTER VI

### MIDDLE REGION FLEXURAL TESTS

#### 6.1 Objective and Scope

The purpose of conducting a flexural test on one of the two specimens in a typical pair of beams was to validate the main type of behavior for which these bridge members are designed, that is, behavior in bending. Generally, the size of a TxDOT prestressed concrete I-beam chosen for a particular span, loading, and beam spacing is based on the flexural capacity of the system, with the shear capacity being assumed to be adequate except for unusual cases. Thus, it was deemed wise to verify that the materials and workmanship that produced each beam would, in fact, provide the bending strength on which a designer would have depended. If this feature of the specimen varied significantly from its expected value, this fact would have to be taken into consideration in interpreting all of the other test results. In particular, the evaluation of the shear tests that are of primary interest would have to be modified.

The flexural tests were set up in a traditional way as shown in Figure 6.1. The 36-foot specimen was supported with standard elastomeric bearing pads on four-foot-high concrete pedestals, and the assumed effective length between vertical reactions was 413 inches. The two equal applied loads were centered about midspan and increased in predetermined load increments as described in Section 3.4. The total applied loads, LVDT deflections, and strain gage strains were recorded on the computer at each load increment, and dial gage deflections were hand recorded at the same intervals. Pictures of cracks were taken less frequently, both

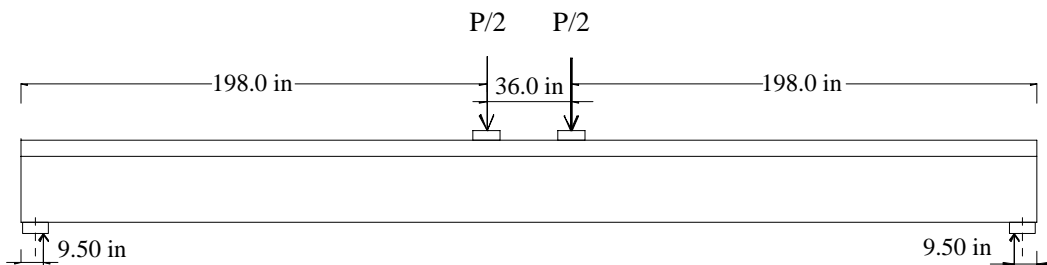


**Figure 6.1** Configuration for the Middle Region Flexural Test

on the marked (east) side with a regular camera and on the unmarked (west) side with a digital cameral. These pictures focused primarily on the central constant-moment region, but the east side pictures also encompassed shear-flexure and shear cracks out as far toward the ends of the beam as these cracks extended. A load-deflection diagram was monitored real time on the computer screen at each increment of loading. There was no need to monitor strand end slips in these tests.

The key results for the flexural tests consisted of load-deflection diagrams, comparisons of the measured load capacities to the theoretical AASHTO capacities, and the cracking in the central, constant-moment region. It should be recalled that these specimens were loaded beyond their theoretical moment capacities but not on material failure to allow the specimens to retain adequate strength for later shear tests on the two ends.

Because the flexural tests results were significantly different for the normal strength concrete (NSC) and high strength concrete (HSC) specimens, the results are grouped into these two categories when presented in this chapter. Within the first category, there were results for specimens with traditional reinforcement, matching WWF reinforcement, simplified WWF reinforcement (uniform wire sizes), and equivalent strength WWF reinforcement (80-ksi wire of uniform size). These different types of shear reinforcement were not expected to affect the bending behavior in these specimens. Again, the tests were simply to verify the flexural performance of the specimens. For high strength concrete, the matching WWF reinforcement case was omitted. In addition, there were no flexural tests on specimens fabricated with the alternate R-bar detail.

## **6.2 Normal Strength Concrete**

There were flexural tests on four specimens with normal strength concrete and different types of reinforcement, as outlined above. The symbol for each of these tests had a second letter “N” for normal strength concrete and ended with an “Fm” to signify a flexural specimen in a middle region flexural test.

### 6.2.1 Load-Deflection Behavior

Load-deflection curves for the four different NSC beams tested in flexure are shown together in Figure 6.2. The horizontal dashed line indicates the load corresponding to the AASHTO moment capacity for the nominal material properties for which the specimens were designed (6-ksi beam concrete, 5-ksi slab concrete, 270-ksi strand strength). All of the specimens reached the expected AASHTO moment capacity, although the stiffnesses and maximum deflections varied somewhat, as discussed below.

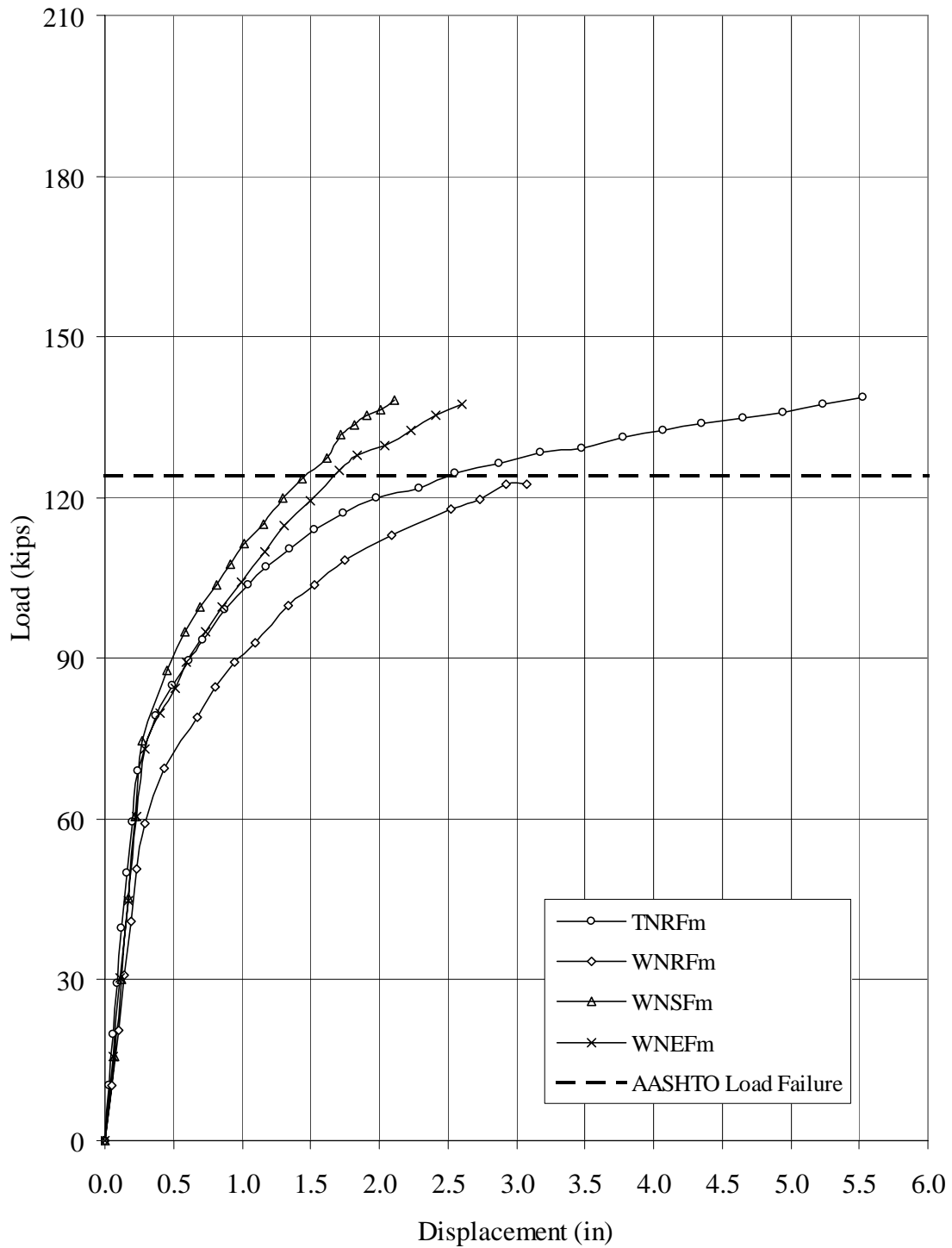


**Figure 6.2** Load-Deflection Curves for NSC Flexural Beam Middle Region Tests

Table 6.1 presents numerical values for the key parameters of the load-deflection curves of Figure 6.2. The parameters in Table 6.1 include the beam stiffness,  $E_b$ , defined as the slope of the initial elastic portion of each curve in kips per inch, the maximum elastic load and deflection, measured at the last load point for which there appeared to be linear behavior, the load at which the first cracks appeared, the load and deflection at the last load before the test was stopped, and the “ductility ratio,” defined as the final deflection divided by the maximum elastic deflection. Table 6.2 shows a comparison between the AASHTO design loads for these specimens and the observed peak loads, plus the criterion used to terminate each test. It should be noted that the AASHTO capacity values in Table 6.2 were determined using experimental concrete strengths for each beam and slab while the corresponding value shown in Figure 6.2 was determined using the design values.

**Table 6.1** Middle Region Flexural Test Load-Deflection Data for Normal Strength Concrete

<b>Beam</b>	<b>Beam</b> Stiffness, $E_b$ (Kips/in)	<b>Max.</b>	<b>Elastic</b>	<b>Cracking</b>	<b>Max.</b>	<b>Final</b>	<b>Ductility</b> Ratio
		Load (Kips)	Deflection (Inches)	Load (Kips)	Load (Kips)	Deflection (Inches)	
<b>TNRF</b>	286	69	0.241	79	139	5.53	23.0
<b>WNRF</b>	203	59	0.291	41	122	3.08	10.6
<b>WNSF</b>	277	75	0.270	88	138	2.11	7.8
<b>WNEF</b>	248	73	0.295	73	137	2.60	8.8



**Table 6.2** Middle Region Flexural Test Terminal Loads for Normal Strength Concrete

Beam	AASHTO Design Capacity (Kips)	Terminal Test Load (Kips)	Ratio	Termination Criterion
TNRF	125	139	1.11	Strains
WNRF	125	122	0.98	Wire Broke
WNSF	124	138	1.11	Strains
WNEF	125	137	1.10	Strains

### 6.2.1.1 Traditional Reinforcement

The load-deflection curve for the traditionally reinforced beam, labeled TNRFm in Figure 6.2, shows that it had a very smooth transition from elastic to inelastic behavior and that it was carried to a considerably larger deflection than any of the WWF-reinforced specimens. Even at the final load, however, there was not a complete loss of stiffness, and the flexural cracks, while large, were evenly spaced and fairly uniform in width. The point at which to terminate the loading was decided by taking the average strain on the top of the slab (as measured by two concrete strain gages), measuring the depth of penetration of flexural cracking up into the slab to estimate the location of the neutral axis in bending, and assuming a linear strain distribution to predict the strain in the strands. The test was terminated when the measured concrete strain reached 0.002 in/in and the strand strain was below 0.035 in/in. The former strain is well below the standard value of 0.003 in/in at which concrete crushing is assumed to occur; the latter value is the strain associated with the guaranteed tensile strength of the strands (including prestressing strain). Both the concrete and steel strains were below their respective limits when the test was stopped.

One of the striking realizations that a person observing this test was bound to have was that the traditionally reinforced beam had a tremendous capacity to deform without failing. The 5.5-inch maximum deflection at the center of the beam at maximum load, shown from an end view in Figure 6.3, made a vivid impression on all observers that a prestressed concrete beam and slab is truly a ductile structural system in bending.

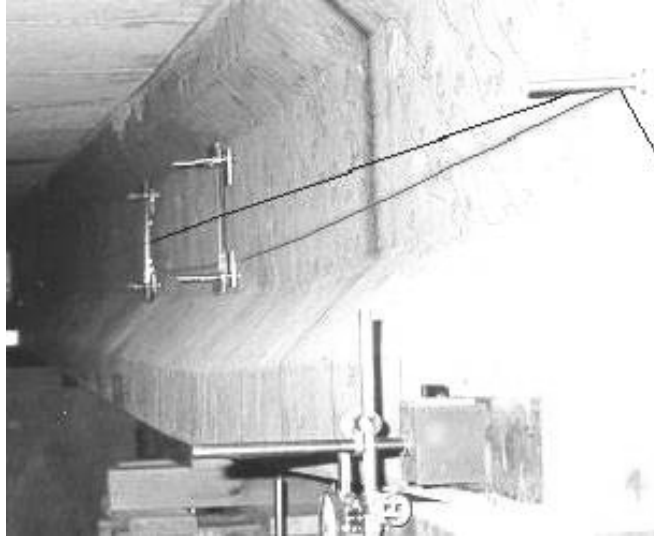


**Figure 6.3** Final Deflected Shape of the Specimen TNRm

#### *6.2.1.2 Matching WWF Reinforcement*

The lowest load-deflection curve in Figure 6.2 is for the flexural test on the specimen using the matching WWF detail that has a one-for-one replacement of the traditional bars with WWF wires, WNRm. It shows a lower initial stiffness than the curve for traditional bars and earlier yielding. Furthermore, the test was stopped just about at the level of the AASHTO capacity load. The only possible reason that could be given for the lower strength of this specimen than the others at comparable deflections was that the flexural cracking in the central, constant-moment region tended to be concentrated at one dominant crack, rather than being distributed more evenly among several cracks.

The reason for the early termination of this test in terms of its applied load was that a loud popping sound was heard at the last load shown, and it was feared that one of the strands had broken. Since the flexural strength of the specimen would be needed for subsequent shear tests on the end portions, the test was stopped at this point, and both corners of the lower flange were reinforced with angles to ensure safety during the later tests. This reinforcement is shown in Figure 6.4. As the result of later tests on the end portions of this and other beams, it was determined that the popping noise was not due to breakage of a strand, but instead was due to breakage of one of the lower longitudinal WWF wires used to complete the WWF cage and provide bottom anchorage of the stirrups. These wires naturally took tension in bending along with the strands. Thus, the test could have been continued to show that the full AASHTO load was exceeded and a larger ductility could have been achieved. However, in the first experience of the phenomenon of longitudinal WWF wire breakage, extra caution was exercised.

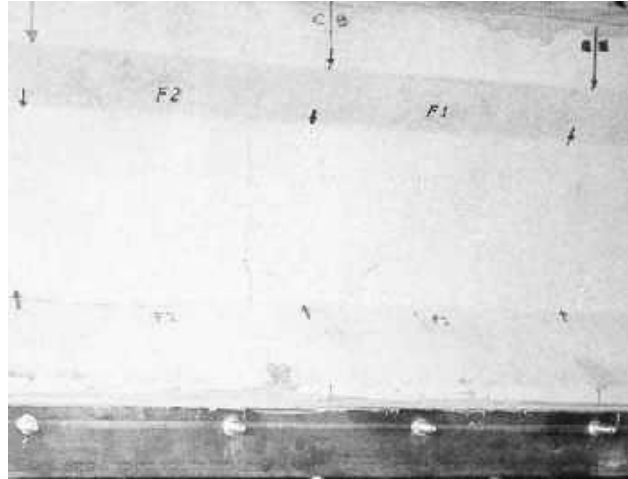


**Figure 6.4** Retrofitted Bottom Flange Reinforcement for Specimen WNR Fm

#### *6.2.1.3 Simplified WWF Reinforcement*

The load-deflection curve in Figure 6.2 for the simplified WWF reinforcement, labeled WNSFm, had almost the same initial stiffness as the traditionally-reinforced beam, and it tracked the initial inelastic portion of that beam's curve very closely as well. However, it exhibited a larger stiffness and strength at larger deflections, perhaps from the added area of the longitudinal WWF wires in the bottom flange. Once again, the loading was terminated before a loss of stiffness was evident. This time it was stopped at a load approximately equal to the maximum load on the traditionally reinforced beam. This allowed crack pictures to be taken at comparable loads without risking a failure of the specimen.

#### *6.2.1.4 Equivalent Strength WWF Reinforcement*

The fourth load-deflection curve in Figure 6.2, the one for the equivalent strength design labeled WNEFm, again showed an almost identical initial stiffness to that of the traditionally-reinforced beam, but a slightly stiffer initial yielding portion as the AASHTO load was approached. This added strength at comparable deflections continued until the test was stopped at a load equal to the maximum load on the traditionally reinforced beam. This difference in behavior can be explained in terms of the added area of the longitudinal WWF wires in the bottom flange. However, these wires were smaller than in the simplified WWF design, so they provided less additional stiffness than in that beam.

#### *6.2.1.5 Summary for Normal Strength Concrete*

In summary for the normal strength concrete flexural tests, there should not have been an effect of the shear reinforcement, either traditional or WWF, in the end regions on the strength in flexure in the middle portions of the beams, but there were measurable differences. The simplified and equivalent strength WWF design exhibited greater inelastic stiffness and strength than the traditionally reinforced beam, apparently due to the tension in the bottom longitudinal WWF wires. However, the WWF specimen with a one-for-one replacement had a lower

stiffness and strength than the traditionally reinforced beam, apparently due to the development of a dominant flexural crack and the breakage of one or more of the bottom longitudinal WWF wires. This breakage prompted early termination of the latter test.

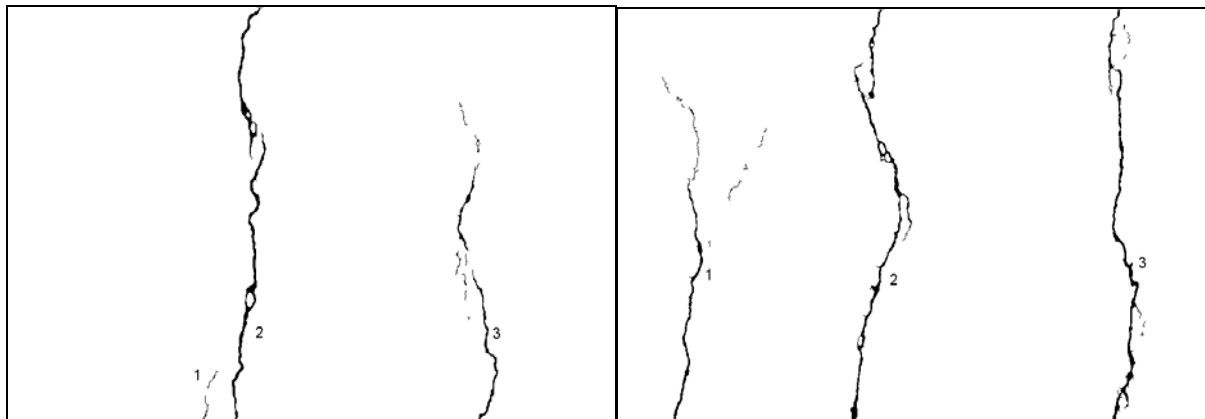
### 6.2.2 Cracking Behavior

For each of the flexural tests, digital pictures were taken at several high load levels of the two 11 x 18-inch regions of the web in the 3-foot constant-moment region. These pictures were then processed by the techniques described in Chapter 5. Also, the cracks on the opposite side of the web were photographed at a number of different load levels after they had been marked in black indicating the length and the load. Only the digital imaging results are presented here, but the other data are available in Texas Tech archives.

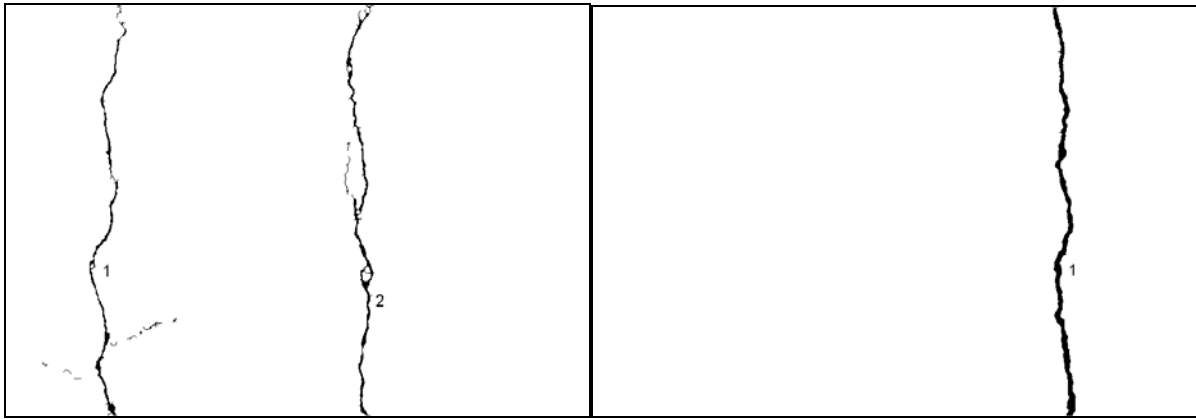
Selected digital imaging crack results for the four normal strength concrete flexural tests of Figure 6.2 are shown in Table 6.3. The two regions considered, F1 and F2, refer to the web areas just to the left and right of the beam centerline, as shown in Figure 5.18. Figure 6.5 shows the cracks in these two regions for the traditionally reinforced beam and for the matching WWF beam at comparable loads of 128 and 123 kips, respectively. In Table 6.3, the numbers of cracks range from three in both regions of the former beam to only one in the F2 region of the latter beam. With an 18-inch image width, three cracks average to a spacing of about 6 inches, which holds except for the region F2 of the WWF specimen (Figure 6.5b). The one crack shown there is much wider than the others because of the lack of distribution of the cracking. This behavior could possibly reflect a weakness in the beam in this region and could account for the lower stiffness and strength of the beam, as discussed earlier.

**Table 6.3** Crack Results for Normal Strength Concrete Flexural Tests

<b>Region</b>		<b>F1</b>				<b>F2</b>			
Test Case	Load Level (Kips)	Number of Cracks	Total Crack Area (in <sup>2</sup> )	Max. Crack Width (in)	Average Crack Width (in)	Number of Cracks	Total Crack Area (in <sup>2</sup> )	Max. Crack Width (in)	Average Crack Width (in)
<b>TNRFm</b>	128	3	1.555	0.069	0.055	3	2.582	0.055	0.051
<b>WNRFm</b>	123	2	1.780	0.051	0.049	1	1.651	0.128	0.128
<b>WNSFm</b>	127	2	0.669	0.038	0.036	3	0.787	0.051	0.039
<b>WNEFm</b>	127	2	0.977	0.056	0.049	2	1.443	0.058	0.055



(a) TNRFm Specimen at 128 kips



(b) WNRfM Specimen at 123 kips

**Figure 6.5** Flexural Cracking in the TNRFm and WNRfM Specimens at 128 & 123 Kips

The total crack areas in Table 6.3 vary quite a bit, from 0.67 square inches to 2.58 square inches. The average crack widths shown were calculated by dividing the total area of cracking by the total length of cracking in the region. The maximum crack widths shown were calculated by dividing the area of each crack by its length and taking the largest value among all the cracks. Thus, these numbers represent average widths, too, but for single cracks. The average widths were fairly consistent except for the F2 region of the matching WWF detail specimen, as discussed above.

It should be recalled that prestressed concrete beams are designed not to crack at service loads, so the crack areas and widths just discussed are simply ways to compare the behavior near flexural failure of specimens with different types of reinforcement. In fact, the flexural test crack results are merely a prelude to the crack studies in the other 3 types of tests on the specimen considered. In the shear tests to failure, the different types of shear reinforcement were expected to have a possible effect on the cracking behavior and the failure load.

### 6.3 High Strength Concrete

There were flexural tests on three specimens with high strength concrete and different types of reinforcement. The “simplified” pattern and not the “regular” pattern was included for 60-ksi design reinforcement. The symbol for each of these tests had a second letter “H” for normal strength concrete and ended with an “Fm” to signify a flexural specimen in a middle region flexural test.

Load-deflection curves for the three high strength concrete beams are shown together in Figure 6.6. The horizontal dashed again line indicates the load corresponding to the AASHTO moment capacity determined using material design values. All of the specimens reached the expected AASHTO moment capacity, but only after a considerable amount of deformation,

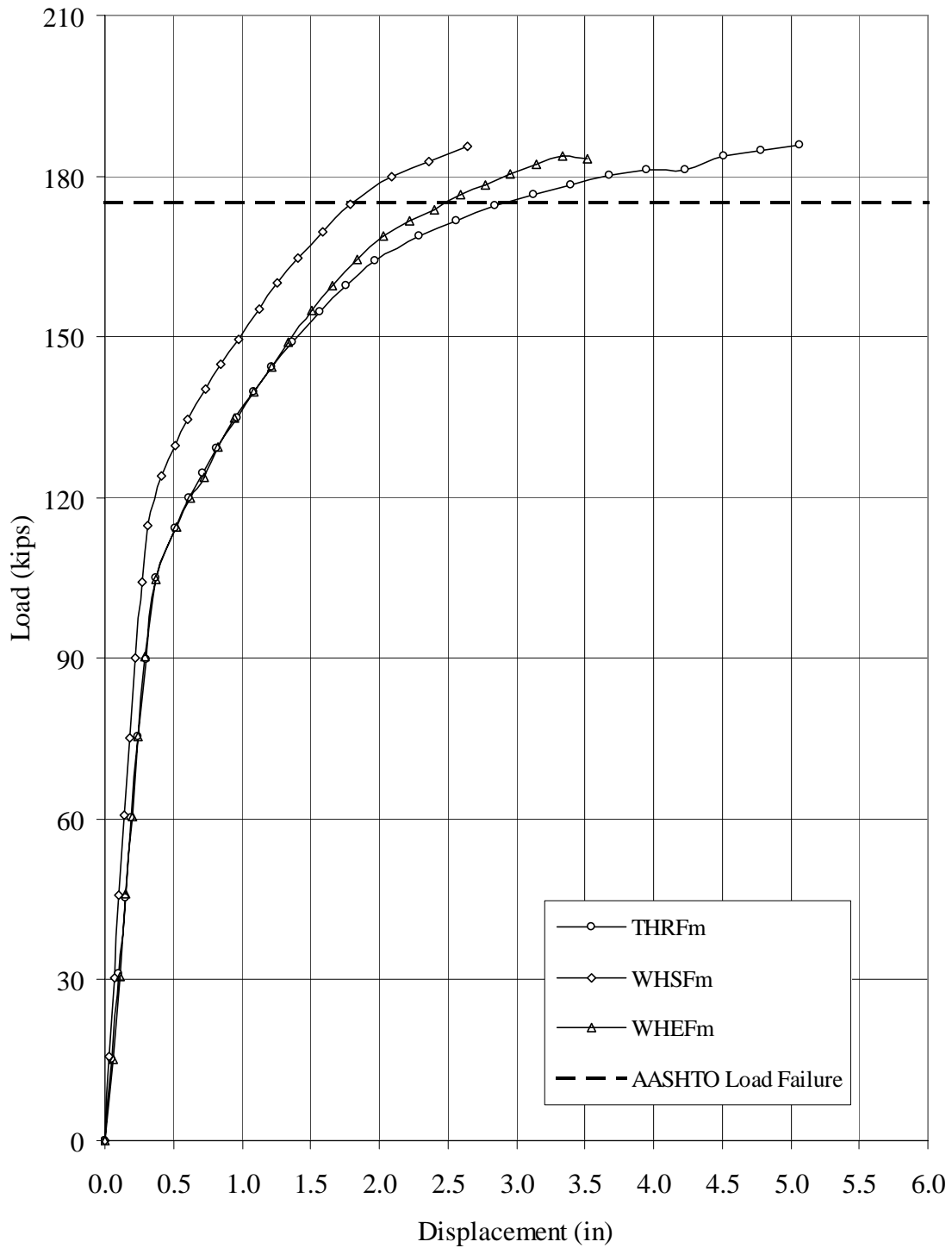


**Figure 6.6** Load-Deflection Curves for HSC NSC Flexural Beam Middle Region Tests

as discussed below. Table 6.4 presents numerical values for the key parameters of the load-deflection curves and Table 6.5 shows a comparison between the AASHTO design loads for these specimens and the observed peak loads, plus the criterion used to terminate each test. Again, the AASHTO design capacities in Table 6.5 were determined using experimental beam and slab concrete strengths.

**Table 6.4** Load-Deflection Data for the HSC Middle Region Flexural Tests

Beam	Beam Stiffness, $E_b$ (Kips/in)	Maximum Elastic		Cracking Load (Kips)	Terminal		Ductility Ratio
		Load (Kips)	Deflection (Inches)		Load (Kips)	Deflection (Inches)	
THRF	286	105	0.367	114	186	5.060	13.8
WHSF	367	115	0.313	115	185	2.640	8.4
WHEF	285	105	0.369	105	183	3.522	9.5

**Table 6.5** Terminal Loads and Failure Modes for the HSC Middle Region Flexural Tests

Beam	AASHTO Design Capacity (Kips)	Terminal Test Load (Kips)	Ratio	Termination Criterion
THRF	175	186	1.06	Strains
WHSF	176	185	1.05	Strains
WHEF	174	183	1.05	Strains

### 6.3.1.1 Traditional Reinforcement

The load-deflection curve for the traditionally reinforced beam, labeled THRF<sub>m</sub> in Figure 6.6, shows that it has a very smooth transition from elastic to inelastic behavior, a fairly consistent second slope after cracking, and then a further loss of stiffness just before it passes the AASHTO design load. The test was terminated again based on the measured and estimated concrete and steel strand strains. While the peak deflection was similar that of the corresponding NSC beam in flexure, the ductility was considerably smaller (a ductility of only 13.8 as compared to 23.0 before). The AASHTO load was exceeded only by six percent at this stage, but the beam evidently could have carried more load if its moment capacity had not been needed for later shear tests. In this test, a popping sound from a bottom WWF wire breaking was not used as a basis to end the test.



### 6.3.1.2 Simplified WWF Reinforcement

The highest load-deflection curve in Figure 6.6 is for the flexural test on the specimen with a uniform pattern of intermediate-size WWF wires, WHSFm. It shows a greater initial stiffness than the curve for traditional bars, slightly more load at yielding, and transition to a third stiffness only after surpassing the AASHTO design load. However, the test was stopped once the load found earlier for the traditionally reinforced specimen was reached and at a considerably smaller deflection. This relationship between the traditionally reinforced and the WWF reinforced flexural specimens is similar to that for the normal strength concrete beams of Figure 6.2.

### 6.3.1.3 Equivalent Strength WWF Reinforcement

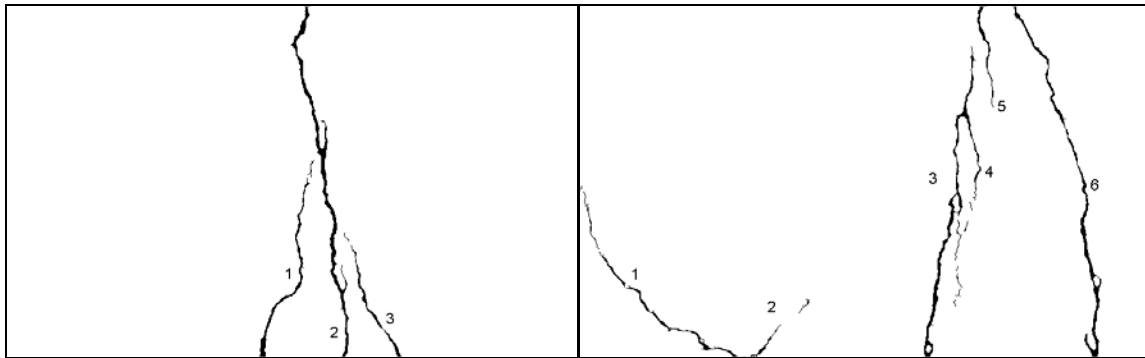
The intermediate curve in Figure 6.6 is for the beam with smaller, 80-ksi steel wires. It matches the curve for the traditionally reinforced beam well into the inelastic range, but maintains its second slope longer and achieves the terminal load of the other two beams at an intermediate final deflection. Once again, the behavior is similar to that in NSC flexural tests: at a given inelastic deflection the equivalent strength (80-ksi steel) WWF specimen carries a greater load than the traditionally reinforced beam, but less than that of the simplified (60-ksi steel) beam.

## 6.3.2 Cracking Behavior

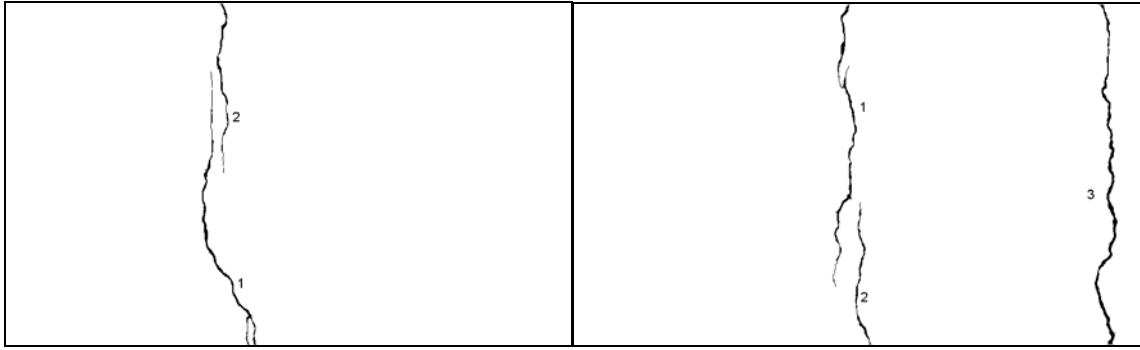
The flexural cracking of the beams with high-strength concrete was quite similar to that of the beams with normal-strength concrete. The summary data for the high-strength beams are presented in Table 6.6 and the processed crack images are given in Figure 6.7. A review of Table 6.6 and Figure 6.7 shows similar crack patterns and sizes for the 3 HSC middle region flexural test specimens. Comparing the numbers in Table 6.6 to those in Table 6.3 for normal-strength concrete, it may be seen that the high-strength beam cracks tended to be somewhat closer together. This could be attributed to the greater number of prestressing strands in the high-strength specimens, which would tend to minimize the crack widths. Recall, however, that because of the greater flexural strength of the high-strength specimens, the loads at which the cracks were compared for the different types of shear reinforcement were higher than for the normal-strength specimens. Thus, a direct comparison between the high- and normal-strength crack results is not possible, even though the moment was approaching the ultimate moment in each case.

**Table 6.6** Crack Results for High Strength Concrete Flexural Tests

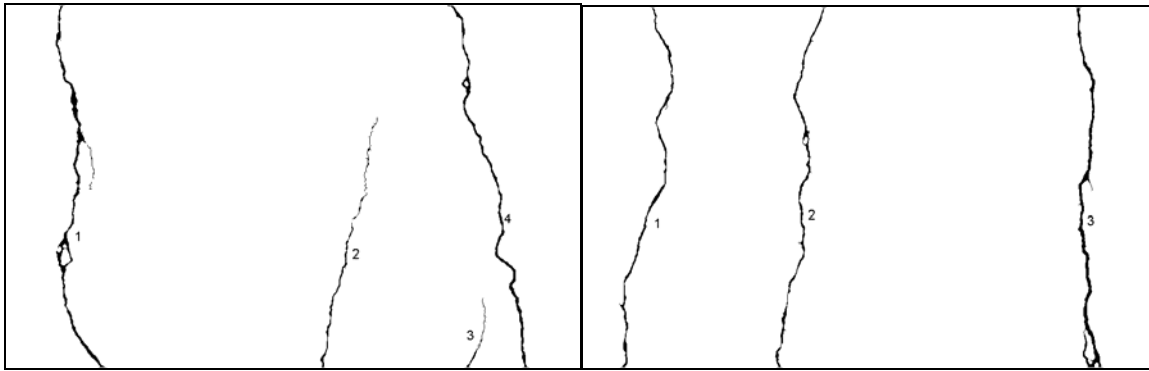
Region		F1				F2			
Test Case	Load Level (Kips)	No. of Cracks	Total Crack Area (in <sup>2</sup> )	Max. Crack Width (in)	Avg. Crack Width (in)	No. of Cracks	Total Crack Area (in <sup>2</sup> )	Max. Crack Width (in)	Avg. Crack Width (in)
<b>THRFm</b>	186	3	1.995	0.086	0.073	4	2.808	0.068	0.054
<b>WHSFm</b>	185	2	0.805	0.050	0.048	3	1.695	0.073	0.059
<b>WHEFm</b>	184	4	2.295	0.064	0.055	3	2.517	0.077	0.061



(a) Final Crack Images of THRFm at 186 kips



(b) Final Crack Image of WHSFm at 185 kips



(c) Final Crack Image of WHEFm at 184 kips

**Figure 6.7** Crack Images for Middle Region Flexural Tests on HSC Specimens

## 6.4 Summary

Again, the responses of the middle region flexural specimens tested during this project were not expected to be significantly affected by the various shear reinforcement details used. However, it was felt that it was important to verify their overall behavior when tested in the primary design mode of a prestressed concrete member. Load-deflection and crack data presented in this chapter shows that the shear reinforcement details used during this project produced members that exhibited adequate flexural responses for both normal and high strength concrete specimens. In most cases, the responses of the members fabricated using the alternative shear reinforcement details exceeded that of the TxDOT standard member.

## CHAPTER VII

### FIRST END REGION SHEAR TESTS

#### 7.1 Objective and Scope

The purpose of the tests called “first end region shear tests” was to compare the shear capacities of the heavily reinforced regions of the beams (where both R and S bars are placed) among specimens with the five alternative types of shear reinforcement considered. Capacities of four alternative types were compared to the capacities of traditionally reinforced beams. As indicated earlier, the four alternative types were: 1) a “matching” WWF detail with a one-for-one replacement of the traditional No. 4 R bars with D20 WWF wires and the traditional No. 5 S bars with D31 WWF wires; 2) a “simplified design” with uniform D26 WWF wires in this region; 3) an “equivalent strength design” with uniform D20 WWF wires of 80-ksi steel; and 4) an “alternate R bar design” with the bottom 90-degree hooks turned parallel to the length of the beam.

In order to determine the shear strength of the first end region of each beam, which for an A-type beam extends 38 inches from the end of the beam as shown in Figure 2.2, the loading and support configuration was set up as shown in Figure 7.1. Since the load nearer the end of the beam was three-fourths of the total, the moment diagram was approximately constant between the two loads. With a standard elastomeric bearing pad at the support, the distance between the resulting support reaction and the first load was approximately 28.5 inches. This horizontal distance was almost the same as the depth of the beam, 28 inches, so the zone of maximum shear, neglecting the slab, was virtually square. Once again, the load was increased in predetermined load increments as described in Section 3.4.

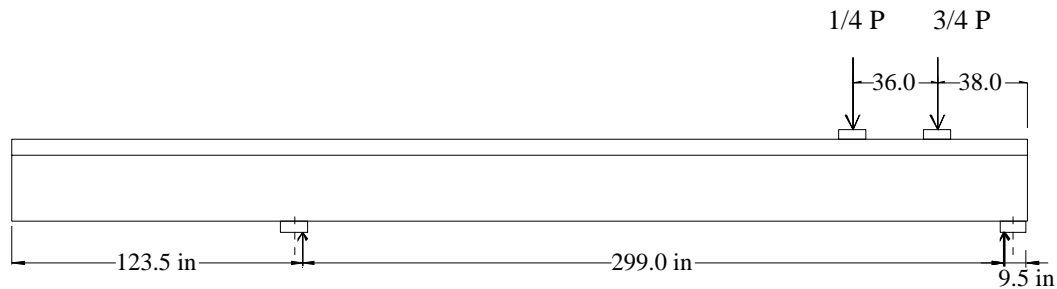


**Figure 7.1** Configuration for the First End Region Shear Test

In these tests, the load was increased to complete failure of the specimen, although failure was not always of the same nature. Because strand slip was expected to play a possible role in the failure of these specimens, it was monitored closely with a digital micrometer. In order to provide a degree of repeatability, two first end region tests were conducted to failure for each type of reinforcement. Except for the alternate R bar tests, the first of each pair of tests was performed on the “flexural specimen” of the pair, that is, the one previously tested in moment as described in Chapter 6. The second specimen was one that had not been tested in flexure, and it was called the “pristine specimen” of the pair. It was observed that cracking during the flexural tests did not extend into the first end regions of the beams, so the ultimate strength results should have been comparable. However, the stiffnesses of the flexural beams were expected to be lower than those of the pristine beams because of their prior cracking. For the alternate R bar specimens, no flexural test was performed, and only one first end region shear test was conducted on a pristine specimen since the alternate R-bar specimens were tested late in the project, and at that time, the intermediate end region shear tests were expected to yield more pertinent data.

Pictures of cracks were taken at every two or three load increments, both on the marked (east) side with a regular camera and on the unmarked (west) side with a digital camera. These pictures focused only on the first end region and the constant moment and shear-flexure regions next to it, that is, regions S1 through S2 in Figure 5.18.

Once again, beams with normal strength concrete and with high strength concrete were included in the test program, although only normal strength beams were considered with the alternate R-bars. As in Chapter 6, the results for the two concrete strengths are presented separately since the flexural reinforcements as well as the concrete strengths were different.

The key results for the first end region tests consisted of load-deflection diagrams, end slip measurements, comparisons of the measured load capacities to the theoretical AASHTO shear capacities, and the cracking in the first end region. These specimens were all carried to failure. In many cases, strand slip clearly precipitated the failure, and in some

cases, a combination of strand slip and diagonal compression between the end support and the nearest load characterized the failure.

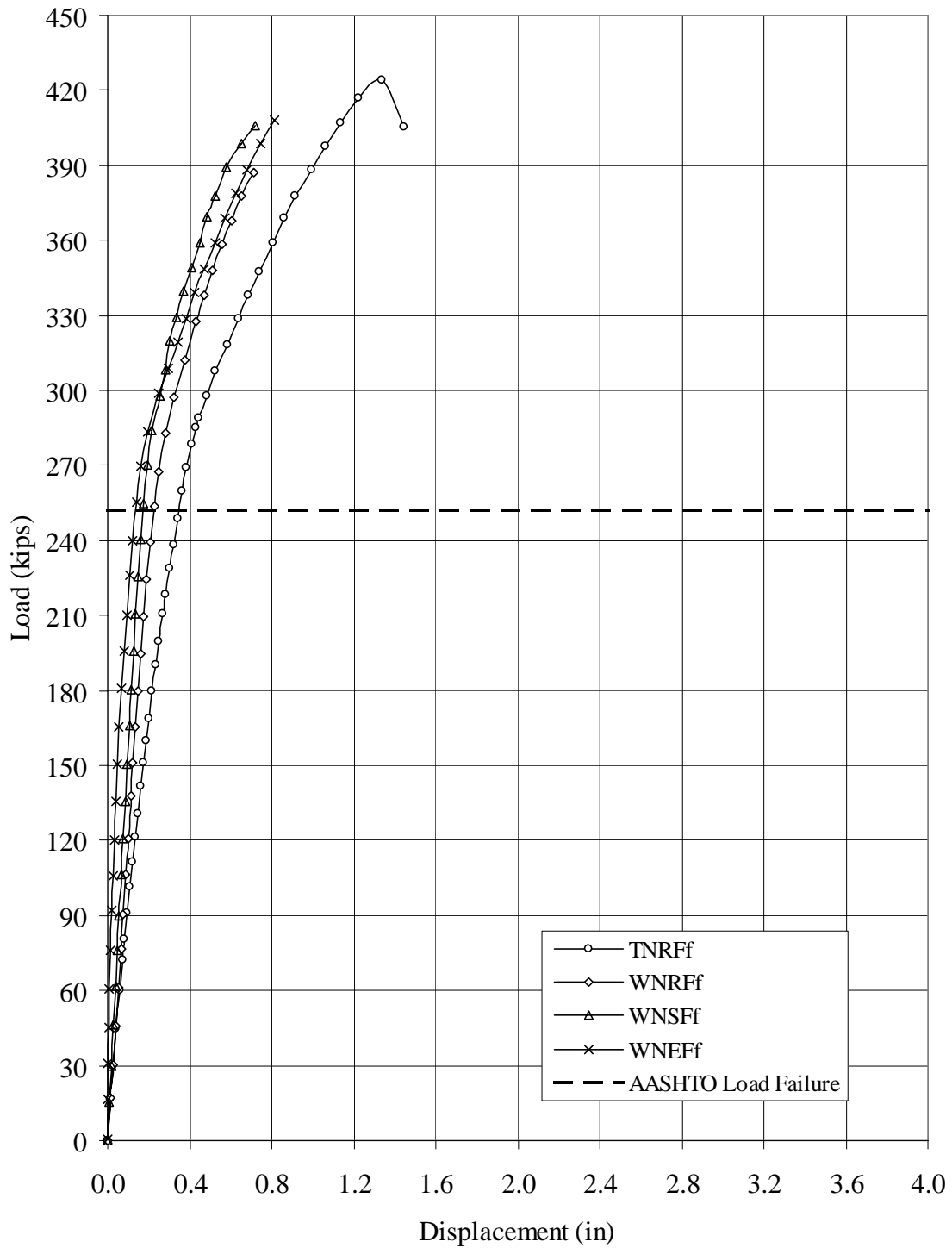
## **7.2 Normal Strength Concrete**

First end region shear tests were conducted on four “flexural specimens” and five “pristine specimens” fabricated with normal strength concrete and different types of reinforcement. The symbol for each of these tests had a second letter “N” for normal strength concrete. Those for the flexural specimens ended with an “Ff” to signify a flexural specimen in a first end region test, while those for the pristine specimens ended with a “Pf” to signify a pristine specimen in a first end region test.

### **7.2.1 Load-Deflection Behavior**

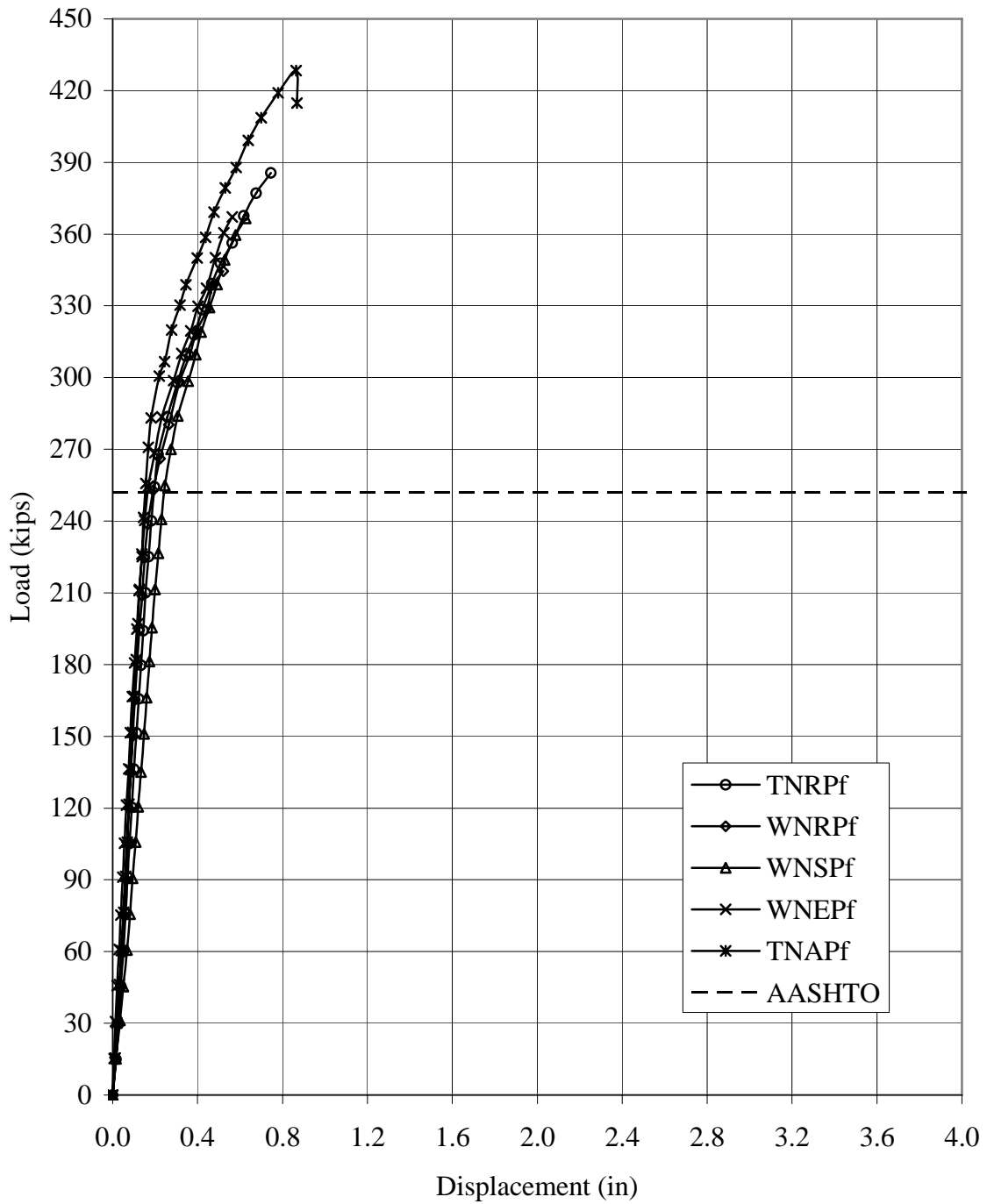
Load-deflection curves for the nine normal strength concrete beams tested in the first end region are shown in Figure 7.2 for the flexural specimens and in Figure 7.3 for the pristine specimens. In each figure, the horizontal dashed line indicates the load corresponding to the AASHTO shear capacity for the nominal material properties for which the specimens were designed (6-ksi beam concrete, 5-ksi slab concrete, 270-ksi strand).

Table 7.1 presents numerical values for the same key parameters of the load-deflection curves of Figures 7.2 and 7.3 as presented in Table 6.1 for the flexural tests. Table 7.2 shows a comparison between the AASHTO design loads for the specimens and the observed peak loads, plus the mode of failure, which varied between strand slip and compression strut failure. While all of the specimens exceeded the expected AASHTO shear capacity by a considerable margin, there were trends that are worth noting.



**Figure 7.2** Load-Deflection Curves for the NSC Flexural Beam First End Region Tests





**Figure 7.3** Load-Deflection Curves for the NSC Pristine Beam First End Region Tests

**Table 7.1** Load-Deflection Parameters for the NSC First End Region Tests

Beam	Beam Stiffness, $E_b$ (Kips/in)	Max.	Elastic	Cracking Load (Kips)	Max.	Final	Ductility Ratio
		Load (Kips)	Deflection (Inches)		Load (Kips)	Deflection (Inches)	
<b>TNRF</b>	761	229	0.301	121	424	1.447	4.8
<b>WNRF</b>	1,114	254	0.228	138	387	0.711	3.1
<b>WNSF</b>	1,406	270	0.192	136	406	0.717	3.7
<b>WNEF</b>	2,112	226	0.107	151	408	0.813	7.6
<b>TNRP</b>	1,247	268	0.215	136	386	0.745	3.5
<b>WNRP</b>	1,437	239	0.166	120	344	0.521	3.1
<b>WNRP</b>	1,036	255	0.246	121	367	0.627	2.5
<b>WNEP</b>	1,527	255	0.167	136	367	0.564	3.4
<b>TNAP</b>	1,623	271	0.167	210	428	0.867	5.2

**Table 7.2** Terminal Loads and Failure Modes for the NSC First End Region Tests

<b>Beam</b>	<b>AASHTO Design Capacity (Kips)</b>	<b>Failure Load (Kips)</b>	<b>Ratio</b>	<b>Failure Mode</b>
<b>TNRF</b>	252	424	1.68	CS+SS+SP
<b>WNRF</b>	251	387	1.54	SS
<b>WNSF</b>	296	406	1.37	CS+SS
<b>WNEF</b>	304	408	1.34	CS+SS
<b>TNRP</b>	256	386	1.51	SS
<b>WNRP</b>	256	344	1.34	SS
<b>WNSP</b>	296	367	1.24	CS+SS
<b>WNEP</b>	304	367	1.21	SS
<b>TNAP</b>	259	428	1.65	SS

CS = Compression strut failure  
SS = Strand Slip failure  
SP = Shear / Punching slab failure

Figures 7.2 and 7.3 show that the initial slopes varied more for the flexural specimens than for the pristine specimens, and that there was no consistent trend for the flexural specimens to have lower slopes, as expected. This was attributed to the problem of initial seating of the beams on their elastomeric bearing pads at the nearby support and the sensitivity of the slope to this effect on the deflection for tests with very large stiffnesses. The loads at initial cracking, at maximum elastic behavior, and at failure were all more consistent than the stiffnesses.

#### *7.2.1.1 Flexural Specimen with Traditional Reinforcement*

The load-deflection curve for the traditionally reinforced flexural beam, labeled TNRFf in Figure 7.1, shows that it had a lower stiffness and a larger maximum deflection than any of the other flexural specimens. This beam also had the largest terminal load by a

slight margin, and its failure was distinguished from all of the other first end region failures by the extent to which compression strut failure seemed to combine with strand slip and pure shear. This feature was evidenced by a shear crack all the way through the slab so that the load point nearest the end appeared to have punched through the slab, as shown in Figure 7.4. Significant strand slip seemed to hold off until the compression strut failure occurred, which was not true in most of the tests. Figure 7.5 shows a side view of the compression strut failure of the TNRFf specimen.

Since strand slip played a role in nearly all of the first end region tests, it is useful to examine it more carefully. Figure 7.6 shows the measured strand slips as functions of the applied load for the TNRFf specimen. The ten strands are shown in Figure 7.7, where

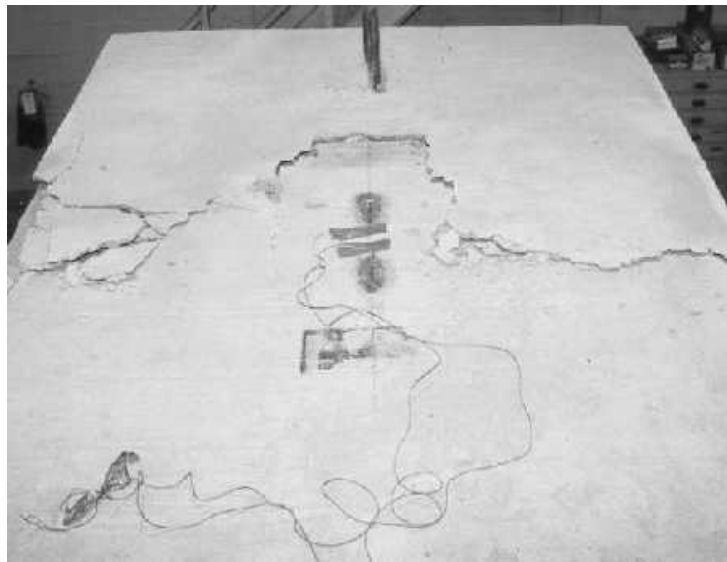


**Figure 7.4** Punching and Shear Failure of the Slab of the TNRFf Specimen



**Figure 7.5** Compression Strut Failure of the TNRFf Specimen

the six unharped ones are numbered from left to right across the bottom row, then from left to right in the top row. Figure 7.6 shows that slip initiated first in the top two unharped strands, which was typical for the normal strength concrete specimens. Apparently, the upward reaction at the end of the beam helped to confine the concrete around the lower strands enough to keep them from slipping first. In Figure 7.6, once slip in all the strands had started, the rate of slip (slope of the slip curve) seemed to be approximately constant up to the failure load in diagonal compression. Note that the largest slip up to failure was only 0.04 inches in this case, and past experience (Burkett, et al, 1999) has shown that a slip failure typically does not develop until a slip of approximately 0.10 inches. This is a further indication that the terminal load in this particular case was controlled by the compression strut failure.

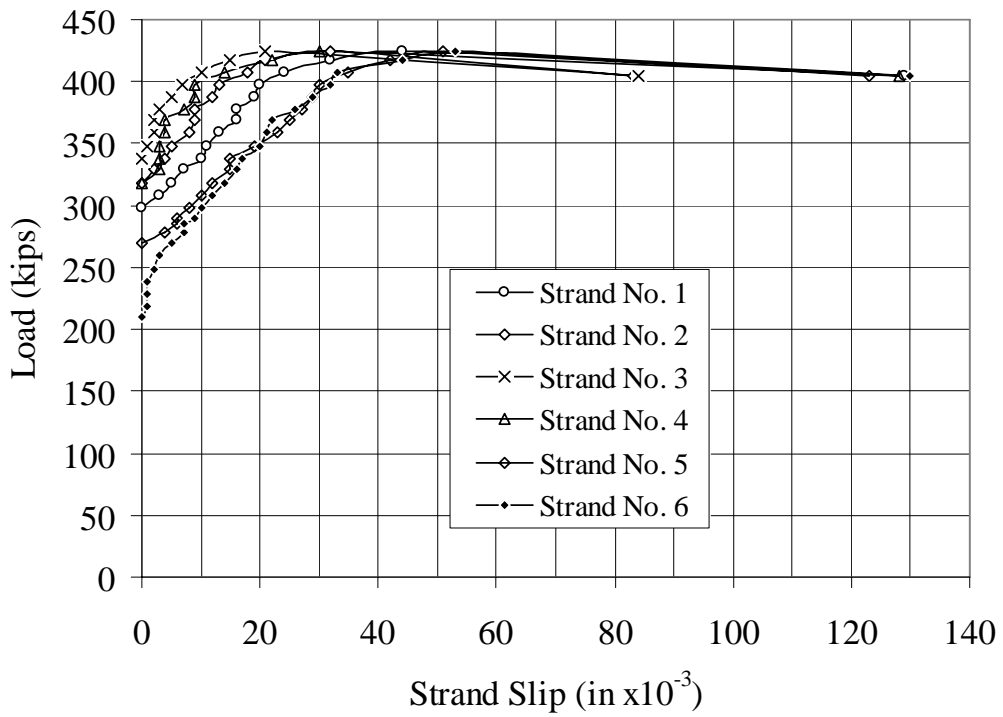


**Figure 7.6** Load vs. Strand Slip for the TRNFf Specimen

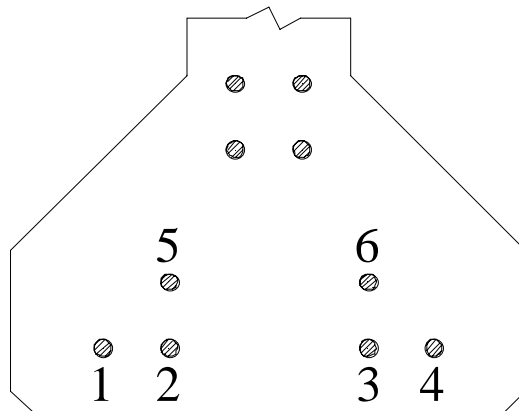


**Figure 7.7** Strand-Slip Numbering Identification

Other features of note in the load-deflection diagram for the TNRFf specimen are that the second slope of the curve is almost linear and that the maximum elastic load is close to the AASHTO design load. The second slope was maintained right up to failure of the beam, showing that a brittle type of failure occurred. By isolating the curve for the TNRFf specimen, Figure 7.8 shows these features more clearly. It should also be noted from Table 7.1 that slight hairline cracking of the beam web started well before the AASHTO load was reached (121 kips vs. 252 kips), and this cracking load did not correlate with the load judged to represent the maximum elastic load, which was 229 kips.

#### 7.2.1.2 Flexural Specimen with Matching WWF Reinforcement

When tested in the first end region, the flexural beam with matching WWF reinforcement had a considerably higher initial stiffness than the traditionally reinforced beam, but about a ten percent lower ultimate load. The lower ultimate load in this test was clearly associated with a strand slip failure, that is, splitting of an end portion of the lower flange through a strand, as seen

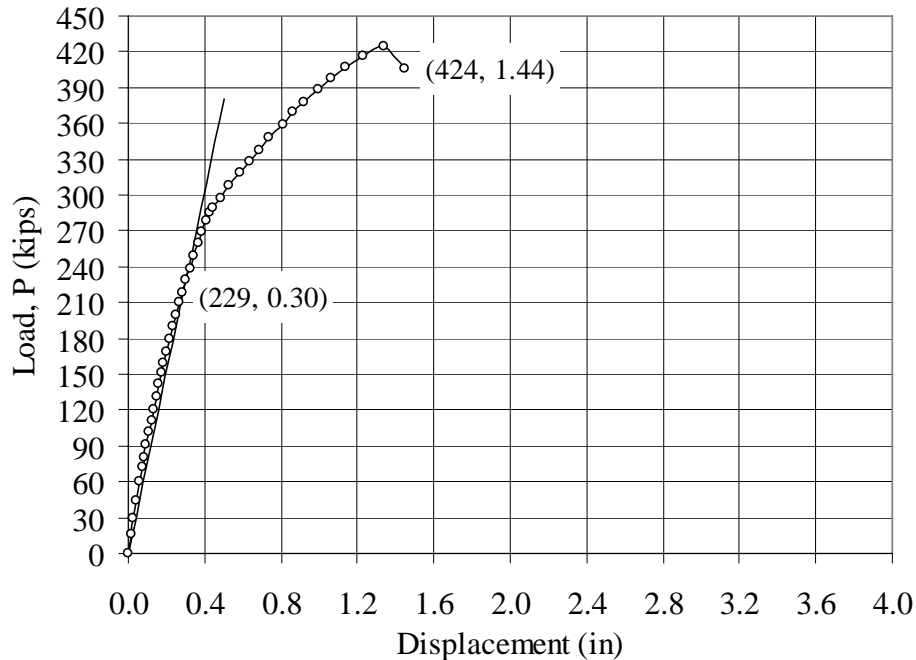


**Figure 7.8** Load-Deflection Curve for the TNRFf Beam

in Figure 7.9, before web failure in compression. In this test, strand slip was first detected in a lower strand (No. 1) at a load of 237 kips as opposed to 308 kips for the TNRFf specimen, so it is not surprising that slightly earlier strand slip failure occurred. In fact, the peak beam moment in the first end regions test was within the transfer length of the strands, so a strand slip failure was highly probable.

Despite the difference in failure mode and a ten percent difference in ultimate load, the specimen with matching WWF, WNRff, had a load-deflection behavior generally comparable to that of the traditionally reinforced specimen, TNRff. In both cases, the behavior was linear up to the AASHTO design load and a sudden (brittle) failure occurred at a load over 50 percent greater than the AASHTO design load.

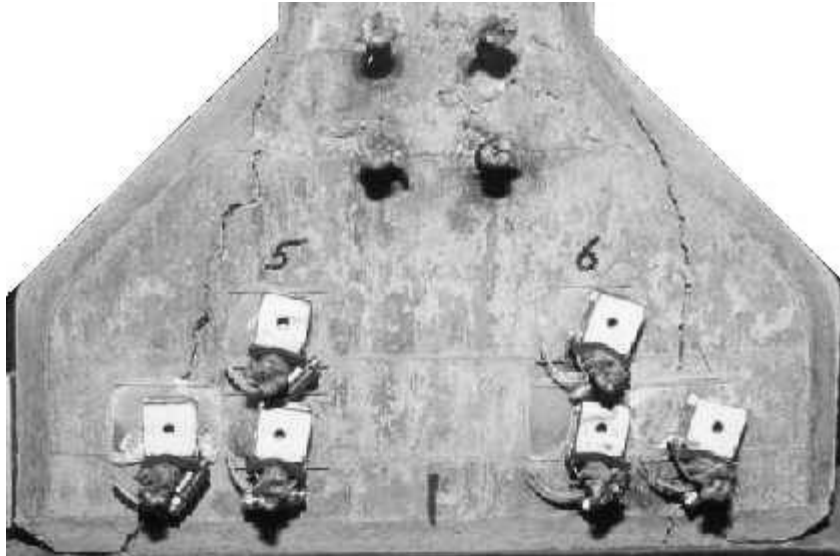


**Figure 7.9** Typical Strand Slip Crack Pattern

#### *7.2.1.3 Flexural Specimen with Simplified WWF Reinforcement*

The curve in Figure 7.2 for the simplified (uniform size) WWF reinforcement specimen, labeled WNSff, very closely matches that of the WNRff specimen just discussed. However, this curve has a slightly greater stiffness, particularly in the portion beyond the AASHTO design load, and a slightly greater ultimate load. In this case, it was not clear whether the failure was precipitated by strand slip or compression strut crushing; the two modes seemed to occur simultaneously.

#### *7.2.1.4 Flexural Specimen with Equivalent Strength WWF Reinforcement*

The specimen with high-strength (80-ksi) steel and a simplified (i.e., uniform size) WWF stirrup design performed almost the same as the one with a normal strength (60-ksi) simplified stirrup design. Their maximum loads were within 0.5 percent, and they both failed in a combination of strand slip and compression strut crushing.



#### 7.2.1.5 Pristine Specimens

With the detailed discussion just presented for the flexural specimens of Figure 7.2, it is easy to compare the load-deflection behavior of the pristine specimens of Figure 7.3 and Tables 7.1 and 7.2. In Figure 7.3, the traditionally reinforced beam does not have the smallest initial stiffness, as before, and all of the specimens exhibit comparable behavior in both the linear and non-linear ranges of loading. The ultimate loads were slightly lower and only one of the five specimens had a combination of compression strut crushing and strand slip, as opposed to pure strand slip, as the mode of failure.

Figures 7.3 and the bottom portions of Tables 7.1 and 7.2 show the results of 5 pristine beam first end region shear tests due to the addition of a specimen fabricated using the alternate R-bar detail (traditional 60-ksi bar with the 4-inch hooks rotated 90°). When compared to TNRPf, the alternate R-bar specimen had a similar elastic stiffness, a slightly increased plastic stiffness, and a 10% increase in ultimate load that was also well above the AASHTO design capacity.

#### 7.2.1.6 Load-Deflection Summary for Normal Strength Concrete

In summary, the load-deflection results from the first end region tests on both flexural and pristine beam specimens showed no signs of weakness in the WWF versions or the alternate R bar versions as compared to the prototype traditionally reinforced versions. The ultimate strength was well above the AASHTO design strength in every case, showing the conservatism in the design equation. The first end region should not fail in shear due to lack of strength in the vertical reinforcement. Rather, it should fail either in strand slip or diagonal compression in the web.

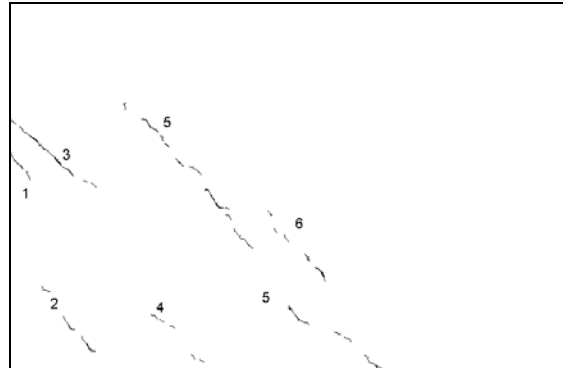
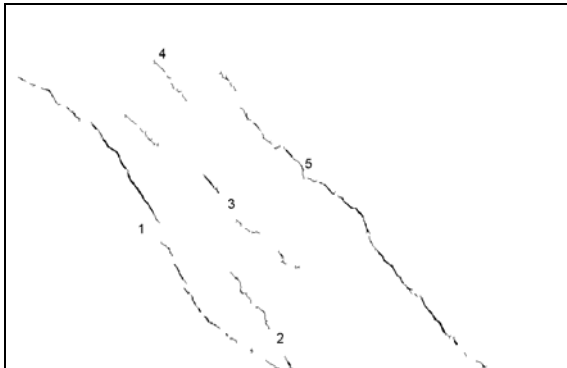
#### 7.2.2 Cracking Behavior

For each of the first end region tests, digital pictures were taken at several high load levels of the three 11 x 18-inch regions of the web nearest the end of the beam, and these pictures were then processed by the techniques described in Chapter 5. Also, the cracks on the opposite side of the web were photographed at a number of different load levels after they had been marked in red, indicating the length and the load. Only the digital imaging results are presented here, but the other data are available in Texas Tech archives.

Digital imaging crack images for the four normal strength concrete first end region tests of Figure 7.2 are shown in Figure 7.10. The applied load was approximately 329 kips in each case. Only the first web region, S1, is shown since it illustrates the key cracking. The corresponding calculated crack properties, based on the method of Chapter 5, are shown in upper part of Table 7.3. It may be seen from both the figures and the table that the cracking was quite comparable in all of the specimens at the selected load level. Even though the total crack area if WNRFf is smaller, its crack distribution and widths are similar.

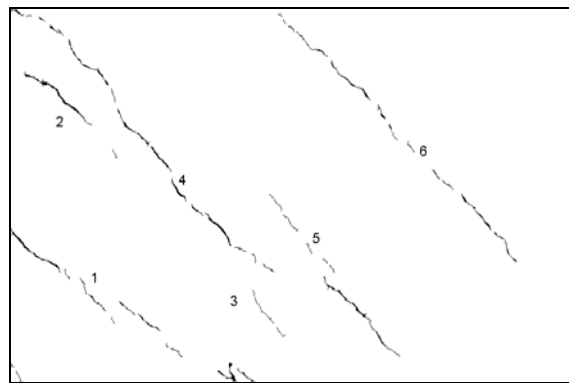
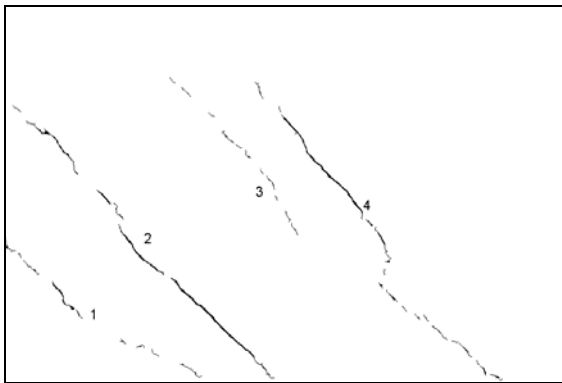
Corresponding processed crack images for the first end region tests for pristine beams with normal strength concrete are shown in Figure 7.11. The numerical data for these cases are also included in Table 7.3. Once again, the results are comparable for

similar cases, although the total crack areas are slightly larger for the NSC pristine beams than for the NSC flexural beams. It may be noted that the cracking in the alternate R-bar specimen, TNAPf, was less than in any other specimen but its crack widths and distribution were also similar. Overall, the shown crack values and distributions are very similar with only isolated points of variation and no undesired trends.



(a) Final Crack Image of TNRFf at 348 kips

(b) Final Crack Image of WNRFF at 348 kips



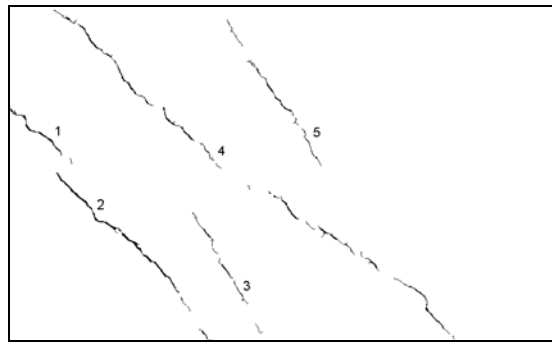
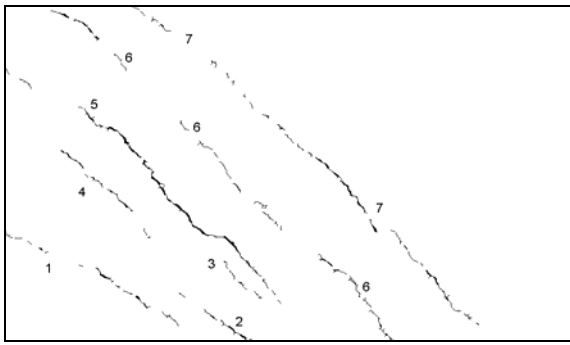
(c) Final Crack Image of WNSFf at 349 kips

(d) Final Crack Image of WNEFf at 349 kips

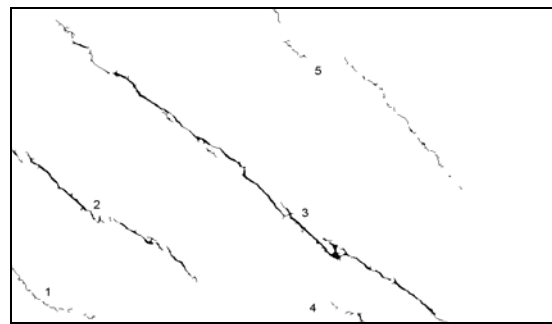
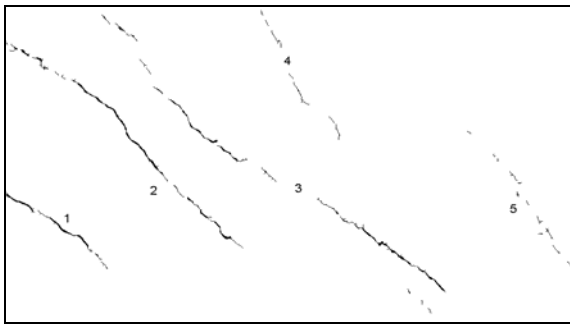
**Figure 7.10** Crack Images for First End Region Tests on NSC Flexural Beams

**Table 7.3** Calculated Crack Results for the NSC First End Region Tests

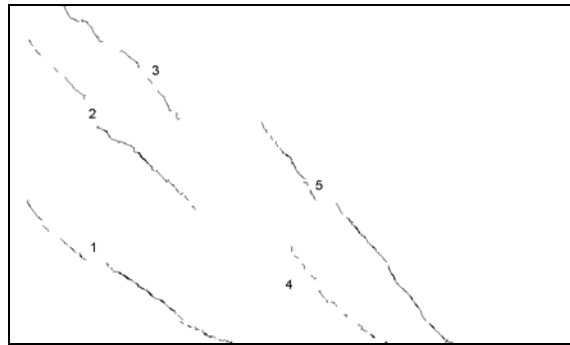
<b>Web Region</b>		<b>S1</b>			
<b>Test Case</b>	<b>Load Level (Kips)</b>	<b>Number of Cracks</b>	<b>Total Crack Area (in<sup>2</sup>)</b>	<b>Max. Crack Width (in)</b>	<b>Average Crack Width (in)</b>
		<b>Flexural Beams</b>			
<b>TNRff</b>	348	5	0.841	0.029	0.026
<b>WNRff</b>	348	6	0.376	0.023	0.021
<b>WNSff</b>	349	4	0.930	0.034	0.028
<b>WNEff</b>	349	5	1.159	0.035	0.027
		<b>Pristine Beams</b>			
<b>TNRpf</b>	348	6	1.290	0.032	0.025
<b>WNRpf</b>	349	4	1.171	0.042	0.031
<b>WNSpf</b>	349	5	1.080	0.033	0.028
<b>WNEpf</b>	350	5	1.592	0.037	0.032
<b>TNAPf</b>	350	5	0.651	0.023	0.021



(a) Final Crack Image of TNRPf at 348 kips (b) Final Crack Image of WNRPf at 349 kips



(c) Final Crack Image of WNSPf at 349 kips (d) Final Crack Image of WNEPf at 350 kips



(e) Final Crack Image of TNAPf at 350 kips

**Figure 7.11** Crack Images for First End Region Tests on NSC Pristine Beams

### 7.3 High Strength Concrete

The specimens with high strength concrete were tested in the same way as those with normal strength concrete in the first end region. However, only the three most critical pairs were tested; one with the traditional bar detail, one with the simplified, 60-ksi, WWF detail, and one with the equal strength, 80-ksi detail.

### 7.3.1 Load-Deflection Behavior

Figures 7.12 and 7.13 show the load-deflection curves for the high-strength concrete flexural and pristine beams, respectively, when tested in the first end region. Tables 7.4 and 7.5 present numerical values for the key parameters of the load-deflection curves and comparisons between the AASHTO design loads and the observed peak loads, plus the mode of failure of each beam. In all cases, the curves showed almost no non-linear behavior prior to reaching their AASHTO design load and achieved, at a minimum, terminal loads approaching 50 percent of their AASHTO design capacity. As in several other cases, the initial stiffness of the traditionally reinforced flexural specimen was lower than those of the other specimens. Also, in both figures, the traditionally reinforced specimen had a lower peak load, and, as expected because of its smaller bars, the WWF specimen with high strength (80-ksi) steel had a slightly lower inelastic stiffness than the one with the usual 60-ksi steel. As can be seen in Table 7.5, the types of failure modes were mixed throughout the various shear reinforcement details and shows no negative trends.

### 7.3.2 Cracking Behavior

Digital crack images for the three high strength concrete first end region tests of the flexural and pristine beams are shown in Figures 7.14 and 7.15, respectively. The applied load was approximately 430 kips in each case. Only cracks in the first web region, S1, are shown. The corresponding calculated crack properties, based on the method of Chapter 5, are shown in Table 7.6. It may be seen from both the figures and the table that the cracking was quite comparable in all of the specimens at the selected load level.

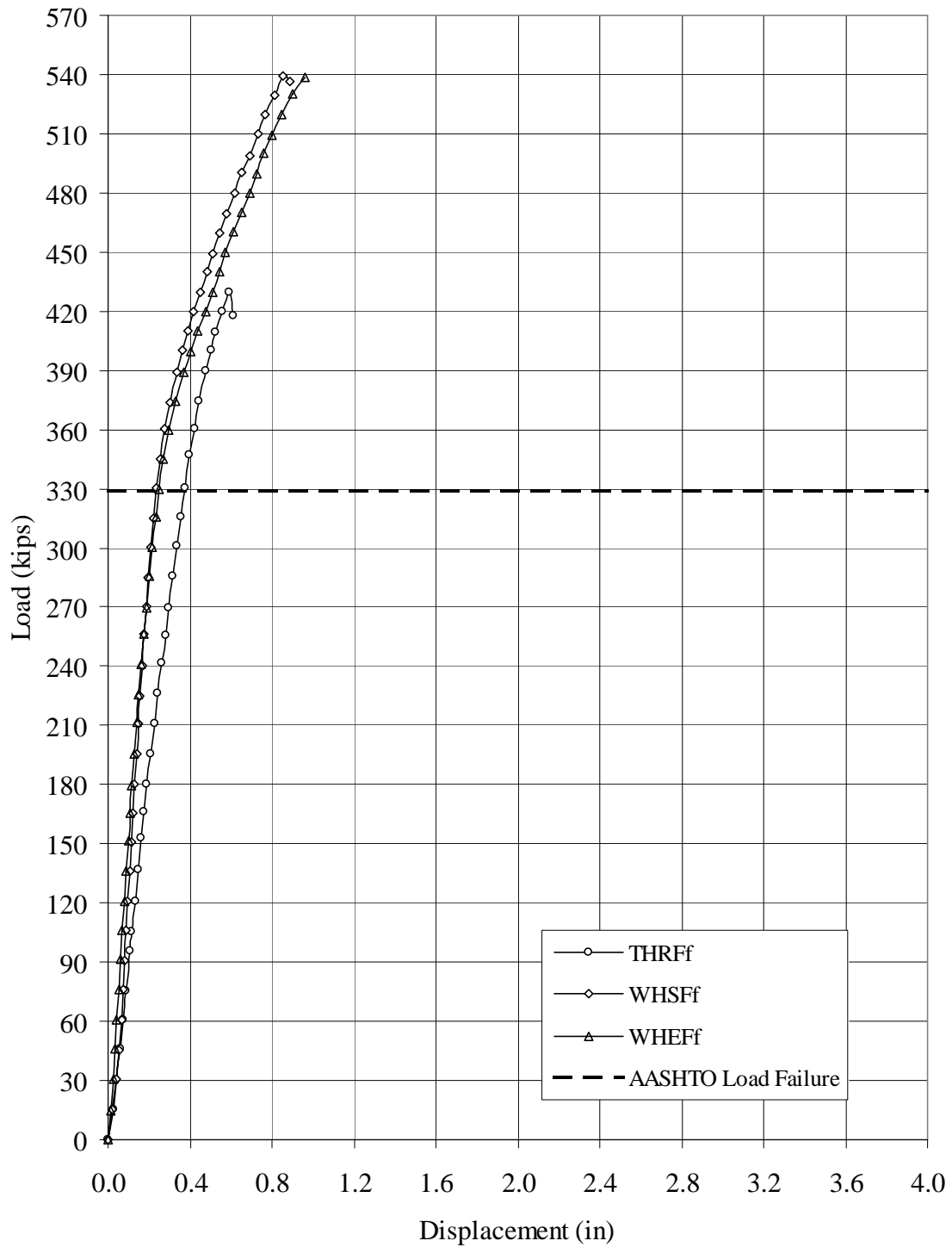


**Figure 7.12** Load-Deflection Curves for the HSC Flexural Beam First End Region Tests

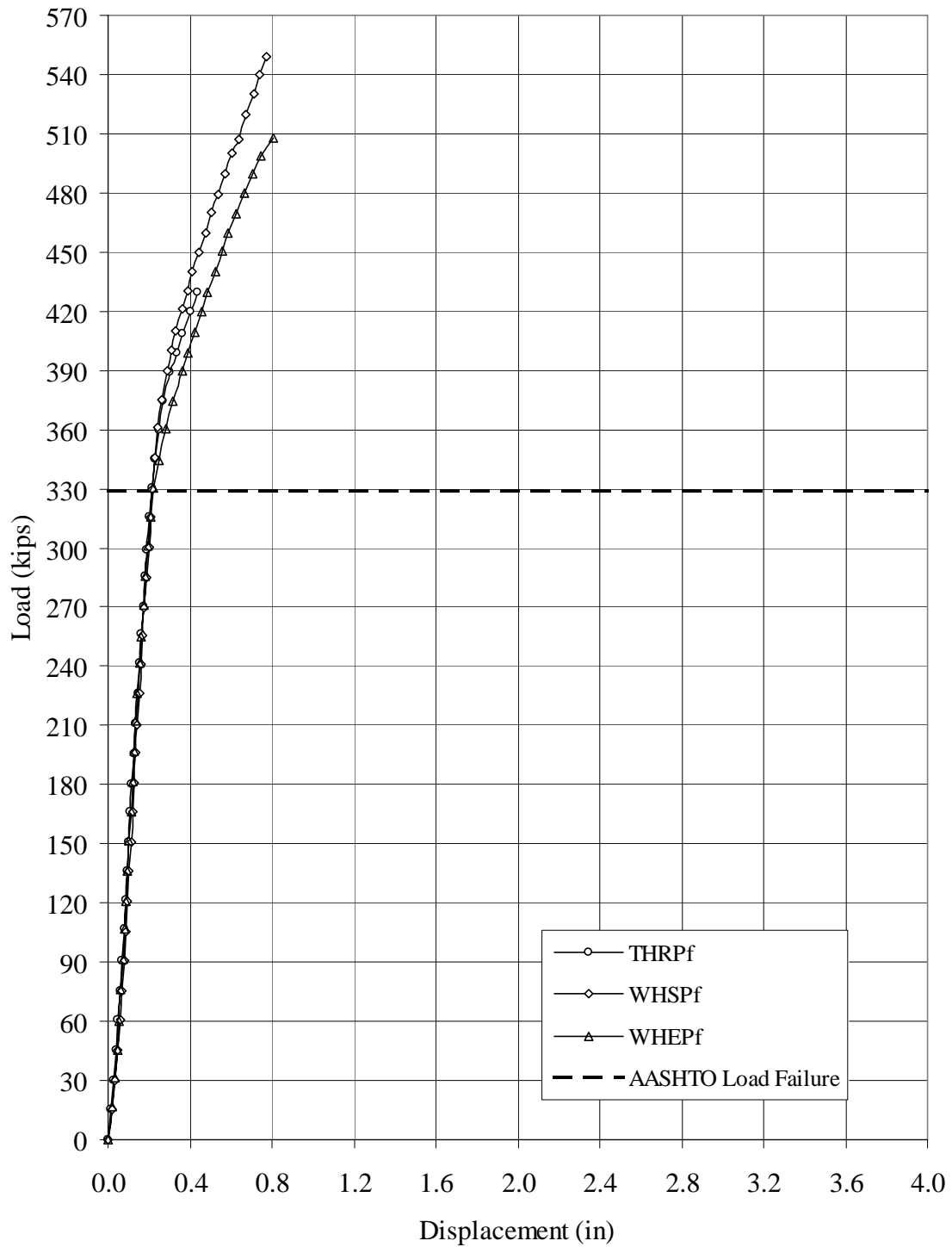


**Figure 7.13** Load-Deflection Curves for the HSC Pristine Beam First End Region Tests

**Table 7.4** Load-Deflection Parameters for the HSC First End Region Tests

Beam	Beam Stiffness, $E_b$ (Kips/in)	Max.	Elastic	Cracking Load (Kips)	Max.	Final	Ductility Ratio
		Load (Kips)	Deflection (Inches)		Load (Kips)	Deflection (Inches)	
<b>THRF</b>	909	270	0.297	180	429	0.589	2.0
<b>WHSF</b>	1,403	331	0.236	166	545	0.888	3.8
<b>WHEF</b>	1,331	330	0.248	180	539	0.959	3.9
<b>THRP</b>	1,570	270	0.172	196	429	0.435	2.5
<b>WHSP</b>	1,492	361	0.242	196	549	0.775	3.2
<b>WHEP</b>	1,473	330	0.224	152	508	0.808	3.6

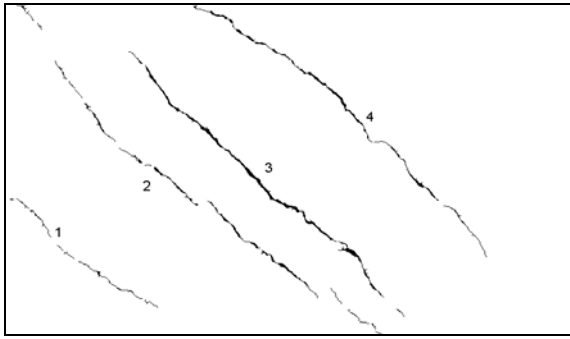


**Table 7.5** Terminal Loads and Failure Modes for the HSC First End Region Tests

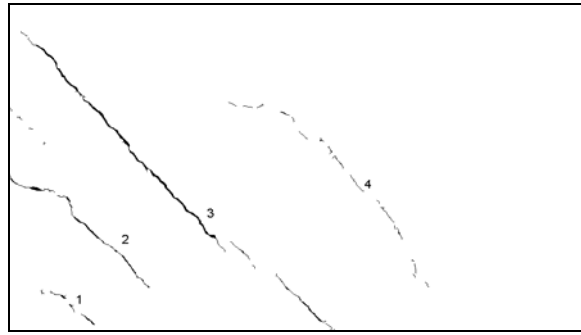
<b>Beam</b>	<b>AASHTO Design Capacity (Kips)</b>	<b>Failure Load (Kips)</b>	<b>Ratio</b>	<b>Failure Mode</b>
<b>THRF</b>	278	429	1.54	SS
<b>WHSF</b>	329	545	1.66	CS
<b>WHEF</b>	329	539	1.64	CS + SS
<b>THRP</b>	278	429	1.54	SS
<b>WHSP</b>	330	549	1.66	CS + SS
<b>WHEP</b>	331	508	1.53	SS

SS = Strand slip failure

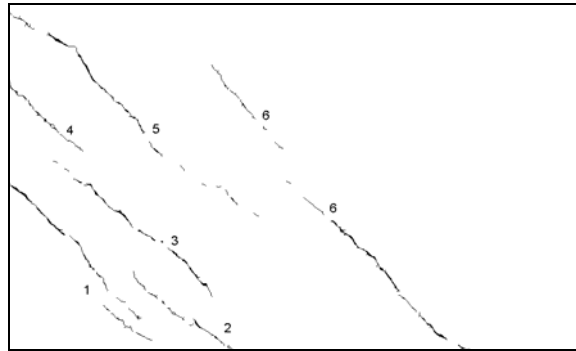
CS = Compression strut failure



(a) THRFf at 429 kips

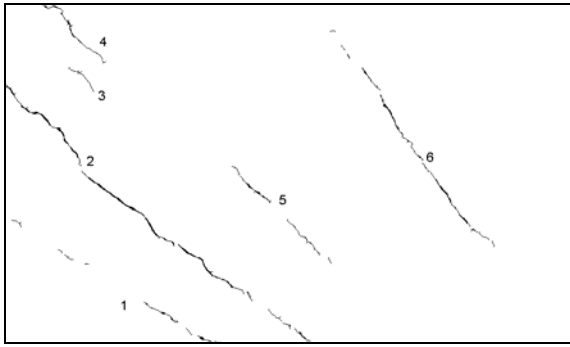


(b) WHSFf at 430 kips

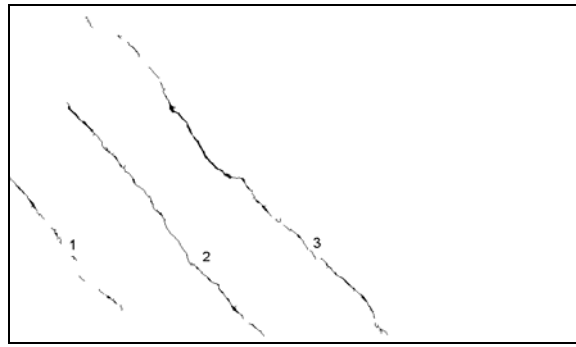


(c) WHEFf at 340 kips

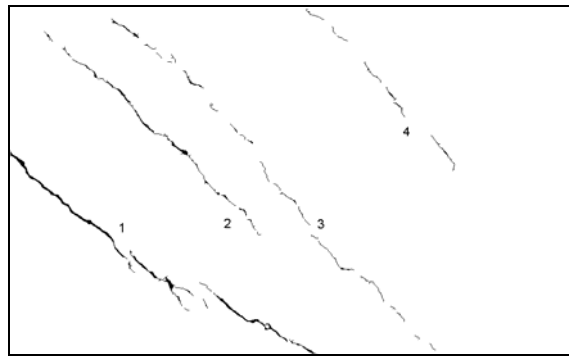
**Figure 7.14** Crack Images for First End Region Tests on HSC Flexural Beams



(a) THRPF at 429 kips



(b) WHSPF at 430 kips



(c) WHEPF at 429 kips

**Figure 7.15** Crack Images for First End Region Tests on HSC Pristine Beams

**Table 7.6** Calculated Crack Results for the HSC First End Region Tests

Web Region		S1			
Test Case	Load Level (Kips)	Number of Cracks	Total Crack Area (in <sup>2</sup> )	Max. Crack Width (in)	Average Crack Width (in)
<b>Flexural Beams</b>					
<b>THRFf</b>	429	4	1.853	0.052	0.036
<b>WHSFf</b>	430	4	0.986	0.040	0.033
<b>WHEFf</b>	430	5	1.061	0.030	0.024
<b>Pristine Beams</b>					
<b>THRPf</b>	429	4	0.941	0.031	0.026
<b>WHSPf</b>	430	3	0.831	0.029	0.027
<b>WHEPf</b>	429	4	1.334	0.042	0.030

#### 7.4 Summary

The first end region tests for both normal and high strength concrete showed the beams to have nearly 50 percent or more load capacity than the AASHTO design equation provides. In almost every case, there was slight web cracking but hardly any loss of initial stiffness up to the AASHTO load, followed by a distinct but still high region of inelastic stiffness until sudden failure. In all but one case the primary failure mechanism was by strand slip, which is not surprising since the maximum moment occurred in the transfer region of the development length of the strand.. In the exceptional case, compression strut failure was dominant, and this mechanism also seemed to combine with strand slip in some other cases. There was extensive but similar cracking in all shear spans up to the failure load. In general, all WWF specimens showed responses similar to their corresponding traditional rebar specimens with no negative trends during the first end region shear tests.

## CHAPTER VIII

### SECOND END REGION SHEAR TESTS

#### 8.1 Objective and Scope

The purpose of the tests called “second end region shear tests” was to compare the shear capacities of the zones where only No. 4 R-bars are spaced at 8 inches on centers in TxDOT Type A bridge I-beams for different types of shear reinforcement. If shear failures could be induced in these regions, they would reflect the effects of the R-bars and their anchorages alone, without the complicating effects of the S-bars that are interspersed among the R-bars in the first end region. Thus, these tests are considered to be more demanding than the previous ones on the traditional and WWF stirrups and their anchorages. The combined shear effect of the R- and S-bars in the first end region was more pronounced for the WWF details since they were both fully anchored by the longitudinal wires, whereas, the S-bars of the traditional detail are straight with no special anchorage at their ends.

The same five types of reinforcement as considered in the first end region tests were examined once again: (1) the traditional reinforcement pattern; (2) the matching, one-for-one replacement of traditional R- and S-bars with comparable WWF wires; (3) substitution of a “simplified” (uniform) pattern of D26 WWF wires in the first end region and D20 wires in the second end region; 4) substitution of “equivalent strength” (smaller, 80-ksi) WWF wires, and (5) substitution of “alternate R-bars” with their bottom hooks turned parallel to the beam.

The second end region tests were set up as shown in Figure 8.1. The support under the previously tested south end of the 36-foot specimen was moved 10 feet inward to avoid failure of that damaged end, and the two applied loads were placed farther from the end to be tested (the north end) than in the first end region tests. Actually, the positions of these two loads were adjusted twice in an effort to induce a shear failure in the second end region, rather than the moment failure in that was initially experienced.

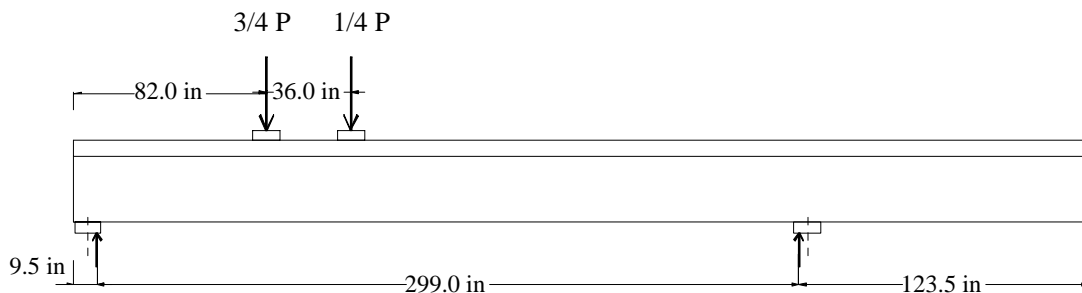


**Figure 8.1** Configuration for the Second End Region Shear Tests

Design calculations indicated that with the first position of the loads, that is, with the nearest one 82 inches away as shown in Figure 8.1, a shear failure would occur first unless the experimental shear capacity was found to be in excess of 18 percent greater than its AASHTO design capacity. In other words, based on the AASHTO moment and shear capacities, there was an 18 percent margin of shear failure over moment failure. However, the first specimen tested did fail in moment instead of shear, so the two applied loads, while being kept three feet apart and in the proportion of three-fourths and one-fourth of the total load, were moved 8 inches closer to the end. This shortened the shear span and caused less moment for the same shear force on the second end region. In this position, calculations indicated that the experimental shear capacity would have to be 26 percent above the AASHTO design value for a moment failure to occur first. Again, however, a moment failure did occur first. Finally, the two loads were moved 8 more inches closer to the end (with the closer one 66 inches from the end), and all the remaining second end region tests kept this loading position. While a moment failure still controlled in many of the tests, it was evident from the cracking that a shear failure was also imminent in almost every test. The reason that the loads were not moved still closer to the end was that diagonal cracks from shear stress in the web in the second end region would have propagated well into the lower flange in the first end region had the loads been so placed. The lower portions of some cracks did, in fact, reach into the first end region.

Once again, the load was increased in predetermined load as described in Section 3.4. The total applied loads, LVDT deflections, and strain gage strains (in the first few specimens) were recorded on the computer at each load increment, and dial gage deflections were hand recorded at the same intervals. Pictures of cracks were taken on both sides of the specimens as before. These pictures focused on the regions marked as N1 through N5 of the beam. Strand end-slip measurements were taken at regular intervals but strand end-slip was small and never appeared to cause any loss of strength in these tests.

Because the second end region test results were significantly different for the normal strength and high strength specimens, once again the results are grouped into these two categories when presented in this chapter.

## **8.2. Normal Strength Concrete**

Second end region tests were conducted on a total of nine specimens with normal strength concrete and different types of reinforcement, as outlined above. The symbol for each of these tests had a second letter “N” for normal strength concrete. The symbol ended with an “Fs” for the four flexural specimens and a “Ps” for the five pristine specimens. Note that the loads were in different places for the first two of these tests than for the remaining seven tests, so some of the load-deflection curves were not truly comparable.

### **8.2.1 Load-Deflection Behavior of Flexural Beams**

Load-deflection curves for the four different flexural (previously tested in flexure) beams subjected to second end region testing are shown together in Figure 8.2. The first two of these tests were the ones with the loads placed out farther from the end than in the other tests. Corresponding curves for the five pristine beams are of greater interest than those for the flexural beams since they all had the loads in the same positions and the

beams had not been previously damaged over a portion of the clear span. The horizontal dashed line in Figure 8.2 again indicates the load corresponding to the AASHTO shear capacity for the design material properties (6-ksi beam concrete, 5-ksi slab concrete, 270-ksi strand). All four of the flexural specimens exceeded the expected AASHTO load capacity, although the stiffnesses and maximum deflections varied somewhat, as discussed below.

The first part of Table 8.1 presents numerical values for the same key parameters of the load-deflection curves of Figures 8.2 as considered for flexural and first end region tests in Chapters 6 and 7, respectively. These parameters include the beam stiffness,  $E_b$ , the maximum elastic load and deflection, the load at which the first cracks appeared, the load and deflection at the last load, and the “ductility ratio.” Table 8.2 shows a comparison between the AASHTO design loads, using experimental concrete strengths, for these specimens and the observed peak loads.

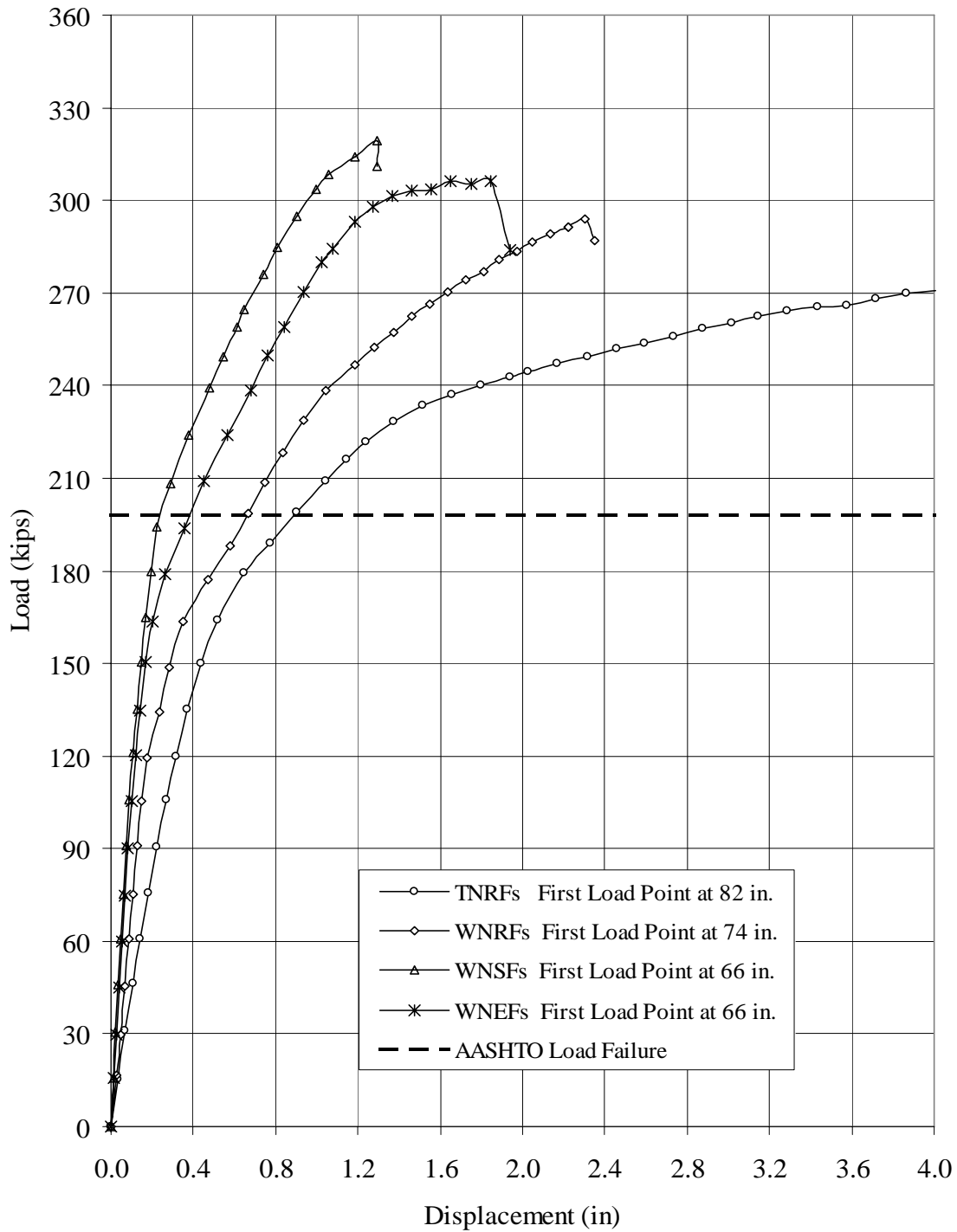


**Figure 8.2** Load-Deflection Curves for Second End Region Tests on NSC Flexural Specimens

**Table 8.1** Load-Deflection Data for Second End Region Shear Tests on NSC Specimens



<b>Beam</b>	<b>Beam Stiffness, E<sub>b</sub> (Kips/in)</b>	<b>Max.</b>	<b>Elastic</b>	<b>Cracking Load (Kips)</b>	<b>Max.</b>	<b>Final</b>	<b>Ductility Ratio</b>
		<b>Load (Kips)</b>	<b>Deflection (Inches)</b>		<b>Load (Kips)</b>	<b>Deflection (Inches)</b>	
<b>TNRF</b>	381	120	0.315	120	271	4.01	12.7
<b>WNRF</b>	678	119	0.176	105	294	2.35	13.4
<b>WNSF</b>	933	180	0.193	135	319	1.29	6.7
<b>WNEF</b>	904	151	0.167	105	306	1.94	11.6
<b>TNRP</b>	1,025	179	0.175	134	330	3.37	19.2
<b>WNRP</b>	926	150	0.156	120	310	2.74	17.6
<b>WNRP</b>	878	180	0.205	120	309	1.60	7.8
<b>WNEP</b>	1,126	179	0.159	120	316	2.07	13.0
<b>TNAP</b>	1,139	164	0.144	135	316	3.58	24.9

**Table 8.2** Terminal Loads for Second End Region Shear Tests on NSC Specimens

<b>Beam</b>	<b>AASHTO Design Capacity (Kips)</b>	<b>Failure Load (Kips)</b>	<b>Ratio</b>	<b>Failure Mode</b>	<b>Wire-Break Load * (Kips)</b>
<b>TNRF</b>	197	271	1.38	SF	---
<b>WNRF</b>	198	294	1.48	SF	295
<b>WNSF</b>	188	319	1.70	SF	318
<b>WNEF</b>	192	306	1.59	SF	303
<b>TNRP</b>	197	330	1.68	SF	---
<b>WNRP</b>	197	310	1.57	SF	310
<b>WNSP</b>	187	309	1.63	SF	249
<b>WNEP</b>	191	316	1.65	Shear	314
<b>TNAP</b>	183	316	1.73	SF	---

SF = Shear / Flexure failure

\* WWF longitudinal smooth wire

### 8.2.1.1 Traditional Reinforcement

In Figure 8.2 for the flexural beams, the load-deflection curve for the traditionally reinforced beam, labeled TNRFs, shows that it had a very smooth transition from elastic to inelastic behavior and that the beam reached a considerably larger deflection than any of the other specimens. Despite the smoothness of the curve, one can detect three regions of stiffness, the first ending before the design load was reached, the second going through the design load to a deflection of approximately 1.4 inches, and the third stretching out to the final deflection of 4.0 inches. Because the loads were applied farther out on the beam for this test than for any of the others, these three stiffnesses were the lowest in the figure. That is, with the loads in a more central position, smaller magnitudes of load were required to produce a given deflection, which was always measured halfway between the two loads. Even at the final load on the traditionally reinforced beam, however, there was not a complete loss of stiffness, and large flexure and shear-flexure cracks were seen in the bottom of the beam. The mode of failure was considered to be a “shear-flexure” failure (SF in Table 8.2). The load of 271 kips when the test was stopped was 38 percent greater

than the design shear capacity. The decision to stop the test was based on a loud popping sound judged to mean that a strand had broken.

#### *8.2.1.2 Matching WWF Reinforcement*

The next-highest load-deflection curve in Figure 8.2 is for the second end region test on the specimen with the matching one-for-one replacement of the traditional bars with WWF wires, WNRFs. It shows a much greater initial and yielding stiffnesses than the curve for traditional bars, but yielding at about the same level. The greater stiffnesses may be attributed to three effects. The most significant one was the placement of the two loads eight inches closer to the end of the beam. In addition, there was less damage to the middle portion of the WWF beam during its flexural test, the bottom longitudinal wires added some stiffness, especially in the post-cracking range, and the stiffness of the WWF reinforcing cages themselves was greater than that of the hand-tied cages of the traditionally reinforced beam. Once again, there appear to be three stiffness ranges. The test was stopped when the load dropped suddenly as a popping sound was heard. Even though a smaller maximum deflection was achieved than with the traditionally reinforced TNRFs beam, the peak load for the WNRFs specimen was 48 percent greater than the AASHTO design capacity as compared to 38 percent greater for the TNRFs specimen. This difference in load capacity is a reflection of putting the loads closer to the end of the beam. Although there was little loss of stiffness near the peak load, the failure was judged to be one of “shear-flexure” (SF in Table 8.2) from observation of the cracking behavior.

#### *8.2.1.3 Simplified WWF Reinforcement*

The load-deflection curve in Figure 8.2 for the simplified WWF reinforcement, labeled WNSFs, had considerably greater initial and inelastic stiffnesses than either of the two previously discussed beams, primarily because the applied loads were placed eight inches still closer to the end of the beam. Also, the terminal load was quite a bit larger (70 percent larger than the AASHTO value, as compared to 38 and 28 percent larger before) due primarily to the different load placement but also due to some extent to the other two factors cited earlier. Despite the load placement, the failure again involved flexure as well as shear, but there was little or no loss of stiffness just prior to the failure, indicating that a pure shear failure was also eminent.

#### *8.2.1.4 Equivalent Strength WWF Reinforcement*

The fourth load-deflection curve in Figure 8.2, the one for the equivalent strength design labeled WNEFs, matched the curve for the simplified design in the elastic range but exhibited a lower inelastic stiffness, a slightly smaller peak load, and a significant loss of stiffness as failure was approached. With the same load placement for this beam and the beam with the simplified design, these results are comparable and understandable. The lower inelastic stiffness, that is, behavior dependent on the steel after cracking has initiated, is due to the presence of smaller, higher-strength wires throughout the design. Despite the stiffness differences, however, the WNEFs specimen had a maximum load 59 percent above the AASHTO design load.

#### *8.2.1.5 Summary for Flexural Beams and Normal-Strength Concrete*

In summary for the second end region tests on “flexural” (previously tested) beams with normal-strength concrete, only the results for the third and fourth specimens are truly comparable because the loads were placed at different positions in the first two tests. Nevertheless, the results show that the load capacities of all three types of WWF-reinforced beams were well above the AASHTO design load and that the smaller wires in the equivalent strength design did result in a reduced stiffness once cracking developed. The load position used on the last two specimens tested in this series was used on the remaining five, second end region shear test on pristine beams is discussed in the following section.

### 8.2.2 Load-Deflection Behavior of Pristine Beams

Load-deflection curves for the five different pristine (undamaged) beams subjected to second end region testing are shown together in Figure 8.3, and selected test data is provided in the lower portions of Tables 8.1 and 8.2. Since the loads were all applied with the exact same geometry on these five specimens, this test data is directly comparable and show a striking amount of consistency. In particular, the stiffness in the elastic region is almost the same for all of the tests, and the failure loads are all in the range between 1.57 and 1.73 times the AASHTO design capacity in shear. As before, the traditionally reinforced specimen exhibited the largest deflection before failure, but the difference was not as great as in some other cases. The two curves in Figure 8.3 for the simplified WWF reinforcement with 60-ksi and 80-ksi steel (WNSPs and WNEPs) fall almost on top of one another.

Another difference in these tests of the WWF specimens from earlier tests was that they were not stopped with the breakage of a longitudinal WWF wire in the bottom flange. Instead, despite a temporary loss of stiffness near failure, the loading was continued and a greater capacity was later attained. Thus, somewhat greater ductility ratios were reached than in the corresponding flexural beam tests (see Table 8.1).

While the results in Figure 8.3 are well within experimental error, there was one major distinction among the types of failure. Unlike the other four specimens, the specimen with high-strength WWF wires exhibited a true shear failure, not a combined shear-flexure failure. A typical shear failure is illustrated in Figures 8.4 and 8.5, where the second end region of the WNEPs specimen is shown after the test. There was breakage of the vertical steel stirrups in tension and a wide separation along a shear crack that extended all the way from the bottom of the beam through the top of the slab. A so-called “dominant” shear crack also developed in the other second end region tests, indicating that a shear failure was imminent, but it never quite caused the type of separation seen in Figures 8.4 and 8.5. Interestingly enough, the WNEPs specimen did not have the smallest ductility despite its true shear failure. The breakage of the WWF stirrups before any type of loss of anchorage in the bottom of the beam certainly illustrates the adequacy of the

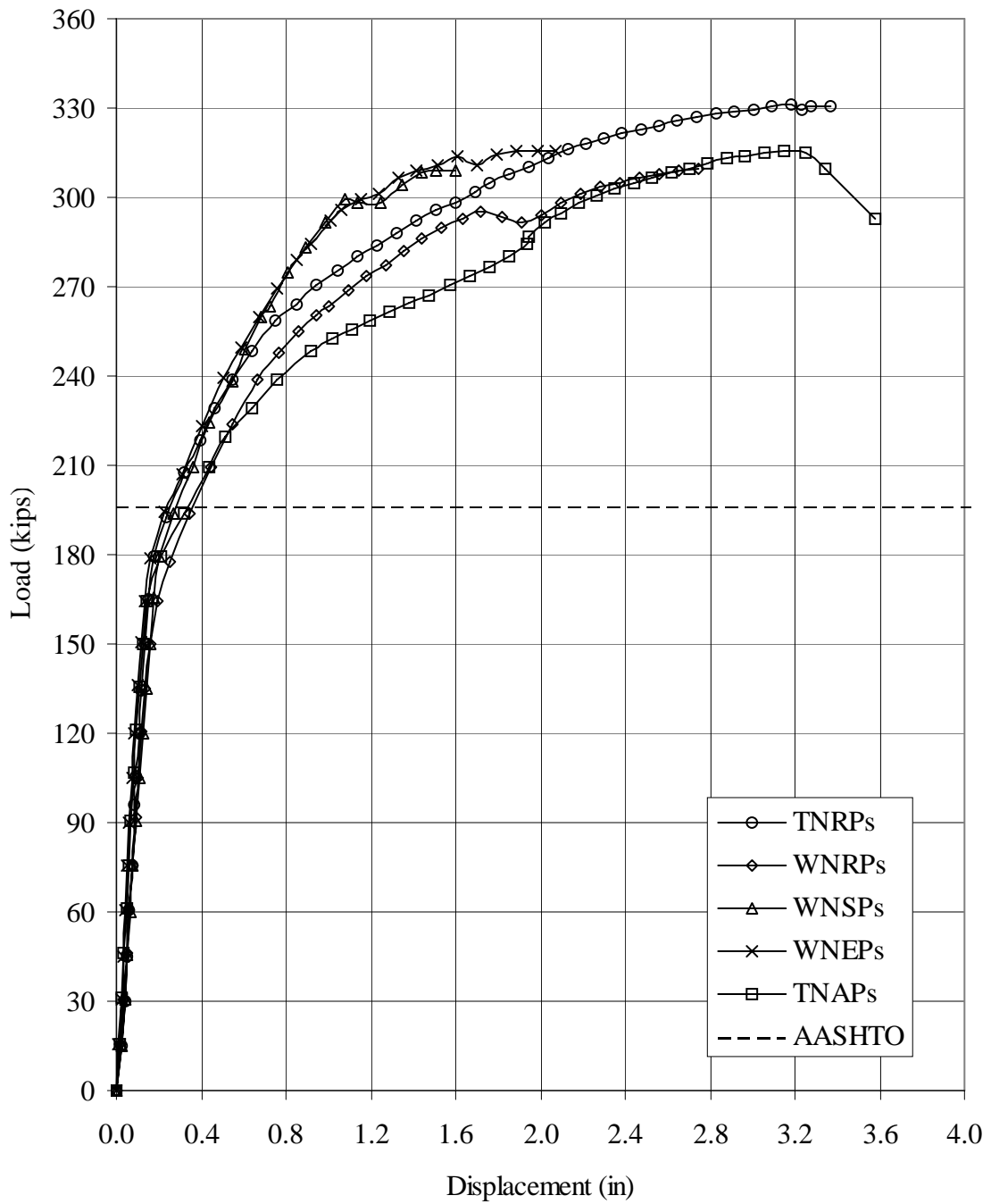


**Figure 8.3** Load-Deflection Curves for Second End Region Tests on NSC Pristine Specimens

bottom longitudinal wires as anchorage for the stirrups. A comparison of the test data from the traditional and alternate R-bar specimens, TNRPs and TNAPs, respectively, shows very similar behaviors. They have similar stiffnesses in their elastic ranges and very large ductility ratios. The most distinctive difference is the slightly reduced plastic stiffness associated with the alternate R-bar specimen test, TNAPs.



**Figure 8.4** Second End Region Shear Failure of the Specimen WNEP

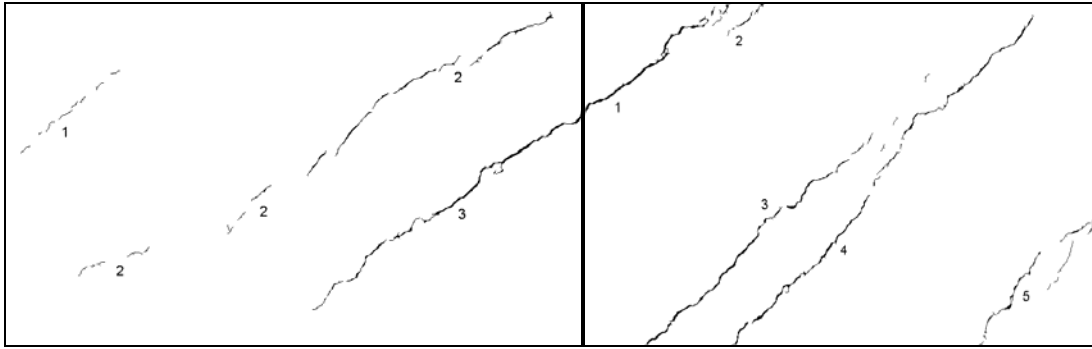


**Figure 8.5** Detail of Second End Region Stirrup Failure in the WNEP Beam

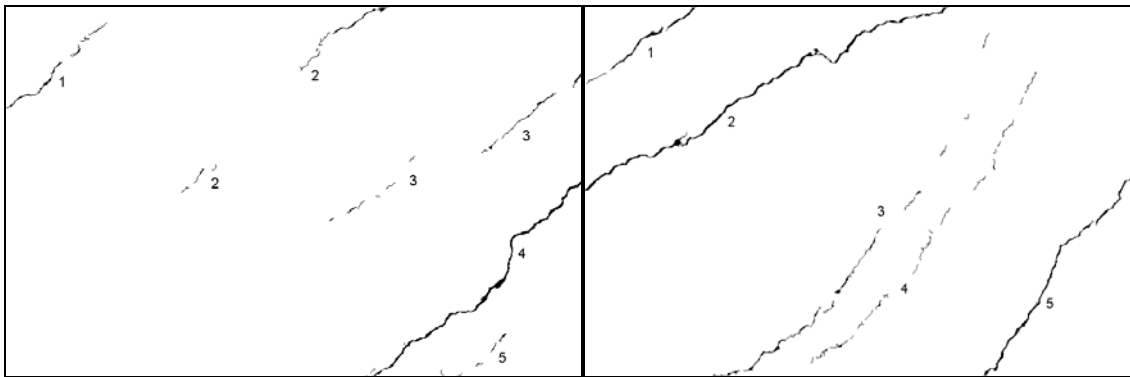
### 8.2.3 Cracking Behavior

For each of the second end region tests, digital pictures were taken at several high load levels of several 11 x 18-inch regions of the web near the end of the specimen. These regions were labeled N1 through N5, as seen in Figure 5.18. These pictures were then processed by the techniques described in Chapter 5. Also, the cracks on the opposite side of the web were photographed at a number of different load levels after they had been marked in green, indicating the length and the load. As in the other tests, only the digital imaging results are presented here, but complete data are available in Texas Tech archives.

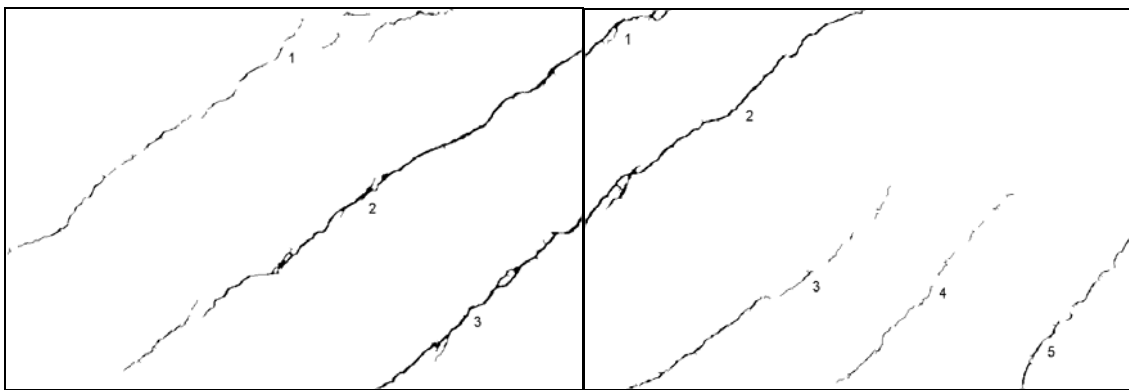
The cracking in the pristine specimens in regions N2 and N3 was the most representative of the shear cracking in the second end region tests. Final N2 and N3 crack images at loads of approximately 308 kips are shown for comparison in Figure 8.6 for the five pristine specimens of Figure 8.3. It may be seen by eye that the spacings, widths, and lengths of the cracks are comparable at this maximum or near-maximum load for each beam, except that there is less cracking in region N2 and more cracking in region N3 of test specimen TNAPs. The digital imaging data of Table 8.3 indicate the same results in numerical form. The previously described change in point location for the flexural specimens tested in the second end region, prevented comparison of the associated crack data. Therefore, only pristine specimen crack data is presented in Table 8.3.



(a) TNRPs at 310 kips (Regions N2 and N3)

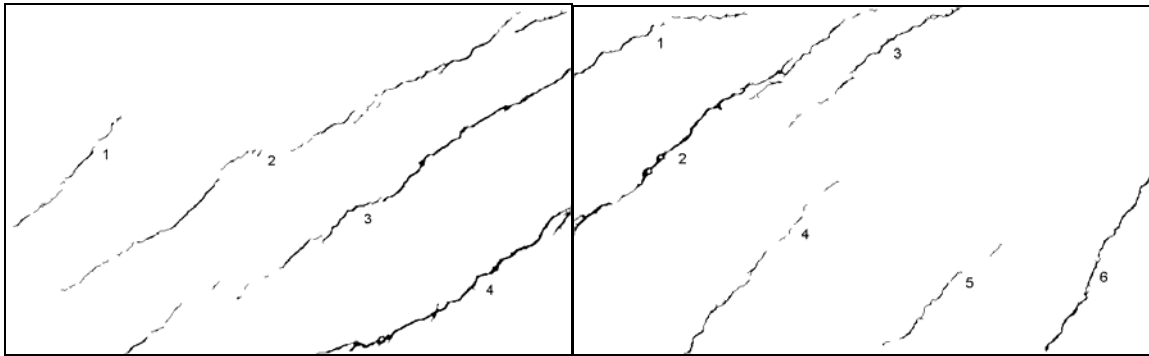


(b) WNRPs at 310 kips (Regions N2 and N3)



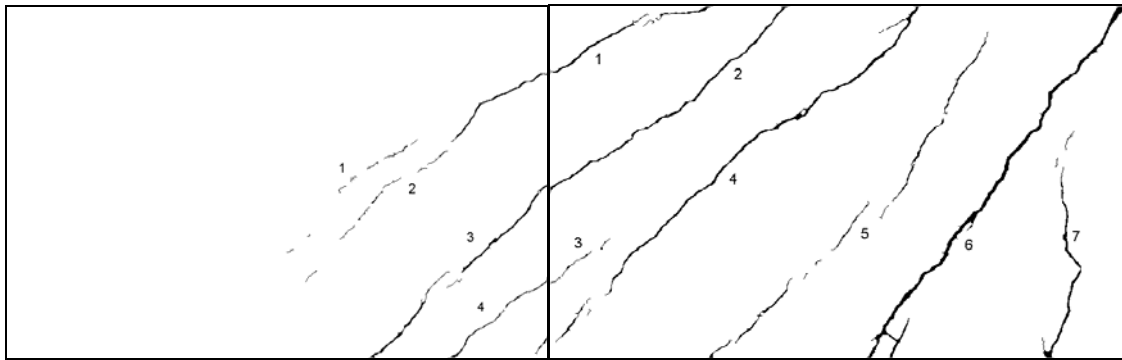
(c) WNSPs at 308 kips (Regions N2 and N3)





(d) WNEPs at 306 kips (Regions N2 and N3)

Figure A.39 Final Crack Image of WNEPs 306 N3



(e) TNAPs at 309 kips (Regions N2 and N3)

**Figure 8.6** Crack Images for Pristine Beams in NSC Second End Region Tests

**Table 8.3** Crack Results in the NSC Second End Region Tests of Pristine Specimens

Region		N2				N3			
Test Case	Load Level (Kips)	No. of Cracks	Total Crack Area (in <sup>2</sup> )	Max. Crack Width (in)	Average Crack Width (in)	No. of Cracks	Total Crack Area (in <sup>2</sup> )	Max. Crack Width (in)	Average Crack Width (in)
TNRPs	310	3	0.913	0.037	0.030	4	1.782	0.042	0.035
WNRPs	310	5	1.011	0.055	0.036	5	1.868	0.045	0.035
WNSPs	308	3	2.106	0.055	0.043	5	1.639	0.053	0.038
WNEPs	306	4	2.293	0.056	0.041	6	1.877	0.045	0.037
TNAPs	309	4	0.900	0.041	0.033	7	4.365	0.083	0.053

### 8.3 High Strength Concrete

Second end region tests were conducted on only three pairs of specimens with high strength concrete. The three pairs were flexural and pristine beams with traditional reinforcement, “simplified” WWF reinforcement, and “equivalent strength” WWF reinforcement. Pairs for one-for-one or “matching” WWF reinforcement were skipped since this pattern was believed to be less advantageous than the simplified pattern. Also, no alternate R-bar tests were conducted with high-strength steel in order to incorporate “intermediate end” tests within the project schedule and budget. Otherwise, the test program closely followed that of the normal strength concrete specimens, although with more strands as well as a higher concrete strength, the applied loads were considerably higher. The symbol for each of these beams had a second letter “H” for high strength concrete.

#### 8.3.1 Load-Deflection Behavior of Flexural Beams

Figure 8.7 shows the load-deflection curves obtained from the three second end region tests on HSC flexural beams. The loads were all placed at the standard 66-inch position from the end of the beam. Numerical summaries of the results are presented in Tables 8.4 and 8.5. It may be seen in Figure 8.7 that the traditionally reinforced beam, labeled THRFs, had a much lower stiffness and maximum load than the two WWF beams. A possible reason for these differences is that the TNRFs specimen was damaged more in its flexural test, something that would normally affect the stiffness more than the strength. It is interesting how far into the inelastic range the WHSFs specimen was able to sustain its maximum load despite multiple breaks in the bottom longitudinal wires, as indicated by the dips in the curve. The equivalent strength WHEFs specimen, on the other hand, had much less ductility as it failed in shear at about half as much total deflection. Once again, as in the normal strength second end region tests, the smaller R-bars of the high-strength

(80-ksi) steel in the WHEFs specimen did not restrict the cracking as much as the larger R-bars in the beams with 60-ksi steel and seemed to allow a full shear failure more readily. Pictures of the shear failure of this specimen are shown in Figure 8.8. All of the flexural specimens of Figure 8.7 showed little if any deviation from elastic behavior until after the AASHTO design load had been passed, although very slight web cracking was detected in each case below the AASHTO value. As before, adequate failure load and ductility ratios can be seen in Tables 8.4 and 8.5 for all of these flexural specimens.

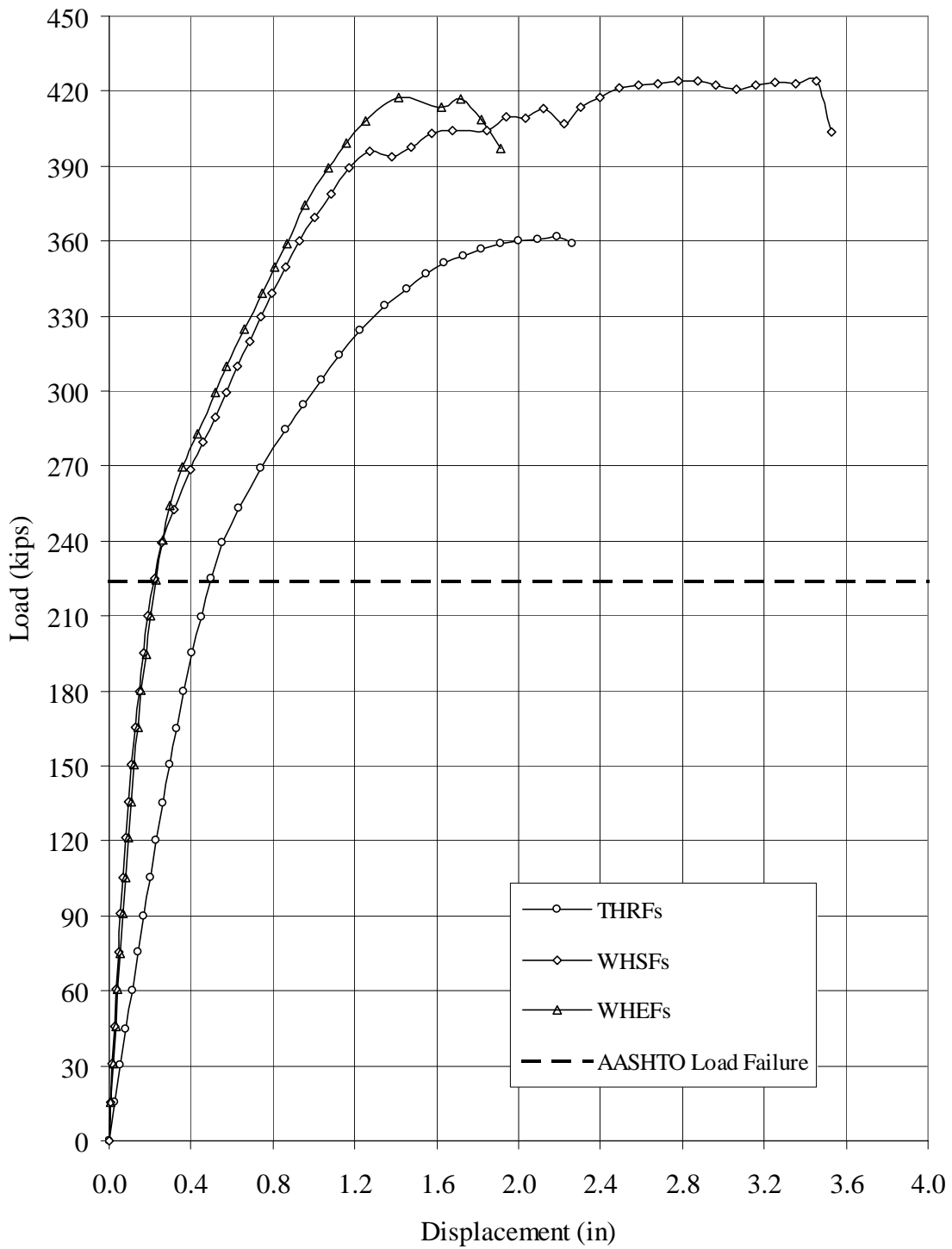


**Figure 8.7** Load-Deflection Curves for Second End Region Shear Tests on HSC Flexural Specimens

**Table 8.4** Load-Deflection Data for Second End Region Shear Tests on HSC Specimens

Beam	Beam Stiffness, $E_b$ (Kips/in)	Max.	Elastic	Cracking Load (Kips)	Max.	Final	Ductility Ratio
		Load (Kips)	Deflection (Inches)		Load (Kips)	Deflection (Inches)	
<b>THRF</b>	483	195	0.404	105	362	2.62	5.6
<b>WHSF</b>	1,099	210	0.191	180	424	3.45	18.1
<b>WHEF</b>	1,024	210	0.205	180	417	1.91	9.3
<b>THRP</b>	1,037	252	0.243	166	394	2.66	10.9
<b>WHSP</b>	1,071	225	0.210	165	402	2.96	14.1
<b>WHEP</b>	1,166	225	0.193	165	390	3.12	16.2

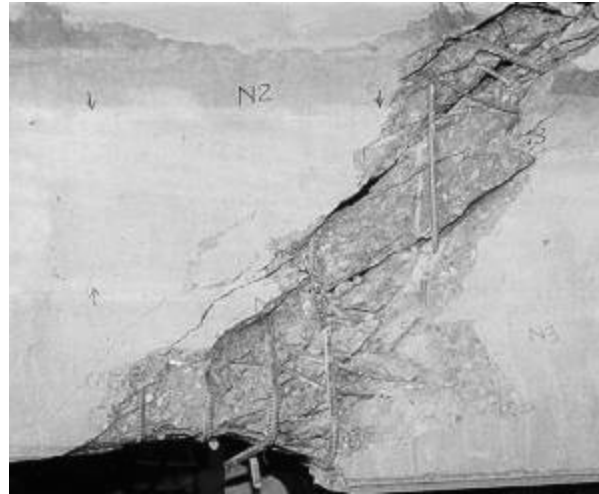
**Table 8.5** Terminal Loads for Second End Region Shear Tests on HSC Specimens

Beam	AASHTO Design Capacity (Kips)	Failure Load (Kips)	Ratio	Failure Mode	Wire- Break Load * (Kips)
<b>THRF</b>	223	362	1.62	SF	---
<b>WHSF</b>	228	424	1.86	Flexure	295
<b>WHEF</b>	221	418	1.89	Shear	318
<b>THRP</b>	223	394	1.77	Flexure	---
<b>WHSP</b>	228	404	1.77	SF	310
<b>WHEP</b>	224	390	1.74	SP	249

SF = Shear / Flexure failure

SP = Shear failure / Punching

\* WWF longitudinal smooth wire



(a) Overall Shear Failure Crack



(b) Detail of the Stirrup Failure

**Figure 8.8** Shear Failure of the Second End Region Test on Specimen WHEFs

### 8.3.2 Load-Deflection Behavior of Pristine Beams

Figure 8.9 shows the load-deflection curves of the three second end region tests on pristine specimens. These curves are remarkably similar, even out to comparable maximum deflections. They also show how much extra strength and ductility is available beyond the AASHTO load, as loads from 74 to 77 percent higher than the AASHTO value and ductilities of 10.9 to 16.2 were reached (see Tables 8.4 and 8.5). Once again, the specimen with high-strength steel, WHEPs, was the only one of the three to experience a shear failure, although the failure might be attributed in part to the punching through of the load pad closest to the end of the beam.

### 8.3.3 Cracking Behavior

The cracking of the beams with high-strength concrete was quite similar to that of the beams with normal-strength concrete in the second end region tests. The summary data for the high-strength beams are presented in Table 8.6. The comparable loads chosen for comparison were all approximately 390 kips. Figure 8.9 shows this to have been the load at which the three pristine beams exhibited a plateau. As can be seen in Table 8.6, the crack data for the high strength concrete test specimens tested in the second end region for shear had similar crack data values throughout the tests with only an occasional stray data point.

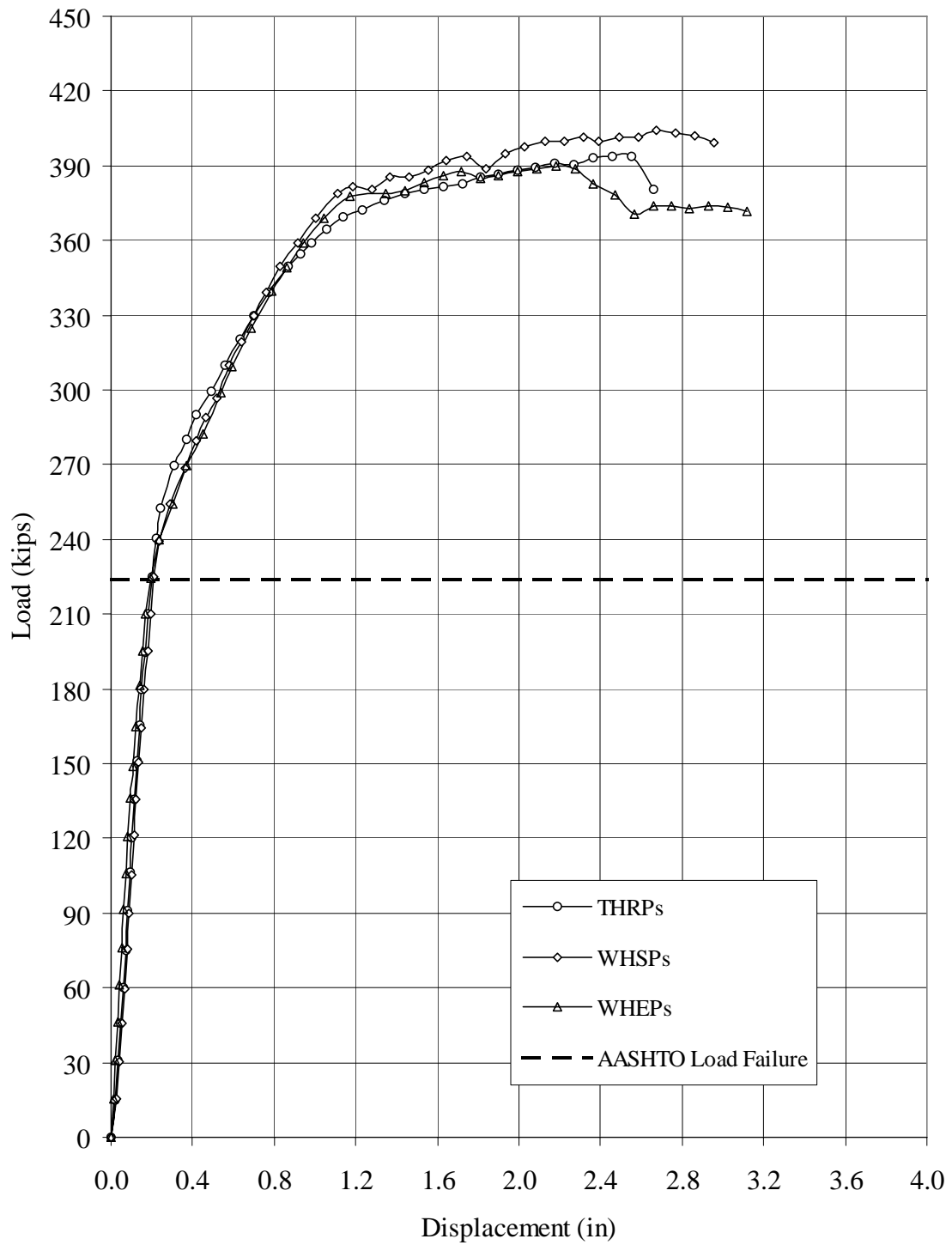


**Figure 8.9** Load-Deflection Curves for Second End Shear Region Tests on HSC Pristine Specimens



**Table 8.6** Crack Results in the High-Strength Concrete Second End Region Shear Tests

Region		N2				N3			
Test Case	Load Level (Kips)	No. of Cracks	Total Crack Area (in <sup>2</sup> )	Max. Crack Width (in)	Avg. Crack Width (in)	No. of Cracks	Total Crack Area (in <sup>2</sup> )	Max. Crack Width (in)	Avg. Crack Width (in)
<b>Flexural Beams</b>									
<b>THRFs</b>	-	-	-	-	-	-	-	-	-
<b>WHSFs</b>	389	4	1.623	0.053	0.032	7	2.353	0.054	0.041
<b>WHEFs</b>	389	4	1.390	0.041	0.031	6	2.186	0.043	0.037
<b>Pristine Beams</b>									
<b>THRPs</b>	391	7	1.810	0.064	0.039	8	3.872	0.068	0.051
<b>WHSPs</b>	392	6	1.687	0.054	0.032	6	3.267	0.069	0.046
<b>WHEPs</b>	390	7	3.154	0.049	0.038	6	3.432	0.070	0.052

- No digital image available due to beam failure before the common load increment

Comparison of the data in Table 8.6 to that in Table 8.3 for normal strength concrete shows that the high-strength concrete specimens had comparable average crack widths but a larger number of cracks in a given region, which produced a greater total area of cracking at maximum load. The maximum load was greater, however, and this should be considered in any comparison between the high- and normal-strength crack results, even though the moment was approaching the ultimate moment in each case.

#### 8.4 Summary

The maximum capacities of the second end region shear tests ranged from 38 to 89 percent greater than their AASHTO capacities calculated using experimental concrete strengths for the NSC and HSC specimens, showing adequate strength. For all the specimens, the minimum ductility ratio was 5.6; again, showing adequate ductility for all of these specimens. In general, all the WWF detail specimens showed responses similar to or better than their corresponding traditional reinforcement detail specimens, with no negative trends during this series of tests.



## CHAPTER IX

### INTERMEDIATE END REGION SHEAR TESTS

#### 9.1 Objective and Scope

The purpose of conducting “intermediate” end regions shear tests was to force a true shear failure in the second end region. These tests were added late in the test program. In the original test plan, it was expected that the first end region shear tests would produce a failure either in shear or diagonal strut compression within the first 38 inches of the beam or develop a strand slip failure, and this expectation was realized. Furthermore, it was expected that the second end region shear tests would produce a shear failure in the portion of the beam just past the 38-inch zone, but this type of failure was rare. Instead, a moment failure was the dominant behavior even with a 40% factor of safety against a flexural failure. While the realistic support and loading conditions of the second end region shear tests gave assurance that in practice the second end region would not fail in shear, it was still of interest to determine for sure if the different WWF reinforcement and alternate R-bar patterns considered were in fact adequate, both in anchorage and in relation to the traditional reinforcement and the AASHTO design capacity.

The intermediate end region shear tests were thus designed with the end support moved to the interior end of the first end region and the nearest load placed 82 inches from the end of the beam as shown in Figure 9.1. This artificial support arrangement meant that the moment arm of the end reaction had a maximum length of only 45.5 inches instead of the length of up to 72.5 inches in the second end region tests (see Figure 8.1), there again would be no strand slip problem, and shear in the second end region would almost certainly be the mode of failure.

Four types of reinforcement details were considered in intermediate end region tests: traditional, simplified WWF, equal strength WWF, and alternate R-bar. Also, only beams with normal strength concrete were included. Two intermediate end region shear tests were conducted on each of the traditional detail and the alternate R-bar detail. To differentiate between these tests, a sixth numeric distinguisher (1 or 2) was added to the initial 5-letter identification code discussed in Chapter 2. Only one intermediate end region shear test was conducted on each of the WWF details, simplified and equal strength. For all of these tests, the configuration shown in Figure 9.1 was applied to either end on the specimen.

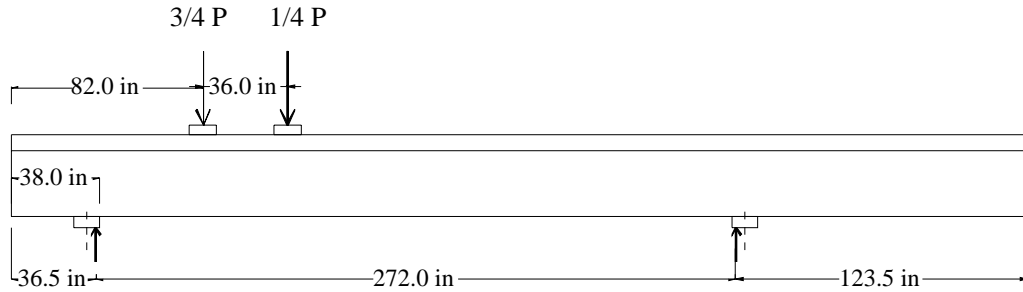


**Figure 9.1** Configuration for the Intermediate End Region Shear Test

## 9.2 Load-Deflection Behavior

Load-deflection curves for the six tests conducted using the intermediate end region arrangement are shown together in Figure 9.2. The horizontal dashed line again indicates the load corresponding to the AASHTO moment capacity and Table 9.1 presents numerical values for the key parameters of the load-deflection curves, and Table 9.2 shows a comparison between the observed peak loads and the AASHTO design load for these specimens. Note the fact that shear was the failure mode in every case except one, TNAPi1. All six specimens had similar values of stiffness, especially in the elastic range, with the transition between and elastic and plastic response occurring beyond the AASHTO design capacity. In addition, all specimens reached a load at least 69 percent greater than the expected AASHTO shear capacity. Also, all the ductility ratios were at least 6.3 as seen in Table 9.1. Thus the anchorage and shear properties of the WWF reinforcement showed to be quite adequate. The fact that the bottom anchorage was adequate is reinforced by the fact that in both of the intermediate end region tests on the beam with the WWF stirrups, the stirrups failed in tension as a pure shear failure occurred, as seen in Figure 9.3. Although a shear failure clearly occurred in the beams using traditional deformed bar, both the standard TxDOT detail and the alternate R-bar detail, total rupture of the stirrups did not appear to happen, see Figure 9.4. Straightening of the 90-degree hooks on the lower ends of the traditional and alternate R-bars was typically seen as they spalled off concrete from the bottom surface of the I-beam. This allowed slippage of the bars to occur in lieu of fracture.

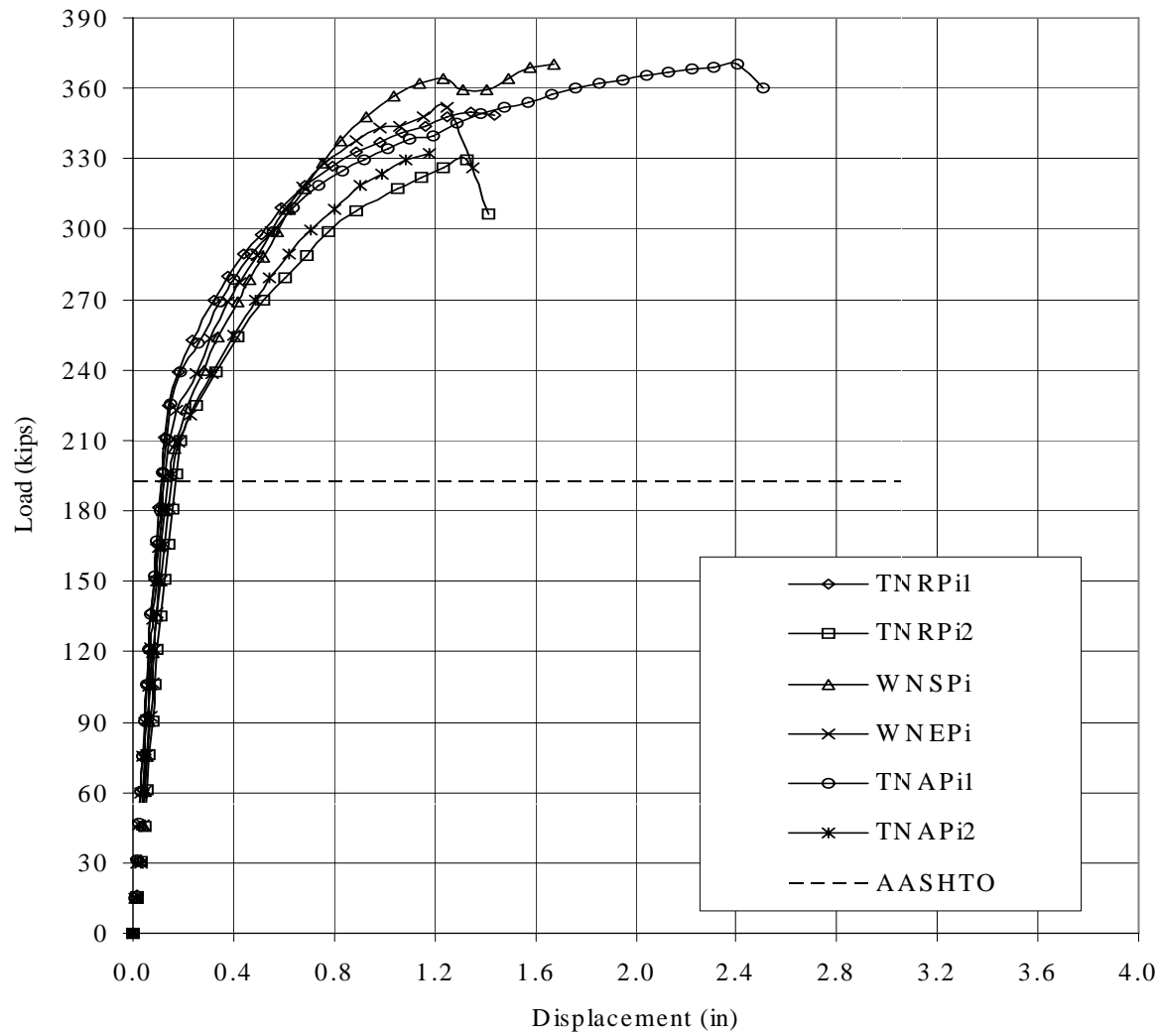


**Figure 9.2** Load-Deflection Curves for Intermediate End Region Shear Tests

**Table 9.1** Load-Deflection Parameters for Intermediate End Region Shear Tests

Beam	Beam Stiffness, $E_b$ (Kips/in)	Max.	Elastic	Cracking Load (Kips)	Max.	Final	Ductility Ratio
		Load (Kips)	Deflection (Inches)		Load (Kips)	Deflection (Inches)	
<b>TNRPi1</b>	1,596	225	0.141	137	350	1.44	10.2
<b>TNRPi2</b>	1,111	210	0.189	136	330	1.41	7.5
<b>WNSPi</b>	1,393	195	0.140	120	370	1.67	11.9
<b>WNEPi</b>	1,451	209	0.144	135	352	1.35	9.4
<b>TNAPi1</b>	1,537	226	0.147	180	370	2.41	16.3
<b>TNAPi2</b>	1,123	210	0.187	150	332	1.18	6.3

**Table 9.2** Terminal Loads and Failure Modes for Intermediate End Region Shear Tests

Beam	AASHTO Design Capacity (Kips)	Failure Load (Kips)	Ratio	Failure Mode	Wire-Break Load (Kips)
<b>TNRPi1</b>	192	350	1.82	Shear	---
<b>TNRPi2</b>	192	330	1.72	Shear	---
<b>WNSPi</b>	192	370	1.93	Shear	360
<b>WNEPi</b>	192	352	1.83	Shear	343
<b>TNAPi1</b>	196	370	1.89	Flexure	---
<b>TNAPi2</b>	196	332	1.69	Shear	---

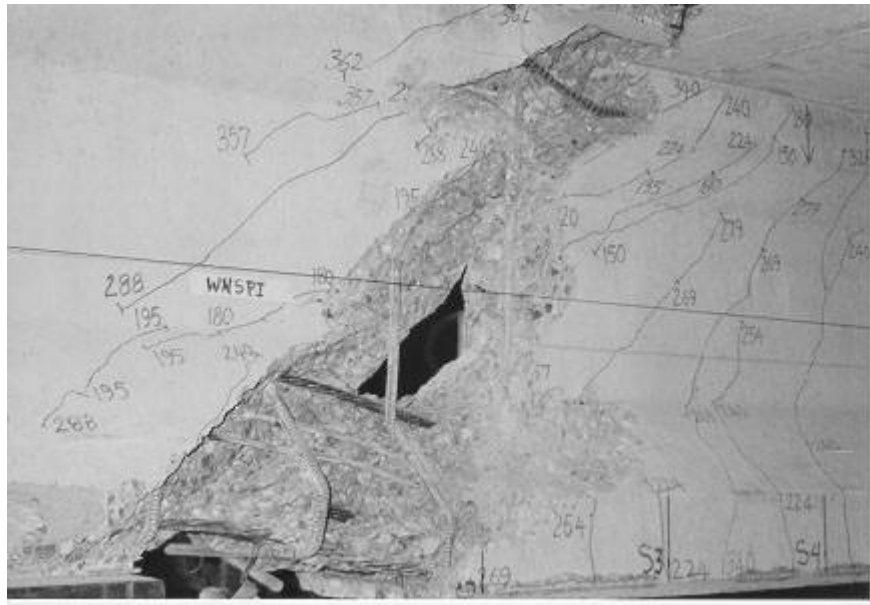


**Figure 9.3** Shear Failure of the Specimen WNSPI

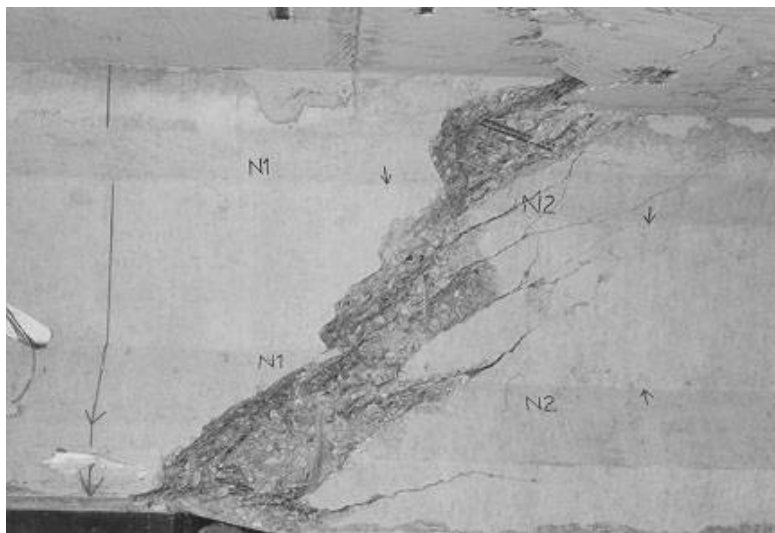


**Figure 9.4** Shear Failure of the Specimen TNRPi2

### 9.3 Cracking Behavior

For each of the intermediate end region shear tests, digital pictures were again taken at several high load levels, this time, of three 11 x 18-inch web regions: regions 1, 2, and 3 from the support. These pictures were then processed by the techniques described in Chapter 5. Selected digital imaging crack results for the six tests of Figure 9.2 are shown in Table 9.3. Data and pictures from only 2 regions of each test (N2 or S2 and N3 or S3), where the major cracking occurred, are provided here. Additional data and pictures are available in Turkyilmaz (2001). In Table 9.3, the numbers of cracks range from 3 to 6 in each region. With an 18-inch image width, three cracks average to a spacing of about 6 inches. Images for regions 2 and 3 are displayed in Figures 9.5 through 9.10. The results are quite comparable for the four reinforcement details considered.



**Figure 9.5** Final Crack Image of TNRPi1 at 319 kips (S3 & S2)

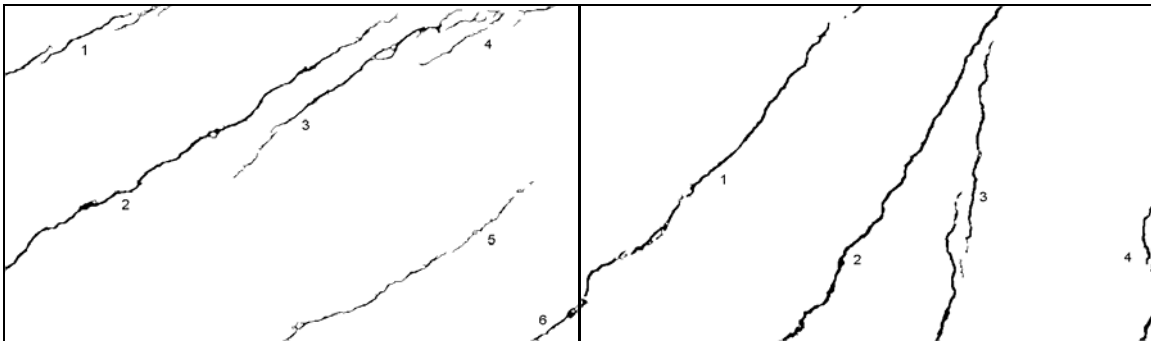


**Figure 9.6** Final Crack Image of TNRPi2 at 318 kips (N2 & N3)



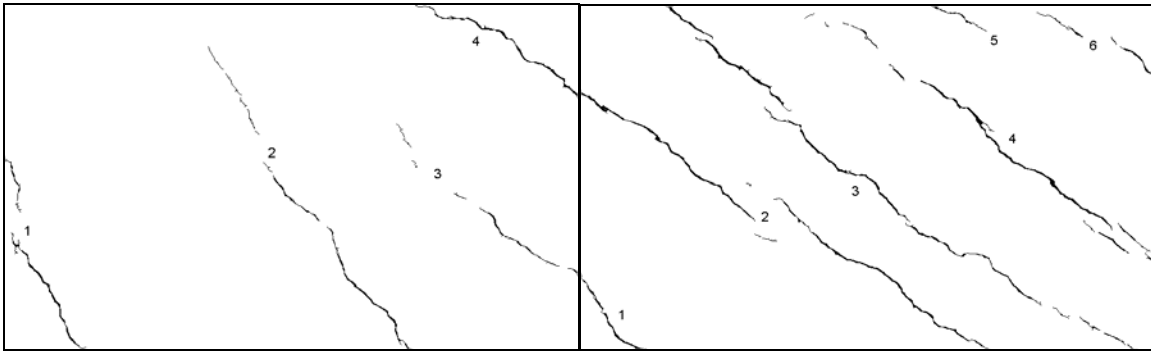


**Figure 9.7** Final Crack Image of WNSPi at 317 kips (S3 & S2)

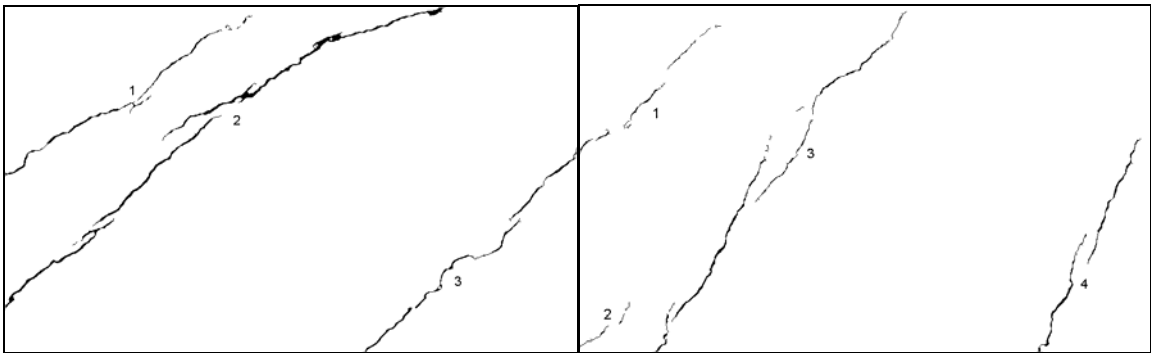


**Figure 9.8** Final Crack Image of WNEPi at 318 kips (N2 & N3)

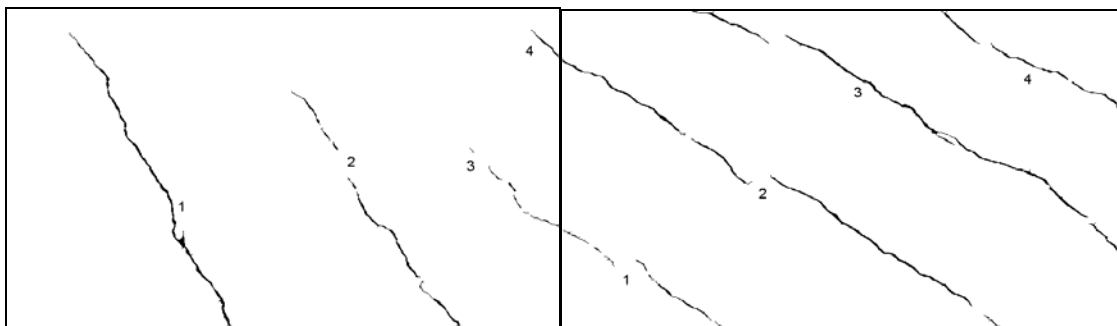


**Figure 9.9** Final Crack Image of TNAPi1 at 319 kips (S3 & S2)

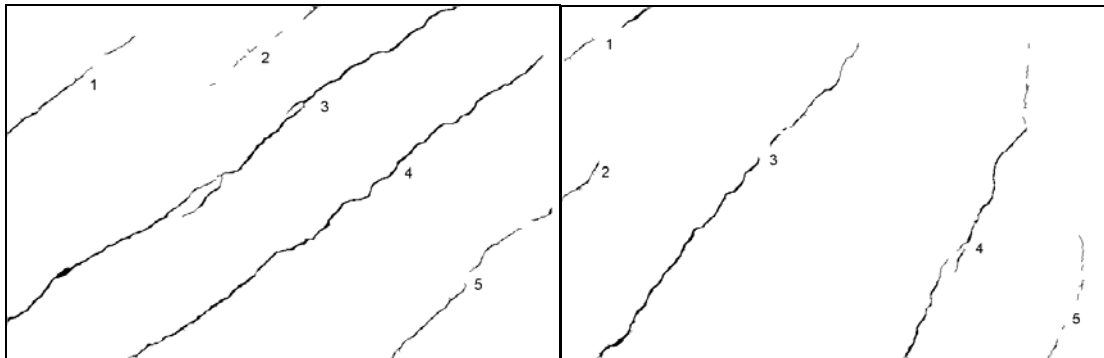


**Figure 9.10** Final Crack Image of TNAPi2 at 319 kips (N2 & N3)

**Table 9.3** Crack Results in NSC Intermediate End Region Shear Tests

Test Case	Load Level (Ksi)	N2 or S2				N3 or S3			
		No. of Cracks	Total Crack Area (in <sup>2</sup> )	Max. Crack Width (in)	Avg. Crack Width (in)	No. of Cracks	Total Crack Area (in <sup>2</sup> )	Max. Crack Width (in)	Avg. Crack Width (in)
<b>TNRPi1</b>	319	3	1.952	0.062	0.050	3	1.493	0.048	0.044
<b>TNRP2</b>	318	5	2.695	0.061	0.043	4	2.179	0.055	0.043
<b>WNSPi</b>	317	6	2.686	0.042	0.039	4	1.100	0.038	0.032
<b>WNEPi</b>	318	3	2.249	0.055	0.046	4	1.230	0.036	0.032
<b>TNAPi1</b>	319	4	2.340	0.052	0.048	4	1.327	0.058	0.048
<b>TNAPi2</b>	319	5	2.642	0.054	0.047	5	1.410	0.051	0.041

#### **9.4 Summary**

Test data for the 6 intermediate end region shear tests conducted in this project show similar responses for the 4 reinforcing details tested using this configuration. Similar stiffness and crack data, as well as large ductilities and ultimate load capacities, show that the WWF and alternate R-bar details perform as well as or better than the standard TxDOT detail.



## CHAPTER X

### POTENTIAL FATIGUE PROBLEMS

#### 10.1 Background

During the experimental testing phase of this project, loud metallic “pops” were heard coming from the test specimens. These noises were originally assumed to be individual wires within the seven-wire prestressing strands breaking prematurely due to flexure. They were considered premature breaks because of the magnitudes of the applied moments and the associated levels of strain in the prestressing strands at the times the “pops” were heard. In addition, the rising slopes of the load-deflection curves, at the time of the breakages, indicated that the prestressing strands were nowhere near their minimum guaranteed strain values of 3.5 percent. Yet, these metallic “pops” consistently occurred in flexural regions of the test specimens as the applied moments approached, but were well below, the specimens’ ultimate moment capacities. The load-deflection curves showed small drops in load immediately after the “pops” followed by further increases in load and a return of the load-deflection curves to their previous slopes as loading was continued. This indicated that something other than breaks in the individual wires of the prestressing strands were causing the “pops.”

Upon further consideration, it was discovered that the lower four longitudinal smooth wires in the WWF cages ran parallel to the prestressing strands in the maximum tension regions of the beams and that the stirrups anchored these wires in the longitudinal direction and allowed them to carry tensile forces caused by the applied moment. Until this time, the smooth longitudinal wires were only considered to anchor the vertical deformed wire stirrups, which allowed the stirrups to resist vertical shear forces. It was the breakage of these four lower smooth wires that caused the loud metallic “pops” which most commonly occurred in multiples of four. Just prior to the first wire breakage, one of the flexure-initiated cracks in or near the maximum moment region of the specimen often began to grow at a faster rate than the other cracks in the region. This crack became the dominant crack in the region as the wire breakages continued until all four lower longitudinal wires broke. This dominant crack allowed the researchers to identify where the breaks were occurring and allowed the concrete to be chipped away following the completion of the load test to expose the four fractured wires. This action was taken in several second and intermediate end region shear tests where sufficient amounts of moment were developed to fracture the wires.

A brittle failure mode at or very near the welded joints of the WWF was observed in almost all of the fractured wires. Only a very few wires failed in a ductile mode away from the welded joint. The heat generated during the electrical resistance welding process used during fabrication most probably caused the brittleness of the WWF at its welded

joints. It is the brittleness of the WWF at its joints that first began to raise the question of fatigue, which is most critical in brittle materials loaded in tension.

## **10.2 Literature Review**

A review of the literature did produce two key articles addressing cyclic loading and fatigue effects on WWF and prestressed concrete beams (Pincheira, et. al., 1989, and Ayyub, et. al., 1994). Pincheria (1989) reported ultimate loads associated with prestressed concrete T-beams with deformed WWF shear reinforcement. Comparisons of ultimate loads were made between two beams, one subjected only to a monotonically increasing static load and one subjected to increasing magnitudes of cyclic loads with 20,000 cycles at each load increment until over 200,000 cycles were applied. The cyclically loaded beam had a 26.5 % decrease in ultimate load capacity when compared to the similar beam that had only been statically loaded, showing a significant fatigue effect. It should be noted that cyclic loads well above service loads were applied and that web-shear cracks developed only after 70,000 cycles. However, this test result does not tell the complete story about fatigue associated with WWF in prestressed concrete beams. Fatigue is also a function of the magnitude of the change in stress as well as the number of stress cycles. Since the reinforcing steel does not carry a significant portion of the load until after cracking and a prestressed concrete beam should remain uncracked at service loads, the magnitudes of the changes in stresses in the WWF of Pincheira's study were much higher than would be expected at service load conditions in a prestressed concrete beam in the field. Therefore, the WWF in his study was much more susceptible to fatigue than the WWF in the prestressed concrete beams of this project.

The second key article, by Ayyub, et. al., (1994), reported test data on the number of cycles to failure of bare WWF reinforcement for four stress ranges from 20 ksi to 50 ksi. WWF test specimens in Ayyub's work were directly loaded in a test machine and were not embedded in a concrete specimen. Of the three WWF specimens that were loaded in the 20-ksi stress range, two successfully completed 10,000,000 cycles with no evidence of fatigue while the third specimen failed at 5,728,460 cycles. However, the fracture of the third specimen occurred at one of the grips where stress concentrations would be expected to occur. During the other tests, the number of cycles to failure decreased as the magnitude of the stress range increased. Also, the failure modes became more fatigue related at or near the welded regions as the stress ranges increased, further indicating potential problems with fatigue in the heat-affected zone of the electrical resistance welds used during the fabrication of WWF.

## **10.3 I-beam Related Concerns and Resolutions**

Two primary fatigue issues associated with WWF were addressed in this project. The first issue was the cyclic tension in the longitudinal smooth wires in the flexural-tension region located in the bottom flange of the beam. Fracture of these wires where they are welded to the R-bar stirrups could cause loss of anchorage for the stirrups and therefore loss of stirrup capacity. The second issue was the cyclic tension in the vertical

deformed wire stirrups near the intersection of the upper beam flange and its web, in the high shear regions near the ends of the beams. Fracture of these wire stirrups, near their upper welds, would also cause overall loss of shear capacity for the beam. Either of these two scenarios would be unacceptable and both were investigated in this project for probability.

The first fatigue issue noted above, fatigue in the lower longitudinal smooth wires, was addressed by a parametric study using TxDOT's computer code PSTRS-14 (1997) for the beam types, spacings, and span lengths shown in Table 10.1, which are typical design values taken from TxDOT standards. The span lengths used in Table 10.1 represent typical minimum, average, and maximum span lengths. PSTRS-14 analyses were run for each of the parameters listed in Table 10.1 using HS-20 loads to determine the maximum lower fiber concrete stress at mid-span caused by the live load (plus impact). Assuming strain compatibility between the steel and the concrete, these stress values were used to estimate the maximum change in stress that would occur in the lower longitudinal smooth wires. Considering all of the cases shown in Table 10.1, the largest live load change in stress was determined to be in the lower longitudinal smooth wire and was estimated to be 8.8 ksi. The value 8.8 ksi was well below the 20-ksi value reported by Ayyub (1994) where the WWF was able to withstand 10 million load cycles with no adverse fatigue effects. In addition, this maximum stress value occurred at mid-span where shear forces are small. At the outside quarter points of the span, the maximum live load steel stress was reduced to 7.1 ksi, even more conservative against a fatigue fracture. In addition, the live load stresses in the lower longitudinal smooth wire remained totally in the compression range from the outside quarter points to the ends of the beam due to the pre-compression in the beam. This fact by itself negates the concern about fatigue in the lower longitudinal smooth wires in the end regions of the beams where the vertical shear forces are the largest.

**Table 10.1** PSTRS-14 Analyses Parameters

Beam Type	Beam c/c Spacing (feet)	Span Length (feet)		
		30	40	50
A	6.7	30	40	50
B	6.7	30	48	65
C	8.0	40	60	80
IV	8.0	40	78	116

The second fatigue issue noted above, the cyclic tension in the vertical deformed wire stirrups near their upper welds where they are also connected to longitudinal smooth wires, was addressed experimentally in tests WNSPI and WNEPI. These tests were conducted on opposite ends of the same test specimen. Here, twenty strain gages (ten at each end of the beam with five on the near side and five on the far side of the beam) were embedded in the concrete using witness bars as described in Section 4.2.1, see Figure 10.1. The strain gages were installed in the upper region of the I-beam near the intersection of the beam's web and upper flange where the shear stresses would be greatest. The gages were oriented in the vertical direction and located near the vertical deformed wire stirrups just inside the second end region near the transition from the 4-inch to 8-inch center-to-center spacing. For the intermediate end region shear tests, this corresponded to the most critical shear region for the stirrups. Just prior to the formation of shear cracks, which appeared at loads of around 120 kips, the strains in the gages were a mix of compression and tension with the maximum value equal to only 42 microstrains. This equates to a stress in the steel of approximately 1.2 ksi when strain compatibility is assumed. A stress level of 1.2 ksi in the vertical wire stirrups is well below the 20-ksi stress level reported by Ayyub (1994) where 10 million cycles were achieved with no noticeable fatigue effects. The strains in these gages increased significantly in magnitude as tensile strains as soon as cracking of the concrete occurred in their immediate regions. However, properly designed prestressed concrete beams will remain uncracked at service load conditions and will produce very low magnitudes of tensile stresses in the vertical shear reinforcement so that the second fatigue issue should not be of concern.



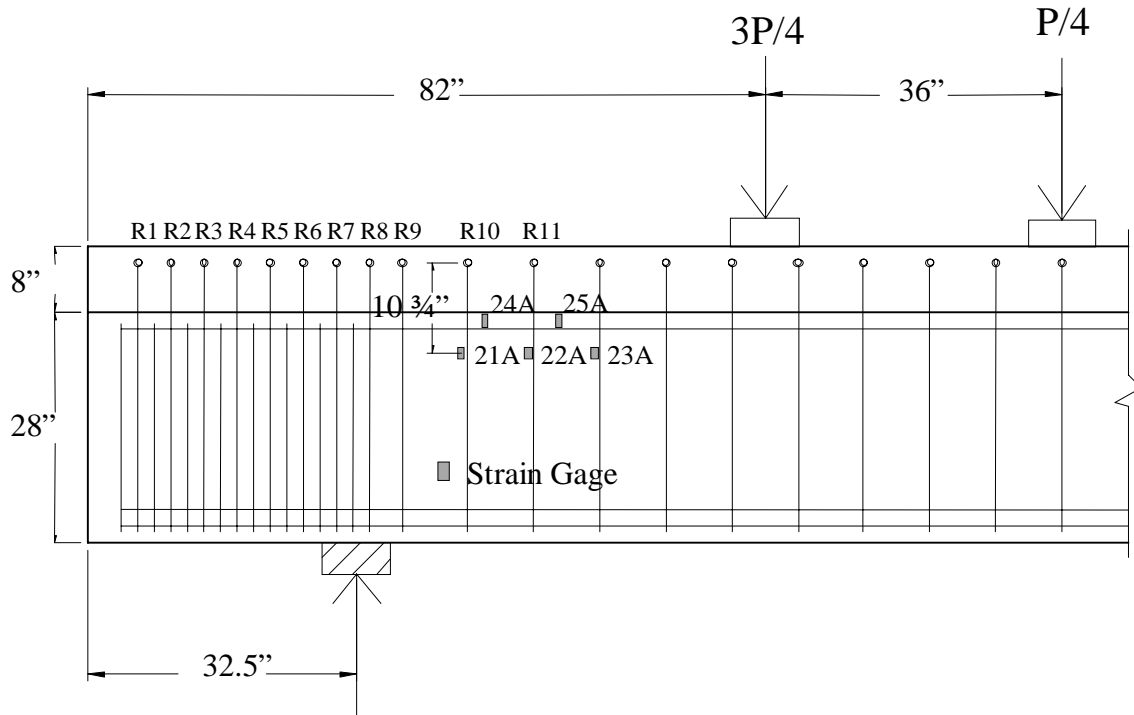


**Figure 10.1** Fatigue Related Strain Gage Installations

#### 10.4 Summary

In summary, the observed brittle fracture mode of the longitudinal smooth wires in the vertical steel cages, at or near the welded joints, raised concern about fatigue causing premature failure of the WWF reinforcement installed in prestressed I-beams. Analytical and experimental methods were used to investigate the presence of large magnitude cyclic tensile stresses in the WWF. These two methods were used in two separate critical regions of the test specimens to determine the potential levels of cyclic tensile stress in the WWF. The brittle nature of WWF near the electrical resistance welds could make it susceptible to fatigue. It was determined in both of the critical regions that the maximum levels of tensile stress were well below the threshold value of 20 ksi, as reported by Ayyub (1994), below which fatigue in WWF was not a problem.



## CHAPTER XI

### SUMMARY, CONCLUSIONS, AND RECOMMENDATIONS

#### 11.1 Summary

##### 11.1.1 Test Program

The purpose of this research project was to determine if welded wire fabric (WWF) could function as well as traditional, individually tied steel bars as shear reinforcement in prestressed concrete bridge beams. In particular, the adequacy of the bottom anchorage of the WWF R-bars as currently specified by ACI, AASHTO, PCI, and WRI needed to be verified. Through a series of 43 load tests on 18 full-scale TxDOT Type A I-beam specimens, the project compared the shear and moment capacities of traditionally reinforced and WWF-reinforced members designed to current TxDOT specifications. Also, the tests explored a range of other parameters of interest: high-strength (10- to 12-ksi) and normal strength (5- to 7-ksi) concrete in the I-beam, 80-ksi and 60-ksi WWF in the shear reinforcing cage, a WWF shear cage with uniform stirrup sizes rather than alternating D31 and D20 bars to match the traditional sizes, and an alternate bottom anchorage of traditional R-bars to avoid the concrete coverage problems sometimes encountered in their installation.

The tests were conducted in the Civil Engineering structures laboratory at Texas Tech University with its structural test deck and a special steel load frame. The specimens were fabricated by the Southwest Prestressed Concrete Company in Amarillo, Texas. Each I-beam had an 8-inch-thick by 6-foot-wide concrete deck slab reinforced according to TxDOT specifications cast on it. Five load tests were performed on a typical matched pair of beams, with the exception of the eighth pair. One test was in flexure, with symmetric loads applied near midspan to verify the moment capacity of the pair, but the test was stopped just short of flexural failure. Then two shear tests to failure were carried out on opposite ends of the same beam, called the “flexural beam,” one test placing only the “first end region” (first 38 inches) in shear to determine the strength of the region heavily reinforced with both R-bars and S-bars, and the other test placing the “second end region” (first 66 inches) in shear. Finally, identical opposite end shear tests to failure were performed on the second specimen of the pair without prior flexural testing. This specimen was called the “pristine beam.” All four ends of the eighth pair of beams were tested using an artificial load configuration designed to force a shear failure in the second end region of the shear reinforcement. These tests were designated “intermediate end region” test. The test parameters used in the eighth pair were selected combinations of previously tested parameters.

The specimens were instrumented for displacements with dial gages, a wire gage, and linear variable displacement transducers (LVDTs) and for strain with concrete strain

gages on the top of the slab and “witness bars” attached to the internal reinforcement for strains in some stirrups. Also, the load applied by the million-pound-capacity hydraulic ram was monitored in three ways, and end-slip measurements were taken of the straight reinforcing strands during two of the three types of shear tests, first and second end regions. Thirty-five millimeter pictures of marked cracks were taken on one side of the I-beam and digital pictures of unmarked cracks were taken on the other side. All of the electronic data were monitored and recorded by a computer to give real-time load-deflection and strain results, while mechanical data were individually read and recorded by hand.

A special study was conducted to quantify the cracking near failure of the differently reinforced beams through digital imaging, and the crack areas and widths were compared with this method.

### 11.1.2 Test Results

The specimens in this test program all performed up to expectations in that, in every case, the capacity of the beam met or exceeded the AASHTO design capacity. Specimen failure load to AASHTO design load ratios from 1.24 to 1.93 for all shear tests. Flexural tests were not loaded to failure but were loaded beyond the AASHTO design moment capacity. In comparing the performance of the beams with WWF reinforcement to those with traditional reinforcement, the WWF specimens had similar or improved responses when comparing ductility ratios, elastic and plastic stiffnesses, and loads at first cracking. This generally comparable behavior was true for the “matching” WWF design, for the “simplified” WWF design, and for the “equivalent strength” WWF design, both with normal strength and high strength concrete. The specimens with alternate R-bars, that is, with the 90-degree hooks at the lower ends of the deformed bar stirrups turned parallel the beam axis, also exhibited similar or improved responses when compared to beams reinforced with traditional R-bars.

Cracking in all the specimens was also comparable at comparable loads near failure. Crack areas and widths, as quantified by the newly developed digital imaging technique, were almost the same for the WWF specimens as for the specimens with traditional reinforcement. Good crack width and crack area results were obtained by digital imaging for cracks of small to large width, but limitations were encountered in attempting to use the method on very narrow (hairline) cracks.

### **11.2 Conclusions**

Both a “matching” WWF cage (one-for-one substitution of welded wire fabric R-bars and S-bars) and a “simplified” WWF cage (uniform bars of average size between the two) are acceptable for the shear reinforcement in TxDOT prestressed bridge beams. However, the simplified design would seem to be more advantageous in that it is less expensive to fabricate in a WWF shop through full automation of the process, and with the average sizes being smaller than the No. 7 traditional bars required for the largest TxDOT

beams, it will permit fabrication using WWF even for these beams. No. 7 bars are beyond the normal size limits of WWF.

The current TxDOT design standards for WWF vertical reinforcement are satisfactory for carrying the maximum shear force that can come upon the beam. Use of nominal 80-ksi as well as nominal 60-ksi WWF wires is acceptable for the vertical shear reinforcement. Although the cracks in the test beams with high-strength wires grew at a faster rate than the cracks in the beams with normal-strength wires, this cracking should not be an issue in prestressed beams since they are designed to carry service loads without cracking.

There should be no restriction against using high-strength (10-plus ksi) concrete in the prestressed beams of TxDOT bridges if a design of the longitudinal reinforcement is carried out to take proper advantage of the strengths of both the steel and the concrete.

It is acceptable to use an alternate detail for the bottom anchorage of traditional R-bars in which the 90-degree hooks are rotated to be parallel to the axis of the beam.

Digital imaging for the measurement of cracking in concrete beams should be considered and possibly tested on existing TxDOT bridges. In the beams of this project, good crack width and crack area results were obtained for cracks of small to large width, but limitations were encountered in attempting to use the method on very narrow (hairline) cracks.

### **11.3 Recommendations**

Based on the results of this research project, the following recommendations are submitted to the Texas Department of Transportation.

#### **11.3.1 TxDOT Policies and Standards**

While both a “matching” WWF” cage (one-for-one substitution of R-bars and S-bars) and a “simplified” WWF cage (uniform bars of average size between the two) are acceptable for the shear reinforcement in TxDOT prestressed bridge beams, the simplified design is recommended in order to take advantage of its less expensive fabrication.

It is recommended that the use of nominal 80-ksi as well as nominal 60-ksi WWF wires be permitted for the design of vertical shear reinforcement.

There should be no restriction against using high-strength (10 to 12- ksi) concrete in the prestressed beams of TxDOT bridges if the design of the longitudinal reinforcement is carried out to take proper advantage of the strengths of both the steel and the concrete.

It is acceptable to use an alternate detail for the bottom anchorage of traditional R-bars in which the 90-degree hooks are rotated to be parallel to the axis of the beam. Hook

lengths should be shortened to 3.5 inches to allow clearance between R-bars in the first end region.

Digital imaging for the measurement of cracking in concrete beams should be considered and possibly tested on existing TxDOT bridges.

### 11.3.2 Future Research

For further understanding and applications that might provide even more economy in the future, it is recommended that a study be conducted of the use of fiber-reinforced concrete in place of some of the smaller first end region bars to prevent congestion and to simplify and speed up the construction process. Tests would be needed to verify that the fiber reinforcement can successfully supplant the bars in preventing unwanted cracking and failure.

It might also be prudent to conduct a limited number of shear tests on prestressed concrete I-beams of a larger size than the Type A beams used in this research project to make sure that some kind of scale factor does not come into play to adversely affect the strength and that the WWF anchorage found to be adequate for the smaller beams is also adequate for larger ones.

Shear capacities as predicted by current AASHTO standards (1996) are extremely conservative. A further study to better understand the shear phenomena and modify existing codes could yield more economical designs. In addition, a comparison of the test data obtained in this project and the new AAHSTO LRFD code design values should be conducted.

Preliminary studies conducted during this project indicate that fatigue is probably not an issue with prestressed concrete I-beams reinforced with WWF, but the observed brittle failure mode of the wires at or near the heat-affected zones of the electrical resistance welds does warrant additional consideration. This could be accomplished by additional full-scale testing with cyclic loading followed by static loading to failure.

The Digital Image Analysis Technique developed during this project for crack evaluation worked well for cracks with small to large widths and has the potential to work equally as well for very narrow (hairline) cracks typically seen in concrete members at service loads. Additional work is required to further develop this technique for use with long-term evaluations of bridges.

## REFERENCES

1. AASHTO, (1996), "Standard Specifications for Highway Bridges," American Association of State Highway and Transportation Officials, 16<sup>th</sup> Edition, Washington, D. C.
2. ACI Committee 318, (1999), "Building Code Requirements for Reinforced Structural Concrete (318-99) and Commentary (318R-99)," American Concrete Institute, Farmington Hills, Michigan.
3. Ayyub, B. M., Chang, P., and Al-Mutairi, N. (1994). "Welded Wire Fabric for Bridges. I: Ultimate Strength and Ductility." *ASCE J. Struc. Engrg.*, 120(6), 1866-1881.
4. Ayyub, B. M., Chang, P., and Al-Mutairi, N. (1994). "Welded Wire Fabric for Bridges. II: Fatigue Strength." *ASCE J. Struc. Engrg.*, 120(6), 989-997.
5. Burkett, W. R., and Kose, M. M., (1999), "Development Length of 0.6-inch Diameter Prestressing Strand at 2-inch Grid Spacing in Standard I-shaped Pretensioned Concrete Beams," Report No. TX / 98 / 1388-2, Texas Tech University, Lubbock, Texas.
6. Cedeno-Rosete, R., (2001), "Alternate Vertical Steel Reinforcement in Prestressed Concrete Beams," Ph.D. Dissertation, Texas Tech University, Lubbock, Texas.
7. Griezic, A., Cook, W. D., and Mitchell, D., (1994). "Tests to Determine Performance of Deformed Welded Wire Fabric Stirrups." *ACI Struc.l J.*, 91(2), 211-220.
8. Lin, C. H., and Perng, S. M., (1998). "Flexural Behavior of Concrete Beams with Welded Wire Fabric as Shear Reinforcement." *ACI Struc Journal*, 95(5), 540-546.
9. Mansur, M. A., Lee, C. K., and Lee, S. L., (1986). "Anchorage of Welded Wire Fabric Used as Shear Reinforcement in Beams." *Magazine of Concrete Research.*, 38(134), 36-46.
10. MATLAB, (2001), "Image Processing Toolbox," The MathWorks, Inc., Version 6.1, Natick, Massachuttes.
11. PCI, (1985), "PCI Design Handbook, Precast and Prestressed Concrete," Prestressed Concrete Institute, 3<sup>rd</sup> Edition, Chicago, Illinois.
12. Pincheira, J. A., Rizkalla, S. H., and Attiogbe, E. K., (1989). "Performance of Welded Wire Fabric as Shear Reinforcement Under Cyclic Loading." *ACI Struc.l J.*, 86(6), 728-735.

13. PSTRS-14, (1997), "TxDOT Prestressed Concrete Beam Program PSTRS-14," Texas Department of Transportation, Version 3.21, Austin, Texas.
14. Robertson, I. N., and Durrani, A. J., (1987). "Shear Strength of Prestressed Concrete T Beams with Welded Wire Fabric as Shear Reinforcement." *PCI Journal* March-April 1987, 46-61.
15. Turkyilmaz, S., (2001), "Characterization of Cracks in Bridge Beams with Welded Wire Fabric Reinforcement Using Image Processing," Master Thesis, Texas Tech University, Lubbock, Texas.
16. WRI, (1993), "Structural Welded Wire Reinforcing Detailing Manual," Wire Reinforcement Institute, Findlay, Ohio.
17. Xuan, X., Rizkalla, S., and Maruyama, K., (1988). "Effectiveness in Pretensional Prestressed Concrete T-Beams." *ACI Struct. J.*, 85(4), 429-436.



APPENDIX A  
BEAM REINFORCEMENT DETAILS

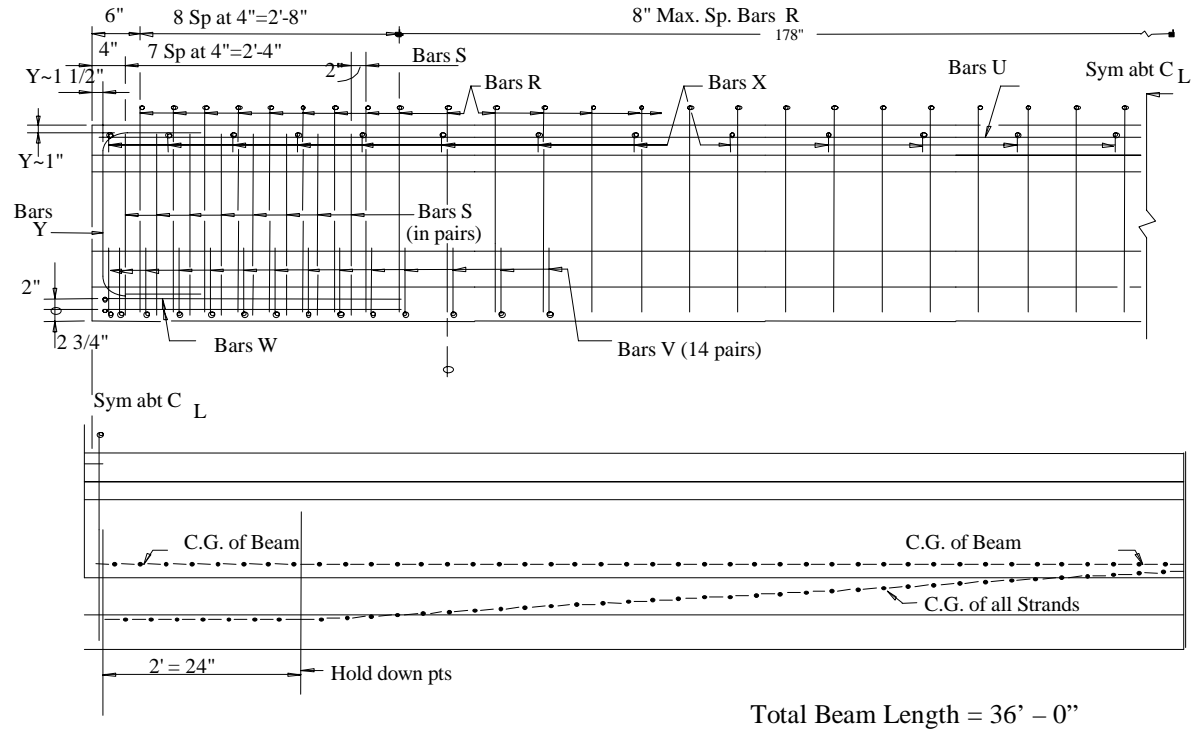
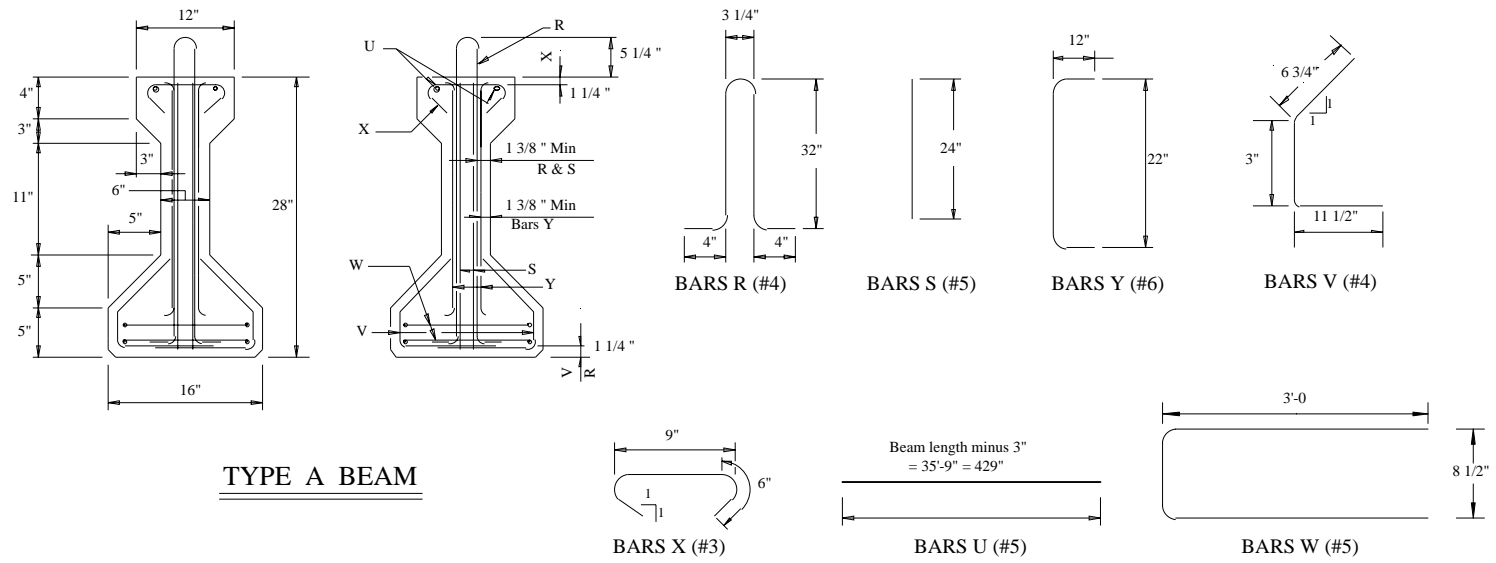


Figure A.1 Longitudinal Reinforcement Detail of the Traditional Specimen



**Figure A.2** Section Reinforcement Detail of the Traditional Specimens

A-4

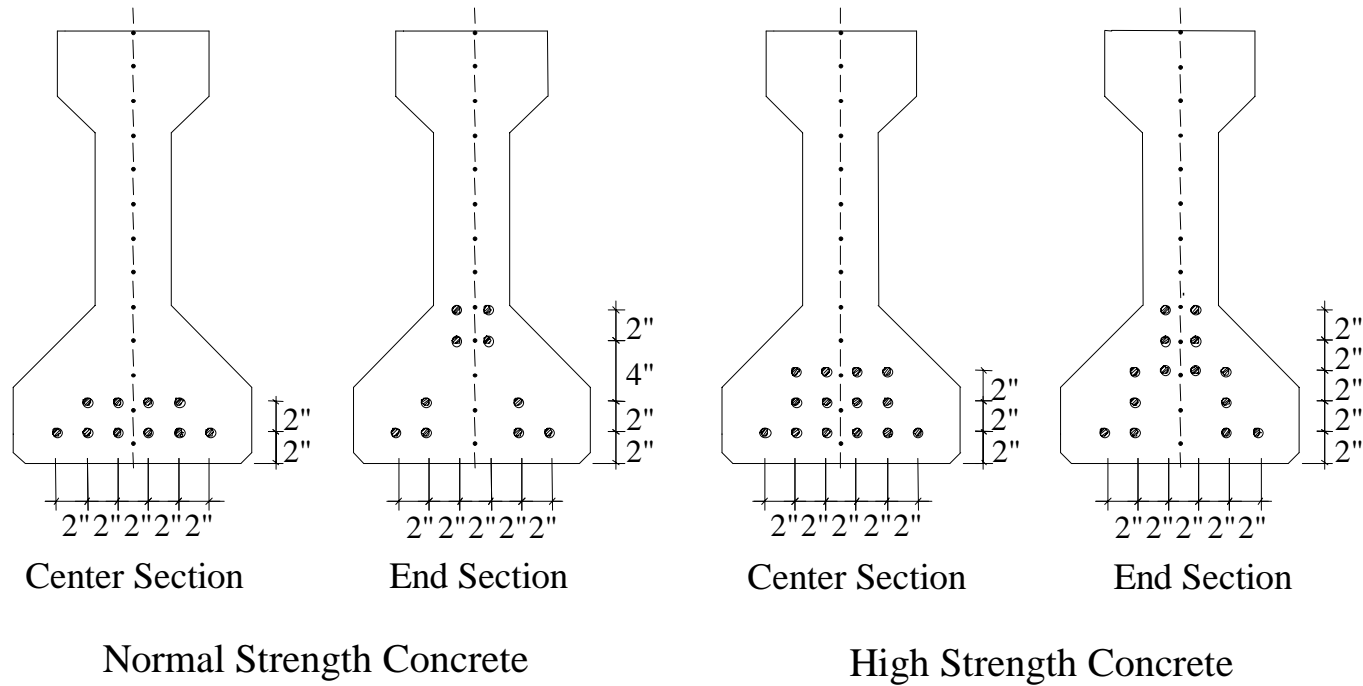
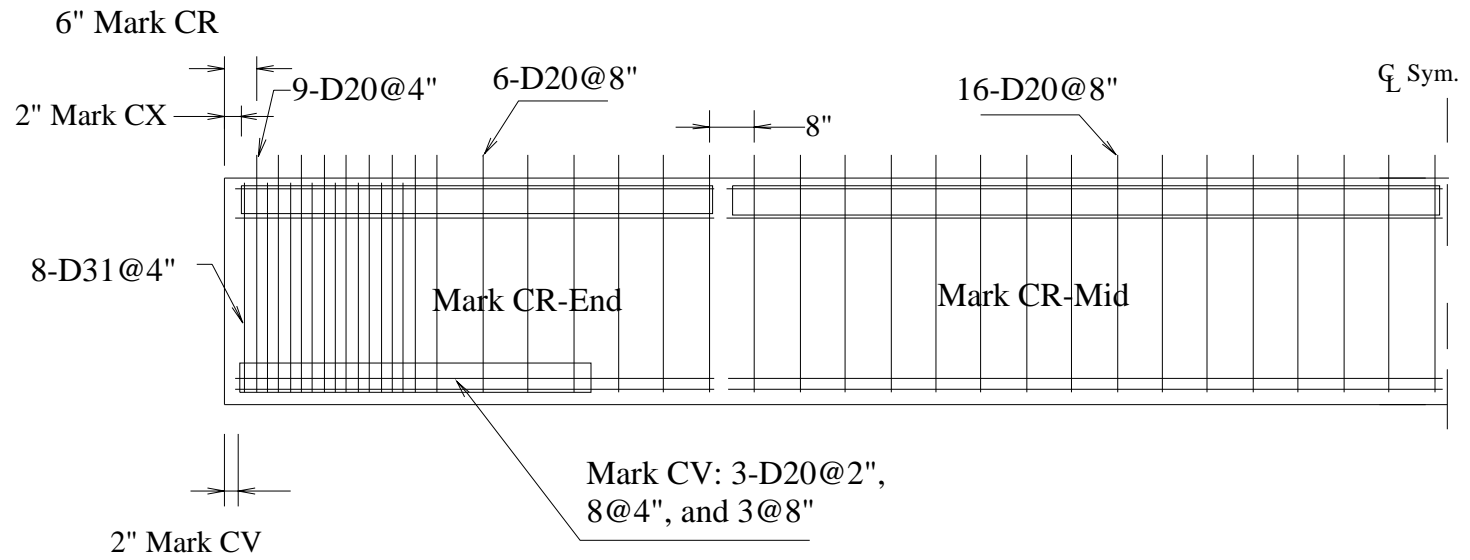


Figure A.3 Strand Position Detail of the Traditional Specimens

A-5



**Figure A.4** Matching Welded Wire Fabric Substitution Longitudinal Section

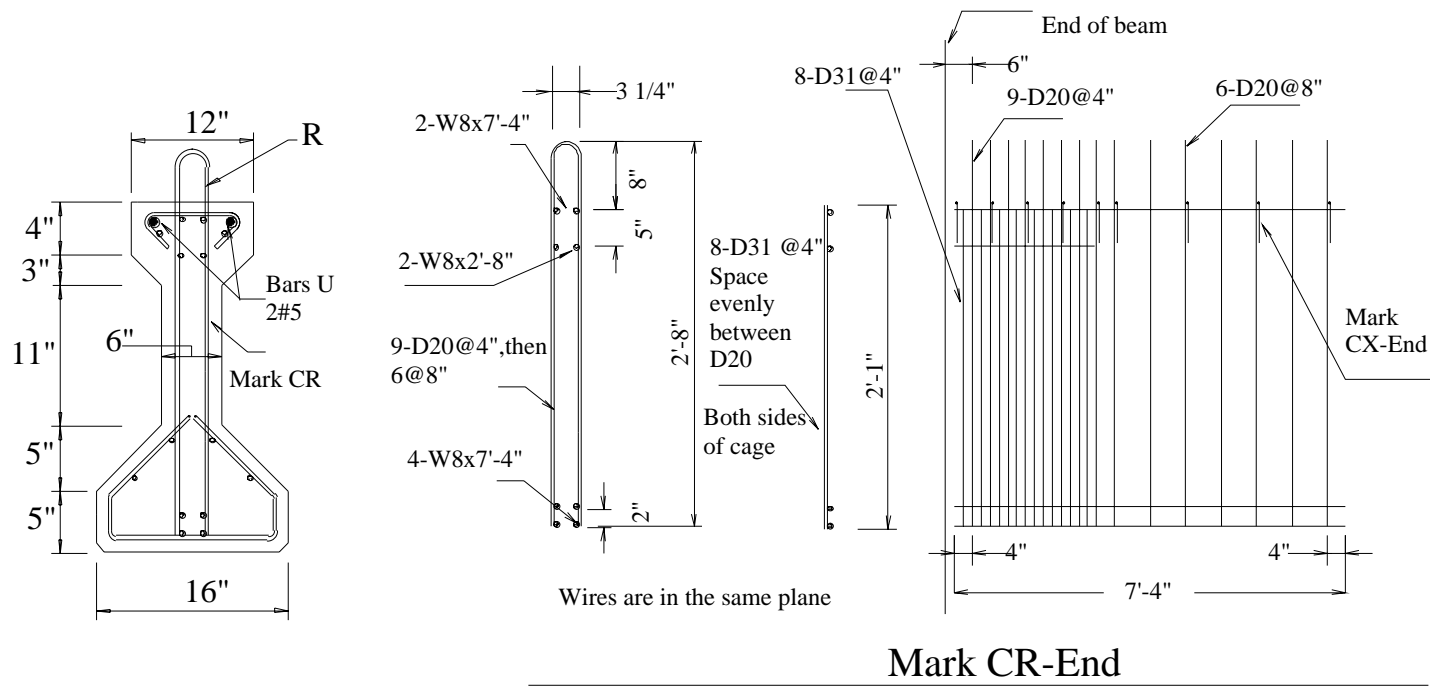
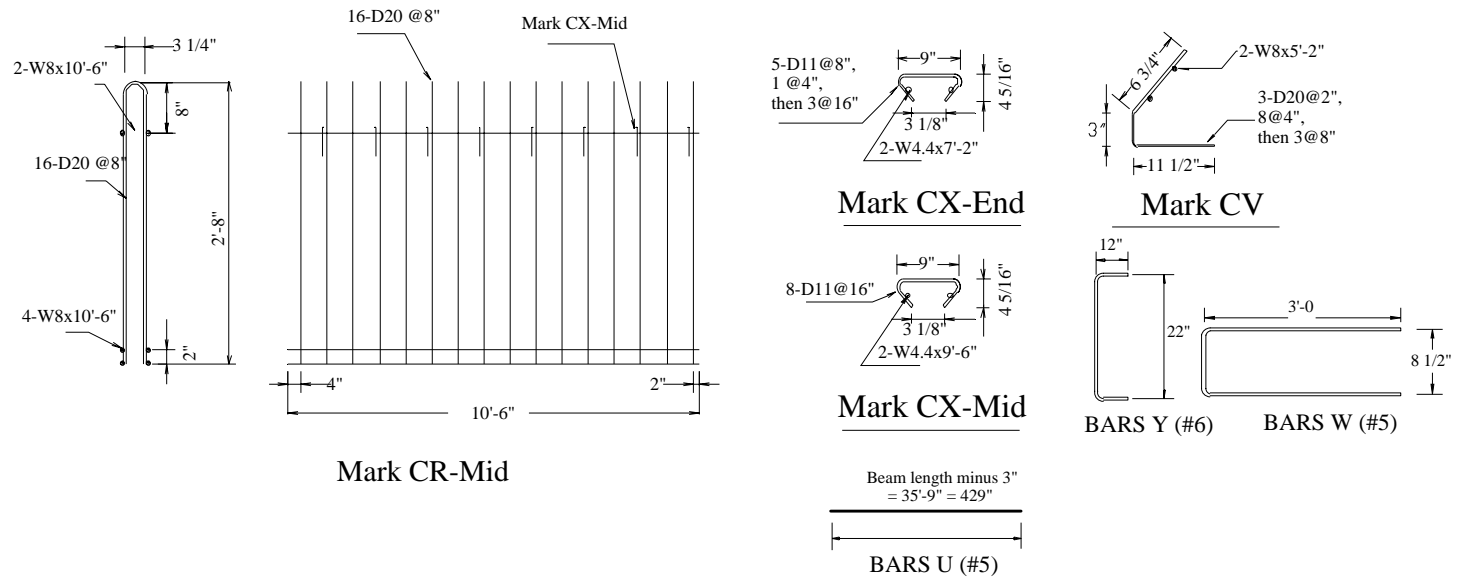
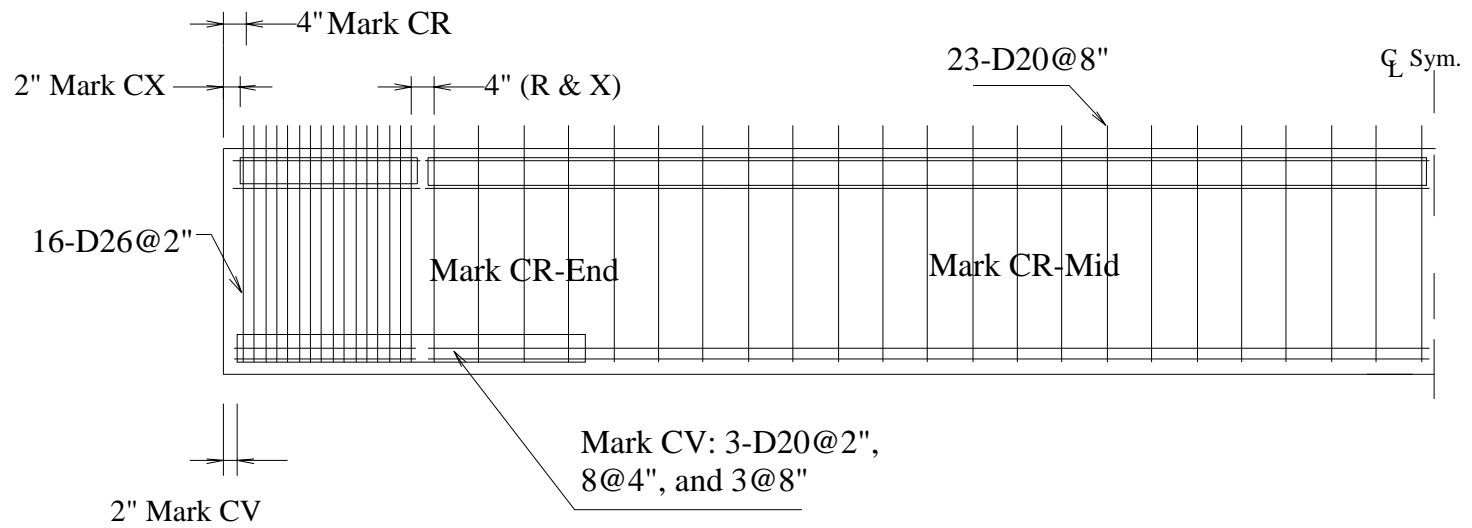


Figure A.5 Matching Welded Wire Fabric Substitution Mark CR-End



**Figure A.6** Matching Welded Wire Fabric Substitution Mark CR-Mid

A-8



**Figure A.7** Simplified Welded Wire Fabric Substitution Longitudinal Section



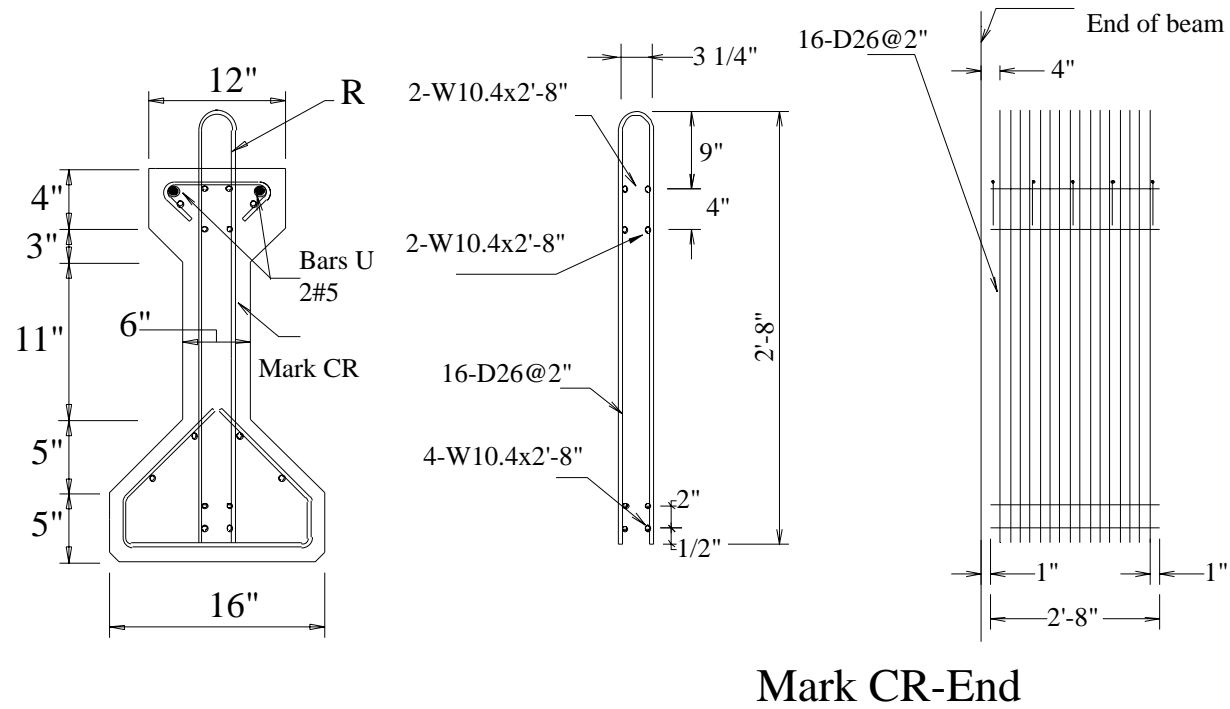


**Figure A.8** Simplified Welded Wire Fabric Substitution Mark CR-End

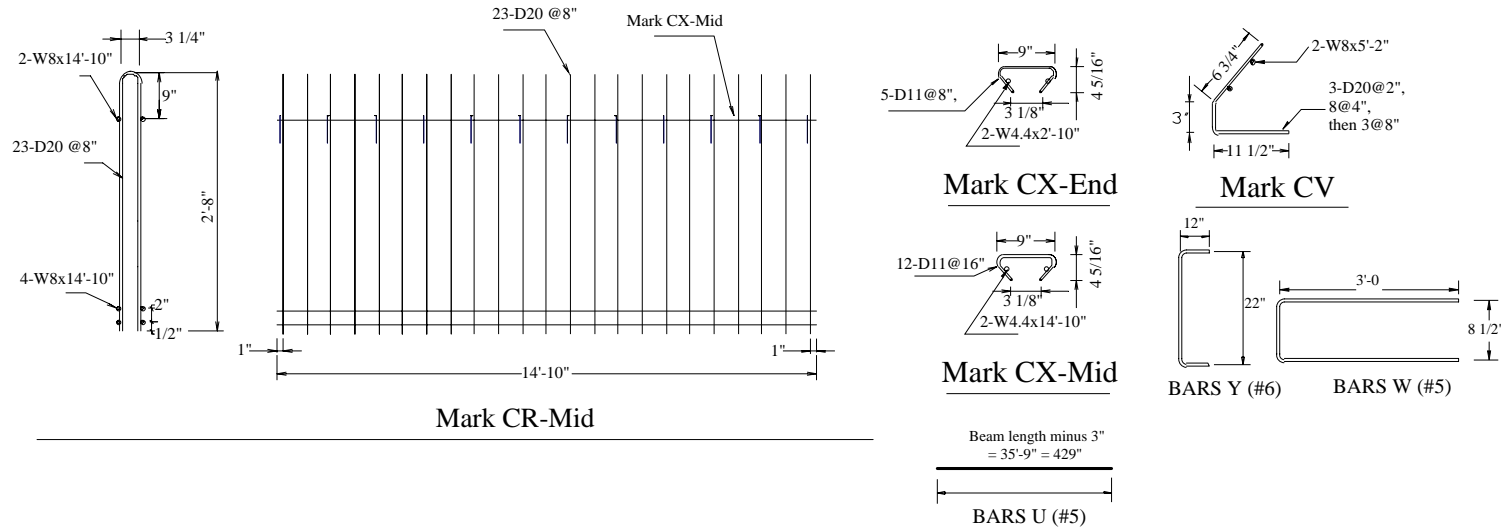


**Figure A.9** Simplified Welded Wire Fabric Substitution Mark CR-Mid

A-11

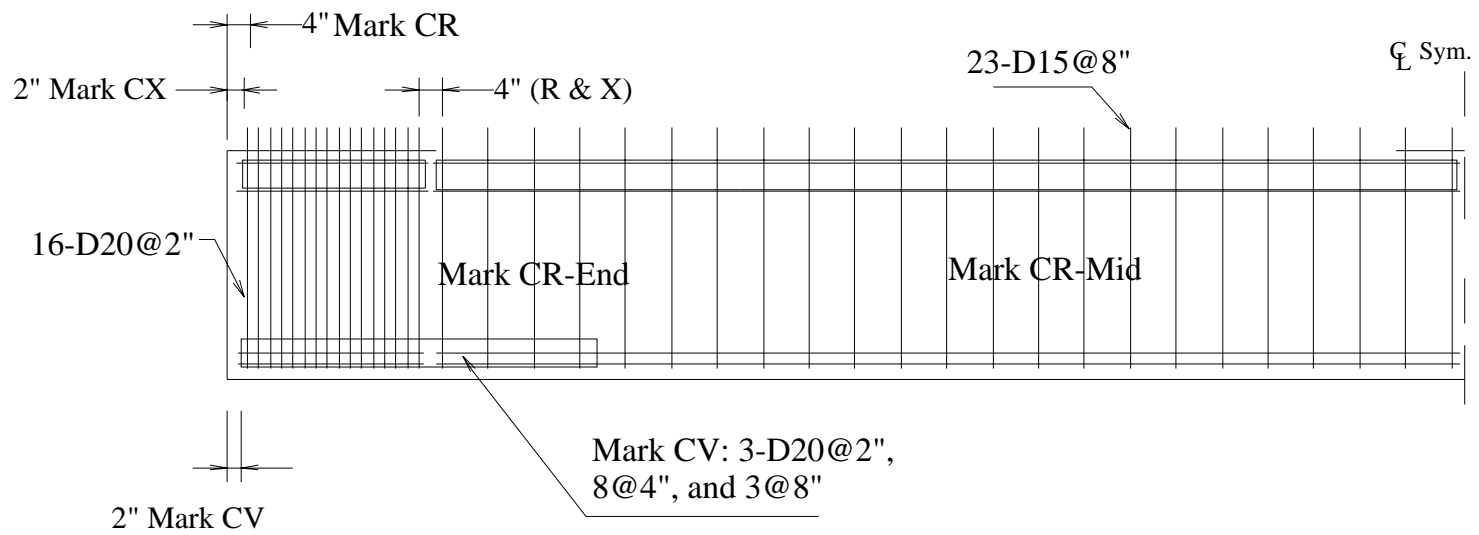


**Figure A.10** Equivalent Strength Welded Wire Fabric Substitution Longitudinal Section

A-12

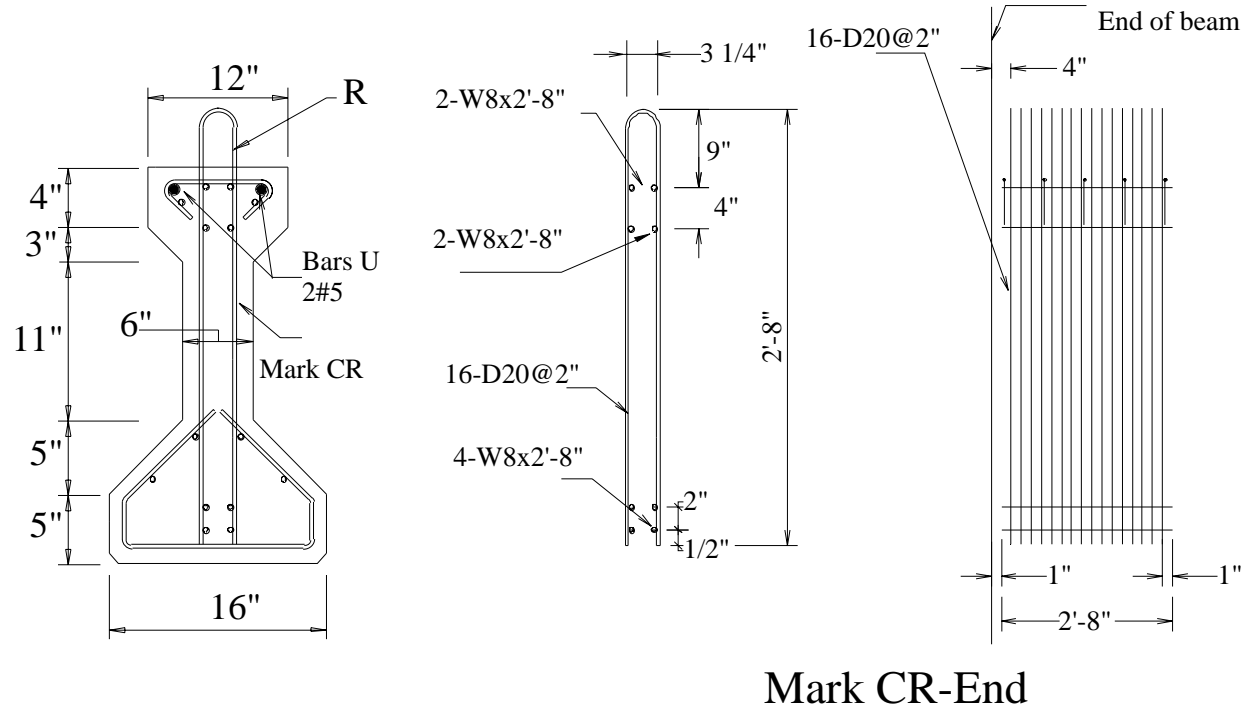
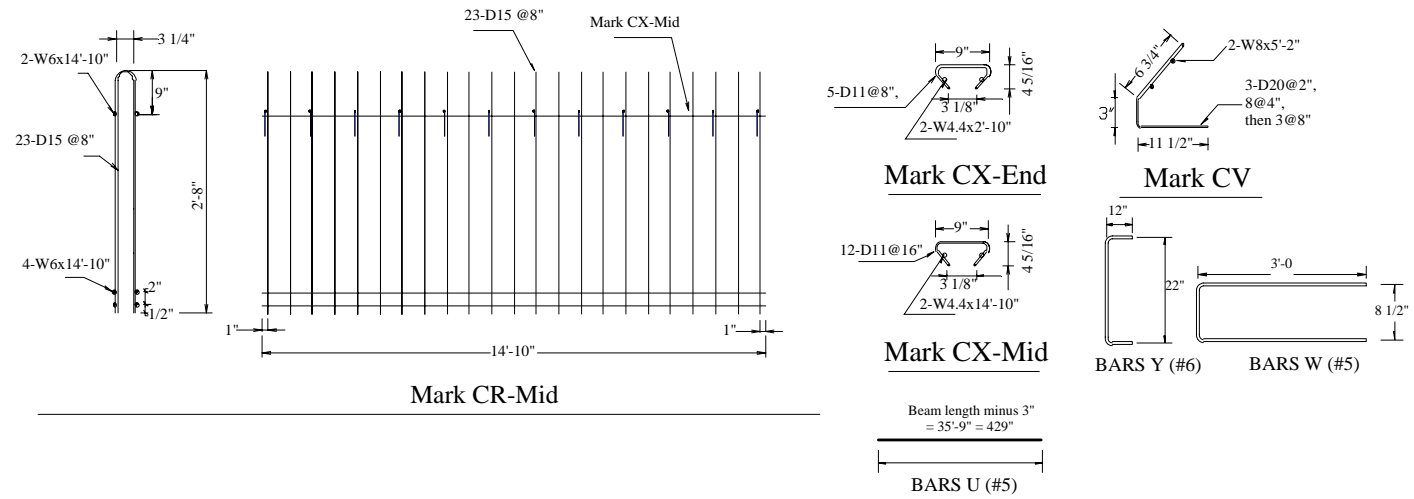
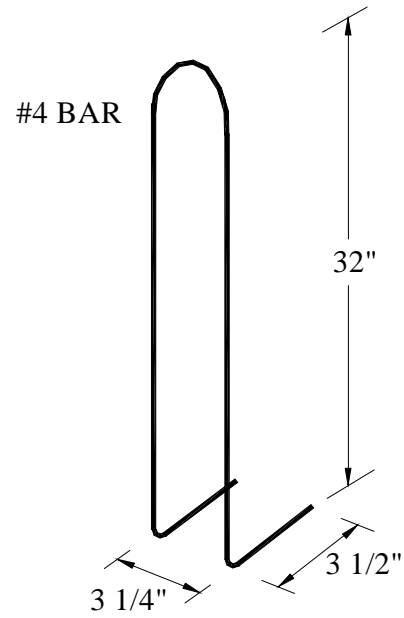


Figure A.11 Equivalent Strength Welded Wire Fabric Substitution Mark CR-End



**Figure A.12** Equivalent Strength Welded Wire Fabric Substitution Mark CR-Mid



Note:

Fabricate Alternate R-bar Specimens per Figures A.1 and A.2, Traditional Beam Detail, but substitute the shown alternate R-bar detail for the traditional R-bar detail. All 90-degree hooks should point towards the centerline of the beam.

**Figure A.13** Alternate R-bar Substitution

APPENDIX B  
ALTERNATE R-BAR SURVEYS

**TxDOT Personnel**

Survey of Alternate Vertical Shear Reinforcement Details  
Used in Prestressed Concrete I-Beams  
Conducted by Texas Tech University (TTU) for  
Texas Department of Transportation (TxDOT)

Name : TxDOT PERSONNEL (7 SENT/4 RECEIVED)  
Company / Division : \_\_\_\_\_  
Title / Position : \_\_\_\_\_  
Address : \_\_\_\_\_  
Phone No. : \_\_\_\_\_  
E-mail : \_\_\_\_\_

Total Years of Prestressed Concrete (P/C) Related Experience : 6 TO 30 YEARS

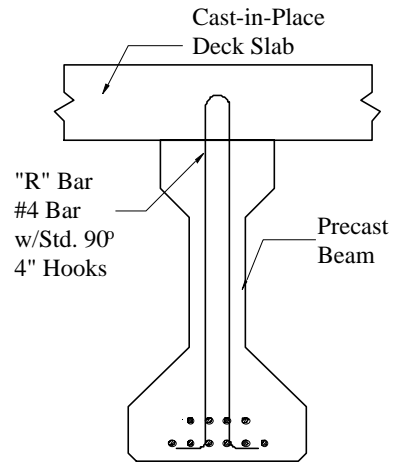
Registered/Professional Engineer: Yes 4 No \_\_\_\_\_

Detail "A" shows a typical P/C I-beam shear reinforcement (R-bar) detail currently use by TxDOT.

1. Have you had any problems with or know of any problems with the use of TxDOT's current R-bar detail?

Yes \_\_\_\_\_ No 4

If yes , describe problem:



Detail "A"

If problem has been corrected, describe how:

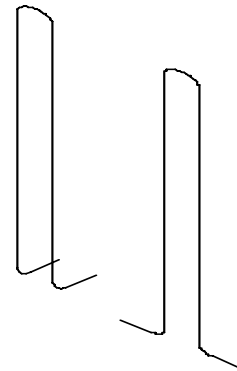


2. The following alternate R-bar details, using conventional reinforcing bar, are currently being considered for full-scale testing and implementation. Please provide comments (positive or negative) about each of the potential R-bar details. Address technical design issues and practical fabrication issues.

- A. Rotate the lower 4" long legs 90° so that they are parallel, in lieu of perpendicular, to the longitudinal axis of the beam.

**Responses:**

- 2 - Design O.K.
- 1 - Minimum cover problem?
- 1 - Problem with tying hooks between strands?



Rotated Hooks and Current Detail

- B. Slightly shorten the vertical legs of the current R-bar detail and place the 4" hooks just above, in lieu of below, the bottom row of strands.

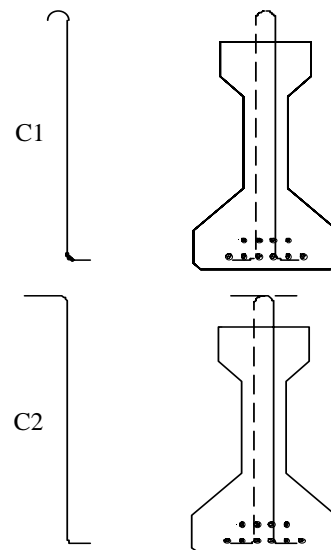
**Responses:**

- 2 - Design O.K.
- 1 - Fabrication problem ?
- 1 - Minimum cover problem ?

- C. Replace one double-leg stirrup with 2 matching single-leg stirrups placed in mirror image pairs. Two possible details are shown: C1 and C2.

**Responses:**

- 2 - Extra labor (double number of bars)
- 1 - Not an improvement
- 1 - C2, Problem with P/C deck panels
- 1 - Problem with overhanging support bracket
- 1 - C2, Upper horizontal leg:
  - Phase line in slab
  - Longitudinal construction joint ?



Note: Matching Bar Dashed for Clarity.

D. Use T-Headed mechanical anchorage devices on the lower end of each R-bar in lieu of the standard 90<sup>0</sup> hooks.

**Responses:**

- 2 - Function O.K.
- 1 - Expensive
- 1 - Improvement
- 1 - Congestion

3. Do you have any suggestions about other alternative R-bar details that should be considered? If yes, please describe/sketch.

**No responses**

4. In your opinion, which of the described R-bar details would be the best, including the current standard TxDOT detail.

**Responses:**

- 4 - Use current TxDOT R-bar detail

Please return this survey by October 13, 2000.

Mail to: William R. Burkett, Ph.D., P.E.  
Box 43107  
Texas Tech University  
Lubbock, TX 79409-3107

FAX to: 806-742-1699

Thank you for your time and participation in this endeavor.

## Texas P/C Fabricators

Survey of Alternate Vertical Shear Reinforcement Details  
Used in Prestressed Concrete I-Beams  
Conducted by Texas Tech University (TTU) for  
Texas Department of Transportation (TxDOT)

Name : TEXAS FABRICATORS (5 SENT/4 RECEIVED)\*  
Company / Division : \_\_\_\_\_  
Title / Position : \_\_\_\_\_  
Address : \_\_\_\_\_  
Phone No. : \_\_\_\_\_  
E-mail : \_\_\_\_\_

\*3 Real responses, 1 response does not fabricate I-beams

Total Years of Prestressed Concrete (P/C) Related Experience : 15 TO 37 YEARS

Registered/Professional Engineer : Yes 1 No 3

Detail "A" shows a typical P/C I-beam shear reinforcement (R-bar) detail currently use by TxDOT.

1. Have you had any problems with or know of any problems with the use of TxDOT's current R-bar detail?

Yes 3 No \_\_\_\_\_

If yes , describe problem:

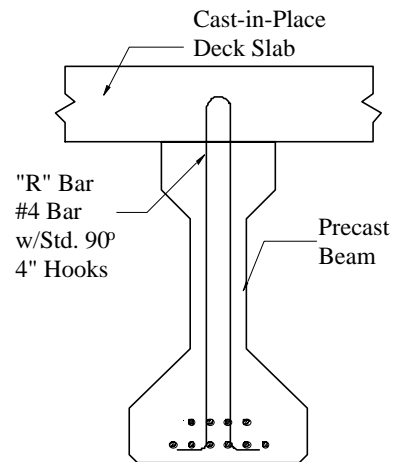
**Responses:**

- 2 - Problems with fitting legs with 4" hooks between strands @ 2" grid
- 2 - 4" hooks in different planes, cover problems

If problem has been corrected, describe how:

**Responses:**

- 1 - Rotate R-bar after insertion between strands
- 1 - Be careful while bending hooks to insure in common plane
- 1 - Replace mis-fabricated R-bars



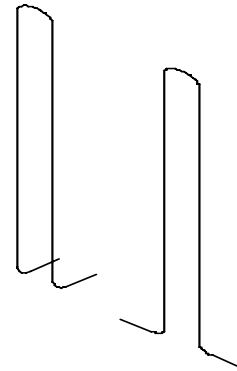
Detail "A"

2. The following alternate R-bar details, using conventional reinforcing bar, are currently being considered for full-scale testing and implementation. Please provide comments (positive or negative) about each of the potential R-bar details. Address technical design issues and practical fabrication issues.

A. Rotate the lower 4" long legs 90° so that they are parallel, in lieu of perpendicular, to the longitudinal axis of the beam.

**Responses:**

- 1 - More difficult to bend in 3-dimensions
- 2 - Better detail, easier to install between the strands



Rotated Hooks and Current Detail

B. Slightly shorten the vertical legs of the current R-bar detail and place the 4" hooks just above, in lieu of below, the bottom row of strands.

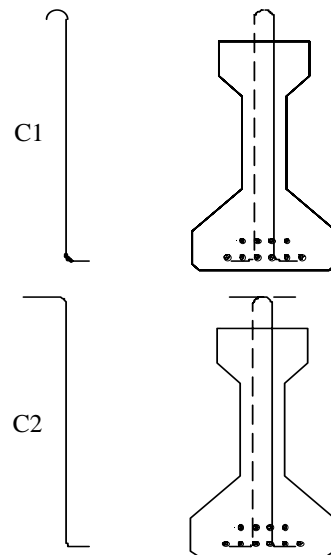
**Responses:**

- 1 - Do not like structurally (PE)
- 1 - Design / function, O.K.
- 1 - Easier to place
- 1 - Raises hooks above plane of V-bars

C. Replace one double-leg stirrup with 2 matching single-leg stirrups placed in mirror image pairs. Two possible details are shown: C1 and C2.

**Responses:**

- 3 - No double bars, increases labor
- 1 - C2, tripping hazard



Note: Matching Bar Dashed for Clarity.

D. Use T-Headed mechanical anchorage devices on the lower end of each R-bar in lieu of the standard 90° hooks.

**Responses:**

3 - Expensive

1 - Add another step to the fabrication process

3. Do you have any suggestions about other alternative R-bar details that should be considered? If yes, please describe/sketch.

**Response:**

1 - Flare out bottom of R-bar to match outline of bottom flange so R-bar will fit over top of strands

4. In your opinion, which of the described R-bar details would be the best, including the current standard TxDOT detail.

**Responses:**

1 - Current TxDOT R-bar detail

2 - Rotate 4" hooks 90-degrees

Please return this survey by October 13, 2000.

Mail to: William R. Burkett, Ph.D., P.E.  
Box 43107  
Texas Tech University  
Lubbock, TX 79409-3107

FAX to: 806-742-1699

Thank you for your time and participation in this endeavor.

**Non-Texas DOT Personnel**

Survey of Alternate Vertical Shear Reinforcement Details  
Used in Prestressed Concrete I-Beams  
Conducted by Texas Tech University (TTU) for  
Texas Department of Transportation (TxDOT)

Name : NON-TEXAS DOT's (19 SENT/12 RECEIVED)  
Company / Division : \_\_\_\_\_  
Title / Position : \_\_\_\_\_  
Address : \_\_\_\_\_  
Phone No. : \_\_\_\_\_  
E-mail : \_\_\_\_\_

Total Years of Prestressed Concrete (P/C) Related Experience: 10 TO 35 YEARS  
Registered/Professional Engineer : Yes 12 No 0

Detail "A" shows a typical P/C I-beam shear reinforcement (R-bar) detail currently use by TxDOT.

1. In bridge / overpass applications, does your state use:

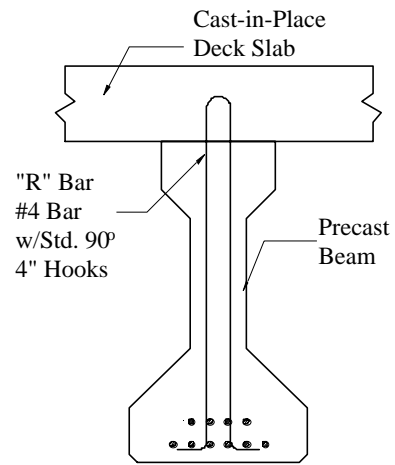
A. AASHTO standard P/C I-Beams?

Yes 8 No 4

B. Some non-standard P/C I-Beams?

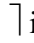
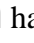

Yes 8 No 3

C. If yes to either 1A or 1B, describe/sketch the details for a typical beam and shear reinforcement or attach a copy of your state



Detail "A"

**Responses:**

- 6 - Similar to C1 or C2, with 1 - field bend top
- 1 -  in matching pairs, left and right side of beam with no bottom anchorage
- 1 - Welded Wire Fabric
- 3 -  hairpin with no bottom anchorage
- 1-  with top hook perpendicular to the beam and the bottom hook parallel to the beam, also in matching pairs on left and right side of beam

2. If information is provided in 1C, have you had any problems with or know of any problems with the use of your typical shear reinforcement detail?

Yes   2   No   8  

If yes , describe problem:

**Responses:**

- 1 - Concrete cover in deck caused by beam camber
- 1 - Multiple bending of bars
- 1 - Engineers express concern with straight lower legs of stirrups, no anchorage

If problem has been corrected, describe how:

**Responses:**

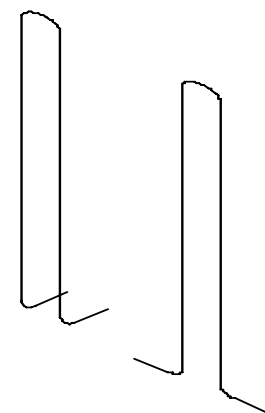
- 3 - Field bending of top of bar to provide proper concrete cover

3. The following alternate R-bar details, using conventional reinforcing bar, are currently being considered for full-scale testing and implementation. Please provide comments (positive or negative) about each of the potential R-bar details. Address technical design issues and practical fabrication issues.

- A. Rotate the lower 4" long legs 90° so that they are parallel, in lieu of perpendicular, to the longitudinal axis of the beam.

**Responses:**

- 3 - Design O.K.
- 2 - Better for beam fabrication
- 1 - Shipping / stacking problem
- 3 - congestion at end of beam if c/c spacing is too close
- 2 - More expensive to make bends
- 2 - More difficult to bend:
  - 3-dimensional bend
  - 2-90° hooks in the same horizontal plane



Rotated Hooks and Current Detail

- B. Slightly shorten the vertical legs of the current R-bar detail and place the 4” hooks just above, in lieu of below, the bottom row of strands.

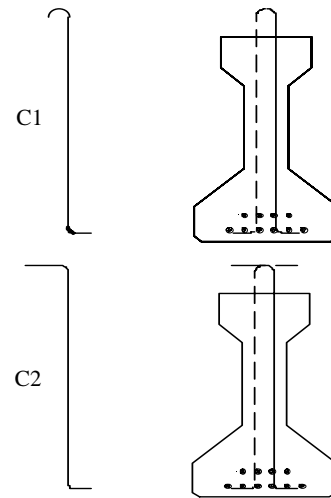
**Responses:**

- 4 - Horizontal leg below bottom strand stronger and protects strand if hit
- 3 - Question whether detail will provide adequate confinement
- 1 - Not practical for fabrication sequence
- 3 - Improves current detail

- C. Replace one double-leg stirrup with 2 matching single-leg stirrups placed in mirror image pairs. Two possible details are shown: C1 and C2.

**Responses:**

- 2 - Design is O.K.
- 2 - Improvement
- 1 - More Flexible with side cover
- 2 - Use similar detail
- 1 - Top of bar is tripping hazard
- 2 - Not practical or no advantage



Note: Matching Bar Dashed for Clarity.

- D. Use T-Headed mechanical anchorage devices on the lower end of each R-bar in lieu of the standard 90° hooks.

**Responses:**

- 1 - Expensive
- 2 - More congestion
- 1 - No confinement of bottom strands
- 1 - Why use
- 1 - Not practical



4. Do you have any suggestions about other alternative R-bar details that should be considered?  
If yes, please describe/sketch.

**Response:**

1 - Welded Wire Fabric,  $\cap$  shape

5. In your opinion, which of the described R-bar details would be the best, including the current standard TxDOT detail.

**Responses:**

2 - Use detail similar to C1 or C2

2 - Use detail similar to current TxDOT

2 - Use two-piece L-shaped stirrup with hook at bottom and top field bent

1 - Use Welded Wire Fabric

1 - Use  $\sqcap$  shape traditional deformed bar with no anchorage at bottom

Please return this survey by October 13, 2000.

Mail to: William R. Burkett, Ph.D., P.E.  
Box 43107  
Texas Tech University  
Lubbock, TX 79409-3107

FAX to: 806-742-1699

Thank you for your time and participation in this endeavor.